Computational neuromorphometry based on structural magnetic resonance imaging

Methods and applications in basic and clinical neuroscience

Thesis

presented

to the Faculty of Arts

of the University of Zurich

for the degree of Doctor of Philosophy

by

Jürgen Hänggi

of Nunningen (SO), Switzerland

Accepted in the summer semester 2007 on the recommendation of

Prof. Dr. rer. nat. Lutz Jäncke
&
Prof. Dr. med. Christoph Hock

Zurich, 2009

Acknowledgements

I would like to thank following people

Andrea, Noah, and Mathis, for everything my family had done for me during my Ph.D. thesis.
My parents, Erwin and Susi, for financial and all other support.
Andreas Buchmann, for interesting discussions, collaborations, and for using some of his data.
Christian Mondadori, for interesting discussions, collaborations, and for using some of his data.
Lutz Jäncke, for his support and interesting discussions of my projects and for being my doctorfather.
Katharina Henke, for giving me the opportunity to research at the Division of Psychiatry Research.
Christoph Hock, for giving me the opportunity to research at the Division of Psychiatry Research.
Roger M. Nitsch, for giving me the opportunity to research at the Division of Psychiatry Research.
Dominique de Quervain and Andreas Papassotiropoulos, for genotyping the participants.
Amanda Aerni and Pascal Vrticka, for help during data acquisition.
Christian Gaser, for using his toolbox for voxel-based morphometry and for his support.
Marko Wilke, for using his script to mask and compute brain volumes and for his support.
John Ashburner and Karl Friston, for using SPM software and for their support.
All other SPM contributors, for using SPM software and for their support.
Bruce Fischl and Anders M. Dale, for using the FreeSurfer analysis suite and for their support.
Douglas N. Greve and Nick Schmanski, for using the FreeSurfer analysis suite and for their support.
All other FreeSurfer contributors, for using the FreeSurfer analysis suite and for their support.
The people from the SPM, FSL, and FreeSurfer mailinglist, for their general support.
Our experimental subjects, for participating in my studies.
Our patients, for using their clinical data for research.
The reader, for showing interest in my Ph.D. thesis and for his/her understanding with respect to my English that is not quite perfect because English is a foreign language for me.

Financial support was granted by

- The EU contract LSHM-CT-2003-503330 (APOPIS).
- Jubilee Foundation of the bank of Basle-Country.
- Handschin Foundation.
- University of Zurich.
- Canton Basle-Country.

Original research articles included in this doctoral thesis

Study 1:

Jürgen Hänggi, Andreas Buchmann, Christian R.A. Mondadori, Katharina Henke, Lutz Jäncke & Christoph Hock (2009). **Sexual dimorphism in the parietal substrate associated with visuospatial cognition independent of general intelligence.** *J. Cogn. Neurosci.*; doi:10.1162/jocn.2008.21175.

Study 2:

Jürgen Hänggi, Christian R.A. Mondadori, Andreas Buchmann, Katharina Henke & Christoph Hock (2009). **A *CYP46* T/C SNP modulates parahippocampal and hippocampal morphology in young subjects.** *Neurobiol. Aging*; doi:10.1016/j.neurobiolaging.2009.07.001.

Study 3:

Jürgen Hänggi, Johannes Streffer, Andri Signorell, Lutz Jäncke & Christoph Hock (2009). **Neuromorphometric profiling in mild cognitive impairment and Alzheimer's disease: Sensitivity and specificity.** (submitted).

Other original research articles not included in this doctoral thesis

Study 4:

Valko, P.**, Hänggi, J.,** Meyer, M. & Jung, H. (2009). **Evolution of striatal generation in McLeod syndrome.** *Europ. J. of Neurol.;* (in press).

Study 5:

Hänggi, J., Koeneke, S., Bezzola, L. & Jäncke, L. (2009). **Structural neuroplasticity in the sensorimotor network of professional female ballet dancers.** *Hum. Brain Mapp.;* (in press).

Study 6:

Jäncke, L., Koeneke, S., Hoppe, A., Rominger, C. & **Hänggi, J.** (2009). **The architecture of the golfer's brain.** *PLoS ONE;* 4(3): e4785.

Study 7:

Jäncke, L., Beeli, G., Eulig, C. & **Hänggi, J.** (2009). **The neuroanatomy of grapheme-colour synesthesia.** *Eur. J. Neurosci.;* 29(6): 1287-1293.

Study 8:

Hänggi, J., Beeli, G., Oechslin, M.S. & Jäncke, L. (2008). **The multiple synaesthete E.S.: neuroanatomical basis of interval-taste and tone-colour synaesthesia.** *Neuroimage;* 43(2): 192-203.

Study 9:

Buchmann, A., Mondadori, C.R.A., **Hänggi, J.**, Aerni, A., Vrticka, P., Luechinger, R., Boesiger, P., Hock, C., Nitsch, R.M., de Quervain, D. J.-F., Papassotiropoulos, A. & Henke, K (2008). **Prion protein M129V polymorphism affects retrieval-related brain activity.** *Neuropsychologia;* 46: 2389-2402.

Study 10:

Huentelman, M.J., Papassortiropoulos, A., Craig, D.W., Hoerndli, F.J., Pearson, J.V., Huynh, K.-D., Corneveaux, J., **Hänggi, J.**, Mondadori, C., Buchmann, A., Reiman, E.M., Henke, K., de Quervain, D.J.-F. & Stephan, D.A. (2007). **Calmodulin-binding transcription activator 1 (CAMTA1) alleles predispose human episodic memory performance.** *Hum. Mol. Genet.*; 16(12): 1469-1477.

Study 11:

Papassortiropoulos, A., Stephan, D.A., Huentelman, M.J., Hoerndli, F.J., Craig, D.W., Pearson, J.V., Huynh, K.-D., Brunner, F., Corneveaux, J., Osborne, D., **Hänggi, J.**, Mondadori, C., Buchmann, A., Reiman, E.M., Caselli, R.J., Henke, K. & de Quervain, D.J.-F. (2006). **Common *Kibra* alleles influence memory performance in humans.** *Science*; 314: 475-478.

Study 12:

Jäncke, L., **Hänggi, J.** & Steinmetz, H. (2004). **Morphological brain differences between adult stutterers and non-stutterers.** *BMC Neurol.;* 4: 23.

Contributions to meetings

Talks & Abstracts

2007

- 3nd Winter Brain Symposium 2007 of the Psychogeriatric University Hospital and the Division of Psychiatry Research, Sils-Maria, Switzerland, February 3-7, 2007. Title of talk: **Neuromorphometric profiles of patients with amnestic mild cognitive impairment and Alzheimer's disease: Sensitivity and Specificity.**

2006

- ZNZ Symposium 2006: Symposium of the Neuroscience Center Zurich (ZNZ), October 20, 2006 at the University of Zurich, Zurich-Irchel. Title of talk: **Gender-specific neuromorphological substrates of human visuospatial intelligence: A computational neuroanatomical study.**
- INS (International Neuropsychological Society) congress 2006 in Zurich, Switzerland, July 26-30, 2006: Topic: From plasticity to rehabilitation. Title of talk: **Computational neuroanatomy supports the diagnosis of dementias in clinical daily routine.**

- 2nd Winter Brain Symposium 2006 of the Psychogeriatric University Hospital and the Division of Psychiatry Research, Sils-Maria, Switzerland, January 29 – February 2, 2006. Title of talk: **Longitudinal effects of β-amyloid immunization (AN1792) on whole brain atrophy rates and hippocampal volumes in patients with Alzheimer`s disease.**

Posters

2009

- NCCR (National Center of Competence in Research) Symposium on neural plasticity and repair 2009, January 30-31, 2009, Berlingen, Switzerland.
  Title of poster: **The architecture of the reverse piano player's brain.**

2008

- ZNZ Symposium 2008: Symposium of the Neuroscience Center Zurich (ZNZ), September 12,

2008 at the Swiss Federal Institute of Technology Zurich, Hönggerberg Zurich, Switzerland.
Title of poster: **Structural neuroplasticity in the sensorimotor system of professional female ballet dancers.**
Title of poster: **The neuroanatomical basis of grapheme-colour synaesthesia – a surface-based morphometry study.**
Title of poster: **Structural brain anomalies in Turner syndrome – revisited.**

- NCCR (National Center of Competence in Research) Symposium on neural plasticity and repair 2008, March 7-8, 2008, Berlingen, Switzerland.
  Title of poster: **Structural neuroplasticity in the sensorimotor system of professional female ballet dancers.**
  Title of poster: **Training-induced structural plasticity in professional handball players: voxel-based morphometry & DTI.**

2007

- ZNZ Symposium 2007: Symposium of the Neuroscience Center Zurich (ZNZ), September 14, 2007 at the University of Zurich, Zurich-Irchel, Switzerland.
  Title of poster: **Neuromorphometric profiles of patients with amnestic mild cognitive impairment and Alzheimer's disease: Sensitivity and Specificity.**

  Title of poster: **Training-induced structural plasticity in professional handball players: voxel-based morphometry & DTI.**

2006

- ZNZ Symposium 2006: Symposium of the Neuroscience Center Zurich (ZNZ), October 20, 2006 at the University of Zurich, Zurich-Irchel, Switzerland. Title of poster: **Gender-specific neuromorphological substrates of human visuospatial intelligence: A computational neuroanatomical study.**

2005

- ZNZ Symposium 2005: Symposium of the Neuroscience Center Zurich (ZNZ), October 21, 2005 at the Swiss Federal Institute of Technology Zurich, Switzerland.
  Title of poster: **Longitudinal effects of β-amyloid immunization on hippocampal volumes in patients with Alzheimer`s disease.**

2003

- Master and Ph.D. congress (Lizentianden- und Doktorandenkongress, LiDoKo,), June 26, 2003, at the Institute of Psychology, University Zurich, Switzerland. Title of poster: **Neuroanatomical anomalies in adults with persistent developmental stuttering (PDS).**

Abbreviations

2D, 3D:	Two-dimensional, three-dimensional
3T, 7T:	Three Tesla, seven Tesla (magnetic field power)
5-HT2a:	5-Hydroxy-Tryptamine (serotonin) 2a receptor
24-OHC:	24*S*-hydroxycholesterol
Aβ:	Amyloid β
AD:	Alzheimer's Disease
ANCOVA:	ANalysis of COVAriance (univariate)
ApoE:	Apolipoprotein E
BA:	Brodmann's Area
BDNF:	Brain-Derived Neurotrophic Factor
CSF:	Cerebro-Spinal Fluid
CYP46:	Cytochrome Pigment 450 46A1 (cholesterol 24*S*-hydroxylase)
DBM:	Deformation Based Morphometry
DOF:	Degrees Of Freedom
fMRI:	Functional magnetic Resonance Imaging
FFE:	Fast Field Echo
FSIQ:	Full Scale Intelligence Quotient
FWHM:	Full Width at Half Maximum
GM:	Grey Matter
g-factor:	Factor for general intelligence
HAWIE-R:	Hamburg Wechsler Intelligenztest für Erwachsene – Revision 1991 (German version of the WAIS-R)
HCS:	Healthy Control Subjects
HMRF:	Hidden Markov Random Field
ICBM:	International Consortium for Brain Mapping
MANCOVA:	Multivariate ANalysis of COVAriance
MARINA:	MAsks for Regions of INterest Analysis software
MCI:	Mild Cognitive Impairment (amnestic type)
MNI:	Montreal Neurological Institute
MRI:	Magnetic Resonance Imaging (Tomography)
MTL:	Medial Temporal Lobe
PET:	Positron Emission Tomography
RAPM:	Raven's Advanced Progressive Matrices
PRADL:	Probable Alzheimer's Disease Late Onset
PRNP:	Prion Protein Gene
SNP:	Single Nucleotide Polymorphism
SPM:	Statistical Parametric Mapping software
SPSS:	Statistical Package for the Social Sciences
SVC:	Small Volume Correction
T1-w.:	T1-weighted
TCSFVplus:	Total Cerebro-Spinal Fluid Volume including scalp, skull, and meninges
TGMV:	Total Grey Matter Volume
TWMV:	Total White Matter Volume
VBM:	Voxel Based Morphometry
VOI:	Volume Of Interest
VSC:	Visuo-Spatial Cognition
WAIS-R:	Wechsler Adult Intelligence Scale – Revised
WM:	White Matter

Summary

General: In the first third of my Ph.D. thesis, I will introduce the individual processing steps of the classical voxel-based morphometry. The second third of the thesis is the experimental part comprised by my three experimental studies. The last part of my Ph.D. thesis deals with shortcomings and drawbacks of the classical voxel-based morphometry methodology and it introduces the approach of surface-based morphometry, which is free of many of the shortcomings described for the classical voxel-based morphometry methods. Furthermore, a fully automated, subcortical, volumetric segmentation procedure is also described and a sparse perspective of the computational, magnetic resonance imaging-based neuromorphometric methodology is scheduled.

Methods: In this Ph.D. thesis, it has been shown that the neuromorphometric methodology based on structural magnetic resonance imaging can be used to investigate the relations between brain structure and brain function. Different computational, neuromorphometric methods were applied to investigate basic neuroscientfic hypotheses about the morphology of brain structures and its associated functions as well as to answer clinical neuroscience questions about pathological conditions of brain structures in disease. The methods described in my thesis focus on cytoarchitecture, investigated with T1-weighted magnetic resonance images. With respect to myeloarchitecture, only volumetric properties of white matter were investigated. In order to investigate the features of white matter connectivity, diffusion-weighted imaging methods are more suitable. With the advent of new high-field magnetic resonance imaging scanners operating at 7 Tesla, new opportunities will be opened for the field of computational, structural neuromorphometry such as the investigation of the laminar pattern of the cortex in vivo.

Study 1: Gender differences in visuospatial cognition (VSC) with male advantage are frequently reported in the literature. There is evidence for sexual dimorphisms in the human brain, one of which postulates more grey matter (GM) in females and more white matter (WM) in males relative to total intracranial volume. We investigated the neuroanatomy of VSC independent of general intelligence (g) in gender-separated populations, homogenous in age, education, memory performance, a memory- and brain morphology-related gene, and g. VSC and g were assessed with the Wechsler adult intelligence scale. The influence of g on VSC was removed using a hierarchical factor analysis and the Schmid-Leiman solution. Structural high-resolution magnetic resonance images were acquired and analysed with voxel-based morphometry. As hypothesised, the clusters of positive correlations between local volumes and VSC performance independent of g were found mainly in parietal areas, but also in pre- and postcentral regions, predominantly in WM in males, whereas in females, these correlations were located in parietal and superior temporal areas, predominantly in GM. Our results suggest that VSC depends more strongly on parietal WM structures in males and on parietal GM structures in females.

This sex difference might have to do with the increased axonal and decreased somatodendritic tissue in males relative to females. Whether such gender-specific implementations of the VSC network can be explained genetically as suggested in investigations into the Turner syndrome, or as a result of structural neural plasticity upon different experience and usage remains to be shown.

Study 2: There is evidence that brain cholesterol metabolism modulates the vulnerability for Alzheimer's disease (AD). Previous data showed that brain β-amyloid load in elderly subjects with the *CYP46* (cholesterol 24*S*-hydroxylase) TT-positive genotype was higher than in *CYP46* TT-negative elderly subjects. We investigated effects of the *CYP46* T/C polymorphism on parahippocampal and hippocampal grey matter (GM) morphology in 81 young subjects using structural magnetic resonance imaging based morphometry. We found that young TT-homozygotes exhibited smallest and CC-homozygotes largest parahippocampal and hippocampal GM volumes with the volumes of the CT-heterozygotes ranging in between. Parahippocampal and hippocampal volumes were positively correlated with delayed memory performance in C-carriers and negatively with immediate memory performance in TT-homozygotes. It has been shown that the brain cholesterol metabolism in general modulates dendrite outgrowth, synaptogenesis, and neuron survival, and it was suggested that *CYP46* indirectly influences β-amyloid metabolism. *CYP46* C-carriers are privileged both in terms of β-amyloid metabolism and in terms of brain reserve due to their larger parahippocampal and hippocampal structures. The exact cellular mechanisms that translate the *CYP46* allelic variation into volumetric brain differences in the parahippocampal gyrus and hippocampus are still unknown and need to be further investigated.

Study 3: Diagnosing Alzheimer's disease (AD) and distinguishing it from other dementia as well as from amnestic mild cognitive impairment (MCI) depends mainly on clinical evaluation, and, ultimately, on investigator's judgement. Clinical evaluation is based primarily on neuropsychological assessments and secondary on biomarkers found in cerebrospinal fluid. The present study explores the potential of volumetric magnetic resonance imaging (MRI) to diagnose AD in vivo and to separate it from patients with amnestic MCI and healthy control subjects (HCS). We acquired 3D volumetric T1-weighted MRI scans of 12 age-matched HCS, 18 patients with amnestic MCI, and 59 patients with probable late onset Alzheimer's disease (PRADL). These MR images were spatially normalised into a stereo-tactic space, segmented into tissue compartments, Jacobian and hidden Markov random field modulated, and the resulted grey matter segments were full automatically parcellated into 45 regions of interest (ROIs) per hemisphere and the volumes of the ROIs were computed. Promising diagnostic values for distinguishing PRADL patients from HCS were found for the total grey matter (sensitivity/ specificity: 88.1%/91.7%), the hippocampi (both 93.2%/91.7%), and the right and left superior parietal gyrus (96.6%/83.3% and 93.2%/83.3%, respectively), for distinguishing MCI from PRADL patients

for the left inferior temporal gyrus (86.4%/72.2%) and the right hippocampus (84.7%/66.7%), and for distinguishing MCI patients from HCS for the left Heschl's gyrus (88.9%/83.3%) and the left superior temporal gyrus (83.3/83.3%). We showed potential diagnostic values of MRI-based neuromorphometric profiling in dementia diagnostics. Therefore, we propose to establish a standardised database of regional brain volumes based on large series of patients and controls. A new patient can then be compared to these norms and statistical measures for a single subject can be derived to support and corroborate the general and differential diagnosis of dementia.

[Zusammmenfassung]

Allgemein: Im ersten Drittel meiner Dissertation führe ich die einzelnen Vorverarbeitungsschritte der klassischen, voxel-basierten Morphometrie ein. Das zweite Drittel meiner Dissertation bildet den experimentellen Teil bestehend aus meinen drei experimentellen Studien. Der letzte Teil meiner Thesis behandelt die Unzulänglichkeiten und Mängel der klassischen voxel-basierten Morphometrie und führt den Ansatz der oberflächen-basierten Morphometrie ein, welche viele dieser Mängel beheben kann. Zusätzlich wird eine vollautomatische, subkortikale Segmentierungsmethode vorgestellt und eine kleine Zukunftsperspektive bgzl. der computationalen, magnetresonanz-tomographie-basierte Neuromorphometrie gegeben.

Methoden: In dieser Dissertation ist gezeigt worden, dass die neuromorphometrische Methodologie basierend auf der strukturellen Magnetresonanz-Tomographie verwendet werden kann, um Beziehungen zwischen Hirnstrukturen und Hirnfunktionen zu untersuchen. Verschiedene computationale, neuromorphometrische Methoden wurden angewendet, um neurowissenschaftliche Hypothesen über die Morphometrie von Gehirnstrukturen und ihren assoziierten Gehirnfunktionen zu untersuchen, und um klinische, neurowissenschaftliche Fragestellungen über pathologische Zustände der Gehirnstruktur bei Krankheiten zu beantworten.

Studie 1: Geschlechtsunterschiede in der visuell-räumlichen Kognition, Männer favorisierend, werden häufig in der Literatur berichtet. Es gibt Evidenz für sexuelle Dimorphismen im menschlichen Gehirn, einer davon postuliert, dass Frauen mehr graue Substanz als Männer und Männer mehr weisse Substanz als Frauen relativ zu ihren intrakraniellen Volumina haben. Wir untersuchten die Neuroanatomie der visuell-räumlichen Kognition unabhängig von allgemeiner Intelligenz in geschlechtergetrennten Populationen, welche homogen bezüglich dem Alter, der Ausbildung, der Gedächtnisleistung, in einem Gen, welches mit Gedächtnis und Morphology assoziiert ist, und bzgl. der allgemeinen Intelligenz. Visuell-räumliche Kognition und allgemeine Intelligenz wurden mit dem Hamburg-Wechsler Intelligenztest für Erwachsene gemessen. Der Einfluss der allgeminen Intelligenz auf die visuell-räumliche Kognition wurde mittels einer hierarchischen Faktorenanalyse und der

Schmid-Leiman-Lösung entfernt. Strukturelle hoch-auflösende Magnetresonanz-Tomographie-Bilder wurden aufgenommen und mit der voxel-basierten Morphometrie analysiert. Wie vorhergesagt, fanden wir Cluster von positiven Korrelationen zwischen lokalen Volumina und der Performanz in der visuell-räumlichen Kognition unabhängig von allgemeiner Intelligenz hauptsächlich in parietalen Arealen, aber auch in pre- und postzentralen Regionen, vorwiegend in der weissen Substanz bei Männern. Bei Frauen waren diese Korrelationen in parietalen und superior temporalen Arealen lokalisiert, vorwiegend in der grauen Substanz. Unsere Resultate sprechen dafür, dass die visuell-räumliche Kognition stärker von der parientalen weissen Substanz bei den Männern, und von der parietalen grauen Substanz bei den Frauen abhängt. Dieser Geschlechtsunterschied hat mit dem erhöhtem axonalen und reduziertem somatodendritischen Gewebevolumen bei Männern relativ zu Frauen zu tun. Ob solche geschlechterspezifische Implementationen des visuell-räumlichen Kognitionnetzwerks genetisch erklärt werden können, wie es Untersuchungen zum Turner Syndrom suggerieren, oder als ein Resultat struktureller neuraler Plastizität aufgrund unterschiedlicher Erfahrung und Gebrauch, bleibt noch zu zeigen.

Studie 2: Es gibt Evidenz, dass der Gehirncholesterolmetabolismus die Vulnerabilität für eine Alzheimer-Demenz moduliert. Frühere Daten habe gezeigt, dass die β-Amyloid-Ladung in älteren Probanden mit dem *CYP46* (Cholesterol 24*S*-Hydroxylase) TT-positiven Genotyp höher ist als in *CYP46* TT-negativen älteren Probanden. Wir untersuchten Effekte eines *CYP46* T/C Polymorphismus auf die parahippokampale und hippokampale Morphologie der grauen Substanz bei 81 jungen, gesunden Subjekten mittels struktureller magnetresonanztomographie-basierender Morphometrie. Wir fanden, dass junge TT-Homozygote die kleinsten und CC-Homozygote die grössten parahippokampalen und hippokampalen Volumina an grauer Substanz aufwiesen, wobei die Volumina der CT-Heterozygote dazwischen lagen. Parahippokampale und hippokampale Volumina waren positiv korreliert mit der Performanz des verzögerten Gedächtnisabrufs in C-Trägern, und negativ korreliert mit der Performanz des unmittelbaren Gedächtnisabrufs bei TT-Homozygoten. Es ist gezeigt worden, dass der Gehirncholesterolmetabolismus im allgemeinen folgende Prozesse moduliert: den dendritischen Auswuchs, die Synaptogenese, und das Überleben der Neurone, und es wurde suggeriert, dass *CYP46* indirekt den β-Amyloidmetabolism beeinflusst. *CYP46* C-Träger sind privilegiert bzgl. dem β-Amyloidmetabolism und bzgl. ihrer Gehirnreserve wegen ihren grösseren parahippokampalen und hippokampalen Strukturen. Die exakten zellulären Mechanismen, welche die *CYP46* allelische Variation in volumetrische Gehirndifferenzen im parahippokampalen Gyrus und im Hippokampus transformieren, sind noch unbekannt und müssen weiter untersucht werden.

Studie 3: Eine Alzheimer-Demenz zu diagnostizieren und sie sowohl von anderen Demenzen als auch von einer amnestischen, leichten kognitiven Beeinträchtigung zu differenzieren, hängt

hauptsächlich von der klinischen Evaluation und daher ultimativ vom Urteil des Untersuchers ab. Die klinische Evaluation basiert primär auf neurpsychologischen Assessments und sekundär auf sogenanten Biomarkern, welche man in der Zerebrospinalflüssigkeit finden kann. Die vorliegende Studie untersucht das Potential mittels der volumetrischen Magnetresonanztomographie und neuromorphometrischen Analysen, eine Alzheimer-Demenz in vivo zu diagnostizieren, und diese Patienten von Patienten mit einer amnestischen, leichten kognitiven Beeinträchtigung und von Gesunden zu separieren. Wir akquirierten 3D volumetrische T1-gewichtete Magnetresonanz-Tomographiebilder von 12 alters-balancierten gesunden Kontrollprobanden, 18 Patienten mit einer leichten kognitiven Beeiträchtigung und 59 Patienten mit möglicher Alzheimer-Demenz mit spätem Beginn. Diese Magnetresonanztomographiebilder wurden räumlich in einen stereotaktischen Raum registriert, segmentiert in die verschiedenen Gewebearten, moduliert mit der Jacobschen Determinante, gewichtet mit einem Hidden Markov Random Field, und die resultierenden Segmente der grauen Substanz wurden vollautomatisch in 45 Regionen per Hemisphäre unterteilt und die Volumen dieser Regionen berechnet. Vielversprechende diagnostische Kennwerte zur Unterscheidung von Alzheimerpatienten von Gesunden wurde gefunden für das Gesamtvolumen der grauen Substanz (Sensitivität/Spezifität: 88.1% / 91.7%), für die beiden Hippokampi (both 93.2% / 91.7%), und für den linken und rechten superioren parietalen Gyrus (96.6% / 83.3% and 93.2% / 83.3%, beziehungsweise). Gute diagnostische Kennwerte zur Unterscheidung von Patienten mit einer leichten kognitiven Beeiträchtigung von denjenigen mit einer Alzheimer-Demenz zeigte der linke inferiore temporale Gyrus (86.4% / 72.2%) und der rechte Hippokampus (84.7% / 66.7%), und zur Unterscheidung von Patienten mit einer leichten kognitiven Beeiträchtigung von Gesunden der linke Heschl'sche Gyrus (88.9% / 83.3%) und der linke superiore temporale Gyrus (83.3 / 83.3%). Wir zeigten potentielle diagnostische Kennwerte von magnetresonanztomographie-basiertem, neuromorphometrischem Profiling. Deshalb schlagen wir vor, eine standardisierte Datenbank von regional Hirnvolumina basierend auf grossen Serien von Patienten und Gesunden zu etablieren. Ein neuer Patient kann dann mit diesen Normen verglichen werden und statistische Masse für einzelne Subjekte können hergeleitet werden, um eine allgemeine oder differenzierte Diagnose einer Demenz zu stellen, zu unterstützen und/oder zu bestätigen.

1 Introduction to neuromorphometry

The aim of this Ph.D. thesis is neither to provide an exhaustive overview about neuroanatomy nor a comprehensive summary about neuromorphometry. Instead, I will focus on some computational, neuromorphometric methods that were applied in my three studies, which constitute the experimental part of my Ph.D. thesis, and show how these approaches can be used to answer basic and clinical neuroscience research questions. Although diffusion tensor imaging (DTI) is also a structural magnetic resonance imaging based method, this kind of neuromorphometric analysis is not part of my Ph.D. thesis. Hence, this thesis deals more with the human cytoarchitecture (neurons, grey matter) than with the myeloarchitecture (glia, white matter). The following introduction focuses on cytoarchitectonic atlases (maps) of the human brain, because these atlases are crucial for computational neuromorphometry with respect to the common stereotaxic space and with respect to the interindividual neuroanatomical variability. This introduction aims at providing some background information about post mortem neuroanatomy in the past to better understand the topics, advantages, and problems of in vivo computational neuromorphometry nowadays. A comprehensive summary about the history of neuromorphometry can be found by Haug (Haug, 1986), an exhaustive overview about human brain atlas construction can be found by Mazziotta, Toga and colleagues (Toga & Mazziotta, 2002; Mazziotta et al., 2001; Toga et al., 2006). The concept of the brain atlas is not new. Cartographic approaches have been used for centuries to identify and target specific regions in the brain and to establish spatial relationships between a coordinate and a brain structure (Toga & Mazziotta, 2002). Early research on the cellular composition of the brain culminated in the development of atlases of the human cerebral cortex, which were pioneered by Brodmann (1909, 1914), Flechsig (1920), Vogt & Vogt (1919), von Economo & Koskinas (1925), and others. These studies continued until the 1960s (Bailey & von Bonin, 1951; Sanides, 1962; Sarkisov et al., 1955). The cortex was segregated into numerous structurally defined areas, based on regional cytoarchitecture (identified mainly by the number of cortical layers, laminar patterns of cell packing density, and by the shape of neuronal cell bodies) or myeloarchitecture (identified mainly by the degree of myelination and the presence or absence of myelinated fibre bundles in the cerebral cortex). These types of architecture were studied by visual inspection under the microscope of Nissl- or myelin-stained histologic sections in single brains. A lot of problems became apparent with these atlases. The most severe problems of these atlases, despite of the known problems associated with post mortem tissue and its fixation, is the absent of a common stereotaxic space (i.e., a common coordinate system), no sharp boundaries of the areas, and with few exceptions, the drawings or descriptions do not show the position of areas and their borders in the cortical sectors that are hidden in the sulci (Toga et al., 2006). Meanwhile, stereological atlases of the human brain, based on postmortem and imaging data, began to

be published (mostly in book form) (Talairach & Szikla, 1967; Talairach & Tournoux, 1988; Mai et al., 1997; Duvernoy, 1991; Ono et al., 1990), primarily in response to needs of neurosurgeons. These atlases overcome many of the problems associated with the maps and atlases of the pioneers mentioned above. These atlases are a central topic when investigating Hundreds of subjects with computational neuroanatomical procedures, both structurally and functionally. Nowadays, there are several digital brain atlases that can be used for analysing structural and functional magnetic resonance tomography (sMRI and fMRI) images of the brain as well as for analyses of functional data acquired with positron emission tomography (PET) and structural analyses of diffusion tensor weighted imaging (DTI). The construction of digital brain atlases was initiated by the Montreal neurological institute (MNI, http://www.bic.mni.mcgill.ca/) and pursued by the international consortium for brain mapping (ICBM, http://www.loni.ucla.edu/ICBM/). In the following introduction, I will focus on the construction of brain atlases in the past and I will show one example of post-mortem atlas reconstruction that is still in progress and will certainly influence the future of neuroimaging. The digital atlases (also called templates, a priori maps, and reference maps) currently used in computational, neuroanatomical (and neurofunctional) procedures will be introduced in section 2. below. Beside cytoarchitectonic and myeloarchitectonic maps, there are efforts to complement these atlases with receptor architectonic information (also called chemoarchitectonic maps) that show the distribution patterns of the receptors of different neurotransmitter systems (Eickhoff et al., 2007).

1.1 Cytoarchitectonics by Korbinian Brodmann, 1909

Korbinian Brodmann (1868-1918), a German neuroanatomist and psychiatrist, who became famous for his definition of the cerebral cortex into 52 distinct regions from their cytoarchitectonic (histologic) characteristics (Brodmann, 1908, 1909, 1914). These areas are now usually referred to as Brodmann's areas (BA, Fig. 1). Some of these areas were later associated with neural functions, such as areas BA 41 and 42 in the temporal lobe (related to auditory functions, A1 and A2), BA 1, 2 and 3 in the postcentral gyrus of the parietal lobe (related to somatosensory functions, S1), BA 4 in the precentral gyrus of the frontal lobe (related to motor functions, M1), and the BA 17 and 18 in the occipital lobe (related to visual functions, V1 and V2). The Brodmann's areas are still used frequently nowadays (complemented with MNI coordinates) as a reference system to report the locations of structural brain differences, functional activity, and brain lesions.

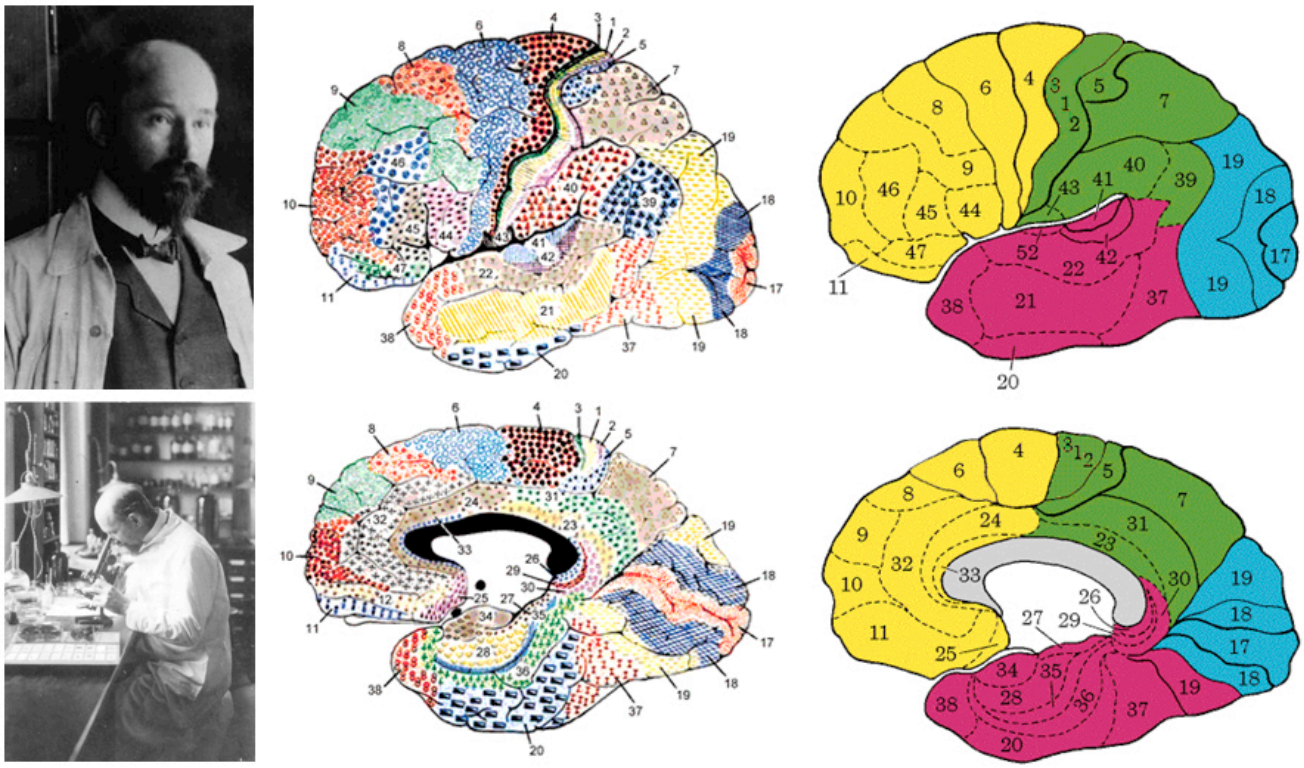

Figure 1: Brodmann's areas.
Left panels: K. Brodmann' portrait and K. Brodmann at work. Figure adopted from http://www.korbinian-brodmann.de. ***Middle panels:*** Original drawings (colorised) by K. Brodmann (***top:*** lateral view, ***bottom:*** medial view). Figure adopted from http://spot.colorado.edu/~dubin/talks/brodmann/brodmann.html. ***Right panels:*** Schematic drawings of Brodmann's areas (***top:*** lateral view, ***bottom:*** medial view). Figure adopted from http://www.umich.edu/~cogneuro/jpg/Brodmann.html.

1.2 Cytoarchitectonics by Constantin von Economo, 1929

Constantine Alexander Freiherr von Economo von San Serff (1876-1931) was a Romanian-Austrian neurologist and psychiatrist, who became famous for his cytoarchitectonic based cortical thickness maps across the whole cerebral mantle (Fig. 2; von Economo & Koskinas, 1925; von Economo, 1929) and for his studies about encephalitis lethargica (sleeping sickness, but another form than that transmitted by the Tsetse fly). The study by Sowell and colleagues (Sowell et al., 2004) can be seen as a proof of principle for the power of the computational neuromorphometric methodology (see below). Note that there is a very good correspondence between the two maps although one map (von Economo's map) was derived from post mortem investigations of adults and the other (Sowell's map) was derived from a T1-weighted MRI in vivo investigation of children.

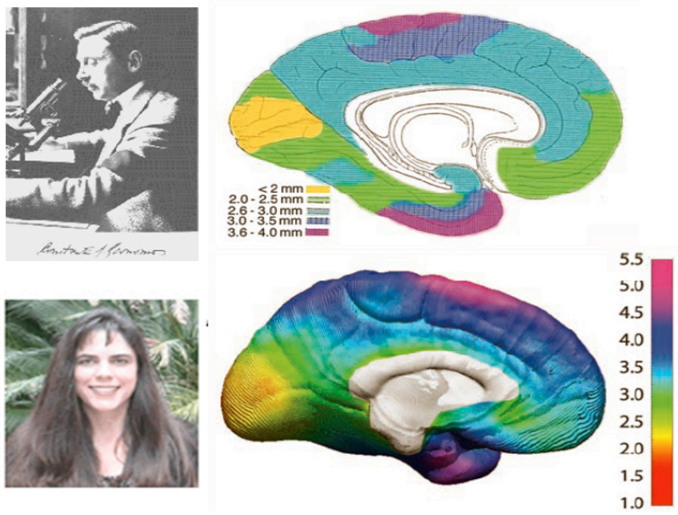

Figure 2: Cortical thickness maps by Constantin von Economo.
Left top panel: C. von Economo at work. Figure adopted from http://www.uic.edu/. ***Right top panel:*** Adapted version of the cortical thickness map of von Economo (1929). Colour coding has been applied over von Economo's original stippling pattern, respecting the boundaries of the original work, to highlight the similarities between the two maps shown in this figure. Figure adopted from Sowell et al., 2004. ***Left bottom panel:*** E. Sowell. Figure adopted from http://www.neurology.ucla.edu/. ***Right bottom panel:*** In vivo average cortical thickness map derived from 45 children between age 7-11 using computational neuroanatomy (cortical pattern matching procedure) (Sowell et al., 2004). Note that there is a very good correspondence between the two maps although one map (von Economo's map) was derived from post mortem investigations of adults and the other (Sowell's map) was derived from a T1-weighted MRI in vivo investigation of children. Figure adopted from Sowell et al., 2004.

1.3 Computational cytoarchitectonic probability maps by Zilles, Amunts, Schleicher, Mohlberg, Eickhoff et al., nowadays

In contrast to the two approaches already mentioned above, which were observer-dependent, a new observer-independent method was developed by the group of Zilles and Amunts (Schleicher et al., 1999). Figure 3 (adopted from Toga et al., 2006) illustrates this procedure. Fig. 3a shows two mean cortical profiles (red and blue curves in the insets) sampled from the grey level index (GLI) image of a cell body-stained histologic section (coronal plane) through the superior and the middle temporal gyri of a human brain. Each mean profile is the average of 20 equally spaced, individual profiles (red lines in panel 3b, top), which were sampled from the rectangular regions of interest (boxes centred around the red or blue arrows). The shape of each profile is described as a feature vector, and is a measure of the cytoarchitecture of the area. High GLI values indicate high volume densities of cell bodies. Fig. 3b (top panel) shows the sliding window procedure used to establish the distance function (bottom panel). The cortical region of interest is divided into a set of profiles (positions shown in red). The positions of the profiles are consecutively numbered starting from n = 1 (at left margin) to k. A sliding window consists of two cortical segments (yellow, to the left and to the right of a central profile) made up of two neighbouring groups of n individual profiles. As an example, sliding windows are shown at positions n = 21 and n = 180. When a certain profile position has been analysed, the sliding window is moved one step (profile) to the next position. The red arrows indicate the direction of the movement of the sliding window across the cortical ribbon. The blue and black arrows indicate positions where the feature vectors show significant changes. TE1.0, TE1.1 and TE2 are distinct cytoarchitectonic areas of

the human auditory cortex. The bottom panel shows the Mahalanobis distance, which indicates the dissimilarity in laminar pattern between two cortical segments and can be calculated from the feature vectors from each profile. The Mahalanobis distance at each position of the sliding window is plotted. Significant maxima at positions n = 40 (blue arrow), n = 97 (black arrow), n = 305, n = 497 and n = 586 indicate the positions of putative areal borders. Performing this procedure in serial histologic sections of several (usually ten) brains, three-dimensional reconstructed histologic data sets of post-mortem brains and their areas are registered to common standard reference space, and cytoarchitectonic probability maps are calculated for each area (Toga et al., 2006; Schleicher et al., 1999).

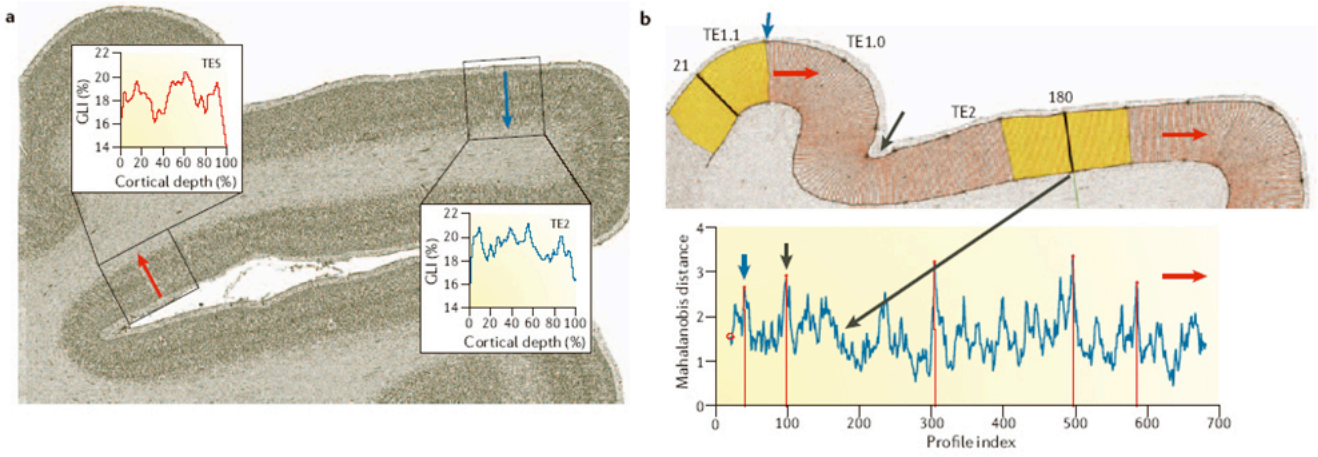

Figure 3: Observer-independent procedure for probabilistic cytoarchitectonic parcellation.
See text for the explanations of these panels. Figure adopted from Toga et al., 2006.

The brain areas mapped up to date are shown in Figure 4 below. These cytoarchitectonic probability maps were implemented in the statistical parametric mapping (SPM) anatomy toolbox (Eickhoff et al., 2005a, 2006; http://www.fz-juelich.de/ime/spm_anatomy_toolbox) and can therefore be used for the localisation and labelling of structural and functional brain differences. In the near future, when the whole brain will completely be mapped by this observer-independent procedure, the reference system (brain atlas) of Talairach & Tournoux, 1988 and that of the Brodmann will be replaced by this new brain atlas that is comprised of theses computational cytoarchitectonic probability maps.

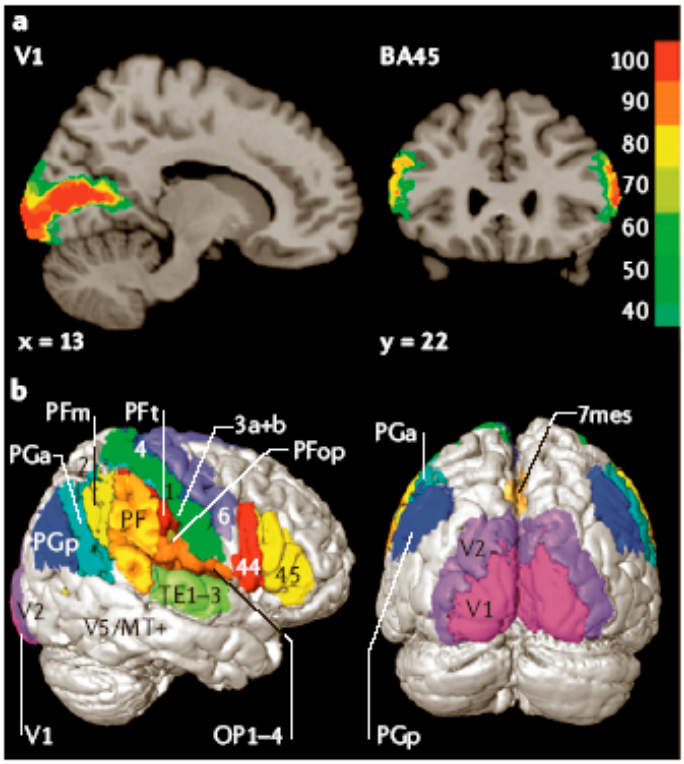

Figure 4: Cytoarchitectonic probability maps of the cortex.
Panel a: Probability maps of the primary visual cortex V1 in a sagittal section (left) and the rostral part (Brodmann's area 45 (BA45); right) of Broca's speech region in a coronal section. x and y refer to the spatial location of the sections in Montreal Neurological Institute (MNI) space. The colour scale indicates the probabilities that the areas are present in a certain voxel of the reference space. ***Panel b:*** Right lateral and occipital views of the maximum probability map in which each voxel of the three-dimensional space has been assigned to the cortical area with the highest probability. Cortical areas shown include areas 44 and 45 (Broca's region), primary motor (4) and premotor (6) areas, the somatosensory cortex (areas 3a, 3b, 1 and 2), inferior posterior parietal association areas (PFt, PFop, PF, PFm, PGa, PGp), parietal opercular areas (OP 1–4), mesial superior parietal area (7mes), auditory areas (TE 1–3) and visual areas (V1, V2 and V5/MT). Figure adopted from Toga et al., 2006.

2 Computational neuromorphometry

There is no doubt about that brain structures are the basis for brain functions. At the level of single neurons, the morphology of axonal and dendritic processes plays a fundamental role in supporting and shaping brain functions. At the level of systems and brain regions, the detailed topographical (topological) organisation, e.g., spatial relationships among ensembles of neurons, influences functional properties in brain networks. The classical field of quantitative neuromorphometry covers a broad range of methods and approaches. Traditional manual approaches typically generate figures, tables, and numbers representing some feature of the brain. At a more advanced level, computerised approaches typically produce larger, more sophisticated, more detailed, and more complex data sets, allowing multidimensional analyses of brain structure and function (Toga et al., 2006). The term computational neuroanatomy is used here to describe computationally demanding, quantitative neuroanatomical analyses, and computational modelling of brain structures and spatial organisation based on such quantitative data. This emerging field is likely to play also a pivotal role in future modelling of brain architecture and its functions. Functional modellers, usually referred to as computational neuroscientists, and computational neuroanatomists increasingly make use of detailed, quantitative neuroanatomical data at multiple levels to produce more advanced and realistic

simulations of brain functions (Bjaalie, 2001; Jennings & Aamodt, 2000). Figure 5 shows the application of mathematical techniques derived from differential geometry, numerical analysis, and the theory of partial differential equations to model structures and processes in brain images. Presented are connections among mathematical concepts used in cortical surface pattern matching (Thompson et al., 2004), i.e., in a particular procedure that produces cortical surface reconstructions (models) that are subsequently transformed to match a particular brain atlas (reference template).

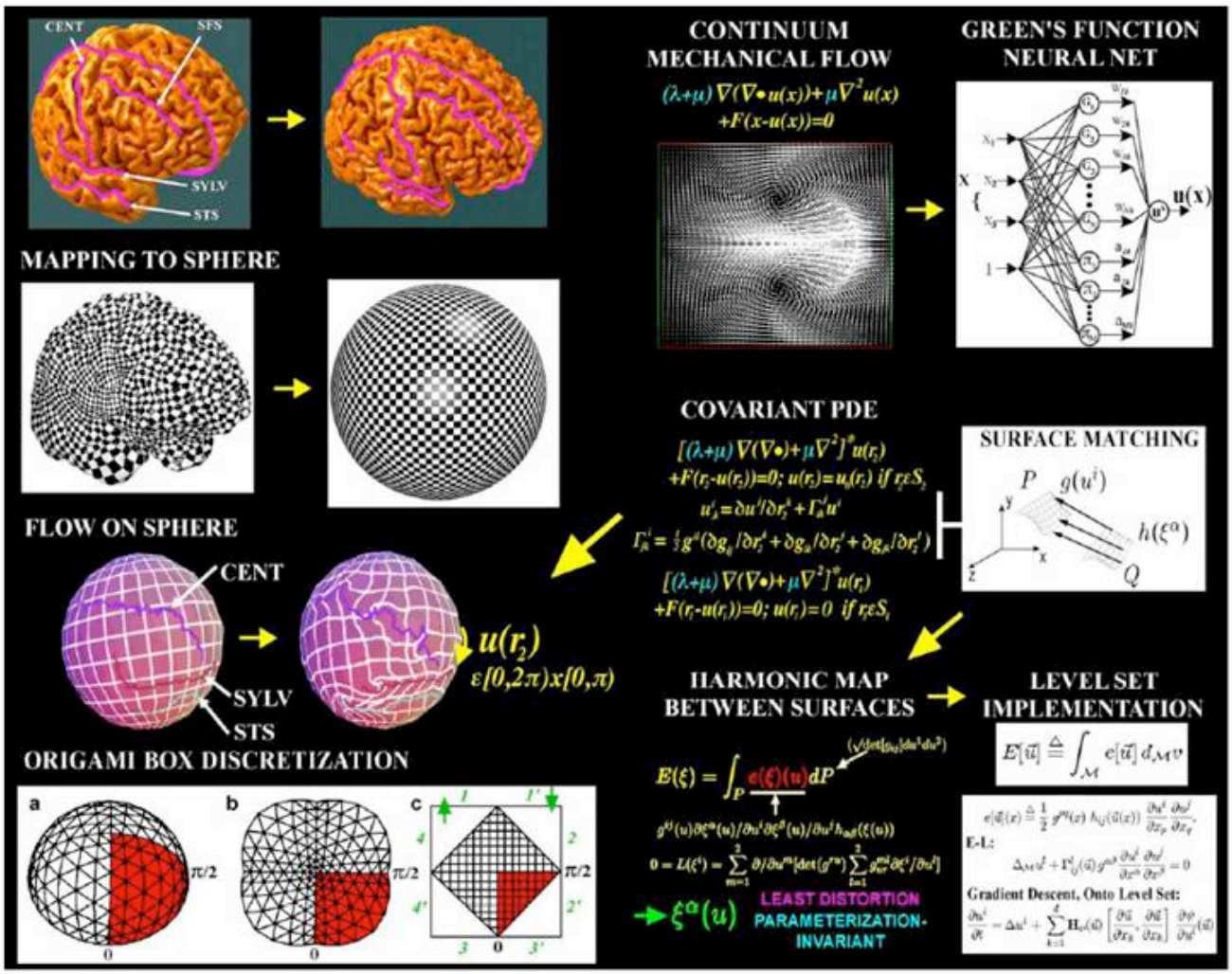

Figure 5: Connections among mathematical concepts used in cortical surface matching procedures.
This schematic illustrates some connections among concepts used in the nonlinear registration (matching) of brain surfaces. When matching two anatomical surfaces, it is often desirable not only to match the entire 3D surface of one subject with another, but also to enforce some higher-order anatomical constraints, such as the exact matching of a range of corresponding sulcal curves (or other landmark points, curves, or regions, such as functional landmarks, if these are known). Figure adopted from Thompson et al., 2004.

An overview about the classes of neuromorphometric methods used in computational neuroanatomy is shown in Table 1 below. Note that this overview is adopted from Thompson et al., 2003 and it is not exhaustive.

Method	Principle	Methods Papers
VBM	Maps group differences in gray matter, white matter, CSF at each voxel in stereotaxic space	Ashburner and Friston, 2000; Davatzikos et al., 2001; Good et al., 2001
DBM	Analyzes brain shape differences based on deformations that map each brain to a common anatomic template	Ashburner et al., 1998; Miller et al., 2002; Gaser, 1999; Thompson et al., 2000
TBM	Analyzes local compression or dilation required to warp a baseline image onto an atlas or onto a later one from the same subject	Davatzikos et al., 1996; Fox et al., 1998; Thompson et al., 2000
Cortical Mapping	Sulcal matching is performed on extracted cortical surface models prior to comparing gray matter measures, shape differences, asymmetries	MacDonald, 1998; Thompson et al., 2001; Fischl et al., 2000
Shape Modeling	3D geometric models of anatomical curves or surfaces are averaged and compared	Thompson et al., 1996; Joshi et al., 1998; Csernansky et al., 1999; Gerig et al., 2001
Parcellation	Regions of interest are manually traced or automatically labeled on images, and volumes are compared across groups	Collins et al., 1995; Kennedy et al., 1998; Fischl et al., 1999

Table 1: Classes of neuromorphometric methods.
While not an exhaustive list of methods, this table describes some key methods for analysing structural MRI data. Each of these methods can be used to identify group differences in brain structures. Abbreviations: VBM, voxel based morphometry; DBM, deformation based morphometry; TBM, tensor based morphometry. Table adopted from Thompson et al., 2003. (Note that Good et al., 2001 in the table refers to Good et al., 2001c in the reference list, and Fox et al., 1998 refers to Freeborough & Fox, 1998 in the reference list; Joshi et al., 1998 in the table refers to Joshi et al., 1997 in the reference list, and Csernansky et al., 1999 in the table refers to Csernansky et al., 1998 in the reference list).

In the following paragraphs, I will describe voxel based morphometry (VBM) that is implemented in the SPM software package (Ashburner & Friston, 2000; http://www.fil.ion.ucl.ac.uk/spm/; http://dbm.neuro.uni-jena.de/vbm/). Computational neuroanatomical procedures are often organised in a processing stream (also called a pipeline or pipe) that implements the different data processing (also called preprocessing) steps serially. In the rest of this Ph.D. thesis, I will not focus on the mathematics, physics, and algorithms behind the different preprocessing steps. Readers who want to deepen into the mathematical concepts behind the processing steps of such computational neuroanatomical analysis pipelines are referred to the methodological articles of the following authors: For VBM in SPM (Ashburner & Friston, 2000, 2003; Ashburner, 2000), for Cortical Pattern Matching software (Thompson & Toga, 2002; Thompson et al., 2004), and for FreeSurfer software (Dale et al., 1999; Fischl et al., 1999a).

The individual steps of VBM in SPM will be presented in more detail below. One other

neuromorphometrical software package, the FreeSurfer software suite (implemented by Fischl & Dale; https://surfer.nmr.mgh.harvard.edu/fswiki) will be shortly described in the paragraph General Discussion after the shortcomings and drawbacks of VBM in SPM are considered and discussed in more detail.

2.1 Prerequisites for computational neuromorphometry

Beside the structural magnetic resonance imaging (sMRI) scans, which are the input data for computational neuromorphometric analyses and will be discussed in the next section under MRI data acquisition, the software and hardware are the most important prerequisites. An overview about different aspects of the three software packages discussed in my Ph.D. thesis is shown in Table 2.

Criteria	SPM5 and VBM5 toolbox	Cortical pattern matching	FreeSurfer
Availability	Free, needs MATLAB	Restricted, apply for	Free
Measures	Density, volume	Density, volume, cortical thickness, curvature indices?	Density, volume, area, cortical thickness, curvature indices
Performance	Well	Better	Best
Publishing	++++++++++	+++	+++++
OS	Win, Mac, Linux	Linux?	Linux, Mac
CPU	Moderate	High?	Very high
RAM	High	Moderate?	Moderate to high
Handling	Easy	Harder	Harder
Personal experience	++++++++++	++	++++++

Table 2: Comparison among three different computational neuroanatomical software packages. Note that these comparisons are subjective and based on my personal experience with these software packages.

The decision which software should be used, or is the best or most appropriate depends also on the topic under investigation and the hypotheses that were posed. The computing performance limiting factor is the hardware. For VBM within the SPM software package that runs under MATLAB (http://www.mathworks.com/) on any platform, "out of memory" problems are more frequent than low performance (long processing time) of the processor when working on common workstations (CPU: about 3 GHz, RAM: about 2 GB). For the FreeSurfer software, the CPU is the limiting factor. For running the whole FreeSurfer pipeline (all steps, i.e., surface reconstruction, subcortical segmentation, and cortical parcellation), processing time is about 20-40 hours per brain, depending on how many topological defects have to be repaired in the surface processing pipeline. Although the FreeSurfer is not fit for parallel computing because steps have to be done in a serial manner, nevertheless can grid computing be used. The advantage of grid computing is that the processing time are still 20-40 hours per brain, but one can run several brains simultaneously by distributing the brains onto several

processors on the grid. At the time, we run FreeSurfer analyses on the Matterhorn cluster (Fig. 6) of the IT services of the university of Zurich (http://www.matterhorn.unizh.ch/). This cluster is composed of 256 nodes with dual Opteron 244 (1.8 GHz) CPUs and 128 nodes with dual Opteron 252 (2.6 GHz) CPUs; all nodes are connected with 100 Mbit and 1 Gbit Ethernet; 128 nodes with additional Myrinet; 2 redundant login nodes; 3 file servers exporting 4 TB file system space via NFS.

Figure 6: Matterhorn cluster of the IT services at the university of Zurich.
We can use this supercomputer for our FreeSurfer analyses in order to finish FreeSurfer analyses in a reasonable amount of time. Figure adopted from http://www.matterhorn.unizh.ch/.

2.2 Voxel based morphometry (VBM) using statistical parametric mapping (SPM) software

The methodological introduction of voxel based morphometry (VBM) into the neuroscience community by Ashburner & Friston was in 2000 (Ashburner & Friston, 2000), although the first article using VBM methodology was published in 1995 (Wright et al., 1995). Together with VBM, these authors also introduced two other morphometric methods called deformation based morphometry (DBM) and tensor based morphometry (TBM) (Ashburner & Friston, 2000, 2003). Although there were some controversies about VBM (Thacker, 2005, http://www.tina-vision.net/docs/memos/2003-011.pdf; Bookstein, 2001; Davatzikos, 2004; Ashburner & Friston, 2001), VBM is the most frequent used computational neuroanatomical procedure to detect structural brain differences between groups of healthy subjects or between patients and control subjects. The main goal of VBM is to assess the significance of structural (grey or white matter) brain differences (volume or density) on a voxel-by-voxel basis between two or more groups of subjects or patients. Supposing a spatial resolution of 1 mm^3 for the brain tissue segments, grey matter segments are composed of about 2 Millions of voxels per brain and white matter segments are composed of about 1 Million voxels per brain.

There is a large body of literature about applications of VBM in basic as well as clinical neuroscience

research. Topics of basic research were learning and training (Draganski et al., 2006a, 2004; Boyke et al., 2008; Driemeyer et al., 2008; Gaser & Schlaug, 2003; Sluming et al., 2002; Golestani et al., 2002; 2007a; Golestani & Pallier, 2007b, Jäncke et al., 2009a), general intelligence (Jung & Haier, 2007; Haier et al., 2005, 2004; Colom et al., 2006a, 2006b; Gong et al., 2005; Wilke et al., 2003; Frangou et al., 2004), visuospatial cognition independent of general intelligence (Hänggi et al., 2009), navigation experience (Maguire et al., 2000), grapheme-colour synaesthesia (Jäncke et al., 2009b), interval-taste and tone-colour synaesthesia (Hänggi et al., 2008), ageing (Tisserand et al., 2004, 2002; Staff et al., 2006), gray matter volume and asymmetries (Lüders et al., 2002; Luders et al., 2004), structural covariance (Mechelli et al., 2005), genetic association studies (Hänggi et al., 2009; Pezawas et al., 2004), and other basic neuroscience research topics. Topics of clinical research were Alzheimer's disease (Hänggi et al., submitted; Testa et al., 2004; Rombouts et al., 2000; Chételat et al., 2002; Baron et al., 2001; Frisoni et al., 2002, 2005; Karas et al., 2003, 2004; Scahill et al., 2002; Busatto et al., 2003), mild cognitive impairment (Hänggi et al., submitted; Pennanen et al., 2005; Karas et al., 2004; Saykin et al., 2006; Chételat et al., 2005), semantic dementia (Rosen et al., 2002; Mummery et al., 2000), frontotemporal dementia (Rosen et al., 2002), dementia with Lewy bodies (Brenneis et al., 2004), schizophrenia (Wright et al., 1995, 1999; Job et al., 2002; Jayakumar et al., 2005; Honea et al., 2005), depression (Bell-McGinty et al., 2002), bipolar disorder (Bruno, 2005; Wilke et al., 2004), traumatic brain injury (Gale et al., 2005), paediatric mesial temporal sclerosis (Cormack et al., 2005), obsessive-compulsive disorder (Pujol et al., 2004), persistent developmental stuttering (Jäncke et al., 2004), narcolepsy (Draganski et al., 2002); limb amputation (Draganski et al., 2006b), restless legs syndrome (Etgen et al., 2005), posttraumatic stress disorder (Jatzko et al., 2006), developmental language disorder (Jäncke et al., 2006), inherited speech and language disorder (Vargha-Khadem et al., 1998), autism (Abell et al., 1999), epilepsy (Woermann et al., 1998, 1999; Keller et al., 2004), genetic association studies (Molko et al., 2004; Shen et al., 2004; Free et al., 2003), malformation of cortical development (Richardson et al., 19997) and other pathologies.

The whole procedure (different preprocessing steps) of the standard VBM (Ashburner & Friston, 2000) will be explained and discussed in the following paragraphs. The steps from the raw MR images to the statistics (statistical parametric maps, SPMs) for the standard VBM are summarised schematically in the flow diagram displayed in Figure 7 below (Senjem et al., 2005). Standard VBM proceeds as follows: (i) perform a 12 degrees of freedom (DOF) affine registration between each subject's MRI image and the MNI template, (ii) perform a nonlinear normalisation of the affine registered subject image to the MNI template, (iii) segment the normalised image using the MNI priors, (iv) apply Jacobian modulation to the segmented GM image, (v) apply a 12-mm full width at half maximum (FWHM) Gaussian spatial smoothing kernel to the modulated GM image. The final

step is statistical comparison, wherein the smoothed, modulated GM images are compared between patient and control populations using a two-sided t-test or an analysis of covariance model (Senjem et al., 2005).

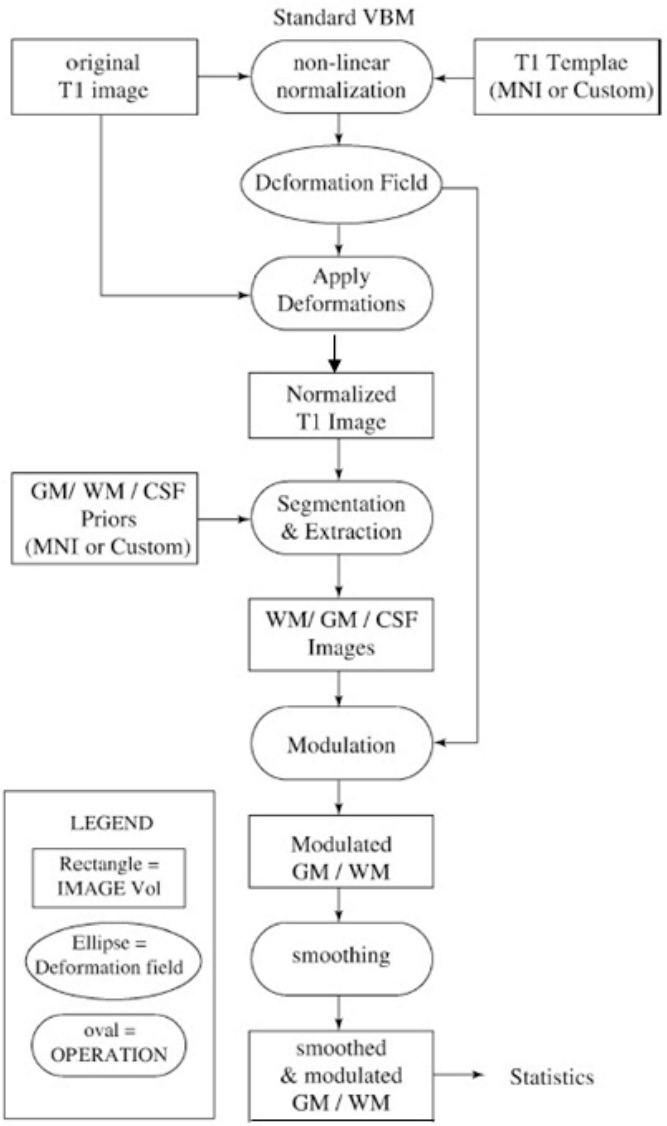

Figure 7: Schematic flow diagram of standard voxel based morphometry (VBM).
This figure illustrates the standard VBM method (Ashburner & Friston, 2000) schematically. Standard VBM algorithm proceeds as follows: (i) perform a 12 degrees of freedom (DOF) affine registration between each subject's MRI image and the MNI template, (ii) perform a nonlinear normalisation of the affine registered subject image to the MNI template, (iii) segment the normalised image using the MNI priors, (iv) apply Jacobian modulation to the segmented GM image, (v) apply a 12-mm full width at half maximum (FWHM) Gaussian spatial smoothing kernel to the modulated GM image. The final step is statistical comparison, wherein the smoothed, modulated GM images are compared between patient and control populations using a two-sided t test or an analysis of covariance model (Senjem et al., 2005). Figure adopted from Senjem et al., 2005.

2.2.1 Magnetic resonance imaging (MRI) data acquisition

In this section, I will briefly describe some important aspects of magnetic resonance imaging (MRI) data acquisition, without explaining the principles of MRI. Because MR images are the basis, i.e., source information, for computational neuroanatomical procedures, they have to be of reasonable quality in order not to bias the subsequent analysis. The following aspects will be discussed: Scanner and field strength; modality and scanning sequence; slice orientation (scanning plane), voxel resolution and matrix; technical parameters; and the number of acquired volumes.

Scanner and field strength: The most frequent used scanners are from the following three manufacturers: General Electrics, Siemens, and Philips. Scanners from Hitachi, Picker, and Bruker are less frequent used. I personally prefer, for reasons not discussed here, Philips and Siemens scanners. Whole body scanners are preferred over only head scanners because the transmission of the radio frequency (RF) impulses and the receiving of the MR signal can be separated, which reduces interferences between the two devices, i.e., between the signals they transmit or receive. When using whole body scanner, transmission of RF impulses should be done with the body coil and receiving the MR signal with the head coil. Scanners operating at 3 Tesla (3T) are preferred over scanners operating at 1.5T. Whether the new developed 7 Tesla (7T) scanners will be superior to 3T scanners had not been shown yet. Clearly, the signal-to-noise ration (SNR) is enhanced at 7T compared with 3T. Unfortunately, the contrast-to-noise ration (CNR), which is a very important quality measure in T1-weighted structural MRI, is commonly somewhat lower at 7T compared with 3T. Our first tests on the 7T Philips scanner here in Zurich were frustrating because the white and grey matter segmentations derived from VBM in SPM on the one hand and the surface reconstructions derived from the FreeSurfer software on the other hand were below the quality compared with the same data acquired on a 3T MR scanner. Besides the somewhat lower CNR, there is also the possibility that geometrical distortions, another problem for computational neuromorphological procedures, will also be enhanced at 7T compared with 3T. The strong dielectric effects at 7T can be reduced by using adiabatic pulse sequences. In my opinion, the most severe problem with respect to T1-w. images acquired at 7T is signal inhomogeneity (nonparametric nonuniform intensity inhomogeneity). This intensity field bias arises from heterogeneous radio frequency head coil B_1 profiles. Meanwhile, an elegant approach to get rid of most of these inhomogeneities was proposed by another group (Van de Moortele et al., 2009). Beside the actual T1-weighted image, a proton density (PD) weighted image, which also contains the inhomogeneity field bias but no T1-weighted contrast, is acquired in addition. By dividing the T1-weighted scan with the PD-weighted image, the inhomogeneity field bias can easily be removed. This procedure removes also confounding contrasts such as the PD-contrast and the T2*-contrast from the T1-weighted image.

Modality and scanning sequence: The choice of the scanning modality depends on the questions and posed hypotheses. If one is interested in grey matter (GM), T1-weighted images have to be acquired. If one is interested in white matter (WM), diffusion tensor imaging (DTI) scans are preferred over T1-, T2- or proton density weighted scans. Sometimes, T2-weighted scans are used in grey matter analyses to enhance the power of segmentation (multimodal, also called multispectral segmentation), because the contrast between GM and cerebrospinal fluid (CSF) is enhanced in T2-weighted compared

to T1-weighted images. Gradient echoes (GRE) are the preferred sequence (no spin echoes). Among the GRE, spoiled gradient echoes (SPGR) are frequently used. Other also frequently used sequences are inversion recovery (IR) and 3D ultra fast echoes. Examples of these sequences for the scanners of different manufacturers can be found in the method sections of my experimental studies.

Slice orientation (scanning plane), voxel resolution, and matrix size: The orientation of the acquired slices are preferentially in the sagittal or transversal plane. Sometimes other planes are used (e.g., coronal, oblique, or a plane perpendicular to the long axis of the hippocampus when specifically interested in this brain structure). Voxel resolutions are 1.0 x 1.0 mm or 0.5 x 0.5 mm in plane and about 120-140 slices (à 1.5 mm) or 160-200 slices (à 1.0 mm). The number of slices depends on the scanning plane. The corresponding matrices are 256 x 256 or 512 x 512. We prefer to acquire T1-weighted images in the sagittal plane in order to minimise susceptibility artefacts in the most inferior brain regions (inferior temporal gyrus). These susceptibility artefacts arise from the abrupt transition between the brain tissue on the one hand and the ossis temporalis (pars petrosa, petrosum) on the other hand.

Technical parameters: Common reported technical parameters are the repetition time (TR; e.g., 12.1 ms), echo time (TE; e.g., 5.16 ms), inversion time (TI; e.g., 450.0 ms), flip angle (FA; e.g., 15°), number of excitations (NEX; e.g., 1 or 2), field of view (FOV; e.g., 24 cm^2), band-width (BW; e.g., 100-200 Hz/pixel), averages = 1-5. For more details about the optimisation of T1-w. MR pulse sequences for neuromorphometry can be found elsewhere (Deichmann et al., 2000; Howarth et al., 2005).

Number of acquired volumes: Until recently, only one structural MRI scan per subject was acquired for computational neuromorphometric analyses. But there is evidence (Holmes et al., 1998) that acquiring more than one volume and average them enhanced the signal-to-noise ration (SNR) as well as the contrast-to-noise ration (CNR). The SNR is expected to increase as the root of the number of contributing volumes (Holmes et al., 1998). In Figure 8, one can see features of the scan resolution and of averaging several brain scans of the same subject. In Figure 9, one can see features of averaging several brain scans of the same subject. In Figure 10, more features of the brain are shown on an average image of 27 T1-w. scans that became only visible after averaging. These features were not observed in a single scan. In the FreeSurfer software, the default value with respect to the number of acquired volumes is two. At our institute, we acquired 2-3 T1-w. MRI scans, 1-2 diffusion weighted sequences, and a single T2-weighted image per subject for a common structural imaging study.

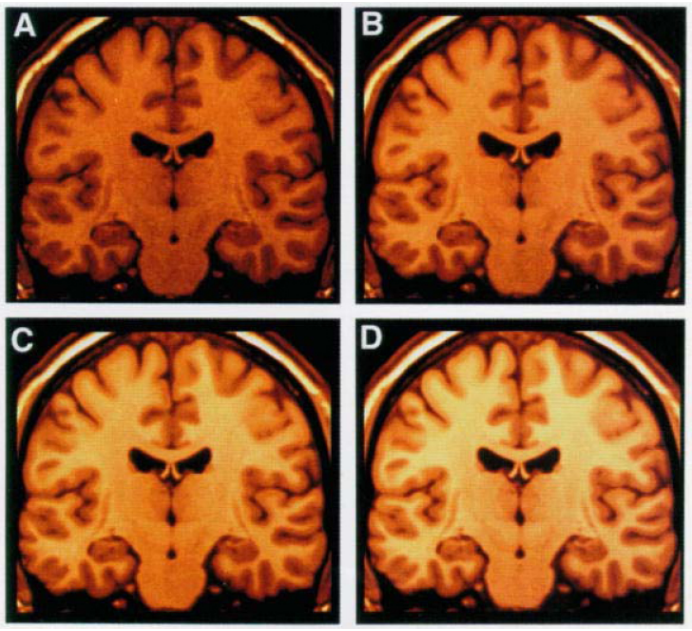

Figure 8: Influences of the scan resolution and of averaging several scans from the same subject on the quality of the MR image.
Panel A: One T1-weighted volume with 0.78 mm^3 voxel size. ***Panel B:*** One T1-weighted volume with 1.0 mm^3 voxel size. Comparing panel A with B, one can see the expected increase in noise when reducing voxel size in MR. ***Panel C:*** Seven T1-weighted volumes with 0.78 mm^3 voxel size after affine registration, resampling at 0.5 mm^3 voxel size, and averaging. ***Panel D:*** Twenty T1-weighted volumes with 1.0 mm^3 voxel size after affine registration, resampling at 0.5 mm^3 voxel size, and averaging. Note that the quality of the average image is greatly enhanced, allowing the delineation of fine structures previously obscured by noise or by an insufficient contrast-to-noise ratio. Figure adopted from Holmes et al., 1998.

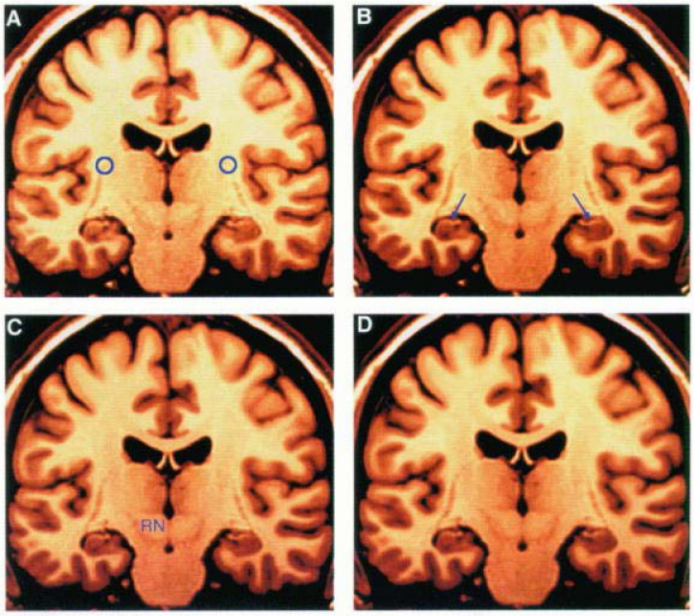

Figure 9: Influences of averaging several scans from the same subject on the quality of the MR image.
In this figure, the result of increasing the n from 5 (Panel A) to 10 (Panel B) to 15 (Panel C) to 20 (Panel D) is presented. ***Panel A:*** The blue circle shows the dorsal tip of the putamen. ***Panel B:*** The blue arrow shows the hippocampus. ***Panel C:*** This panel shows the red nucleus. ***Panel D:*** Compare these three features as the n increases. The details of these features become fully apparent only at high n. In addition, the boundaries of discrete structures of one tissue class embedded in another become more defined. Figure adopted from Holmes et al., 1998.

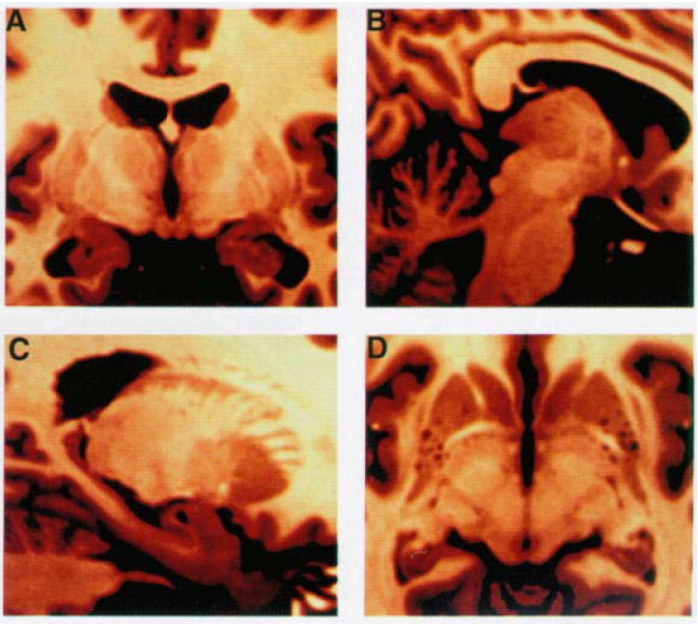

Figure 10: Features visible after averaging several scans from the same subject.
Panel A: Shows nuclear boundaries and fascicles within the thalamus and hippocampus. ***Panel B:*** Shows distinct brain stem divisions. ***Panel C:*** Shows the component of the basal ganglia and their interconnections (grey bridges between caudate nucleus and putamen. ***Panel D:*** Shows small penetrating vessels in the perforated substance. Figure adopted from Holmes et al., 1998.

As stated above, the SNR and CNR are expected to increase as the root of the number of contributing volumes (Holmes et al., 1998), means that when two volumes were acquired the SNR is increased theoretically by the factor 1.414 compared when only acquiring one volume. But acquiring more than two or three volumes (although the scan time per volume is only 8-12 minutes) is mostly neither feasible in research nor in clinical practise due to the restriction in the time during a subject or patient can lay calmly in the scanner bore. In our neuromorphological studies we also acquire diffusion tensor imaging (DTI) data, for which several acquisitions per diffusion gradient are also recommended to enhance the SNR. Hence, we acquire about 3-4 T1-w. images and 2-3 diffusion-weighted sequences during the 50-70 minutes scanning periods. An alternative to acquiring multiple volumes in separate runs with the same scanning sequence or with different scanning sequences is the use of multiecho sequences. One such example is a multiecho (ME) fast low angle shot (FLASH) sequence (called MEF) proposed by Fischl and colleagues (Fischl et al., 2004). This sequence has eight echoes following each excitation pulse and hence produces eight differently "weighted T1-w." MR images within an acquisition time of about 8 minutes. When running this MEF sequence twice with two different flip angles (FA), one gets T1-weighted MR images with a FA of 30° and proton density weighted scans with a FA of 5°. An additional advantage of this kind of sequence is that the acquisition of data at varying echo times allows the explicit estimation of T2*-contrast from a single 8 minutes T1-weighted or proton density weighted scan set. Fischl and colleagues aimed at optimising the MR acquisition with respect to the segmentation procedure in the FreeSurfer software. They concluded that their optimisation reveals that the ambiguity in the subcortical segmentation as well as cortical parcellation is minimised by the conjunction of proton density and T1-weighted images, in

contrast to the more standard practice of acquiring two or more strongly T1-w. MR images and averaging them (Fischl et al., 2004).

Miscellaneous: When investigating brain anatomy with neuromorphometric methods, there might be some confounding factors during MR scanning that potentially influence the further preprocessing of the MR data and/or the results of computational neuromorphometric techniques. In functional brain imaging a lot of confounders such as psychological stressors, posture, hydrostatics, common blood thinners (such as aspirin), vasoconstrictors (such as caffeine), or psychiatric drugs (such as fluoxetine) can potentially skew the outcomes of both cognitive processing and brain hemodynamics (Raz et al., 2005). In contrast to functional imaging, structural imaging can be confounded by dehydration of the brain (Duning et al., 2005). These authors showed that a lack of fluid intake for 16 hours prior to MR scanning reduced the whole brain volume by 0.55% (SD: ± 0.69%), and after rehydration (after drunk 1.5 litre of water and waited for 20-30 minutes) total cerebral volume increased by 0.72% (SD: ± 0.21%) (Duning et al., 2005).

2.2.2 Nonparametric, nonuniform intensity inhomogeneity normalisation (bias field correction)

The first step of a typical VBM analysis is a nonparametric, nonuniform intensity inhomogeneity normalisation (also called bias field correction, not explicitly shown in Fig. 7). Magnetic Resonance (MR) signal intensity measured from homogeneous tissue is seldom uniform; rather it varies smoothly across an image. This intensity nonuniformity is usually attributed to poor radio frequency (RF) coil uniformity, gradient-driven eddy currents, and patient anatomy both inside and outside the field of view. Although these 10%-20% intensity variations have little impact on visual diagnosis, the performance of automatic segmentation techniques which assume homogeneity of intensity within each class can be significantly degraded. A robust, automatic, and inexpensive means of correcting for this artefact is essential for such automatic processing techniques to be accurate in labelling each voxel with a tissue type (Sled et al., 1998). An example of nonparametric, nonuniform intensity inhomogeneity normalisation is displayed in Figure 11. The most common used algorithm is the one implemented in N3 (Sled et al., 1998).

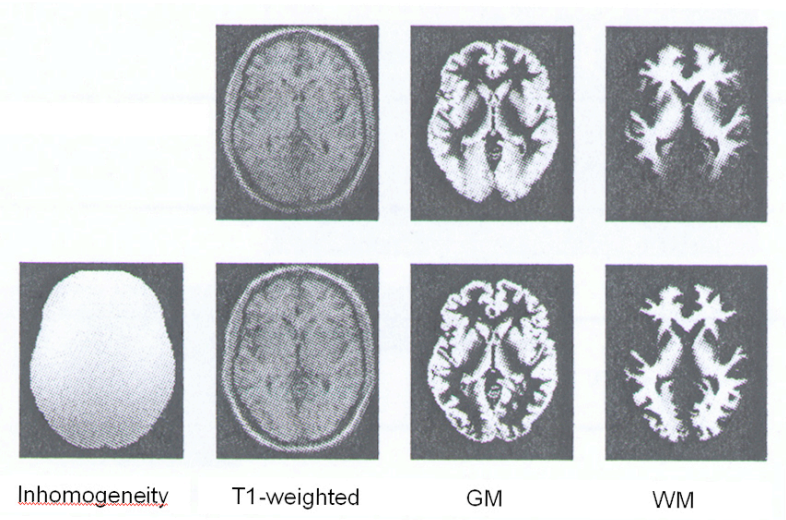

Figure 11: Nonparametric, nonuniform intensity inhomogeneity normalisation. ***Top row:*** T1-weighted image with nonparametric nonuniform intensity inhomogeneity and the resulting overestimation of grey matter (GM) and underestimation of white matter (WM) in posterior areas after segmentation. ***Bottom row:*** The modelled inhomogeneity applied to the T1-weighted image and the resulting segments without overestimation or underestimation. Figure adopted from C.Gaser, SPM Course, Hamburg 2005.

2.2.3 Spatial normalisation (registration)

Spatial normalisation (also called spatial registration or transformation) is an important step in all structural and functional brain analyses. The main aim is to bring the brains of different subjects into a common stereotaxic space (standard coordinate system) and to map corresponding (homologous) structures across individual brains. This process is quite difficult due to the large interindividual variability in neuroanatomy. Spatial normalisation procedures are commonly divided into label based and non-label based procedures. Label based techniques identify homologous spatial structures, features or landmarks in two images and finds the transformation that best superposes the labelled points. Non-label based approaches identify a spatial transformation that minimises some index of the difference between an object and a reference image, where both images are treated as unlabelled continuous processes (Friston et al., 1995a). The main disadvantage of label based techniques is the fact that they are not fully automated yet and therefore very labour intensive because the labels have to set manually. This manual intervention makes these procedures also more prone to bias, because the localisation of the labels is subjective and hence observer-dependent. Here, I focus only on non-label based spatial normalisation approaches. A further division of spatial normalisation techniques is into linear normalisation (also called affine when 12 parameters are used) and nonlinear normalisation (also called warping). Whereas the linear normalisation is similar across different software packages, the techniques of nonlinear normalisation are more heterogeneous across the different implementations (see below).

2.2.3.1 Linear spatial normalisation (registration)

Linear spatial normalisation corrects for different brain sizes and for different head positions during scanning and is a global linear change of the whole brain. There are actually four operations that can

be applied in three directions. There are translations, rotations, zooms (scales), and shears in the x, y, and z direction (axis). The rigid body transformation uses only 3 translations and 3 rotations and adjusts only for the pose of the subject in the scanner. The Procrustes transformation uses 3 translations, 3 rotations, and one scale. The affine transformation uses all 12 parameters (or degrees of freedom, DOF). Sometimes, linear transformations are also denoted affine although less than 12 parameters (mostly 9 parameters) are used. An affine transformation adjusts additionally for size and partially for shape differences, although the adjustment for shape differences is limited. In the context of VBM using statistical parametric mapping (SPM) software, the affine normalisation procedure is implemented with the following term (a 3x3 matrix, a system of linear equations):

$$\mathbf{x_1 = a_1x + b_1y + c_1z + k_1}$$
$$\mathbf{y_1 = a_2x + b_2y + c_2z + k_2}$$
$$\mathbf{z_1 = a_3x + b_3y + c_3z + k_3}$$

The aim is to find the parameters that minimise the sum of squared differences between an image and a template – and also the square of the number of standard deviations away from the expected parameter values (Ashburner & Friston, 1997). Figure 12 shows the four different operations that can be applied during linear normalisation procedures. Without spatial constraints or with poor data, this simple parameter optimisation approach can produce some extremely unlikely transformations. By incorporating prior information into the optimisation procedure, a smooth transition between fixed and fitted parameters can be achieved. The approach adopted here is essentially a maximum a posteriori (MAP) Bayesian approach (Ashburner & Friston, 1997). Because the mathematical formulation of the Bayes rule is much more complex in its continuous form, it will not be discussed in details in this Ph.D. thesis. The interested reader is referred to the literature (Ashburner & Friston, 1997, 1999).

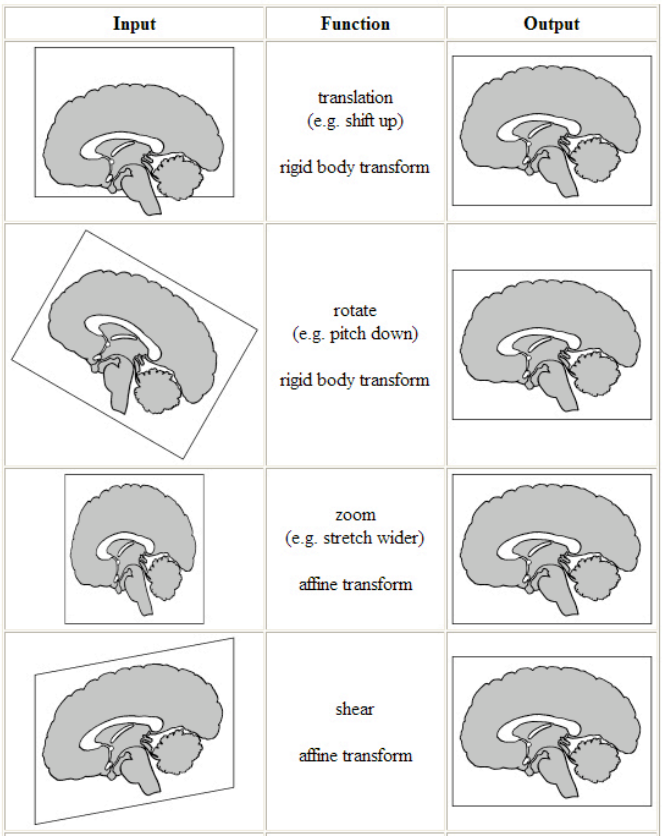

Figure 12: Operations (functions) applied during linear (affine) spatial normalisation. Shown are examples of all four different operations (translation, rotation, zoom, and shear) that can be applied during spatial linear normalisation. Figure adopted from http://www.sph.sc.edu/comd/rorden/mritut.html.

2.2.3.2 Nonlinear spatial normalisation (warping)

Nonlinear spatial normalisation (warping) corrects for local brain shape differences due to interindividual neuroanatomical variability and is a local nonlinear change of specific brain structures within the brain (Fig. 13).

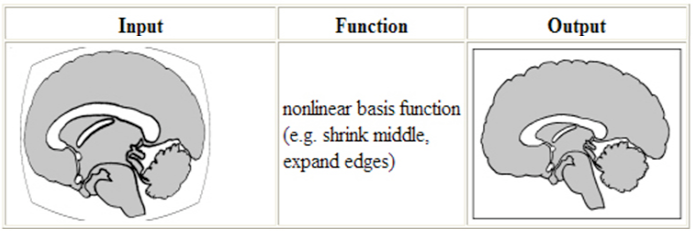

Figure 13: Scheme of the influence of nonlinear basis functions applied during nonlinear spatial normalisation (warping). Figure adopted from http://www.sph.sc.edu/comd/rorden/mritut.html.

There are a number of approaches to nonlinear spatial normalisation, but only methods that attempt to perform spatial nonlinear normalisation in an automatic manner are considered. There is a potentially enormous number of parameters that could be solved for in spatial normalisation problems, i.e., the problem is very high dimensional. The forms of spatial normalisation tend to differ in how they cope with the large number of parameters required to define the transformations (Ashburner & Friston, 1997). Some have abandoned conventional optimisation approaches, and use viscous fluid models

(Christensen et al., 1994, 1996) to describe the warps. In these models, finite-element methods are used to solve the partial differential equations that model one image as it ‘‘flows’’ to the same shape as the other. The major advantage of these methods is that they are able to account for large nonlinear displacements and also ensure that the topology of the warped image is preserved, but they do have the disadvantage that they are computationally very expensive. Not every unit in the functional and structural imaging field has the capacity to routinely perform spatial normalisation using these methods. Others adopt a multiresolution approach whereby only a few of the parameters are determined at any one time (Collins et al., 1994). Usually, the entire volume is used to determine parameters that describe global low-frequency deformations. The volume is then subdivided, and slightly higher-frequency deformations are found for each subvolume. This continues until the desired deformation precision is achieved.

Statistical parametric mapping (SPM) software used a linear combination of basis functions, i.e., the model for defining the nonlinear warps uses deformations that consist of a linear combination of the three dimensional discrete cosine transform or function (DCT). An example of a two dimensional discrete cosine transform and that of a two dimensional discrete Fourier transform together with the formula for the DCT (type I) and the different types of DCTs are shown in Figure 14. In SPM, for speed and simplicity, a relative small number of parameters (approximately 1000) are used to describe the nonlinear components of the registration (Ashburner & Friston, 1999).

The model for defining the nonlinear warps uses deformations that consist of a linear combination of basis functions. So, the transformation from coordinates x, to coordinates y is:

$$\boldsymbol{y_1 = x_1 + \sum_j t_{y1}\, b_{j1}\,(\mathbf{x})}$$
$$\boldsymbol{y_2 = x_2 + \sum_j t_{y2}\, b_{j2}\,(\mathbf{x})}$$
$$\boldsymbol{y_3 = x_3 + \sum_j t_{y3}\, b_{j3}\,(\mathbf{x})}$$

where t_{yd} is the ith coefficient for dimension d, and b_{yd} (x) is the jth basis function at position x for dimension d (Ashburner & Friston, 1999).

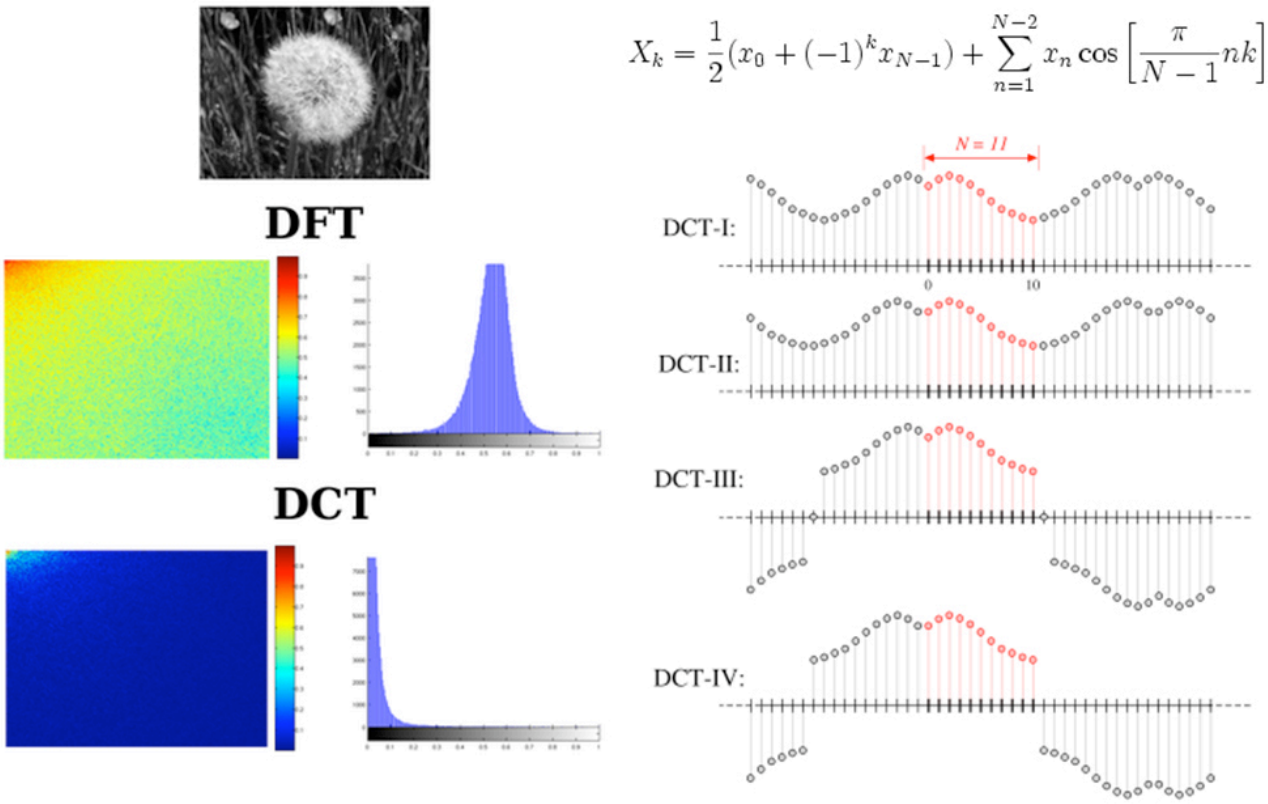

Figure 14: Examples of two dimensional discrete cosine transforms (DCT).
Left panel: Two dimensional DCT (type II) compared to the two dimensional discrete Fourier transform (DFT). For both transforms, there is the magnitude of the spectrum on left and the histogram on right; both spectra are cropped to 1/4, to zoom the behaviour in the lower frequencies. The DCT concentrates most of the power on the lower frequencies. ***Right panel: Top:*** Formula of DCT-I (type I). ***Bottom:*** Illustration of the implicit even/odd extensions of DCT input data, for N=11 data points (red dots), for the four most common types of DCT (types I-IV). Figures adopted from http://en.wikipedia.org/wiki/Discrete_cosine_transform.

In order to model the nonlinear transformations, the two dimensional discrete cosine transforms are extended to three dimensions and combined. An example of the lowest frequency basis functions of a two dimensional DCT is shown in Figure 15 (left panel) and a schematic example of a deformation based upon the DCT and its application to an image is shown in Figure 15 (right panel).

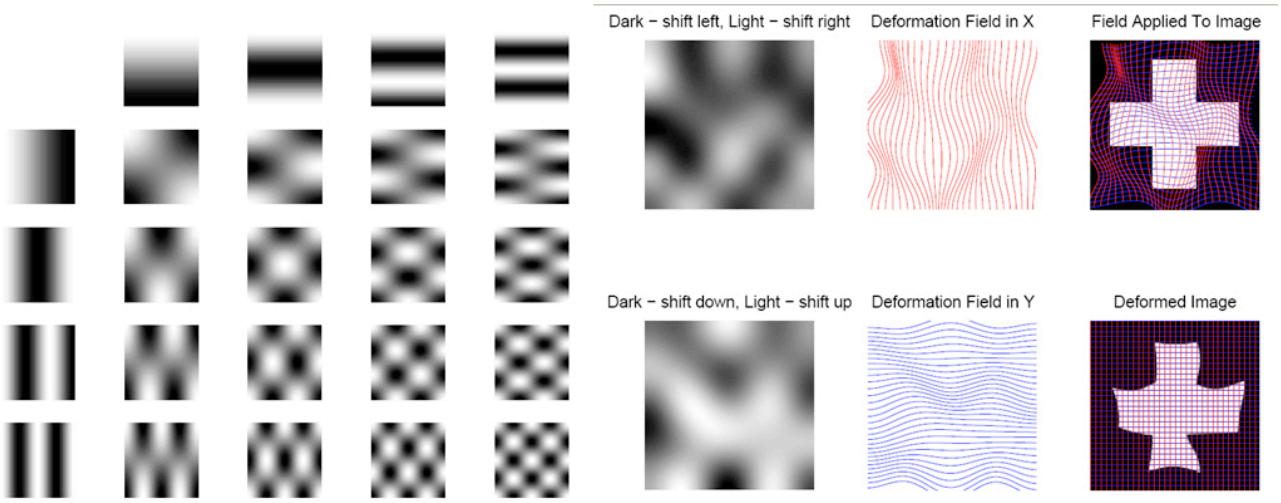

Figure 15: Example of the lowest frequency basis functions of a two dimensional DCT and a schematic example of a deformation based upon the DCT.
Left panel: An example of the lowest frequency basis functions of a two dimensional DCT and its combinations. ***Right panel:*** For the two-dimensional case, the deformation field consists of two scalar fields: one for horizontal deformations (top), and the other for vertical deformations (bottom). Images at left column show the deformation fields as a linear combination of the basis images (see left panel). The centre column shows deformations in a more intuitive sense. The deformation field is applied by overlaying it on the object image, and resampling (right column). Figures adopted from Ashburner & Friston, 1999.

In order to decide which transformations are the most appropriate when transforming an object image onto a template image, a quality factor is needed. The optimisation involves minimising the sum of squared differences between the object image (f) and a template image (g). The images may be scaled differently, so an additional parameter (w) is needed to accommodate this difference. The squared distance between the parameters and their known expectations are also minimised (regularisation, see below). The second minimisation term is equivalent to the bending energy (also called Laplacians) of the deformations (Ashburner & Friston, 1999).

This algorithm can introduce unnecessary deformations that only reduce the residual sum of squares by a tiny amount. Therefore, another function called regularisation is needed to prevent the algorithm to introduce unlikely and unnecessary deformations. The objective of spatial normalisation is to warp the images such that homologous regions of different brains are moved as close together as possible. A large number of parameters are required to encompass the range of possible nonlinear warps. With many parameters relative to the number of independent observations, the errors associated with the fit are likely to be very larger. The use of constraints (such as preserving a one-to-one mapping between image and template) can reduce these errors, but they still remain considerable. For this purpose, the simple minimisation of differences between the images is not sufficient. Although the normalised images may appear similar to each other, the data may in fact have been "over-fitted", resulting in truly homologous regions being moved further apart (Ashburner & Friston, 1999). Other researchers

circumvent this over-fitting problem by restricting their spatial normalisation to just an affine transformation. A properly implemented Bayesian approach should attempt to reach an optimum compromise between these two extremes. Although the incorporation of an optimally applied maximum a posteriori (MAP) approach into nonlinear registration has the effect of biasing the resulting deformations to bee smoother than the true deformations, it is envisaged that homologous voxels should be registered more closely than for unconstrained deformations. The regularisation procedure in SPM follows a Bayesian-like approach and is achieved by minimising the sum of squares difference between the template and the warped image, while simultaneously minimising the sum of squares of the derivatives of the deformation field (Ashburner & Friston, 1999).

2.2.3.3 Jacobian determinant modulation

Because of the nonlinear spatial normalisation, the volumes of certain brain regions will grow, whereas others will shrink. This has implications for the interpretation of what VBM is actually testing for. The objective of VBM is to identify regional differences in the concentration of a particular tissue (grey or white matter). In order to preserve the actual amounts of GM within each structure, a further processing step that multiplies the partitioned images by the relative voxel volumes can be incorporated. These relative volumes are simply the Jacobian determinants of the deformation field (Ashburner & Friston, 2000). This augmented (optimised) VBM can therefore be considered as a combination of VBM and tensor based morphometry (TBM), in which the TBM employs the testing of the Jacobian determinants. VBM can be thought of as comparing the relative concentration of GM (i.e., the proportion of GM to other tissue types within a region). With the adjustment for volume change (Jacobian modulation), VBM would be comparing the absolute amounts of GM in the different regions. It is envisaged that, by incorporating this correction, a continuum will arise with simple VBM (with low-resolution spatial normalisation) at one end of the methodology spectrum and statistical tests based on the Jacobian determinants at the other (with high-resolution spatial normalisation) (Ashburner & Friston, 2000).

2.2.4 Tissue segmentation using the Bayes' theorem

The aim of tissue segmentation is to divide the whole brain into its different tissue types. Healthy brain tissue can generally be classified into three broad tissue types on the basis of an MR image. These are grey matter (GM), white matter (WM), cerebrospinal fluid (CSF), and three other background classes, using a modified mixture model cluster analysis technique (Ashburner & Friston, 2000). These authors

extended their previously described tissue classification method (Ashburner & Friston, 1997b) so that it includes a correction for image intensity nonuniformity that arises for many reasons in MR imaging (see paragraph 2.2.2). The tissue segmentation process is based by the voxel intensities on one hand and by a priori information of the distribution of the different tissue types throughout the brain on the other hand (Ashburner & Friston, 1997b). Segmentation in SPM is obtained from the intensity distribution of the image and a priori information about the spatial distribution for the respective tissue classes. To visualise and analyse image intensity distribution we can plot all values of the image into a histogram as shown in Figure 16. The histogram represents the frequencies of the intensity values in a T1-weighted MR image.

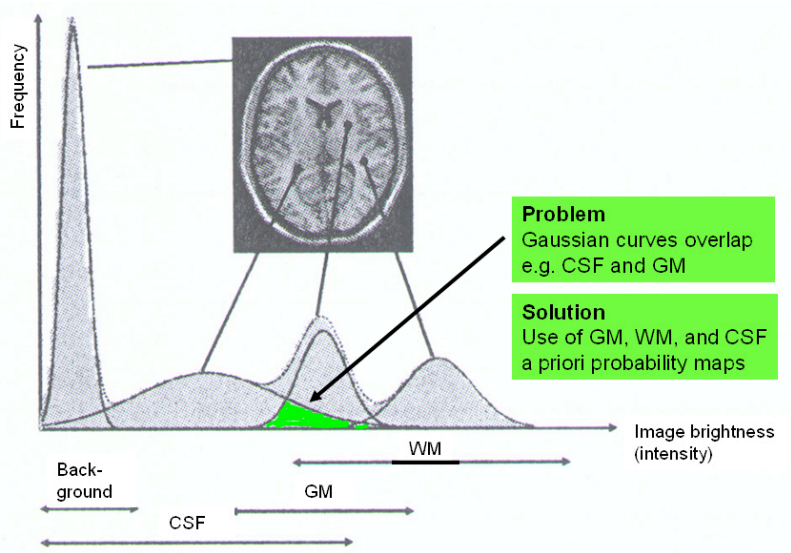

Figure 16: Histogram of the intensity distribution in a T1-weighted MR image. The x-axis shows (from left to right) increasing image intensities and we can differentiate different Gaussian curves for each tissue class and background. The y-axis shows the frequencies of the intensities. Because the Gaussian curves overlap (green), we can not differentiate all voxels properly when only using the voxel intensity information. Therefore a priori information about the spatial distribution of the different tissue types has to be incorporated into the segmentation procedure. Figure adopted from C.Gaser, SPM Course, Hamburg 2005.

The whole segmentation procedure using the Bayes' theorem to integrate a priori information about the spatial distribution of the different tissue types (the so called tissue a priori maps) is illustrated in Figure 17. If we only use intensity information of the whole image there are several misclassifications outside the cortex (see Fig. 17). This is because image intensity around the scalp is similar to that of grey matter as shown in the two black circles.

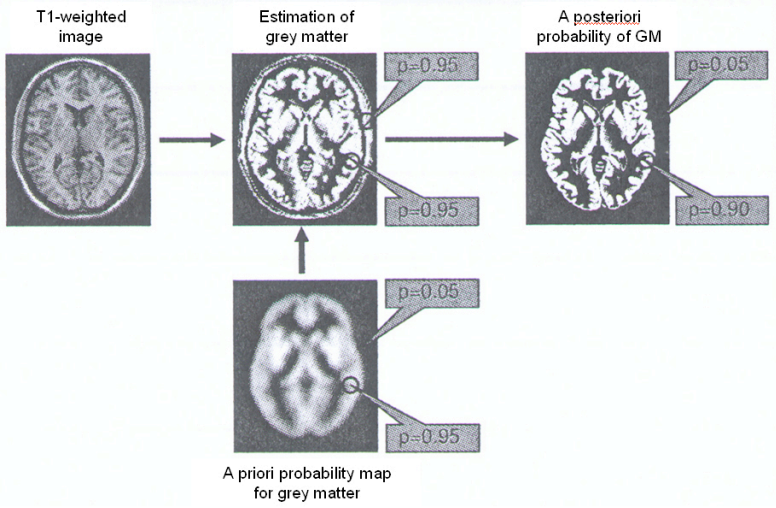

Figure 17: Tissue segmentation process using the Bayes' theorem.
Based on the voxel intensity of the T1 weighted image (top left brain) the probability that a particular voxel belongs to grey matter is estimated. Two voxels (black circles) with equal intensities (p = 0.95) are shown (top middle brain), from which one voxel is really grey matter whereas the other is localised outside the brain and consists of tissue of the scalp. By incorporating an a priori probability map of grey matter (bottom middle brain), we can compute the a posteriori probability that a particular voxel belongs to grey matter (top right brain). Figure adopted from C.Gaser, SPM Course, Hamburg 2005.

In the case of the SPM software, there are actually only two different tissue a priori maps (GM and WM). The third a priori map comprises a mixture of CSF, meninges, scalp, and skull. As I heard from the SPM mailinglist, it is intended to incorporate further a priori tissue maps (like fat, meninges, skull, scalp, muscles, vessels) in future SPM releases (SPM8) to enhance the segmentation procedure. Although a priori information is used to restrict segmentation to the cortex there are still some misclassifications (often at the border between GM and CSF) non-connected non-brain voxels (see Fig. 18). These rims can be tried to remove using morphological operations. Conditional dilatations and erosions based on GM and WM segmentations are used to create a mask to clean up the segmentations. It begins by taking the WM and eroding it a couple of times to get rid of any odd voxels. The algorithm continues on to do conditional dilatations for several iterations, where the condition is based upon GM or WM being present. This identified region is then used to clean up the GM and WM partitions, and has a slight influence on the CSF partition.

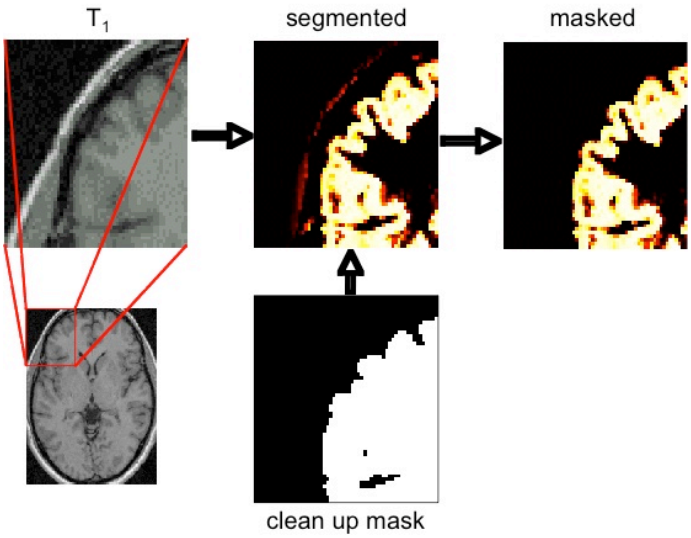

Figure 18: Clean up segmentations.
An overview of the clean up procedure to remove non-connected non-brain voxels from the segmented images. In the initial segmented image a small rim around the cortex is still present (top middle image). Using conditional dilatations and erosions we can create a clean up mask (bottom middle image) to remove these non-connected parts from the segmented images (top right image). Figure adopted from C.Gaser, SPM Course, Hamburg 2005.

A further improvement step in the segmentation procedure, based on the hidden Markov random field theory, can be obtained by incorporating spatial constraints between the voxels throughout the brain as will be discussed in the next paragraph.

2.2.4.1 Hidden Markov random field (HMRF) weighting

Here I present you the hidden Markov random field (HMRF) model which is implemented in the VBM5 toolbox for SPM5 (http://dbm.neuro.uni-jena.de/vbm/markov-random-fields/). We can optionally use prior information by applying a hidden Markov random field (HMRF) model. Using this model we introduce spatial constraints based on neighbouring voxels of a 3x3x3 cube. The centre voxel has 26 neighbours and we can calculate MRF energy by counting the number of neighbouring voxels (see Fig. 19).

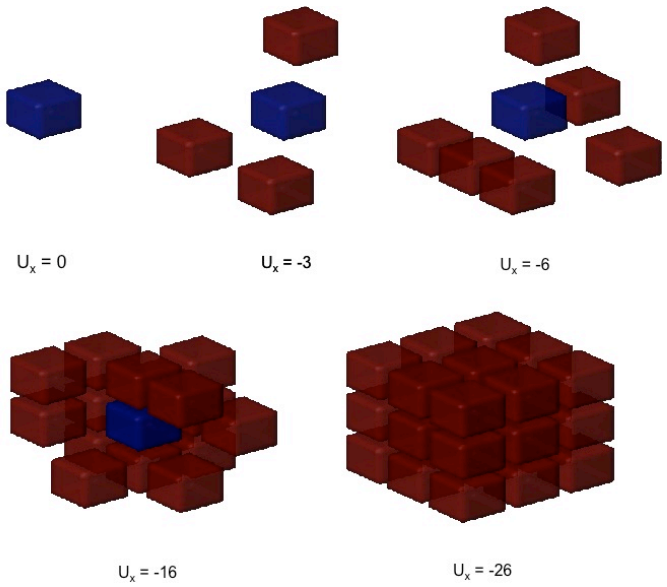

Figure 19: Computation of the Markov random field (MRF) energy.
MRF energy Ux is calculated by counting the number of neighbouring voxels of one tissue class in a 3x3x3 cube. From upper left to lower right there are different configurations shown from Ux = 0 (no neighbours) up to Ux = -26 (maximum number of 26 neighbours). Figure adopted from http://dbm.neuro.uni-jena.de/vbm/markov-random-fields/.

Neighbouring voxels are expected to have the same class labels. The prior probability of the class and the likelihood probability of the observation are combined to estimate the maximum a posteriori (MAP) probability. Prior probability can be weighted between 0 (no HMRF) and 1 (maximum HMRF for very noisy data) to cover different levels of noise. Parts of the version implemented in VBM5 are based on an implementation of a Gaussian hidden Markov random field (GHMRF) approach (Cuadra et al., 2005). The idea is to remove isolated voxels of one tissue class which are unlikely to be member of this tissue type. It also closes holes in a cluster of connected voxels of one tissue type. In the resulting segmentation the noise level will be minimised. Depending on your scanner and the used MR

sequence your T1-images will contain at least 3% noise level. Hence, it is recommend for most images a medium HMRF weighting of 0.3. If your images are affected by more noise level you can choose a larger HMRF weighting. There is also the opportunity to use an adaptive HMRF weighting procedure. Based on the MRF energy we can calculate MRF prior probabilities for each tissue class. This prior information is combined with the likelihood probability from the segmentation step to a joint posterior probability. The amount to which this prior information is used can be controlled with a weighting factor beta. The incorporation of the MRF energy into the segmentation procedure is presented in Figure 20. For further details about HMRF modulation in SPM2 and SPM5 and an evaluation of the approach can be found under http://dbm.neuro.uni-jena.de/vbm/markov-random-fields/. As can be seen in Figure 20, after applying the HMRF modulation to the GM segment, many of the misclassified voxels disappeared (compare the three insets).

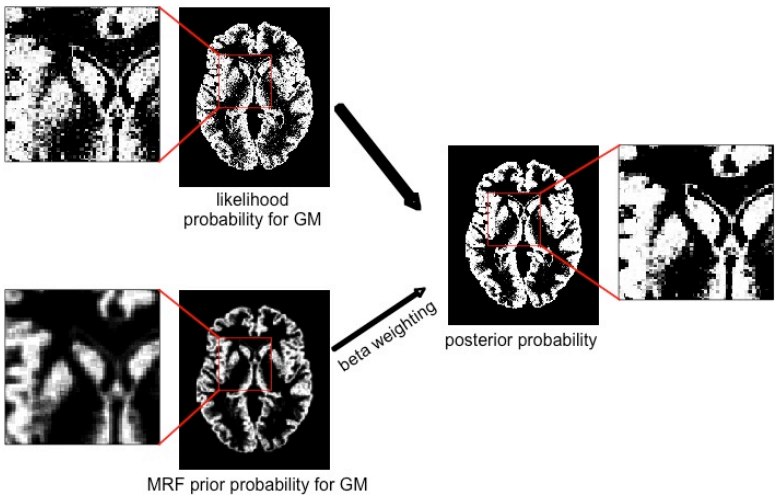

Figure 20: Incorporation of the Markov random field (MRF) energy into the segmentation procedure.
Based on the MRF energy we calculate MRF a priori probabilities for each tissue class. This prior information is combined with the likelihood probability from the segmentation step to a joint posterior probability. The amount to which this prior information is used can be controlled with a weighting factor beta. Figure adopted from http://dbm.neuro.uni-jena.de/vbm/markov-random-fields/.

2.2.5 Spatial smoothing (spatial blurring)

After intensity inhomogeneity correction, spatial normalisation, and tissue segmentation, the GM images are now smoothed by convolving with an isotropic Gaussian kernel (see Fig. 21). This makes the subsequent voxel-by-voxel analysis comparable to a region of interest (ROI) approach, because each voxel in the smoothed images contains the average concentration of GM from around the voxel (where the region around the voxel is defined by the form of the Gaussian smoothing kernel). By the central limit theorem, smoothing also has the effect of rendering the data more normally distributed, increasing the validity and power of parametric statistical tests. Whenever possible, the size of the smoothing kernel should be comparable to the size of the expected regional differences between the brains of the groups under investigation. The smoothing step also helps to compensate for the inexact

nature of the spatial normalisation procedure (Ashburner & Friston, 2000). Smoothing affects the accuracy of spatial localisation negatively.

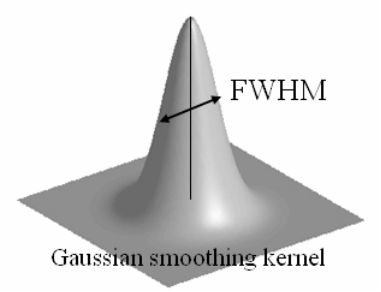

Figure 21: Isotropic Gaussian spatial smoothing (blurring) kernel.
Shown is a isotropic Gaussian spatial smoothing (blurring) kernel. The size of the kernel is determined by the Full Width at Half Maximum (FWHM) measure in mm. In most VBM studies, isotropic Gaussian smoothing kernels with FWHM between 8 mm and 12 mm are used. The origin of the figure is unknown.

2.2.6 Voxel-wise statistical analysis between groups

This paragraph is divided into several parts. The first part deals with the general linear model in SPM, the second part focuses on the problem of multiple dependent and independent comparisons when testing statistical parametric maps (SPMs), the third part discusses the problem of global covariates, fourth part deals with nonparametric, statistical tests such as permutations (statistical nonparametric maps, SnPM), and the last part focuses on how to report voxel-based morphometry studies in the scientific literature. For a more detailed review about statistical issues in SPM, the reader is referred to the SPM book edited by Friston and colleagues (Friston et al., 2007).

General linear model: Statistical parametric analysis in SPM, using the general linear model (GLM), is applied to identify regions of grey matter differences in GM concentration/density or in GM volume that are significantly related to the particular effect under study (Friston et al., 1995b). Grey matter volume is referred to as real absolute volume differences between groups of subjects or patients. Grey matter concentration is often referred to as relative "grey matter density", but should not be confused with cell packing density measured cytoarchitectonically. Normally, it is referred to "grey matter concentration" to avoid confusion. See also paragraph 2.2.3.3 about the Jacobian determinant modulation. The GLM is a flexible framework that allows many different tests to be applied, ranging from group comparisons and identifying regions of GM concentration or volume that are related to specified covariates such as disease severity or age to complex interactions between different effects of interest. Standard parametric statistical procedures (t tests and F tests) are used to test the hypotheses, so they are valid providing the residuals, after fitting the model, are independent and normally distributed. If the statistical model is appropriate there is no reason why the residuals should not be independent, but there are reasons why they may not be normally distributed. The original segmented images contain values between 0 and 1, of which most of the values are very close to either

of the extremes. Only by smoothing the segmented images does the behaviour of the residuals become more normally distributed. Following the application of the GLM, the significance of any differences is ascertained using the theory of Gaussian random fields (GRF) (Worsley et al., 1996; Friston et al., 1996, 2007). A voxel-wise statistical parametric map (SPM) comprises the result of many (up to Millions) statistical tests, and it is necessary to correct for these multiple dependent comparisons (see below).

In the SPM software, there are three different levels on which inferences can be drawn: the set, cluster, and voxel level. Common statistical inference levels reported are the cluster and voxel level, although and unfortunately a mixture of these levels is frequently reported in the neuroimaging literature, i.e., the number of voxels (k_E) derived from the cluster level is combined with the t-value or p-value of a local maxima or minima derived from the voxel level. For more details about the advantages and disadvantages of the different levels of inference please see Friston and colleagues (Friston et al., 1996). Two very important statistical measures used in neuroimaging statistics are the height threshold (error probability of the magnitude) and the extent threshold (error probability of the spatial extent of the magnitude). These error probabilities are ascertained using the theory of Gaussian random fields (Worsley et al., 1996; Friston et al., 1996). With a strong a priori hypothesis about the location of the expected structural difference, there is a consensus in the community that a height threshold of $p < 0.001$ uncorrected for multiple comparisons is appropriate, especially in VBM analyses with small sample sizes. The extent threshold is often chosen somewhat arbitrary. One can guide this choice by the expected size of the structural difference (e.g., 10-200 voxels with a resolution of 1 mm^3 each), or the extent threshold can also be corrected by the theory of Gaussian random fields.

Corrections for multiple dependent or independent comparisons: In cases of strong a priori hypotheses with respect to the anatomical location, statistics without a multiple comparison correction procedure is possible (Friston, 1997). The most popular method to correct for multiple dependent or independent statistical comparisons is the Bonferroni correction (Shaffer, 1995). This procedure accounts for multiple comparisons by dividing the nominal alpha error probability of $p = 0.05$ by the number of statistical tests applied. In a standard VBM study that is analysed voxel-wisely there are about 2 Millions of voxels that have to be compared; hence, about 2 Millions of statistical tests have to be done. If the Bonferroni correction would be used in such a VBM study the actual error probability for declaring a voxel statistically significant would be $p < 2.5*10^{-8}$. Due to the physiological dependence of neighbouring voxels as well as the dependence introduced by the spatial smoothing procedure, a Bonferroni correction is too conservative with respect to the alpha error probability.

In the context of structural and functional neuroimaging two other corrections are common. One is

based on Gaussian random field theory and is called family wise error correction (FWE). The FWE correction can be applied to correct the voxel height threshold as well as to correct the cluster extent threshold (Friston et al., 2007). In cases where FWE correction is used to control the cluster extent threshold, one has also to correct for nonstationarity of the smoothness (Hayasaka et al., 2004), although nonconstant smoothness and nonisotropic deformations are also an important issue in most other kinds of statistical inferences based on statistical parametric maps (Worsley et al., 1999). The other one is denoted false discovery rate correction (FDR) (Genovese et al., 2002). Whereas Bonferroni corrects for the number of statistical tests that were applied, FDR corrects the probability for false positives. This correction is based only on the number of statistical tests declared significant not on the number of tests applied; hence, it is less conservative with respect to the type I error compared with Bonferroni. FWE is more conservative than FDR with respect to false positives. On the other hand, FDR is less conservative than FWE with respect to false negatives. Recently, it has been shown that there are some problems with the FDR in the context of topological inferences using Gaussian random fields (Chumbley & Friston, 2009).

Global covariates: There are ongoing discussions about the correction for global measures in functional and structural neuroimaging studies. When investigating local brain activity, should one control for global brain activity? When investigating local brain volume, should one control for global brain volume? In functional imaging studies, there seems to be less consensus about corrections for global measures (especially in second level analyses for random effects) than in the field of neuromorphometry (Aguirre et al., 1998; Andrade et al., 1999). When analysing local GM volumes (Jacobian determinant modulated images), it is mandatory to control for global GM volumes because most of the volumes of local GM structures are proportional to the global GM volume; hence, local GM volume is confounded (correlated) by global GM volume. When analysing local GM densities (not Jacobian determinant modulated images), controlling for global measures are commonly omitted. But bear in mind that not the entire volume difference is encoded in the linear transformations and in the deformation fields applied during spatial normalisation, so that one might also wish to control for residual global volume differences.

Nonparametric statistical tests (permutations): In cases where the statistical assumptions for parametric analyses are not met, a nonparametric statistics like permutations can be used. For functional and structural neuroimaging data, a toolbox called statistical nonparametric mapping (SnPM) is available (Nichols & Holmes, 2001; http://www.sph.umich.edu/ni-stat/SnPM/). This toolbox provides an extensible framework for voxel level non-parametric permutation/randomisation

tests of functional and structural neuroimaging experiments with independent observations. The SnPM toolbox provides an alternative to the statistics section of SPM. SnPM uses the general linear model (GLM) to construct pseudo *t*-statistic images, which are then assessed for significance using a standard non-parametric multiple comparisons procedure based on randomisation/permutation testing. It is most suitable for single subject PET/SPECT analyses, or designs with low degrees of freedom available for variance estimation. In these situations the freedom to use weighted locally pooled variance estimates or variance smoothing, makes the non-parametric approach considerably more powerful than conventional parametric approaches, as are implemented in SPM. Further, the non-parametric approach is always valid, given only minimal assumptions (Nichols & Holmes, 2001).

How to report voxel-based morphometry studies in the literature: With respect to the scientific publication of VBM studies there are no strict rules about which information and facts including technical parameters should to be reported in the method section of a publication. However, there are guidelines that, when abided by neuroimaging scientists, help to compare the results between different structural neuroimaging studies as well as help to replicate experimental designs accurately. Ten simple rules for reporting VBM studies can be found in more details elsewhere (Ridgway et al., 2008). These rules are: 1) Set out the rational for your study and describe the data fully; 2) Explain how the brain segmentations are produced; 3) Describe the method of intersubject spatial normalisation; 4) Make your statistical design transparent; 5) Be clear about the significance of your findings; 6) Present results unambiguously; 7) Clarify and justify any non-standard statistical analyses; 8) Guard against common pitfalls; 9) Recognise the limitations of the technique; and 10) Interpret your results cautiously and in context (Ridgway et al., 2008). Similar rules were recently also published for reporting the results of functional imaging studies (Poldrack et al., 2008).

2.2.7 Creation of a customised template and customised a priori maps

In cases where the brains of the population under investigation deviates from the distributions of GM, WM, and CSF in the canonical template and a priori maps, it is recommended to create a customised template and corresponding customised a priori maps. Mostly this is the case when investigating paediatric populations, patients with neurodegenerative diseases (e.g., patients with Alzheimer's disease), or patients with diffuse lesions. With respect to the spatial normalisation of customised a priori maps, mostly they will be created by only rigid-bodily or affinely registered images. These linear transformations are unable to account for the whole interindividual neuroanatomical variability. I would prefer to work with customised a priori maps that were derived from linearly as well as non-

linearly spatially normalised images. The schematic flow diagram of the creation process of customised templates and a priori maps is illustrated in Figure 22 below.

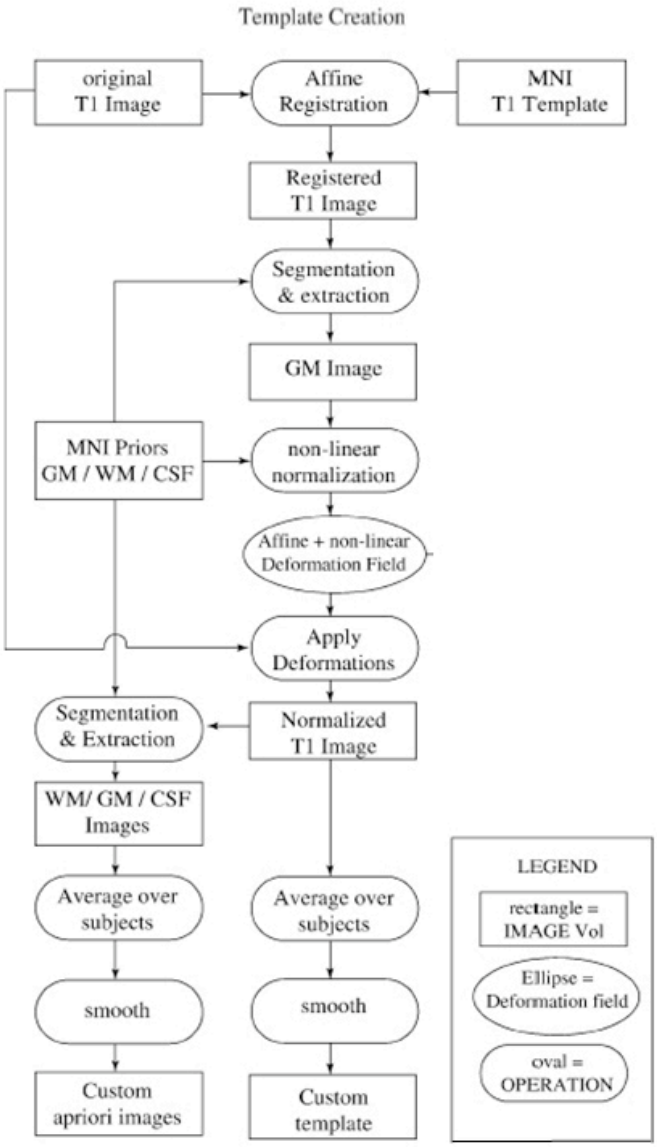

Figure 22: Schematic flow diagram of the creation of a customised template and customised a priori maps.
This figure illustrates the creation of a customised template and customised a priori maps schematically. This algorithm proceeds as follows: (i) perform a 12 degree of freedom (DOF) affine registration between each subject's MRI image and the MNI template; (ii) segment the affine registered image using the MNI priors; (iii) perform a nonlinear normalisation of the segmented GM image to the MNI GM a priori map; (iv) segment the normalised subject image using the MNI a priori maps; (v) average together all the normalised whole head, GM, WM, and CSF images to obtain a customised template and customised GM, WM, and CSF a priori maps, respectively; (vi) apply an 8-mm full width at half maximum (FWHM) Gaussian smoothing kernel to the customised template and customised a priori maps (Senjem et al., 2005). Figure adopted from Senjem et al., 2005.

2.2.8 Optimised voxel based morphometry (VBM)

Because of some limitations of the originally proposed standard voxel based morphometry (VBM), especially its dependence from the templates that are used to spatially normalise and segment the images, a procedure called optimised VBM was initially developed by Good and colleagues (Good et al., 2001a, 2001b; Senjem et al., 2005; Mechelli et al., 2005b). The optimised VBM procedure is schematically summarised in Figure 23 below and proceeds as follow: (i) perform a 12 degrees of freedom (DOF) affine registration between each subject's MRI image and the MNI template; (ii)

segment the affine-registered image using the MNI a priori maps; (iii) perform a nonlinear normalisation of the segmented GM image to the MNI GM a priori map, applying the parameters obtained to the original whole head image; (iv) segment the normalised whole head image using the MNI a priori maps; (v) apply Jacobian modulation to the segmented GM image; (vi) apply a 12 mm full width at half maximum (FWHM) Gaussian spatial smoothing kernel to the modulated GM image, and proceed to the statistics stage.

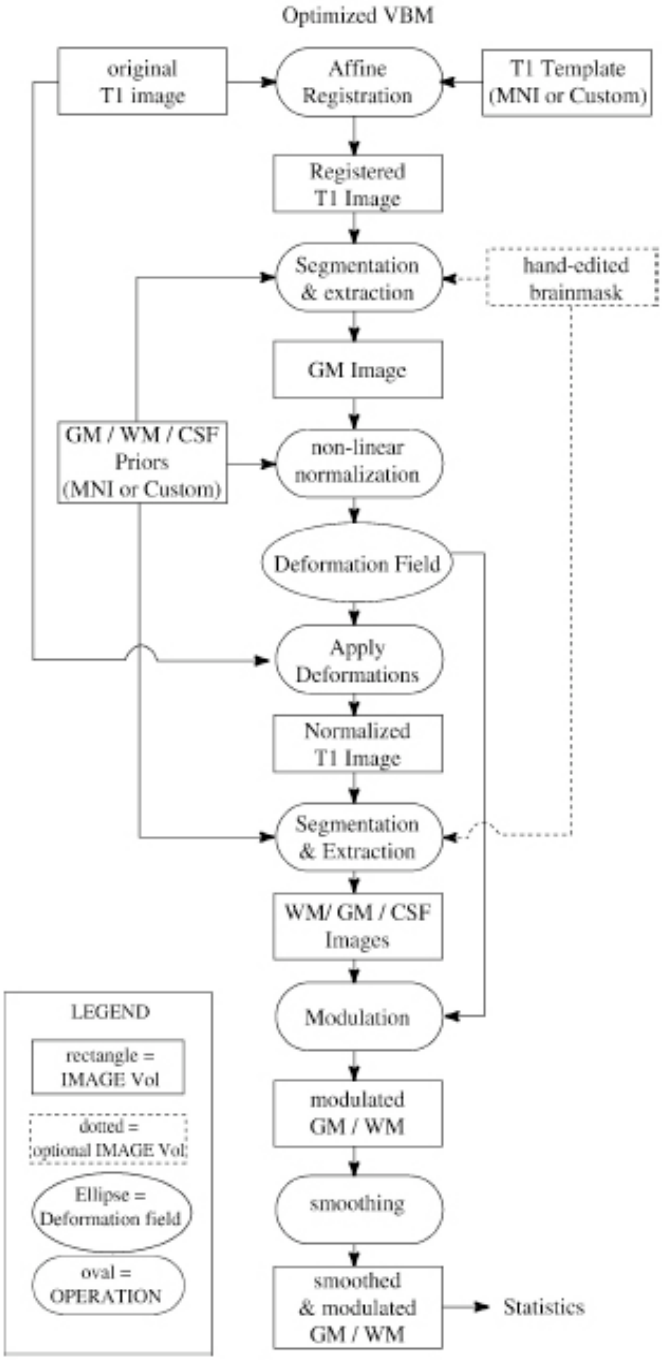

Figure 23: Schematic flow diagram of optimised voxel based morphometry (VBM).
This figure illustrates the optimised VBM method (Ashburner & Friston, 2000; Good et al., 2001a) schematically. The optimised VBM algorithm proceeds as follows: (i) perform a 12 degrees of freedom (DOF) affine registration between each subject's MRI image and the MNI template; (ii) segment the affine-registered image using the MNI a priori maps; (iii) perform a nonlinear normalisation of the segmented GM image to the MNI GM a priori map, applying the parameters obtained to the original whole head image; (iv) segment the normalised whole head image using the MNI a priori maps; (v) apply Jacobian modulation to the segmented GM image; (vi) apply a 12 mm full width at half maximum (FWHM) Gaussian spatial smoothing kernel to the modulated GM image.The final step is statistical comparison, wherein the smoothed, modulated GM images are compared between patient and control populations using a two-sided t test or an analysis of covariance model (Senjem et al., 2005). Figure adopted from Senjem et al., 2005.

The use of a customised template and of customised a priori maps instead of the canonical template and the canonical a priori maps derived from the Montreal neurological institute (MNI) or the international consortium for brain mapping (ICBM) is an option that can be used in both the standard and optimised VBM method. In contrast to the standard VBM method, the optimised VBM procedure differs in the following steps: Spatial normalisation of each individual volume is based on matching the initial GM segment with the GM a priori map (Good et al., 2001a), whereas in standard VBM, spatial normalisation is performed on the volume proper, using the MNI whole brain template as a target for normalisation (Ashburner & Friston, 2000). In standard VBM the segments are generated from an affine and nonlinear normalised image, whereas in optimised VBM the segments are initially generated from only an affine normalised image and in a second step again generated from a warped (nonlinear) image. In this way, the dependency of the VBM procedure from the templates that are used can be diminished.

The canonical T1 template and the canonical a priori maps distributed with the SPM software differ between the two most recent versions. In SPM2, the T1 template and the a priori maps are derived from the MNI305 reference atlas. The ICBM152 T1 template and the corresponding a priori maps are used when working only with SPM5. When using the VBM5 toolbox in SPM5, the ICBM452 T1 a priori maps are used as reference templates.

2.2.9 Unified segmentation in statistical parametric mapping 5 – the new algorithm

As a consequence of the dependency of the normalisation and segmentation procedure from each other and from the templates that are used, the new algorithm in SPM5 tries to reduce these dependencies (Ashburner & Friston, 2005).

Many investigators currently use the tools within SPM for a technique that has become known as “optimised” voxel-based morphometry (VBM) (Good et al., 2001). VBM performs region-wise volumetric comparisons among populations of subjects. It requires the images to be spatially normalised, segmented into different tissue classes, and smoothed, prior to performing statistical tests. The optimised preprocessing strategy involves spatially normalising subjects’ brain images to a standard space by matching grey matter in these images to a grey matter reference. The historical motivation behind this approach was to reduce the confounding effects of non-brain (e.g., scalp) structural variability on the registration. Tissue classification in SPM requires the images to be registered with tissue probability maps (Ashburner and Friston, 1997b). After registration, these maps represent the prior probability of different tissue classes being found at each location in an image (Evans et al., 1994). Bayes rule can then be used to combine these priors with tissue type probabilities

derived from voxel intensities to provide the posterior probability.

This procedure is inherently circular, because the registration requires an initial tissue classification, and the tissue classification requires an initial registration. In the new SPM5 algorithm, this circularity is resolved by combining both components into a single generative model. This model also includes parameters that account for image intensity nonuniformity, although it is now fairly standard to include intensity nonuniformity correction in segmentation (Wells III et al., 1996) and registration (Friston et al., 1995a; Studholme et al., 2004) methods. Estimating the model parameters (for a maximum a posteriori solution) involves alternating among classification, bias correction, and registration steps. This approach provides better results than simple serial applications of each component separately. The new SPM5 algorithm is shown in Figure 24. The algorithm starts with 40 iterations on segmenting, followed by 40 iterations on bias field correction and 20 iterations on warping (nonlinear normalisation). This loop runs as many times as no significant change in the estimate occurs (Ashburner & Friston, 2005).

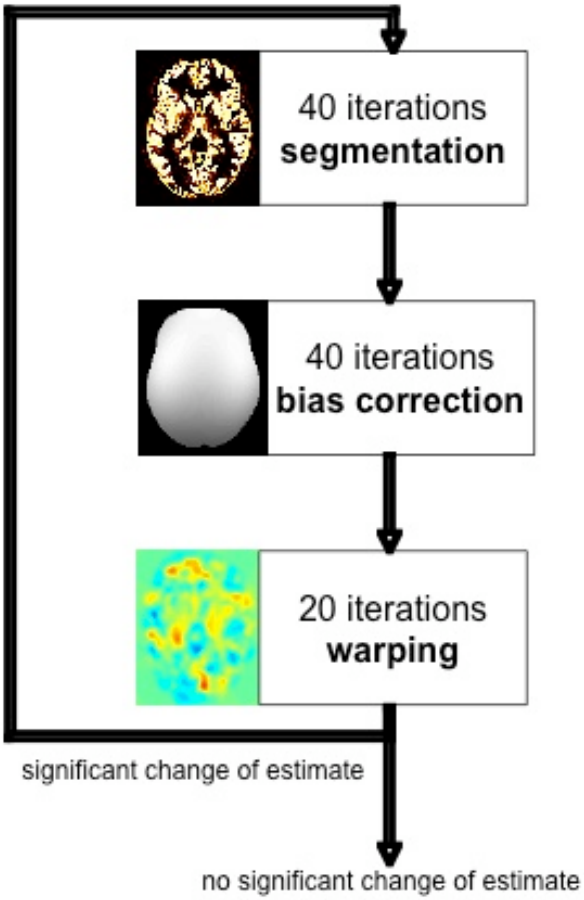

Figure 24: Unified segmentation in statistical parametric mapping 5 software.
This figure illustrates the new algorithm of unified segmentation in SPM5 (Ashburner & Friston, 2005) schematically. The algorithm starts with 40 iterations on segmenting, followed by 40 iterations on bias field correction and 20 iterations on warping (nonlinear normalisation). This loop runs as many times as no significant change in the estimate occurs (Ashburner & Friston, 2005). Figure adopted from http://dbm.neuro.uni-jena.de/vbm/vbm5-for-spm5/.

2.2.10 Parcellation of neuroanatomy

Instead of doing voxel-wise statistics with the normalised, segmented, modulated, and smoothed GM or WM images which is the standard analysis technique in VBM, one can divide the GM tissue segment further into specific volumes of interest (VOIs). This parcellation procedure is similar to the conventional neurovolumetric approaches where a region or volume of interest (ROI or VOI) is chosen and its borders or landmarks then manually delineated on the raw or preprocessed MR images. Manual approaches to the volume of other features of neuroanatomy (like cortical thickness) have many disadvantages. They are very labour intensive (only one or few structures can be investigated), they are subjective (intrarater and interrater reliabilities have to be established that sometimes are insufficient), they are dependent from the protocol used to trace a particular structure (too many protocols are used, therefore huge variability in the measures obtained and badly comparability across different studies), and not applicable to all brain structures (some structures are difficult or impossible in order to be distinguished from neighbouring structures). Most of these shortcomings of manual neurovolumetry can be overcome by fully or semifully automated parcellation methods like the ones proposed here. In this paragraph, I will present you two parcellation approaches that can be implemented in the SPM software. In paragraph 6 General Discussion, I will present you an additional, more sophisticated parcellation (segmentation) procedure (Fischl et al., 2002; Desikan et al., 2006; Makris et al., 2006) where subcortical and cortical structures are labelled in two separate processing streams (volume- and surface-based processing pipeline, respectively) that are implemented in the FreeSurfer software suite developed at the Massachusetts General Hospital (https://surfer.nmr.mgh.harvard.edu/fswiki).

2.2.10.1 Individual brain atlases using statistical parametric mapping (IBASPM)

A toolbox called individual brain atlases using statistical parametric mapping (IBASPM) is available for parcellating cortical and subcortical grey matter into smaller structural divisions like gyri or parts of gyri (http://www.thomaskoenig.ch/Lester/ibaspm.htm). A flowchart of the processing steps applied by IBASPM software is shown in Figure 25.

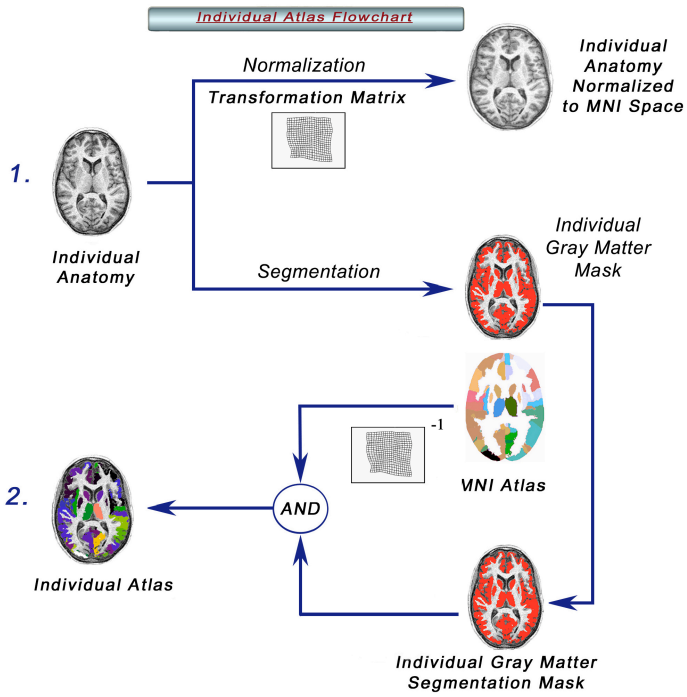

Figure 25: Flowchart of the processing steps used by individual brain atlases using statistical parametric mapping (IBASPM) software. This figure illustrates the steps applied in individual brain atlases using statistical parametric mapping (IBASPM). In step 1, the MR image is normalised to the MNI space in order to obtain the spatial transformation (normalisation) matrix. Additionally, in this step individual MR images are also segmented into three different brain tissue types: grey matter, white matter, and cerebral spinal fluid. In step 2, each individual grey matter voxel is labelled based on the MNI anatomical atlas (constructed by manual or automatic segmentation of a group of brains) and the transformation matrix obtained in the previous step. By multiplying each labelled VOI with the grey matter segment one obtains a binary mask that only contains the GM within that VOI. The volume of theses VOIs can then be computed. Figure adopted from http://www.thomaskoenig.ch/Lester/ibaspm.htm.

In step 1, the MR image is normalised to the MNI space in order to obtain the spatial transformation (normalisation) matrix. Additionally, in this step individual MR images are also segmented into three different brain tissue types: grey matter, white matter, and cerebral spinal fluid. In step 2, each individual grey matter voxel is labelled based on the MNI anatomical atlas (constructed by manual or automatic segmentation of a group of brains) and the transformation matrix obtained in the previous step. By multiplying each labelled VOI with the grey matter segment one obtains a binary mask that only contains the GM within that VOI. The volume of theses VOIs can then be computed.

Other previous works have developed a similar strategy for obtaining the segmentation of individual MR image into different anatomical structures using a standardised brain atlas. Have to be mentioned the approach introduced by the Montreal neurological institute (MNI) that merges the information coming from the ANIMAL (automatic nonlinear image matching and anatomical labelling) algorithm, that warps one image to match a previously labelled template (reference atlas), and from the INSECT (intensity normalised stereotaxic environment for the classification of tissue) algorithm, that assign each voxel a tissue label, for obtaining a suitable gross cortical structure segmentation (Collins et al, 1999).

2.2.10.2 Own parcellation approaches

In two of my studies (see paragraph original research articles) I used the following customised parcellation procedure to obtain the volumes of local grey matter structures. There were three reasons

not to use the IBASPM tool. First, and most important, we wished to apply the whole preprocessing of VBM (incl. the hidden Markov random field modulation). Second, there was actually no peer reviewed published paper about the IBASPM tool. Thirdly, and minor important, additional MATLAB (http://www.mathworks.com/) software modules other than the core had to be bought when one wishes to work with IBASPM. In these two studies, we aimed at parcellating the cortical and subcortical GM into 45 volumes of interest (VOIs) per hemisphere and computing their volumes. In the literature, sometimes this parcellation procedure is also called masking. A similar approach was used by other researchers (Wilke et al., 2003). The masks for the parcellation were derived from the software MARINA (masks for region of interest nnalysis; Walter et al., 2003; http://www.bion.de). These masks were originally drawn by others (Tzourio-Mazoyer et al., 2002) on the MNI single-subject brain (Holmes et al., 1998). There are two different ways how the masks can be adjusted to the population under investigation. We can use the same masks for all subjects (population masks; Figure 26) or we can use individual masks for each subject (individual masks; Figure 27). The preprocessing and the two different ways of parcellation procedures are in brief summarised below.

Parcellation of neuroanatomy using population masks: (I) After have run a first VBM in SPM5, we created customised a priori maps from the normalised, segmented, Jacobian and HMRF (with 0.3) modulated, unsmoothed GM, white matter (WM), and cerebrospinal fluid (CSF) images of the study population. (II) We then segmented the native T1-weighted images again with the customised a priori maps created in the first step. (III) We also segmented the MNI single-subject brain (Holmes et al., 1998), on which the masks were originally drawn (Tzourio-Mazoyer et al., 2002), with the customised a priori maps created in step I. In this way, we got the warping parameters (deformations) that have to be used to adjust the MNI single-subject brain onto the customised a priori maps. (IV) All masks implemented in the MARINA software were saved individually and some of them were combined to avoid too small VOIs. Note that this masks were physically stored in neurological convention, i.e., left is left instead left is right. (V) We then applied the warps that were computed in step III (with the Deformations tool in SPM5) to the masks to bring them in congruence with the structures within the customised a priori maps. (VI) Next we multiplied (using ImCalc) each mask with the unsmoothed GM image of the subjects obtained in step II. (VII) The new binary images now contain only the GM that is localised within an individual mask. (VIII) In the last step, we used an in-house MATLAB script to compute the volumes within these VOIs.

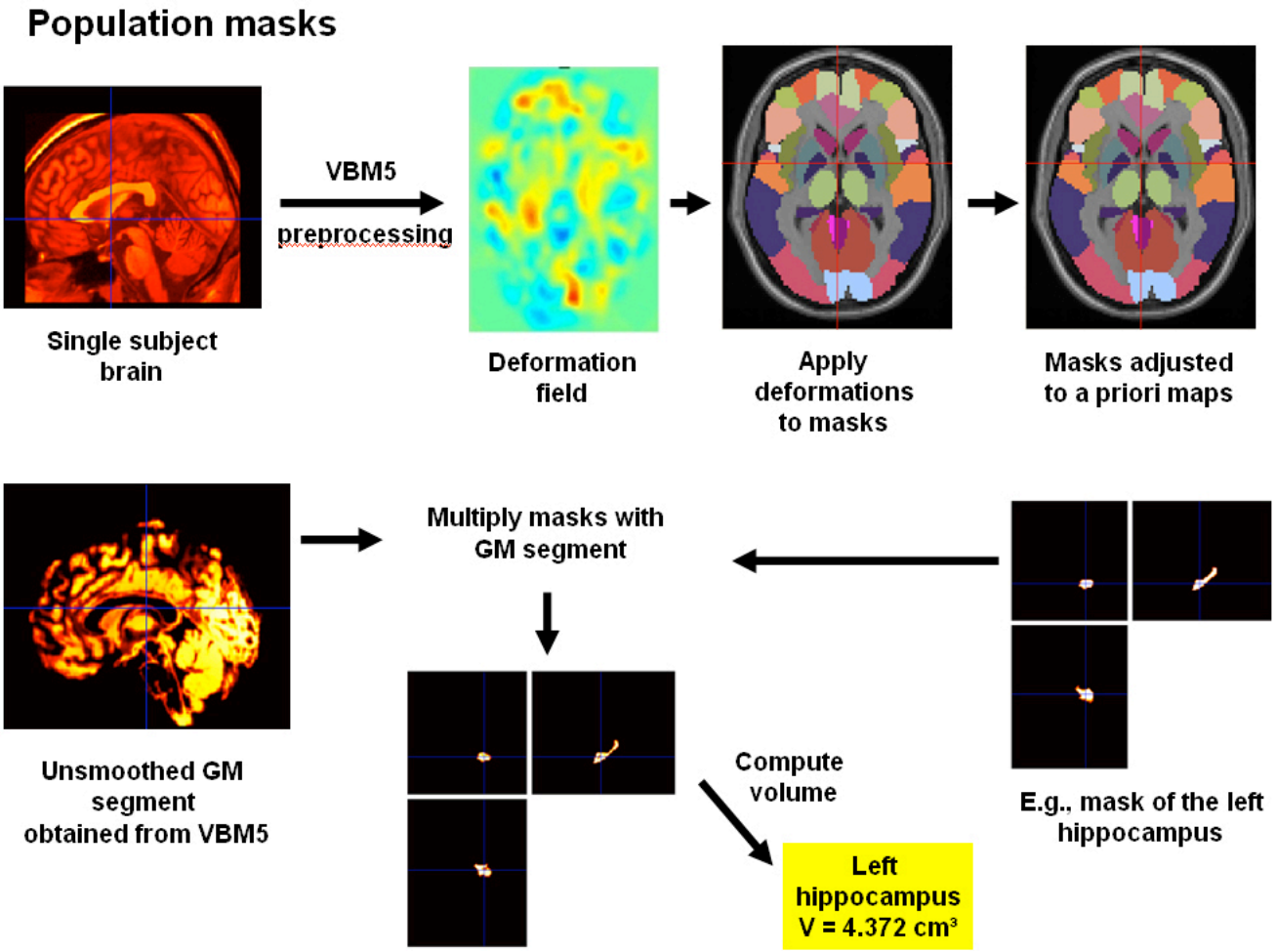

Figure 26: Processing steps used for construction of population masks by our own parcellation approach. This figure illustrates the steps applied in our own parcellation approach to construct population masks. The upper row shows the adjustment of the masks onto the specific template of the population under investigation. The bottom row shows the procedure to compute the volumes.

The most important advantage of our approach with population masks is that it does not require a method paper in order to establish the accuracy of the masking procedure. Because the same masks are used for all subjects, the accuracy of the parcellation is mainly determined by the normalisation and segmentation procedure of VBM5 preprocessing in SPM5. The accuracy of these preprocessing steps are well established (Ashburner & Friston, 2005).

Parcellation of neuroanatomy using individual masks: Because our parcellation procedure is not absolutely accurate with respect to the congruence between the masks and the corresponding brain structures when using population masks. This congruence can be optimised (at least theoretically) by forcing the source image (from where the masks were derived) to match each subject's brain exactly. In this way, the deformation field that exactly matches the brain structure of the source image onto an

individual brain can be obtained. By applying these deformations onto the masks one obtains masks that are adjusted to the anatomy of each individual.

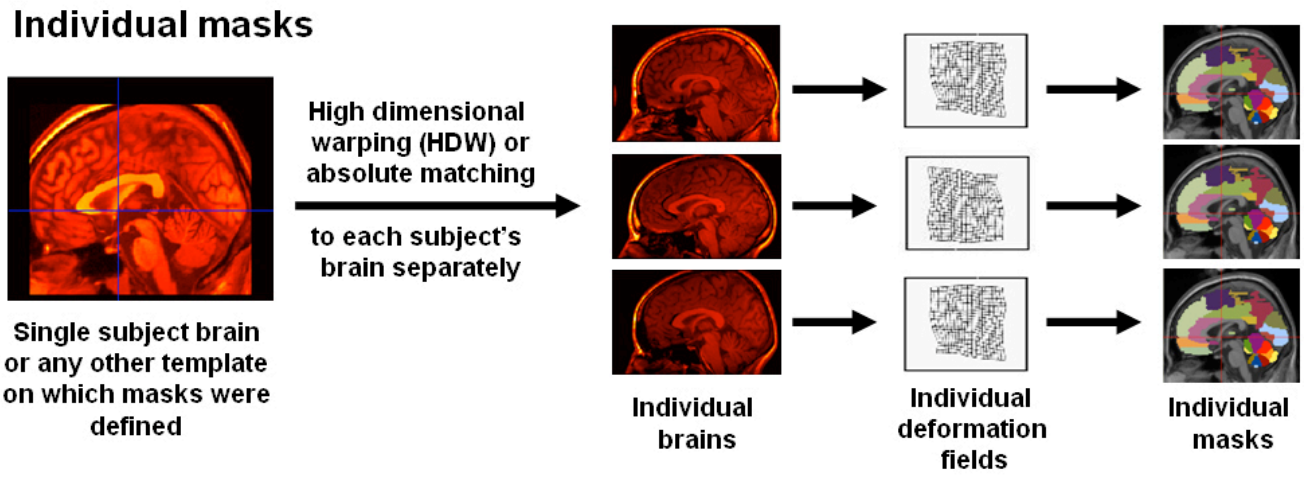

Figure 27: Processing steps used for construction of individual masks by our own parcellation approach. This figure illustrates the steps applied in our own parcellation approach to construct individual masks. The upper row shows the adjustment of the masks onto the brain of each subject under investigation. The steps to compute the volumes of the masks are analogue to that of Figure 26.

The masks we used were drawn by Tzourio-Mazoyer and colleagues (Tzourio-Mazoyer et al., 2002) on the single subject brain (Holmes et al., 1998). Beside the MARINA software (Walter et al., 2003; http://www.bion.de) these masks are also implemented in the Anatomical Automatic Labelling software (AAL; http://www.cyceron.fr/freeware/). This software can be used to label localised functional brain activations as well as structural brain differences. There also existing brain atlases that were derived from several subjects (http://www.fmrib.ox.ac.uk/fsl/data/atlas-descriptions.html).

2.2.11 Deformation based morphometry (DBM) and tensor based morphometry (TBM)

Beside voxel based morphometry there are two further morphometric analysis techniques that can be applied in SPM. The terms deformation based and tensor based morphometry (DBM and TBM, respectively) are used as reference to methods for studying brain shapes that are based on deformation fields obtained by nonlinear normalisation (warping) of brain images onto an atlas (template) image. When comparing groups of subjects, DBM uses deformation fields to identify differences in the relative positions of structures within the subjects' brains, whereas the term TBM is used to refer to those methods that localise differences in the local shape of brain structures (Ashburner & Friston, 2000; Ashburner et al., 1998). Note that DBM does not directly localise brain regions with different

shapes, but rather identifies those brain structures that are in relative different positions. In order to localise structures whose shapes differ between groups, some form of TBM is required to produce statistical parametric maps of regional shape differences (Ashburner & Friston, 2000).

The steps of analysis in DBM are presented in Figure 28. An example is shown for a single subject in one axial slice. The single object brain (image a) has been corrected for orientation and overall size to the template brain (c). Nonlinear normalisation removes most of the anatomical differences between the two brains by introducing local deformations to the object brain, which then (b) looks as similar as possible to the template. Note that these slices only represent two-dimensional information, whereas the method actually works in three dimensions. Image (e) shows the deformations applied to the object brain by a deformed grid and a magnification of the ventricles is displayed in (d). Analysis for DBM can be either multivariate using these x-y-z displacements of the entire 3-D deformation field or univariate using the local Jacobian determinant as a derivative of the field (f) (Gaser et al., 2001). For further information about DBM in general see Gaser, 2001; Gaser et al., 2001; Chung et al., 2001 and Ashburner et al., 1998. Whereas VBM is preferred in cross-sectional study designs, DBM and TBM is more suitable for longitudinal study designs.

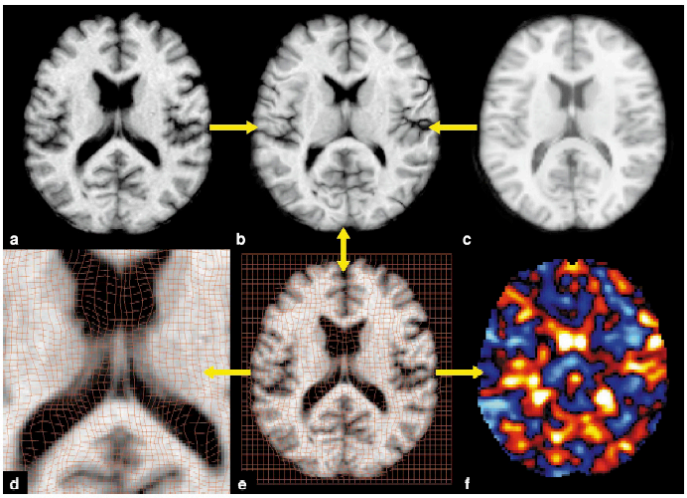

Figure 28: Steps of analysis in deformation based morphometry (DBM).
This figure illustrates the steps of analysis in Deformation Based Morphometry (DBM). An example is shown for a single subject in one axial slice. The single object brain (image a) has been corrected for orientation and overall size to the template brain (c). Nonlinear normalisation removes most of the anatomical differences between the two brains by introducing local deformations to the object brain, which then (b) looks as similar as possible to the template. Note that these slices only represent two-dimensional information, whereas the method actually works in three dimensions. Image (e) shows the deformations applied to the object brain by a deformed grid and a magnification of the ventricles is displayed in (d). Analysis for DBM can be either multivariate using these x-y-z displacements of the entire 3D deformation field or univariate using the local Jacobian determinant as a derivative of the field (f). Figure adopted from Gaser et al., 2001.

Tensor based morphometry (TBM) localises differences in the local shape of brain structures (Ashburner & Friston, 2000; Ashburner et al., 1998). A tensor obtained in TBM is a measure of local variability of brain structures (shape) that encodes the place, the magnitude, and the direction of this neuroanatomical variability. This kind of tensor should not be confused with the diffusion tensor obtained by diffusion tensor imaging (DTI) which is a measure of the diffusion of water molecules in

brain tissue. An example of such a tensor map obtained from TBM is shown in Figure 29. These tensor maps reveal the directional biases in normal cortical variability (n = 20 elderly normal subjects). Tensor maps can be used to visualise the complex patterns of gyral pattern variation at the cerebral cortex. Colour distinguishes regions of high variability (pink) from areas of low variability (blue). In (a) and (b) ellipsoidal glyphs indicate the principle directions of variation: they are most elongated along directions where there is greatest anatomical variation across subjects. Each glyph represents the covariance tensor of the vector fields that map individual subjects onto their group average anatomical representation. The resulting information can be leveraged to distinguish normal from anormal anatomical variants using random field algorithms and can define statistical distributions for feature labelling at the cerebral cortex. (c) Probabilistic confidence limits on normal anatomical variation: tensor field representation. Again, tensor maps reveal the preferred directions of cortical variation, after sulcal pattern correspondences are taken into account. Variability is greatest in the temporoparietal cortex. Confidence ellipsoids are shown, coloured by the determinant of the covariance tensor, which measures the magnitude of anatomical variability at each location (Thompson et al., 2001).

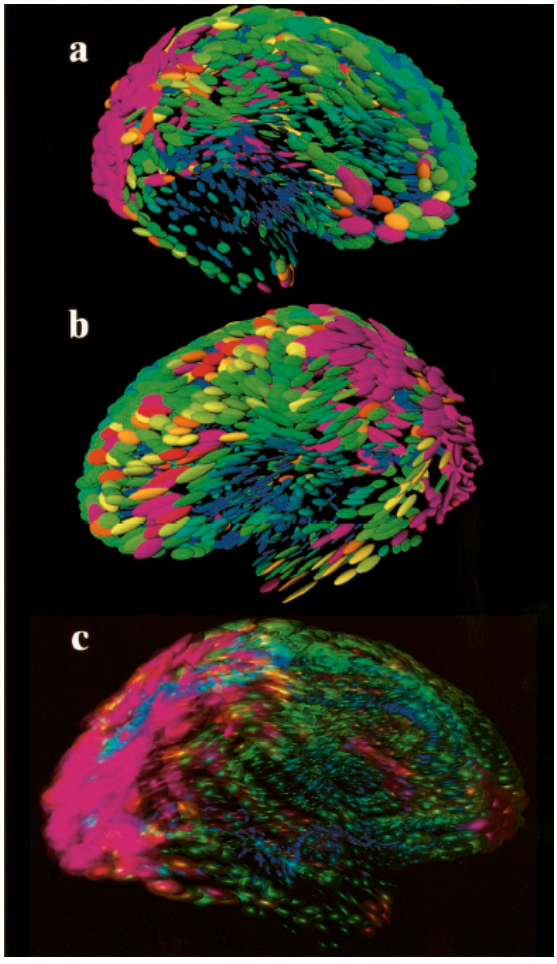

Figure 29: Tensor based morphometry (TBM) maps revealing the directional biases in normal cortical variability.
Tensor maps reveal directional biases in normal cortical variability (n = 20 elderly normal subjects). Tensor maps can be used to visualise the complex patterns of gyral pattern variation at the cerebral cortex. Colour distinguishes regions of high variability (pink) from areas of low variability (blue). In (a) and (b) ellipsoidal glyphs indicate the principle directions of variation: they are most elongated along directions where there is greatest anatomical variation across subjects. Each glyph represents the covariance tensor of the vector fields that map individual subjects onto their group average anatomical representation. The resulting information can be leveraged to distinguish normal from anormal anatomical variants using random field algorithms and can define statistical distributions for feature labelling at the cerebral cortex. (c) Probabilistic confidence limits on normal anatomical variation: tensor field representation. Again, tensor maps reveal the preferred directions of cortical variation, after sulcal pattern correspondences are taken into account. Variability is greatest in the temporoparietal cortex. Confidence ellipsoids are shown, coloured by the determinant of the covariance tensor, which measures the magnitude of anatomical variability at each location. Figure adopted from Thompson et al., 2001.

2.2.12 Cross validation of voxel based morphometry (VBM) with classical manual volumetric approaches and functional activations

There are several studies which validated the accuracy of VBM by comparing its results with that obtained from classical manual volumetric approaches (region of interest (ROI) measurements) and from functional data (Testa et al., 2004; Maguire et al., 2000; Mummery et al., 2000; Woermann et al., 1998, 1999; Richardson et al., 1997; Abell et al., 1999; Vargha-Khadem et al., 1998). Testa and colleagues compared ROI-based and VBM-based hippocampal measurements for the separation of 27 patients with Alzheimer's disease (AD) from 25 healthy elderly control subjects. They used receiver operating characteristic (ROC) curve to characterise the diagnostic power of the two different methods. The area under the curve (AUC), a measure of the diagnostic accuracy, was 0.89 for the ROI-based analysis and 0.96 for the VBM-based analysis. If both measures were combined, the AUC was 0.99 (out of maximal 1.0) means that from 100 diagnoses based on the hippocampal measures only one person will get the wrong diagnosis (Testa et al., 2004). Maguire and colleagues investigated the brains of taxi drivers in London with VBM and a pixel counting method (stereology) and obtained similar results from both methods (Maguire et al., 2000).

3 Original research articles

In the following three paragraphs I will present you three original research articles where the methods described in my Ph.D. thesis until now were applied in order to answer three different questions.

The first paper deals with gender-specific neuromorphological substrates of human visuospatial cognition independent of general intelligence. In this paper we will show evidence that beside the already known gender difference in visuospatial abilities and in functional brain activations during visuospatial processing (maybe indicating the use of different strategies between the genders) there are also neuromorphological differences between the genders in regions important for visuospatial information processing (i.e., parietal lobe).

In the second study, we investigated the influence of a single nucleotide polymorphism (SNP) (genetic mutation) in the gene that encodes for the most important cholesterol degrading enzyme in the brain. This enzyme is called cholesterol 24*S*-hydroxylase (CYP46) and degrades brain cholesterol to 24*S*-hydroxycholesterol. In the literature, this SNP is discussed as a potential risk factor for Alzheimer's disease (AD), although the evidence is not still conclusive. In contrast to the already published studies that investigated the influence of the CYP46 SNP in patients with AD and in healthy elderly control subjects, we investigated this potential AD risk factor in a population of healthy young Swiss subjects of Caucasian origin.

The last study investigated the diagnostic power and accuracy (sensitivity and specificity) of neuroanatomical measures obtained from computational structural neuroanatomy in distinguishing between healthy elderly control subjects, patients with amnestic mild cognitive impairment (MCI), and patients with Alzheimer's disease. These MRI-based morphometric measures can be used to diagnose and corroborate the general and differential dementia diagnosis.

3.1 Study 1: Sexual dimorphism in the parietal substrate of visuospatial cognition independent of general intelligence

Sexual dimorphism in the parietal substrate associated with visuospatial cognition independent of general intelligence

Jürgen Hänggi[a,b*], Andreas Buchmann[b], Christian R.A. Mondadori[c], Katharina Henke[d], Lutz Jäncke[a], and Christoph Hock[b]

[a] Division of Neuropsychology, Institute of Psychology, University of Zurich, Switzerland
[b] Division of Psychiatry Research, Psychiatric University Hospital, University of Zurich, Switzerland
[c] Neuropsychology Unit, Department of Neurology, University Hospital Zurich, Switzerland
[d] Department of Psychology, University of Bern, Switzerland

[*] Corresponding author: J.Hänggi (j.haenggi@psychologie.uzh.ch)

Corresponding author and main affiliation:

Jürgen Hänggi, Ph.D.
Division of Neuropsychology
Institute of Psychology
University of Zurich
Binzmuehlestrasse 14 / PO Box 25
8050 Zurich
Phone: 0041 44 635 73 97
Fax: 0041 44 635 74 09
Email: j.haenggi@psychologie.uzh.ch

Affiliations of the other authors:

Division of Psychiatry Research
Psychiatric University Hospital
University of Zurich
Lenggstrasse 31
8032 Zurich, Switzerland

Neuropsychology Unit
Department of Neurology
University Hospital Zurich
Frauenklinikstrasse 26
8091 Zurich, Switzerland

Department of Psychology
University of Bern
Muesmattstrasse 45
3000 Bern 9, Switzerland

Abstract

Gender differences in visuospatial cognition (VSC) with male advantage are frequently reported in the literature. There is evidence for sexual dimorphisms in the human brain, one of which postulates more grey matter (GM) in females and more white matter (WM) in males relative to total intracranial volume. We investigated the neuroanatomy of VSC independent of general intelligence (g) in gender-separated populations, homogenous in age, education, memory performance, a memory- and brain morphology-related gene, and g. VSC and g were assessed with the Wechsler adult intelligence scale. The influence of g on VSC was removed using a hierarchical factor analysis and the Schmid-Leiman solution. Structural high-resolution magnetic resonance images were acquired and analysed with voxel-based morphometry. As hypothesised, the clusters of positive correlations between local volumes and VSC performance independent of g were found mainly in parietal areas, but also in pre- and postcentral regions, predominantly in WM in males, whereas in females, these correlations were located in parietal and superior temporal areas, predominantly in GM. Our results suggest that VSC depends more strongly on parietal WM structures in males and on parietal GM structures in females. This sex difference might have to do with the increased axonal and decreased somatodendritic tissue in males relative to females. Whether such gender-specific implementations of the VSC network can be explained genetically as suggested in investigations into the Turner syndrome, or as a result of structural neural plasticity upon different experience and usage remains to be shown.

Introduction

Visuospatial cognition (VSC) may be defined as the ability to generate, retain, retrieve, and transform well-structured visuospatial images. Visuospatial abilities occupy a pivotal position in all models of human ability (Jäncke & Jordan, 2007). For example, most models of human abilities state that together with verbal abilities visuospatial cognition captures more variance than any other dimensions in large, representative batteries of ability tests (Thurstone, 1938). Visuospatial abilities have been measured with various tests such as form boards, block manipulation, paper-folding tasks, and mental rotation tests. Many of these tasks are used in contemporary intelligence tests as measures of performance or nonverbal intelligence (i.e., fluid intelligence) such as the block design task from the Wechsler adult intelligence scale – revised (WAIS-R) (Wechsler, 1981). According to the manual of the WAIS-R, the block design task measures visuospatial and motor skills and therefore indicates the degree of functioning of the parietal and frontal lobes (Wechsler, 1981; Warrington et al., 1986; Jäncke & Jordan, 2007). VSC is not a homogenous concept. It comprises at least the three different factors visuospatial perception, mental rotation, and spatial visualisation (Linn & Petersen, 1985). As

operationalised in our study, VSC encompasses all three of these factors. According to the current view, a fourth factor representing spatial navigation can be added to this three-factor solution (Jäncke & Jordan, 2007). To date, most functional neuroimaging-based research on these factors has focused on the cognitive domain of mental rotation. Important for mental rotation is the visuospatial ability of imagery through which the appearance of spatially rotated objects can be imagined (Jäncke & Jordan, 2007).

General intelligence, as operationalised by the psychometric factor termed g, is a theoretical construct describing individual differences in cognitive abilities assessed with psychometric tasks. This concept emerges from empirical observations of positively correlated performance in almost all cognitive tasks, no matter which cognitive domain is assessed (Spearman, 1904). Whether general intelligence is better viewed as one single factor or as several factors specific for cognitive subfunctions (Deary & Caryl, 1997) is still disputed. The g-factor comprises all these cognitive abilities in one common factor, although human general intellectual functioning includes more than sixty individual cognitive abilities (Caroll, 1993). The block design task is one of the highest g-loading tasks of the WAIS-R battery (Colom et al., 2006b); hence, this task is strongly confounded by the g-factor. The g-factor and the intelligence quotient (IQ) have been shown to be associated with structural brain differences that are mainly located in frontal and parietal lobes (Jung & Haier, 2007; Colom et al., 2006a, 2006b; Haier et al., 2004). Gender differences in the structures associated with the IQ were also reported (Haier et al., 2005).

The study of VSC or g in isolation from each other is hampered by the following problem. All intelligence measures tap g plus specific cognitive abilities and skills (Jung & Haier, 2007; Colom et al., 2006b; Jensen, 1998). This means that common intelligence measures deliver composite scores derived from both specific cognitive abilities and skills on one hand and g on the other hand. This implies that a particular performance in a cognitive domain results from a combination of g and domain specific abilities and skills. When either interested in g or domain specific abilities and skills one has to disentangle the contributions of these two cognitive concepts on a particular subject's performance. The investigation of VSC in isolation therefore requires controlling for the g-loading of the considered visuospatial measures. One way of achieving this is to remove g-specific variance shared by the remaining WAIS subtests (which together represent g) in order to reveal the specific visuospatial component of the considered measure. An appropriate statistical method for estimating the g-loading of any given cognitive measure is the hierarchical factor analysis obliquely rotated with an additional transformation called the Schmid-Leiman solution (Jensen, 1998; Schmid & Leiman, 1957; Wolff & Preising, 2005).

There is a large body of evidence showing that the parietal lobes are the most important brain structure

for spatial (including visuospatial) information processing. A comprehensive empirical review of 275 functional imaging studies in cognition unequivocally demonstrate that the parietal cortex in both hemispheres is involved in mental processes such as spatial working memory, spatial perception, spatial imagery, problem solving, attention on orientation, episodic memory encoding of spatial content, and motor skill learning (Cabeza and Nyberg, 2000). More direct support can be derived from functional imaging studies on mental rotation. These studies have reported consistent activations in the parietal cortex during mental rotation tasks (Jordan et al., 2001, 2002; Hugdahl et al., 2006; Unterrainer et al., 2000; Thomsen et al., 2000; Butler et al., 2006). Further evidence of the involvement of parietal structures in VSC is provided by studies investigating patients with parietal lesions. Such studies confirm the importance of the parietal cortex in VSC processing by showing that parietal lesions, such as those observed in patients with spatial neglect, Balint-Holmes' syndrome, Gerstmann's syndrome, and other spatial disorders, are accompanied by impairments in brain functions associated with spatial information processing (Vallar, 2007; Warrington et al., 1986).

Most studies investigating visuospatial abilities used mental rotation tasks of real 3D objects such as the figures of Shepard & Metzler (Shepard & Metzler, 1971). In the case of the block design task from the WAIS-R (Wechsler, 1981) employed in our study, the patterns presented on the cards and, once reconstructed using cubes, the corresponding patterns are actually only in 2D. Earlier studies revealed that there are no topological activation differences in mental rotation tasks regardless of whether 2D or 3D objects are used (Jordan et al., 2001), except that the magnitude of these activations was higher when using real 3D relative to 2D objects.

There are further functional imaging studies that support the theory of gender-specific strategies by showing different activation patterns between the genders when subjects are forced to use visuospatial transformations as required in mental rotation tasks (Cohen et al., 1996; Jordan et al., 2002; Hugdahl et al., 2006; Unterrainer et al., 2000). Whether these activation differences between the genders as well as the commonly observed higher performance in VSC in males are indeed evoked by a gender-specific neural implementation of the VSC processing network is still unknown. The usually observed advantage in VSC in males compared with females (Voyer et al., 1995), the different activation patterns between the genders during mental rotation tasks (Jordan et al., 2002; Hugdahl et al., 2006; Unterrainer et al., 2000), and the presence of sexually dimorphic brain structures globally in the whole brain (Gur et al., 1999; Allen et al., 2003) as well as locally in the parietal lobes (Nopoulos et al., 2000; Verchinski et al., 2000; Allen et al., 2003; Im et al., 2006) might indicate that the origin of the VSC performance differences between the genders observed in the general population (Voyer et al., 1995) is rooted in structural brain differences in the VSC processing network.

The present study aimed to establish the relationship between VSC independently of g on the one hand

and local GM and WM volume differences on the other hand, while simultaneously controlling for known genetic influences on brain morphology and memory by a single nucleotide polymorphism (SNP) of the gene encoding for the brain-derived neurotrophic factor (BDNF) (Pezawas et al., 2004; Egan et al., 2003). We applied the WAIS-R (Wechsler, 1981) to assess g and used a lower order factor, mainly comprised by the block design task performance, derived from the same intelligence test battery to assess VSC independent of g. We hypothesised that g-independent VSC correlates positively with GM and WM volume differences in the parietal lobes (Cohen et al., 1996; Jordan et al., 2001, 2002; Hugdahl et al., 2006; Unterrainer et al., 2000; Thomsen et al., 2000; Butler et al., 2006), preferentially in the spatial processing dominant right hemisphere (Harris et al., 2000; Warrington et al., 1986; Jäncke & Jordan, 2007) and more pronouncedly in males than females (Voyer et al., 1995). Stronger correlations for males were expected because, normally, males outperform females in VSC performance in the general population (Voyer et al., 1995).

The sexual dimorphism hypothesis suggested by Gur and colleagues postulates that in women, a smaller skull size is compensated during development by a relative increase in the somatodendritic tissue (reflected in GM) necessary for information processing, rather than being compensated for by connecting axons (reflected in WM) for transportation of information (Gur et al., 1999). Although this hypothesis was originally postulated globally, that is, for the whole brain, we applied it to the parietal lobe and linked it to VSC. Hence, we expected more structural correlates of VSC in the WM in males due to their relative decrease of somatodendritic tissue in the parietal lobes and due to their relatively larger brains, whereas in females we expected more structural correlates in the GM due to their relative increase of somatodendritic tissue in the parietal lobes and due to their relatively smaller brains.

Methods

Subjects: The 43 participants were drawn from a larger sample of 354 healthy young subjects (de Quervain et al., 2003). These 43 subjects participated in a functional magnetic resonance imaging (fMRI) study that investigated brain activity elicited by episodic memory tasks between different allele carriers (Mondadori et al., 2006). Our sample is homogenous with respect to age, education (in years), episodic memory performance, a memory- and brain morphology-related gene (see below), and general intelligence. Taking this age homogeneous sample limits/excludes the impact of maturational processes in younger subjects or early age-related neurodegenerative alterations in older subjects on our measures. The subjects reported no past or current psychiatric, neurological, and neuropsychological problems and denied taking illegal drugs or medication. All subjects gave written

informed consent to participate in the study after the nature and possible consequences of the study had been explained. The local ethics committee approved the experiment. The subjects were paid for participating in the study.

Neuropsychology: Domains of intelligence were assessed with the German version of the Wechsler Adult Intelligence Scale – Revised (WAIS-R) (Wechsler, 1981) [German version: Hamburg Wechsler Intelligenztest für Erwachsene – Revision 1991 (HAWIE-R)] (Tewes, 1991). We applied all eleven subtests from the WAIS-R and extracted, using hierarchical factor analysis (see below), general intelligence (g, the highest order factor) in order to control visuospatial cognition (VSC) performance (one of the lowest order factor). VSC independent of g is represented in the lowest order factor on which the block design task from the WAIS-R loads highest, with some small contributions from other WAIS-R subtests with visuospatial content. The block design task requires putting sets of cubes together to match patterns presented on cards. The faster the cubes are put together the more points are obtained. The maximum of raw scores is 51. We used raw scores because using standardised scores in our study would lead to a minimisation of the variance in the block design task performance because WAIS age categories are quite coarse; hence, most subjects would fall into the same category due to the limited age range. In order to rule out any gender differences in memory (especially working memory) capacity that might also influence VSC performance the Wechsler Memory Scale – Revised (WMS-R) in German (Härting et al., 1999) was also applied to control for potential gender-differences in memory performance.

Hierarchical factor analysis and the Schmid-Leiman solution: In order to account for the confounding effect in VSC performance by g, we conducted a hierarchical factor analysis with an additional Schmid-Leiman solution (SLS; Schmid & Leiman, 1957) with syntax written by others (Wolff & Preising, 2005). In short, we first used principal axis factoring with an oblique rotation (PROMAX rotation, kappa = 4) to do a hierarchical factor analysis. In this way we extracted the pattern matrices that represent only common variance of variables excluding unique variance. Note that principal factor analysis has to be used in this context, while the more common principal component analysis is not appropriate here because only the common variance of variables has to be isolated excluding unique contributions of variables. These pattern matrices were then entered into a higher (third) order hierarchical factor analysis with the Smith-Leiman solution (SLS). The Schmid-Leiman solution is a convenient tool with which to determine the independent influence of first and higher order factors on a set of primary variables and thus eases the interpretation of factors of differing levels (Wolff & Preising, 2005). Finally, the factor score coefficients were computed. This approach to factor analysis of the variables of the WAIS-R produces the highest-order factor as representing g and the next lower-order factors representing verbal, and performance (nonverbal)

intelligence quotients (IQs), with the lowest-order factors representing specific cognitive abilities and skills. The specific lowest-order factor on which the block design task loads highest was termed visuospatial cognition (VSC) independent of g.

MRI data acquisition: Magnetic resonance imaging (MRI) scans were acquired on a 3T Philips Intera whole body scanner (Philips, Best, the Netherlands) equipped with a transmit-receive body coil and a commercial eight-element head coil array. A volumetric 3D T1-weighted gradient echo sequence (FFE, fast field echo) scan was obtained with a measured spatial resolution of 1 mm x 1 mm x 1.5 mm (acquisition matrix 224 x 224 pixels) and a reconstructed resolution of 0.9 mm x 0.9 mm x 0.8 mm, echo-time TE = 2.3 ms, repetition-time TR = 20 ms, flip angle FA $\theta = 20°$. Scan time was about 10 min. MRI data acquisition and neuropsychological assessments took place within a four weeks period.

Pre- and postprocessing of MRI data: Image pre- and postprocessing and statistical analyses were performed with the statistical parametric mapping (SPM, version 5) software package (http://www.fil.ion.ucl.ac.uk/spm) using MATLAB 7.0.1 R14, SP1 (http://www.mathworks.com) on a Windows workstation. Based on the volumetric 3D T1-weighted structural MRI scans, which covered the whole brain, we applied voxel-based morphometry (VBM) (Ashburner and Friston, 2000) implemented in the VBM5 toolbox (http://dbm.neuro.uni-jena.de/vbm.html) for SPM5. With this approach we sought to verify our proposal that local differences in parietal gray (GM) and white matter (WM) volumes correlate with VSC performance independently of g. Because SPM5 enables image registration, tissue classification, and bias field correction within the same generative model (Ashburner & Friston, 2005), the procedure called optimised VBM (Good et al., 2001a; Senjem et al., 2005) is no longer needed when working with SPM5 (Ashburner & Friston, 2005). Additionally, a Hidden Markov Random Field (HMRF) model was used to enhance the segmentation process (Cuadra et al., 2005; http://dbm.neuro.uni-jena.de/vbm/markov-random-fields/). For spatial normalisation and tissue class segmentation the International Consortium For Brain Mapping (ICBM) 452 standard a priori maps were used. Images were modulated for the affine and nonlinear transformations.

Statistical analyses: For correlating local GM and WM volumes with the factor score coefficients of the lowest order factor "VSC independent of g", a factor mainly comprised by the performance in the block design task of the WAIS-R, we used multiple regression analysis based on the general linear model implemented in the SPM5 software package. We used the following measures as nuisance covariates: Total GM volume (TGMV) for GM analysis, total WM volume (TWMV) for WM analysis, and education, age, and handedness for both analyses. We also controlled for a single nucleotide polymorphism (SNP) because it has been shown that it influences brain morphology (Pezawas et al., 2004). This SNP occurs in the gene that codes for the brain-derived neurotrophic

factor (BDNF) (Egan et al., 2003). For the analysis of the pooled sample we additionally used gender as a nuisance covariate. Given our a priori hypotheses about the expected location of brain structural differences, we set the statistical height threshold to $p = 0.001$ (uncorrected for multiple comparisons) and the cluster extent threshold was set to $k = 50$ voxels. Additionally, we also report results that were corrected for multiple comparisons as well cluster sizes that were corrected for non-stationary smoothness. We applied a false discovery rate (FDR; $p = 0.05$) correction combined with a small volume correction using a sphere of 30 mm diameter.

We used the classical approach of voxel counting and consecutive chi-square (χ^2) testing as well as the lateralisation index (LI) tool (Wilke and Schmithorst, 2006; Wilke and Lidzba, 2007) to assess lateralisation differences between the genders in the brain structures that correlate with VSC independent of g. This new approach is based on threshold-dependent laterality curves and on combined bootstrap/histogram analysis. In the classic approach, we summed up all supra-threshold voxels in all clusters located in the parietal lobes. In the LI tool, we assessed the lateralisation index voxel-wisely in both parietal lobes using the non-thresholded correlation maps as input. Here, we report threshold-weighted mean LIs, i.e., more significant voxels were weighted stronger. The formula to compute the LI classically is: $LI = ((voxel_{left} - voxel_{right})/(voxel_{left} + voxel_{right}))$. A value of 1 indicates an absolute left lateralisation and a value of -1 indicates an absolute right lateralisation. It is important to note that these two approaches differ in several aspects; hence, their results may be different. To compare tissue type and gender we computed a tissue type index (TTI) based only on supra-threshold voxels according to the formula: $TTI = ((voxel_{GM} - voxel_{WM})/(voxel_{GM} + voxel_{WM}))$. Here, a value of 1 indicates exclusively GM voxels and a value of -1 indicates exclusively WM voxels.

Genotyping: Information on the polymorphic site was derived from the database of single nucleotide polymorphisms (dbSNP) established by the National Center for Biotechnology Information (http://www.ncbi.nlm.nih.gov/SNP/index.html). Genotyping procedure for the brain-derived neurotrophic factor (BDNF) gene has been described elsewhere (Egan et al., 2003). We decided to control for this SNP because it has been shown to influence not only memory performance, but also medial temporal and prefrontal brain morphology (Pezawas et al., 2004). Furthermore, when we regressed the BDNF genotypes against voxel-wise local GM and WM volumes we found a differential effect of this genotype on posterior parietal structures, i.e., decreased WM volumes in male BDNF val66met carriers. As suggested by functional neuroimaging studies on mental rotation, which have consistently revealed prefrontal activations in mental rotations tasks (Cohen et al., 1996; Jordan et al., 2001, 2002; Hugdahl et al., 2006; Unterrainer et al., 2000; Thomsen et al., 2000; Butler et al., 2006), there may also be structural correlates of the VSC network located in prefrontal brain regions.

Results

A summary of the demographic characteristics, cognitive indices, and compartmental brain volumes of the pooled study population and the gender-separated groups is depicted in Table 1. In brief, there were no significant differences between the genders with respect to age, education, block design task performance, full-scale intelligence quotient (FSIQ), handedness, and BDNF allele frequencies (all $p > 0.25$). As expected, males and females differed in their compartmental brain volumes. Males had significantly larger total grey (GM) and total white matter (WM) volumes than females (all $p < 0.0005$). In clear contrast to findings in the pertinent psychological literature (Voyer et al., 1995), neither performance in the block design tasks or the factor score coefficient of the VSC factor differed significantly between males and females in our study. There were no differences in memory capacity in any of the 12 subtests (the information and orientation test was omitted) of the WMS-R between the genders.

	Male (n = 18)				**Probability**	**Female (n = 25)**				**Total (N = 43)**			
	Mean	**S.D.**	**Minimum**	**Maximum**	**t- / χ^2-test**	**Mean**	**S.D.**	**Minimum**	**Maximum**	**Mean**	**S.D.**	**Minimum**	**Maximum**
Age (y)	22.2	2.2	19.0	27.0	p = 0.834	22.4	2.7	19.0	32.0	22.3	2.5	19.0	32.0
Education (y)	13.9	1.8	10.5	17.0	p = 0.791	14.0	1.4	12.0	17.5	14.0	1.6	10.5	17.5
Block design (raw)	42.3	6.2	30.0	50.0	p = 0.995	42.3	6.3	31.0	51.0	42.3	6.2	30.0	51.0
FSIQ	123.3	7.74	105.0	136.0	p = 0.820	124.0	11.4	98.0	137.0	123.7	9.9	98.0	137.0
TGMV (cm^3)	**810.3**	**60.4**	**713.2**	**946.6**	**p < 0.0005**	**743.4**	**54.5**	**628.7**	**886.7**	771.4	65.5	628.7	946.6
TWMV (cm^3)	**485.1**	**46.2**	**401.8**	**596.8**	**p < 0.0005**	**434.7**	**31.5**	**359.4**	**493.8**	455.8	45.4	359.4	596.8
TCSFV (cm^3)	368.1	73.3	268.7	491.8	p = 0.744	376.6	89.3	239.5	566.4	373.0	82.2	239.5	566.4
TICV (cm^3)	**1,663.1**	**128.3**	**1,396.0**	**1,906.9**	**p < 0.01**	**1,554.6**	**131.3**	**1,319.8**	**1,786.5**	1,600.3	139.6	1,319.8	1,906.9
	Frequency					**Frequency**				**Frequency**			
Handedness (r/l/a)	16 / 2 / 0				p = 0.333	22 / 1 / 2				38 / 3 / 2			
	Amino acids					**Amino acids**				**Amino acids**			
BDNF val66met	9 val/val	9 val/met	0 met/met		p = 0.267	17 val/val	7 val/met	1 met/met		26 val/val	16 val/met	1 met/met	

Significant differences between the genders are highlighted in bold (two-tailed t-test for independent samples and two-tailed ^{2}-test). Abbreviations: TGMV, total gray matter (GM) volume; TWMV, total white matter (WM) volume; TCSFV, total cerebrospinal fluid (CSF) volume; TICV, total intracranial volume; r, right; l, left, a, ambidexter; BDNF, brain-derived neurotrophic factor; val, valine; met, methionine; y, years; raw, raw data; S.D., standard deviation; FSIQ, full scale intelligence quotient.

Table 1. Demographic characteristics, cognitive indices, and compartmental brain volumes in the pooled sample and the gender-specific groups.

Positive correlations in the pooled sample

For a summary of all clusters found in the pooled sample see Table 2. In our pooled sample, we found clusters of positive correlations between local GM volumes and visuospatial cognition (VSC) independent of g in the left inferior parietal lobule / precuneus, left angular gyrus, left and right superior parietal lobule, and in both pre- and postcentral gyri (Fig. 1A-C and Table 2). Clusters of positive correlations between local WM volumes and VSC were found in the left and right angular gyrus, left inferior parietal lobule, right superior parietal lobule / precuneus, right postcentral gyrus, right superior temporal gyrus, and in the right supplementary motor area (Fig. 1A-C and Table 2).

Using the classical approach of voxel counting and chi-square (χ^2) tests, we further tested whether the voxels with positive correlations between local GM or WM volumes and VSC independent of g are

stochastically independent from the hemisphere (left or right). The distributions of significant correlations over hemispheres showed a tendency for grey matter voxels toward the left hemisphere (3,499 supra-threshold GM voxels in the left and 1,583 in the right hemisphere; lateralisation indices LI_{GM} = 0.38, left lateralisation) and for white matter voxels toward the right hemisphere (345 supra-threshold WM voxels in the left and 778 in the right hemisphere; LI_{WM} = -0.39; right lateralisation), which was statistically significant (χ^2 = 3.93; degree of freedom df = 1; p = 0.047). The LIs derived from the lateralisation tool and based on the non-thresholded correlation maps across the parietal lobes were LI_{GM} = -0.35, right lateralisation; LI_{WM} = 0.06, no lateralisation.

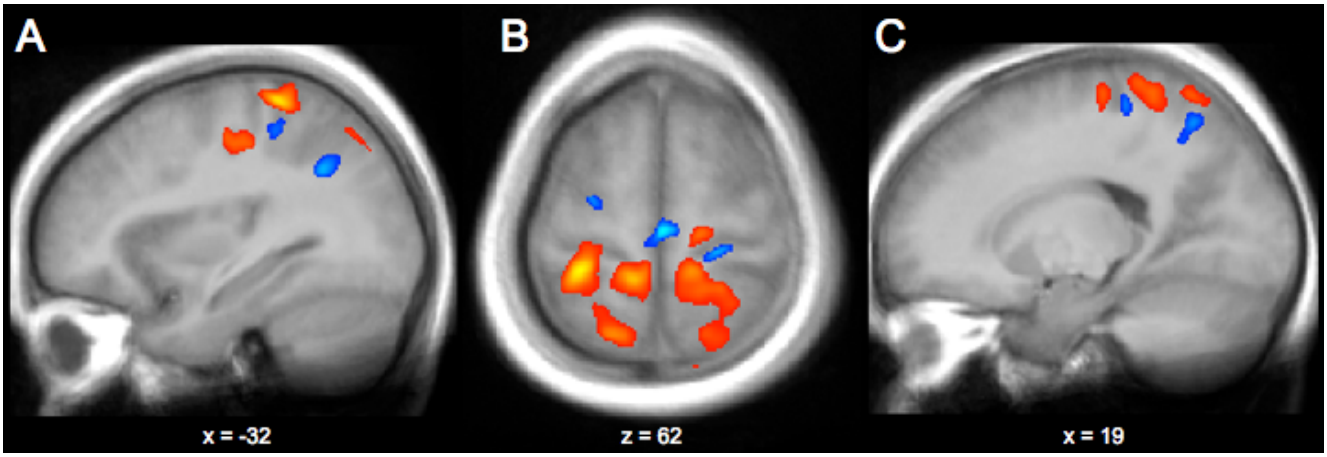

Figure 1. Positive correlations between local grey (red-yellow) or white matter (blue-lightblue) volumes and visuospatial cognition performance independent of general intelligence in the pooled sample. Structural brain differences were overlaid on the average template of the pooled sample. Coordinates are in Montreal Neurological Institute space. Slices are shown in neurological convention. Sagittal plane (A, C) and axial plane (B). Statistical parametric maps for the figures were thresholded with p < 0.005, uncorrected.

Tissue	Anatomical location	Hem.	Brodmann area	MNI coordinates x	y	z	Cluster extent k = 50 voxels	Nonstationarity corrected	t-value (df=36) p < 0.001 uncor.	SVC* p (FDR)	Correlation r	Effect size d
Gray matter	Postcentral gyrus / inferior parietal lobule	left	2	-30	-36	63	2654	4257	6.00	0.001	0.68	1.87
	Postcentral gyrus / precuneus	left	4	-10	-40	62			4.99	0.005	0.61	1.56
	Angular gyrus	left	39	-52	-62	37	479	1429	4.71	0.015	0.59	1.47
	Middle temporal gyrus / angular gyrus	left	39	-54	-65	22	173	418	4.51	0.018	0.58	1.41
	Postcentral gyrus	right	3	13	-37	62	1239	1636	4.31	0.010	0.56	1.35
	Superior parietal lobule	right	5	25	-44	64			3.83	0.010	0.51	1.20
	Superior parietal lobule	left	7	-17	-61	63	193	488	4.19	0.029	0.55	1.31
	Superior parietal lobule	right	40	39	-41	54	344	530	3.96	0.040	0.53	1.24
	Superior parietal lobule	right	7	30	-47	56			3.86	0.021	0.52	1.21
	Precentral gyrus	right	4	16	-23	63	135	231	3.82	0.041	0.51	1.19
	Middle occipital gyrus	right	19	30	-66	29	194	327	3.79	0.057	0.51	1.18
	Precentral gyrus	left	4	-32	-19	44	311	469	3.71	0.027	0.50	1.16
White matter	Lingual gyrus	right	17	8	-80	-4	221	238	4.37	0.017	0.56	1.36
	Postcentral gyrus	right	3	24	-30	58	209	428	4.31	0.050	0.56	1.35
	Supplementary motor area	right	6	2	-22	61	192	422	4.30	0.046	0.56	1.34
	Superior parietal lobule / precuneus	right	7	15	-63	51	314	639	4.25	0.025	0.55	1.33
	Angular gyrus	left	39	-35	-57	35	206	250	4.06	0.066	0.54	1.27
	Angular gyrus	right	40	36	-55	35	255	514	4.05	0.053	0.53	1.27
	Inferior parietal lobule	left	40	-44	-33	41	139	273	3.88	0.075	0.52	1.21
	Superior temporal gyrus	right	42	54	-37	13	142	169	3.80	0.077	0.51	1.19

Table 2. Correlations between local grey or white matter volumes and visuospatial cognition performance independent of general intelligence in the pooled sample. Effect size (d) was computed according to the formula: $d = 2r/(\sqrt{(1-r^2)})$. Abbreviations: df, degree of freedom; FDR, false discovery rate; Hem., hemisphere; MNI, Montreal Neurological Institute; SVC, small volume correction, * with a sphere of 30 mm diameter.

Positive correlations within the gender-separated groups

For a summary of all clusters found see Table 3 for females and Table 4 for males. In females, VSC performance correlated positively with local GM volumes in both superior parietal lobules, the right inferior parietal lobule, the left angular gyrus, the right cuneus, the lateral occipital cortex, the left superior temporal pole, and the right superior temporal gyrus (Fig. 2A-C and Table 3). With respect to WM in females VSC performance correlated positively with local WM volumes in the right precuneus, the left supramarginal gyrus, the right lingual gyrus, the left parahippocampal gyrus, and the left supplementary motor area (Fig. 2A-C and Table 3).

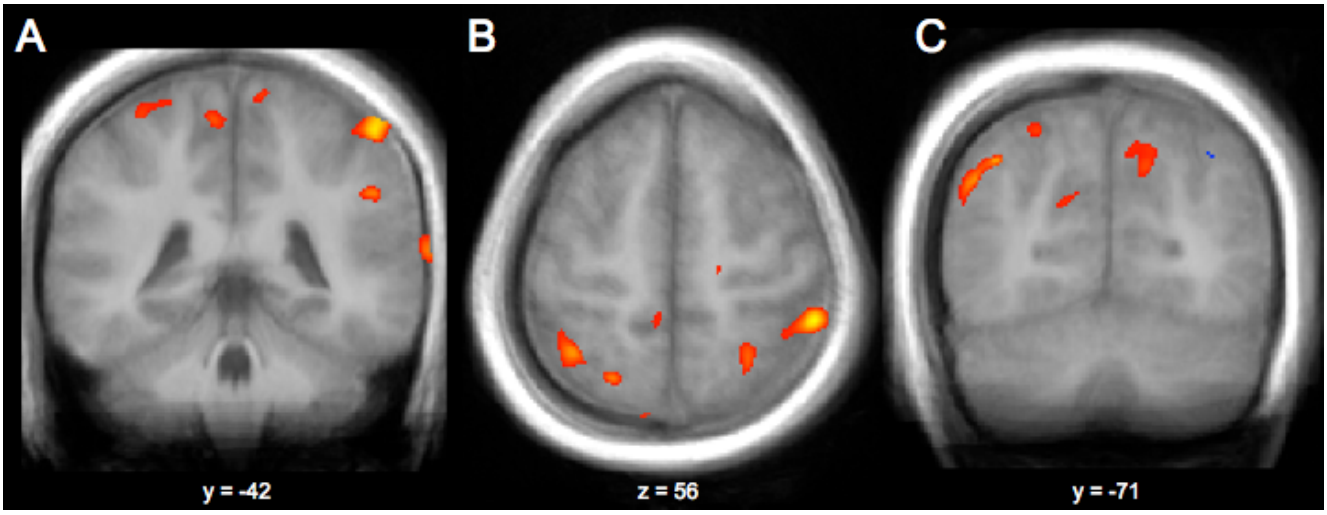

Figure 2. Positive correlations between local grey (red-yellow) or white matter (blue-lightblue) volumes and visuospatial cognition performance independent of general intelligence in females. Structural brain differences were overlaid on the average template of the females. Coordinates are in Montreal Neurological Institute space. Slices are shown in neurological convention. Coronal plane (A, C) and axial plane (B). Statistical parametric maps for the figures were thresholded with $p < 0.005$, uncorrected.

Tissue	Anatomical location	Hem.	Brodmann area	MNI coordinates x	y	z	Cluster extent k=50 voxels	Nonstationarity corrected	t-value (df=19) p < 0.001 uncor.	SVC* p (FDR)	Correlation r	Effect size d
Gray matter	Inferior / superior parietal lobule	right	40	53	-40	55	359	390	5.15	0.012	0.73	2.15
	Superior temporale pole	left	38	-35	25	-29	365	815	5.01	0.013	0.72	2.09
	Superior temporal gyrus	right	22	72	-37	10	319	353	4.88	0.016	0.71	2.04
	Superior parietal lobule	left	7	-19	-58	63	155	582	4.53	0.069	0.69	1.89
	Superior parietal lobule	left	7	-22	-62	56			3.82	0.066	0.62	1.59
	Superior parietal lobule	left	7	-36	-53	55	90	385	4.53	0.075	0.69	1.89
	Angular gyrus	left	19	-39	-70	38	366	1649	4.38	0.042	0.67	1.83
	Lateral occipital cortex	left	39	-49	-67	33			4.35	0.029	0.67	1.81
	Angular gyrus	left	39	-51	-61	38			4.11	0.033	0.65	1.71
	Cuneus	right	19	1	-86	28	140	104	4.01	0.057	0.64	1.67
White matter	Lingual gyrus	right	18	7	-79	-3	167	281	4.95	0.021	0.72	2.06
	Supplementary motor area	left	6	-4	-15	52	88	315	4.74	0.077	0.70	1.98
	Precuneus	right	7	16	-60	49	136	461	4.44	0.082	0.68	1.85
	Parahippocampal gyrus	left	19	-18	-47	0	67	145	4.09	0.149	0.65	1.71
	Supramarginal gyrus	left	40	-43	-34	41	93	187	4.04	0.096	0.64	1.68

Table 3. Correlations between local grey or white matter volumes and visuospatial cognition performance independent of general intelligence in females. Effect size (d) was computed according to the formula: $d = 2r/(\sqrt{(1-r^2)})$. Abbreviations: df, degree of freedom; FDR, false discovery rate; Hem., hemisphere; MNI, Montreal Neurological Institute; SVC, small volume correction, * with a sphere of 30 mm diameter.

In males VSC performance correlated positively with local GM volumes in the left postcentral gyrus / precuneus, the right occipito-parietal cortex, the right paracentral lobule, and the right precentral gyrus / middle frontal gyrus (Fig. 3A-C and Table 4). With respect to WM in males VSC performance correlated positively with local WM volumes in the right superior and inferior parietal lobule, both postcentral gyri, the right precentral gyrus, both angular gyri, and both middle frontal gyri (Fig. 3A-C and Table 4).

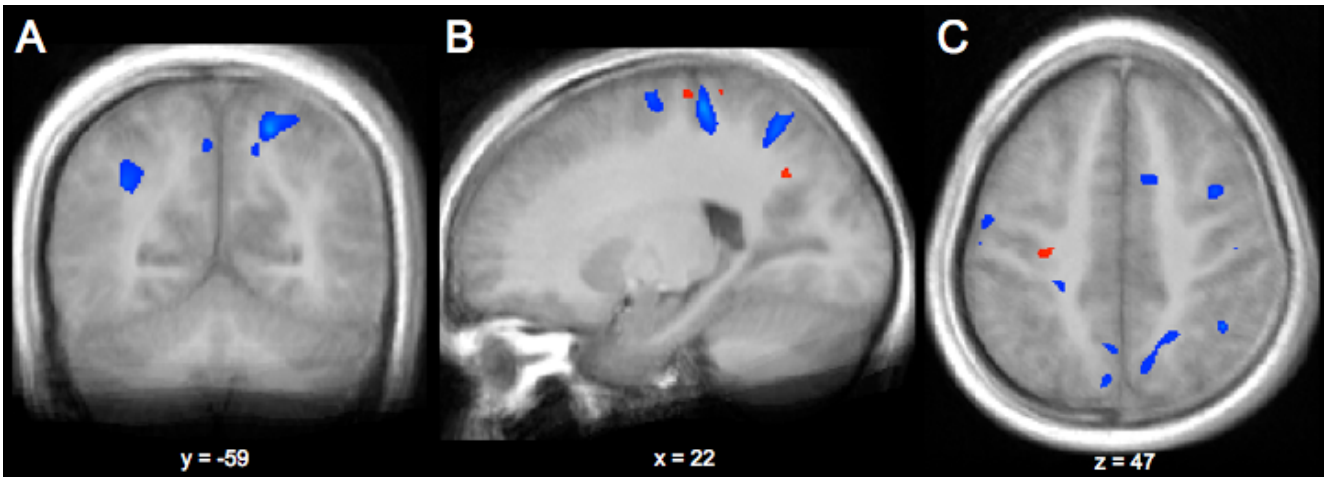

Figure 3. Positive correlations between local grey (red-yellow) or white matter (blue-lightblue) volumes and visuospatial cognition performance independent of general intelligence in males. Structural brain differences were overlaid on the average template of the males. Coordinates are in Montreal Neurological Institute space. Slices are shown in neurological convention. Coronal plane (A), sagittal plane (B), and axial plane (C). Statistical parametric maps for the figures were thresholded with $p < 0.005$, uncorrected.

Tissue	Anatomical location	Hem.	Brodmann area	MNI coordinates x	y	z	Cluster extent k=50 voxels	Nonstationarity corrected	t-value (df=12) p < 0.001 uncor.	SVC* p (FDR)	Correlation r	Effect size d
Gray matter	Occipito-parietal cortex	right	7	27	-63	30	315	2984	7.44	0.007	0.88	3.72
	Paracentral lobule	right	5	7	-33	53	571	1360	5.97	0.017	0.83	2.99
	Postcentral gyrus / preuneus	left	3	-9	-40	64	320	875	5.33	0.04	0.80	2.67
	Precentral / middle frontal gyrus	right	9	40	4	32	133	643	4.98	0.081	0.78	2.49
White matter	Post- / precentral gyrus	right	4	27	-28	59	741	4674	11.1	0.0002	0.94	5.55
	Superior parietal lobule	right	7	19	-59	53	407	1692	7.21	0.010	0.87	3.61
	Inferior parietal lobule	right	40	41	-51	49	56	961	6.44	0.023	0.85	3.22
	Postcentral gyrus	right	3	48	-19	53	167	795	5.71	0.050	0.82	2.86
	Precentral gyrus	right	6	47	-1	37	122	552	5.56	0.053	0.81	2.78
	Middle frontal gyrus	right	6	36	2	45	101	432	5.43	0.058	0.81	2.72
	Middle frontal gyrus	left	9	-39	29	27	76	288	4.84	0.128	0.77	2.42
	Angular gyrus	left	39	-35	-58	33	224	537	4.8	0.058	0.77	2.40
	Angular gyrus	right	40	34	-51	34	160	224	4.78	0.120	0.77	2.39
	Postcentral gyrus	left	1	-51	-20	58	60	200	4.62	0.058	0.76	2.31

Table 4. Correlations between local grey or white matter volumes and visuospatial cognition performance independent of general intelligence in males. Effect size (d) was computed according to the formula: $d = 2r/(\sqrt{(1-r^2)})$. Abbreviations: df, degree of freedom; FDR, false discovery rate; Hem., hemisphere; MNI, Montreal Neurological Institute; SVC, small volume correction, * with a sphere of 30 mm diameter.

The distributions of significant correlations over hemispheres in females showed a slight tendency for grey matter voxels toward the left hemisphere (611 supra-threshold GM voxels in the left and 499 in the right hemisphere; $LI_{GM} = 0.10$, left lateralisation), but a moderate tendency for white matter voxels

toward the right hemisphere (93 supra-threshold WM voxels in the left and 136 in the right hemisphere; LI_{WM} = -0.19; right lateralisation), which was not statistically significant (χ^2 = 0.51; df = 1; p = 0.475). In males, the distributions of significant correlations over hemispheres showed no tendency for GM voxels (320 supra-threshold GM voxels in the left and 315 in the right hemisphere; LI_{GM} = 0.008, no lateralisation), but a strong tendency for WM voxels toward the right hemisphere (284 supra-threshold WM voxels in the left and 1,531 in the right hemisphere; LI_{WM} = -0.69; right lateralisation), which was statistically significant (χ^2 = 5.37; df = 1; p = 0.020). When lateralisation was measured across the whole parietal lobes with the LI tool, LIs were as follow: for grey matter LI_{Female} = -0.20 and LI_{Male} = -0.16; and for white matter LI_{Female} = -0.12 and LI_{Male} = 0.45.

Tissue type indices (TTIs), which assess the relation between tissue type and gender, revealed a tendency for GM in the left (TTI = 0.74), the right (TTI = 0.57), and in the combined hemispheres (TTI = 0.66) in females. In males, there was no tendency for WM in the left hemisphere (TTI = 0.06), but a strong tendency for WM in the right and combined hemispheres (TTI = -0.66 and TTI = -0.48, respectively). Hence, there was a significant difference in the distributions of tissue types between genders in the left hemisphere (χ^2 = 5.95; df = 1; p = 0.015), and highly significant differences in the right and combined hemispheres (χ^2 = 14.06; df = 1; p = 0.0001 and χ^2 = 12.84; df = 1; p = 0.0003, respectively).

Negative correlations

Since we expected only positive correlations due to the literature and for theoretical reasons, i.e., negative correlations are rarely reported in the structural neuroimaging literature and are difficult to explain, we did not hypothesised negative correlations a priori. Nevertheless, we also assessed negative correlations between VSC independent of g and local GM and WM volumes and report these correlations for completeness. Generally, clusters of negative correlations were not as frequent as clusters of positive correlations, smaller in size, less significant than the clusters of positive correlations, and not located in our a priori predicted brain regions. In the pooled sample, clusters of negative correlations between VSC and local brain volume were found in the right lingual gyrus, right lateral occipital cortex, and in both middle frontal gyri (MFG) for GM and in the left anterior superior temporal gyrus (STG) for WM. In females, clusters of negative correlations were found in the left pars opercularis, left premotor cortex (PMC), and in the right MFG for GM and in the right STG, left supplementary motor area, left postcentral gyrus, and in the right PMC for WM. In males, clusters of negative correlations between VSC and local brain volume were found bilaterally in the occipital pole, left frontal pole, left MFG, and in both lingual gyri for GM and in the left superior and right lateral occipital cortex, and in the right frontal pole for WM.

Discussion

We used voxel-based morphometry (VBM) to investigate the neuroanatomical substrates of visuospatial cognition (VSC) independent of general intelligence (g) in gender-separated populations. As hypothesised, we found clusters of positive correlations between VSC independent of g and local grey (GM) and white (WM) matter volumes, mainly in the parietal lobes, but also in pre- and postcentral regions in the pooled sample. When genders were analysed separately, the clusters of correlations between local volumes and VSC were found in males in parietal, pre- and postcentral areas, predominantly located in WM, whereas in females, these correlations were found in parietal and superior temporal areas, predominantly located in GM. The clusters were lateralised in such a way that there was a preponderance of clusters in the left hemisphere in females and in the right hemisphere in males.

The following three questions will be discussed in detail below: (1) is connectivity among parietal areas more important in the male than in the female brain? (2) Does the preponderance of clusters of correlations between local tissue volumes (mainly GM in females and WM in males) and VSC independent of g in the case of females in the left hemisphere and in the case of males in the right hemisphere point to a gender-specific lateralisation of the VSC processing network? (3) Is the involvement of regions associated with motor or somatosensory information processing such as the pre- and postcentral gyri indicative of a differential or additional neural recruitment of a motor or even a somatosensory structure in the VSC processing network in males compared with females?

Gender differences in brain structures correlated with visuospatial cognition independent of g

Whether connectivity of parietal areas is more important in males than females can be considered from a theoretical point of view. In a neural network, neural interconnectivity, which is physiologically implemented as fibre bundles and hence reflected in WM structures, between the distant processors, which are physiologically implemented as assemblies of neurons and hence reflected in GM structures, might be more important in the male than in the female brain to due the relative decrease in parietal somatodendritic tissue in males compared with females as well as due to the larger male brain. This is the view taken by Gur and colleagues in their sexual dimorphism hypothesis that refers to the brain as a whole. The sexual dimorphism hypothesis proposes that the smaller skull size of women is compensated during development by a relative increase in the somatodendritic tissue (reflected in GM) necessary for information processing, rather than being compensated by connecting axons (reflected in WM) for transportation of information (Gur et al., 1999). This hypothesis was initially postulated globally and independently of any cognition. When it is applied locally to the parietal lobes this hypothesis can be linked to VSC performance.

The ‘parietal sexual dimorphism hypothesis of VSC (independent of g)’ was strongly corroborated by our data. Clusters of positive correlations between VSC performance and local brain volumes were predominantly located in WM (reflecting increased connectivity) in males, whereas in females these clusters were predominantly located in GM (reflecting increased somatodendritic tissue). Other studies lend support to our finding by showing that males and females differ in their global, neural, compartmental ratios. Chen and colleagues demonstrated that men have a higher WM to total intracranial volume (ICV) ratio, whereas women have a higher GM to ICV ratio (Chen et al., 2007), and in another study, larger re-scaled GM volumes in females and larger re-scaled WM volumes in males were reported, while the re-scaled total brain and cerebrospinal fluid (CSF) volumes did not show any significant gender effect (Luders et al., 2005). Kruggel showed that the relative amount of GM is slightly higher in female brains, which is also reflected in the lower ratio of GM/WM in males (Kruggel, 2006). Further evidence of larger relative WM volumes in males and GM volumes in females was reported in other studies (Lemaître et al., 2005; Gur et al., 1999), although there are also conflicting findings, at least as far as GM volumes are concerned (Good et al., 2001b).

At a lobar level, the parietal lobe has been shown as a whole to be highly sexually dimorphic for WM volume (Allen et al., 2003). In that study, the GM/WM ratio effect size for the right parietal lobe was the largest for any of the regions measured, as corroborated by Nopoulos and colleagues (Nopoulos et al., 2000), who showed that the most sexual dimorphic region, that is, with proportionally more GM in females, was the right parietal lobe. Verchinski and colleagues found increased GM density in parietal areas in women compared with men (Verchinski et al., 2000). Im and colleagues used surface-based morphometry and found that women compared with men also showed increased cortical thickness in the parietal lobes (Im et al., 2006), whereas Luders and coworkers used the cortical pattern matching method (Thompson et al., 2000) and revealed increased gyrification (cortical complexity) in women than in men in parietal and frontal regions (Luders et al., 2004). Developmental studies show that, on one hand, males have a 19.1% reduction in GM volume between 6 and 18 years of age compared with a 4.7% reduction in females, and on the other hand, that males have a 45.1% increase in WM volume and a 58.5% increase in corpus callosum area compared with 17.1% and 27.4% increases in females, respectively (de Bellis et al., 2001).

Most visuospatial tasks are performed under time constraints, meaning that faster processing is beneficial, depending of course on the extent of any speed-accuracy trade-off, because more points are obtained, as reflected in the block design task. Increased WM volume that reflects increased interconnectivity might subserve increased speed of information transfer between the parietal visuospatial processing network nodes and hence, resulting in higher visuospatial task performance in males compared with females as ordinarily observed in the general population. This only happens if

increased interconnectivity is implemented by myelin thickening or by increased axonal diameters. Otherwise, if increased connectivity is realised by an increased number of axons or by longer distances of the axons, a decrease in speed of information transfer must be expected. Unfortunately, the cellular basis of the macroscopically observed structural brain differences cannot be investigated by structural neuroimaging. Therefore, we were unable to determine whether increased WM volumes in parietal areas correlated with VSC observed in males are evoked by myelin thickening of the axons or by an increase in the number and distance of the axons. Diffusion tensor MRI might provide information on this issue.

Gender-specific lateralisation of brain structures correlated with visuospatial cognition independent of g

Besides the single dissociation between the genders found for the GM (more pronounced in females) and WM (more pronounced in males) parietal volumes correlated with VSC independent of g, a double dissociation emerged from the analysis of lateralisation of these volumetric brain differences. In females, the GM clusters correlated with VSC were mainly located in the left hemisphere, whereas in males the WM clusters were mainly located in the right hemisphere. The general view is that there is a right-hemispheric dominance for visuospatial processing and a left-sided dominance for language, while the relative extent of lateralised domain dominance is greater for language functions. Therefore, our findings might help to explain the generally observed higher level of visuospatial processing performance in males (Voyer et al., 1995) by showing that in females, the parietal areas in the spatial processing non-dominant, left hemisphere seem to be more involved in visuospatial processing compared with males whose visuospatial processing relies more on a parietal network in the right hemisphere. We are not aware of any functional imaging study that supports this pattern of lateralisation. The question of lateralisation is further complicated by the fact that there are laterality shifts in spatial processing depending on the menstrual cycle (Rode et al., 1995). Furthermore, one electroencephalographic (EEG) study revealed that a simple two-dimensional mental rotation task was associated with more left-parietal than right-parietal activation in men and more right-parietal than left-parietal activation in women (Roberts & Bell, 2003), the opposite lateralisation pattern of the one observed in our study. The complex three-dimensional mental rotation task in the same study was associated with greater right-parietal than left-parietal activation in both genders (Roberts & Bell, 2003). It is important to note that the relationship between EEG power and GM and WM volumes is still uncharacterised and that the performance in the complex three-dimensional mental rotation task was not matched between the genders. Whether the right hemisphere is the dominant side for visuospatial processing at all is still a matter of controversy. Functional imaging studies consistently

revealed almost bilateral parietal activations during mental rotation tasks (Jäncke & Jordan, 2007; Cohen et al., 1996; Jordan et al., 2001, 2002; Hugdahl et al., 2006; Unterrainer et al., 2000; Thomsen et al., 2000; Butler et al., 2006; Harris et al., 2000).

The two different approaches to compute lateralisation indices applied in our study revealed discrepant results. This discrepancy is mainly derived from the inclusion of voxels correlated at the sub-threshold level in the computation of the LIs with the LI tool. Since we were only interested in supra-threshold correlations, we based on the LIs that were derived from the classical approach of voxel counting. This classical approach revealed a weak left lateralisation of GM voxels in females (LI = 0.10) and no lateralisation of GM voxels in males (LI = 0.008), whereas there was a weak-to-moderate right lateralisation of WM voxels in females (LI = -0.19) and a strong right lateralisation of WM voxels in males (LI = -0.69). Therefore, VSC processing seems to be more dependent on WM parietal structures in the right than the left hemisphere, at least in males for whom the difference between the number of significantly correlated voxels in the left and right hemisphere was statistically significant ($p = 0.020$).

Gender differences in the visuospatial cognition processing strategy

A number of brain structures correlated with VSC independent of g. Leaving aside the clusters located in the parietal lobes, the clusters found in pre- and postcentral gyrus in males might reflect a motor (or even a somatosensory) processing component in VSC in general, similar to what was specifically proposed for mental rotation tasks by other researchers. Kosslyn and colleagues (Kosslyn et al., 1998, 2001) suggest that such a motor, or egocentric strategy, results when people mentally rotate a visual mental image in the same way they rotate an actual object physically. They found activations in the primary motor area when subjects mentally rotated a hand compared with rotating other objects mentally (Kosslyn et al., 1998, 2001). Besides the already mentioned WM and GM clusters that positively correlated with VSC independent of g located in the pre- and postcentral gyri of males, further clusters supporting a motor component in visuospatial processing in males were found in the GM of the right paracentral lobule and in WM of the right and left middle frontal gyrus (see Table 4). In females, there was only one such motor-related cluster located in the left supplementary motor area (see Table 3).

Other functional imaging studies support the theory of gender-specific strategies by showing different activation patterns when subjects are forced to use visuospatial transformations as required in mental rotation tasks (Jordan et al., 2002; Hugdahl et al., 2006; Unterrainer et al., 2000). Other authors suggested that males use a “gestalt” strategy and females use a “serial” reasoning strategy when approaching mental rotation tasks (Thomsen et al., 2000), reminiscent of the earlier speculations about “holistic” and “analytic” processing strategies in the psychological literature. This means that males

generally tend to use more effective visuospatial holistic strategies in which the object is mapped in the mind and then rotated as a whole, and that females tend to prefer less efficient analytic strategies that result in a more piecemeal (analytic) mental rotation process. Butler and colleagues (Butler et al., 2006) referred to more effortful and conscious "top-down" (analytic) processing in females and to more effective and unconscious "bottom-up" (holistic) processing in males. In contrast to the motor, or egocentric strategy, proposed by Kosslyn and colleagues (Kosslyn et al., 1998, 2001), which is supported by our findings, the "holistic" (bottom up) and "analytic" (top down) strategy distinction (Butler et al., 2006) would imply that structural correlates of VSC should be expected in the prefrontal cortex in females due to their analytic strategy in visuospatial information processing. This expectation is not supported by our structural data, although functional studies in mental rotation tasks revealed strong evidence of activation differences in prefrontal brain areas between genders (Thomsen et al., 2000; Hugdahl et al., 2006), hence supporting the "holistic" (bottom up) strategy in males and the "analytic" (top down) strategy in females. In order to investigate different cognitive processing strategies in mental rotation and VSC, functional imaging techniques are more suitable than structural methods.

Possible mechanisms mediating a gender-specific implementation of the VSC processing network

To explain the parietal sexual dimorphism of VSC independent of g, biological (genetic, hormonal, evolutionary) and environmental (spatial activities, socialisation) factors are often discussed (Casey et al., 1999; Casey, 1996; Kimura, 1999). Genetic and hormonal factors may exert considerable effects on the VSC processing network. For example, females with Turner syndrome (X-chromosome deficiency) are impaired in visuospatial information processing and have structural anomalies in the parietal lobes (Brown et al., 2004; Molko et al., 2003, 2004), therefore X-chromosome-linked influences on parietal structures have to be assumed, and might help to further elucidate the observed gender-specific pattern of structures correlated with VSC, i.e., GM in females versus WM in males. Besides genetic factors, sexual hormones exert a considerable effect on cognitive performance, at least in females (Sherwin, 2003; Rode et al., 1995; Bayer et al., 2008), and might modulate GM and WM volumes even in the parietal lobes (Goldstein et al., 2001).

However, to explain the structural brain differences between genders from an environmental point of view, we would like to highlight the influence of regular training and frequent usage, as shown in other contexts by Draganski and colleagues (Draganski et al., 2004, 2006). These two seminal studies indicate that learning- and training-induced cortical plasticity is also reflected at the structural level. With respect to the time scale, such structural changes are already detectable 7 days after training commencement (Driemeyer et al., 2008) and also in older subjects (Boyke et al., 2008). The impact of

these environmental factors during longer time periods was also shown in other populations, for example, in taxi drivers of London (Maguire et al., 2000), in professional musicians (Gaser and Schlaug, 2003; Münte et al., 2002), and in mathematicians (Aydin et al., 2007). The direction of cause and effect is not yet fully understood in these populations, although the positive correlations between GM density and expertise point to a preference of environmental over genetic explanations.

The structural brain differences found in our study might reflect the simple fact that boys move more frequently (and faster) than girls (Campbell & Eaton, 1999); hence, boys encounter more differentiated environments (and faster alterations) that place greater demands on visuospatial information processing. These gender-specific differences in locomotion probably affect visuospatial processing abilities, that is, boys may acquire different strategies and/or more experience in visuospatial information processing, which in turn modulates parietal lobe structures. Further studies revealed that gender-stereotyped space-related activities predict visuospatial performance and that females improve in (visuo-)spatial information processing performance when engaged in male-associated space-related activities (e.g., video-games and sports) (Signorella et al., 1989; Devlin, 2004; Ginn & Pickens, 2005).

The cellular basis of these structural alterations is still not fully understood and cannot be investigated using structural neuroimaging methods. Such events may include synaptogenesis, dendritic expansion, myelin thickening, increased neuronal sizes, or the genesis of glial or even neuronal cells. We prefer to relate our finding of macroscopic brain differences to changes in myelo- and cytoarchitectonics because it has been shown that the T1-weighted intensity profiles in structural MRI are best explained by a weighted sum of myelo- and cytoarchitectonic profiles (Eickhoff et al., 2005b). Imaging results have to be compared with histologic data for the identification of the structural basis at the microscopic level.

Our finding in the context of a parieto-frontal integration theory of intelligence

According to Jung and Haier, there is converging evidence derived from functional and structural neuroimaging studies for a parieto-frontal integration theory (P-FIT) of intelligence (Jung and Haier, 2007). We also evaluated the neuroanatomy of VSC performance uncorrected for g. This analysis revealed only a quantitative difference in the correlates of VSC uncorrected for g compared with the analysis for which VSC was corrected for g. Particularly, there were less and smaller parietal clusters when general intelligence variance was not removed. Actually, we expected any involvement of prefrontal brain regions when VSC is not controlled for g because it has been shown that from all WAIS-R subtests the block design task loads highest on the g-factor on the one hand (Colom et al., 2006a) and prefrontal brain regions were proposed to be involved in the network of intelligence on the other hand (Jung and Haier, 2007). We found correlates of VSC (corrected as well as uncorrected for

g) mainly in the parietal lobes, whereas Colom and colleagues found correlates of the block design task performance (uncorrected for g) across all lobes with a preponderance in the parietal and frontal lobe, but also in subcortical and limbic structures (Colom et al., 2006a). In view of the high g-loading of the block design task, it is really surprising that the results differ only slightly between the analysis for which g was controlled for compared with the analysis where intelligence variance was not removed. The high correlation between the block design task and g means that much variance was partialised out when VSC was controlled for g, so the results should look different. However, the sample sizes are almost equal between our (N = 43) and the study of Colom and colleagues (N = 48), whereas the age ranges are quite different between the studies (19-32 years in our and 18-84 years in the Colom study) and might in part be responsible for the discrepant results. Beside the age factor, there are methodological differences between these two studies (SPM2 vs. SPM5; density vs. volume; no HMRF-weighting vs. HMRF-weighting; MR images from one scanner vs. images from two different scanners). Further differences between the results of the two studies could be explained by differences in memory performance and the more homogenous nature of our sample with respect to other demographical measures such as education. In a combined magnetic resonance spectroscopy (MRS) and morphometry study, block design task performance and global GM volume were stronger correlated in females (r = 0.45) than in males (r = 0.29), whereas block design task performance and global WM volume were correlated positively in males (r = 0.25) and weakly negatively in females (r = -0.08) (Jung et al., 2005), results that are consistent with the sexual dimorphism hypothesis. The *N*-acetylaspartate (NAA) concentration in a left occipito-parietal WM region was strongly correlated with block design task performance in females (r = 0.68), whereas these measures were not correlated in males (r = 0.05) (Jung et al., 2005). Although these correlations differ between the genders, it is still unknown for what NAA is a marker for; hence, we did not tried to interpret these correlations.

The current study contributes to a growing body of evidence demonstrating that even if gender is not associated with differences in VSC performance (in our study independent of g), the neural substrate of VSC is different. In future studies, it would be interesting to dissect the interplay between the genetic/hormonal (nature) and exposure/usage (nurture) basis on the parietal lobe structures correlated with VSC performance independent of g.

Acknowledgments

We thank H.-G. Wolff for his syntax and the help with the Schmid-Leiman solution and acknowledge the participation of the subjects in our study. The study was supported by the Swiss National Science Foundation (3100-067114 to K.H.), by the EU contract LSHM-CT-2003-503330 (APOPIS), and by

the National Centre of Competence in Research on Neural Plasticity and Repair (NCCR, grant to C.H.). We also thank Marcus Cheetham for improving the English manuscript. Jürgen Hänggi expresses his thanks to the Handschin Foundation and the Jubilee Foundation of the Bank of the Canton Basle-Country for their support, and for the grants received from the University of Zurich and from the Canton Basle-Country.

Author contributions

K.H., A.B. and J.H. proposed the project. K.H., A.B., C.R.A.M. and J.H. planned the study and acquired the behavioural and imaging data. J.H. preprocessed and analysed the data and wrote the preliminary version of the manuscript. C.H., K.H., L.J., A.B., and C.R.A.M. discussed and edited the manuscript and critically evaluated the results.

Competing interests statement

The authors declare that they have no competing financial interests.

References

Allen, J. S., Damasio, H., Grabowski, T. J., Bruss, J., and Zhang, W. (2003). Sexual dimorphism and asymmetries in the gray-white composition of the human cerebrum. *Neuroimage, 18,* 880-894.

Ashburner, J., and Friston, K. J. (2000). Voxel-based morphometry – The methods. *Neuroimage, 11,* 805-821.

Ashburner, J., and Friston, K.J. (2005). Unified segmentation. *Neuroimage 26,* 839-851.

Aydin, K., Ucar, A., Oguz, K.K., Okur, O.O., Agayev, A., Unal, Z., Yilmaz, S., and Ozturk, C. (2007). Increased Gray Matter Density in the Parietal Cortex of Mathematicians: A Voxel-Based Morphometry Study. *American Journal of Neuroradiology, 28,* 1859-1864.

Bayer, U., Kessler, N., Güntürkün, O., and Hausmann, M. (2008). Interhemispheric interaction during the menstrual cycle. *Neuropsychologia*, (in press, doi:10.1016/j.neuropsychologia.2008.02.028).

Boyke, J., Driemeyer, J., Gaser, C., Büchel, C., and May, A. (2008). Training-induced brain structure changes in the elderly. *Journal of Neuroscience, 28(28),* 7031-7035.

Brown, W. E., Kesler, S. R., Eliez, S., Warsofski, I. S., Haberecht, M., and Reiss, A. L. (2004). A volumetric study of parietal lobe subregions in Turner syndrome. *Developmental Medicine and*

Child Neurology, 46, 607-609.

Butler, T., Imperato-McGinley, J., Pan, H., Voyer, D., Cordero, J., Zhu, Y.-S., Stern, E., and Silbersweig, D. (2006). Sex differences in mental rotation: Top-down versus bottom-up processing. *Neuroimage, 32,* 445-456.

Cabeza, R., and Nyberg, L. (2000). Imaging cognition II: An empirical review of 275 PET and fMRI studies. *Journal of Cognitive Neuroscience, 12(1),* 1-47.

Campbell, D. W., and Eaton, W. O. (1999). Sex Differences in the Activity Level of Infants. *Infant and Child Development, 8,* 1-17.

Caroll, J. B. (1993). Human Cognitive Abilities. Cambridge, UK: Cambridge University Press.

Casey, M. B., Nuttall, R. L., and Pezaris, E. (1999). Evidence in support of a model that predicts how biological and environmental factors interact to influence spatial skills. *Developmental Psychology, 35,* 1237-1247.

Casey, M. B. (1996). Gender, sex, and cognition: Considering the interrelationship between biological and environmental factors. *Learning and Individual Differences, 8,* 39-53.

Chen, X., Sachdev, P. S., Wen, W., and Anstey, K. J. (2007). Sex differences in regional gray matter in healthy individuals aged 44-48: A voxel-based morphometric study. *Neuroimage, 36,* 691-699.

Cohen, M. S., Kosslyn, S. M., Breiter, H. C., DiGirolamo, G. J., Thompson, W. L., Anderson, A. K., Bookheimer, S. Y., Rosen, B. R., and Belliveau, J. W. (1996). Changes in cortical activity during mental rotation: A mapping study using functional MRI. *Brain, 119,* 89-100.

Colom, R., Jung, R. E., and Haier, R. J. (2006a). Distributed brain sites for the g-factor of intelligence. *Neuroimage, 31,* 1359-1365.

Colom, R., Jung, R. E., and Haier, R. J. (2006b). Finding the g-factor in brain structure using the method of correlated vectors. *Intelligence, 34(6),* 561-570.

Cuadra, M. B., Cammoun, L., Butz, T., Cuisenaire, O., Thiran, J. P. (2005). Comparison and Validation of Tissue Modelization and Statistical Classification Methods in T1-Weighted MR Brain Images. *IEEE Transaction in Medical Imaging 24(12),* 1548-1565.

Deary, I. J., and Caryl, P. G. (1997). Neuroscience and human intelligence differences. *Trends in Neuroscience, 20,* 365-371.

de Bellis, M. D., Keshavan, M. S., Beers, S. R., Hall, J., Frustaci, K., Masalehdan, A., Noll, J., and Boring, A. M. (2001). Sex differences in brain maturation during childhood and adolescence. *Cerebral Cortex, 11,* 552-557.

de Quervain, D. J.-F., Henke, K., Aerni, A., Coluccia, D., Wollmer, M. A., Hock, C., Nitsch, R. M., and Papassotiropoulos, A. A functional genetic variation of the 5-HT2a receptor affects human memory. *Nature Neuroscience, 6(11),* 1141-1142.

Devlin, A. S. (2004). Sailing experience and sex as correlates of spatial abilities. *Perception and Motor Skills, 98,* 1409-1421.

Draganski, B., Gaser, C., Busch, V., Schuierer, G., Bogdahn, U., and May, A. (2004). Changes in grey matter induced by training. *Nature, 427,* 311-312.

Draganski, B., Gaser, C., Kempermann, G., Kuhn, H. G., Winkler, J., Büchel, C., and May, A. (2006). Temporal and Spatial Dynamics of Brain Structure Changes during Extensive Learning. *Journal of Neuroscience, 26(23),* 6314-6317.

Driemeyer, J., Boyke, J., Gaser, C., Büchel, C., and May, A. (2008). Changes in gray matter induced by learning – Revisited. *PLoS One, 3(7),* e2669.

Egan, M. F., Kojima, M., Callicott, J. H., Goldberg, T. E., Kolachana, B. S., Bertolino, A., Zaitsev, E., Gold, B., Goldman, D., Dean, M., Lu, B., and Weinberger, D. R. (2003). The BDNF val66met polymorphism affects activity-dependent secretion of BDNF and human memory and hippocampal function. *Cell, 112(2),* 257-269.

Eickhoff, S., Walters, N. B., Schleicher, A., Kril, J., Egan, G.F., Zilles, K., Watson, J. D. G., and Amunts, K. (2005). High-Resolution MRI Reflects Myeloarchitecture and Cytoarchitecture of Human Cerebral Cortex. *Human Brain Mapping, 24,* 206-215.

Gaser, C., and Schlaug, G. (2003). Brain structures differ between musicians and non-musicians. *Journal of Neuroscience, 23(27),* 9240-9245.

Ginn, S. R., and Pickens, S. J. (2005). Relationships between spatial activities and scores on the mental rotation test as a function of sex. *Perception and Motor Skills, 100,* 877-881.

Goldstein, J. M., Seidman, L. J., Horton, N. J., Makris, N., Kennedy, D. N., Caviness Jr., V. S., Faraone, S. V., and Tsuang, M. T. (2001). Normal Sexual Dimorphism of the Adult Human Brain Assessed by *In Vivo* Magnetic Resonance Imaging. *Cerebral Cortex, 11,* 490-497.

Good, C. D., Johnsrude, I. S., Ashburner, J., Henson, R. N. A., Friston, K. J., and Frackowiak, R. S. J. (2001a). A Voxel-Based Morphometric Study of Ageing in 465 Normal Adult Human Brains. *Neuroimage, 14,* 21-36.

Good, C. D., Johnsrude, I. S., Ashburner, J., Henson, R. N. A., Friston, K. J., and Frackowiak, R. S. J. (2001b). Cerebral Asymmetry and the Effects of Sex and Handedness on Brain Structure: A Voxel-Based Morphometric Analysis of 465 Normal Adult Human Brains. *Neuroimage, 14,* 685-700.

Gur, R. C., Turetsky, B. I., Matsui, M., Yan, M., Bilker, W., Hughett, P., and Gur, R. E. (1999). Sex Differences in Brain Gray and White Matter in Healthy Young Adults: Correlations with Cognitive Perfomance. *The Journal of Neuroscience, 19(10),* 4065-4072.

Härting, C., Markowitsch, H.J., Neufeld, H., Calabrese, P., Deisinger, K., and Kessler, J. (1999).

Deutsche Adaptation der revidierten Fassung der Wechsler Memory Scale. Bern, Switzerland: Verlag Hans Huber.

Haier, R. J., Jung, R. E., Yeo, R. A., Head, K., and Alkire, M. T. (2005). The neuroanatomy of general intelligence: sex matters. *Neuroimage, 25,* 320-327.

Haier, R. J., Jung, R. E., Yeo, R. A., Head, K., and Alkire, M. T. (2004). Structural brain variation and general intelligence. *Neuroimage, 23,* 425-433.

Harris, I. M., Egan, G. F., Sonkkila, C., Tochon-Danguy, H. J., Paxinos, G., and Watson, J. D. G. (2000). Selective parietal lobe activation during mental rotation: A parametric PET study. *Brain, 123,* 65-73.

Hugdahl, K., Thomsen, T., and Ersland, L. (2006). Sex differences in visuospatial processing: An fMRI study of mental rotation. *Neuropsychologia, 44,* 1575-1583.

Im, K., Lee, J.-M., Lee, J., Shin, Y.-W., Kim, I.Y., Kwon, J.S., and Kim, S.I. (2006). Gender difference analysis of cortical thickness in healthy young adults with surface-based methods. *Neuroimage, 31,* 31-38.

Jäncke, L., and Jordan, K. (2007). Functional neuroanatomy of mental rotation performance. In Mast, F. W., and Jäncke, L. (Ed.), Spatial processing in Navigation, Imagery, and Perception (pp. 183-207). New York: Springer Science and Business Media, LLC.

Jensen, A.R. (1998). The g factor: the science of mental ability. Westport, CT: Praeger.

Johnson, W., Jung, R. E., Colom, R., and Haier, R. J. (2007). Cognitive abilities independent of IQ correlate with regional brain structure. *Intelligence, 36,* 18-28.

Jordan, K., Heinze, H.-J., Lutz, K., Kanowski, M., and Jäncke, L. (2001). Cortical Activations during the Mental Rotation of Different Visual Objects. *Neuroimage, 13,* 143-152.

Jordan, K., Wüstenberg, T., Heinze, H. J., Peters, M., and Jäncke, L. (2002). Women and men exhibit different cortical activation patterns during mental rotation tasks. *Neuropsychologia, 40,* 2397-2408.

Jung, R. E., and Haier, R. J. (2007). The Parieto-Frontal Integration Theory (P-FIT) of intelligence: Converging neuroimaging evidence. *Behavioral and Brain Sciences, 30,* 135-154.

Jung, R. E., Haier, R. J., Yeo, R. A., Rowland, L. M., Petropoulos, H., Levine, A. S., Sibbitt, W. L., and Brooks, W. M. (2005). Sex differences in *N*-acetylaspartate correlates of general intelligence: An ^{1}H-MRS study of normal human brain. *Neuroimage, 26,* 965-972.

Kimura, D. (1999). Sex and cognition. Cambridge, MA: MIT Press.

Kosslyn, S. M., DiGirolamo, G. J., Thompson, W. L., and Albert, N. M. (1998). Mental rotation of objects versus hands: neural mechansisms revealed by positron emission tomography. *Psychophysiology, 35(2),* 151-161.

Kosslyn, S. M., Thompson, W. L., Wraga, M., and Albert, N. M. (2001). Imagining rotations by endogenous versus exogenous forces: distinct neural mechanisms. *Neuroreport, 12(11),* 2519-2525.

Kruggel, F. (2006). MRI-based volumetry of head compartments: Normative values of healthy adults. *Neuroimage, 30,* 1-11.

Lemaître, H., Crivello, F., Grassiot, B., Alpérovitch, A., Tzourio, C., and Mazoyer, B. (2005). Age- and sex-related effects on the neuroanatomy of healthy subjects. *Neuroimage, 26,* 900-911.

Linn, M. C., and Petersen, A. C. (1985). Emergence and characterization of sex differences in spatial ability: a meta-analysis. *Child Development, 56(6)*, 1479-1498.

Luders, E., Narr, K. L., Thompson, P. M., Rex, D. E., Jancke, L., Steinmetz, H., and Toga, A. W. (2004). Gender differences in cortical complexity. *Nature Neuroscience, 7(8),* 799-800.

Luders, E., Narr, K. L., Thompson, P. M., Woods, R. P., Rex, D. E., Jancke, L., Steinmetz, H., and Toga, A. W. (2005). Mapping cortical gray matter in the young adult brain: Effects of gender. *Neuroimage, 26,* 493-501.

Maguire, E. A., Gadian, D. G., Johnsrude, I. S., Good, C. D., Ashburner, J., Frackowiak, R. S. J., and Frith, C. D. (2000). Navigation-related structural change in the hippocampi of taxi drivers. *Proceedings of the National Academy of Science of the United States of America, 97,* 4398-4403.

Molko, N., Cachia, A., Rivière, D., Mangin, J.-F., Bruandet, M., LeBihan, D., Cohen, L., and Dehaene, S. (2003). Functional and Structural Alterations of the Intraparietal Sulcus in a Developmental Dyscalculia of Genetic origin. *Neuron, 40,* 847-858.

Molko, N., Cachia, A., Rivière, D., Mangin, J.-F., Bruandet, M., LeBihan, D., Cohen, L., and Dehaene, S. (2004). Brain Anatomy in Turner Syndrome: Evidence for Impaired Social and Spatial-Numeric Networks. *Cerebral Cortex, 14(8),* 840-850.

Mondadori, C. R. A., de Quervain, D. J.-F., Buchmann, A., Mustovic, H., Wollmer, M. A., Schmidt, C. F., Boesiger, P., Hock, C., Nitsch, R. M., Papassotiropoulos, A., and Henke, K. (2006). Better Memory and Neural Efficiency in Young Apolipoprotein E ε4 Carriers. *Cerebral Cortex, 17(8),* 1934-1947.

Münte, T. F., Altenmüller, E., and Jäncke, L. (2002). The musician's brain as a model of neuroplasticity. *Nature Reviews Neuroscience, 3,* 473-478.

Nopoulos, P., Flaum, M., O'Leary, D., and Andreasen, N. C. (2000). Sexual dimorphism in the human brain: evaluation of tissue volume, tissue composition and surface anatomy using magnetic resonance imaging. *Psychiatry Research Neuroimaging, 98,* 1-13.

Pezawas, L., Verchinski, B. A., Mattay, V. S., Callicott, J. H., Kolachana, B. S., Straub, R. E., Egan, M. F., Meyer-Lindenberg, A., and Weinberger, D. R. (2004). The brain-derived neurotrophic

factor val66met polymorphism and variation in human cortical morphology. *Journal of Neuroscience, 24(45),* 10099-10102.

Roberts, J. E., and Bell, M. A. (2003). Two- and three-dimensional mental rotation tasks lead to different parietal laterality for men and women. *International Journal of Psychophysiology, 50,* 235-246.

Rode, C., Wagner, M., and Güntürkün, O. (1995). Menstrual cycle affects functional cerebral asymmetries. *Neuropsychologia, 33 (7),* 855-865.

Schmid, J., and Leiman, J. N. (1957). The development of hierarchical factor solutions. *Psychometrica, 22,* 53-61.

Senjem, M. L., Gunter, J. L., Shiung, M. M., Petersen, R. C., and Jack Jr., C. R. (2005). Comparison of different methodological implementations of voxel-based morphometry in neurodegenerative disease. *Neuroimage, 26,* 600-608.

Sherwin, B. B. (2003). Estrogen and cognitive functioning in women. *Endocrine Reviews, 24(2),* 133-151.

Shepard, R. N., and Metzler, J. (1971). Mental Rotation of Three-Dimensional Objects. *Science, 171,* 701-703.

Signorella, M. L., Jamison, W., and Hansen Krupa, M. (1989). Predicting Spatial Performance From Gender Stereotyping in Activity Preferences and in Self-Concept. *Developmental Psychology, 25(1),* 89-95.

Spearman, Ch. (1904). General intelligence objectively determined and measured. *American Journal of Psychology, 15,* 201-293.

Tewes, U. (1991). HAWIE-R. Hamburg-Wechsler Intelligenztest für Erwachsene Revision 1991. Bern, Switzerland: Verlag Hans Huber.

Thomsen, T., Hugdahl, K., Ersland, L., Barndon, R., Lundervold, A., Smievoll, A. I., Roscher, B. E., and Sundberg, H. (2000). Functional magnetic resonance imaging (fMRI) study of sex differences in a mental rotation task. *Medical Science Monitor: International Medical Journal of Experimental and Clinical Research, 6,* 1186-1196.

Thompson, P. M., Woods, R. P., Mega, M. S., and Toga, A. W. (2000). Mathematical/Computational Challenges in Creating Deformable and Probabilistic Atlases of the Human Brain. *Human Brain Mapping, 9,* 81-92.

Thurstone, L. L. (1938). Primary mental abilities. Chicago: University of Chicago Press.

Unterrainer, J., Wranek, U., Staffen, W., Gruber, T., and Ladurner, G. (2000). Lateralized Cognitive Visuospatial Processing: Is It Primarily Gender-Related or Due to Quality of Performance? A HMPAO-SPECT Study. *Neuropsychobiology, 41,* 95-101.

Vallar, G. (2007). Spatial neglect, Balint-Holmes' and Gerstmann's syndrome, and other spatial disorders. *CNS Spectrums, 12(7),* 527-536.

Verchinski, B., Meyer-Lindenberg, A., Japee, S., Kohn, P., Egan, M., Bigelow, L., Callicott, J., Bertolino, A., Mattay, V., Berman, K., and Weinberger, D. (2000). Gender Differences in Gray Matter Density: A Study of Structural MRI Images Using Voxel-Based Morphometry. *Neuroimage, 11(5),* S228.

Voyer, D., Voyer, S., and Bryden, M. P. (1995). Magnitude of Sex Differences in Spatial Abilities: A Meta-Analysis and Consideration of Critical Variables. *Psychological Bulletin, 117(2),* 250-270.

Warrington, E. K., James, M., and Maciejewski, C. (1986). The WAIS as a lateralizing and localizing diagnostic instrument: a study of 656 patients with unilateral cerebral lesions. *Neuropsychologia, 24(2),* 223-239.

Wechsler, D. (1981). Wechsler Adult Intelligence Scale – Revised. San Antonio, Texas: Psychological Corporation.

Wilke, M., and Lidzba, K. (2007). LI-tool: A new toolbox to assess lateralization in functional MR-data. *Journal of Neuroscience Methods, 163,* 128-136.

Wilke, M., and Schmithorst, V. J. (2006). A combined bootstrap/histogram analysis approach for computing a lateralization index from neuroimaging data. *Neuroimage, 33,* 522-530.

Wolff, H.-G., and Preising, K. (2005). Exploring item and higher order factor structure with the Schmid-Leiman solution: Syntax codes for SPSS and SAS. *Behavior Research Methods, 37(1),* 48-58.

3.2 Study 2: A *CYP46* T/C SNP modulates parahippocampal and hippocampal morphology in young subjects

A *CYP46* T/C SNP modulates parahippocampal and hippocampal morphology in young subjects

Jürgen Hänggi [a,b], Christian R.A. Mondadori [c], Andreas Buchmann [d], Katharina Henke [e], Christoph Hock [b]

[a] Division of Neuropsychology, Institute of Psychology, University of Zurich, Binzmühlestr. 14/25, 8050 Zurich, Switzerland

[b] Division of Psychiatry Research, Psychiatric University Hospital Zurich, Lenggstr. 31/1931, 8032 Zurich, Switzerland

[c] Neuropsychology Unit, Department of Neurology, University Hospital Zurich, Frauenklinikstr. 26, 8091 Zurich, Switzerland

[d] Children's Hospital, University of Zurich, Steinwiesstr. 75, 8032 Zurich, Switzerland

[e] Department of Psychology, University of Bern, Muesmattstr. 45, 3000 Bern 9, Switzerland

Corresponding author:
Jürgen Hänggi, PhD
Division of Neuropsychology
Institute of Psychology
University of Zurich
Binzmühlestrasse 14/25
8050 Zurich
0041 44 635 73 97 (phone)
0041 44 635 74 09 (fax)
j.haenggi@psychologie.uzh.ch

Abstract

There is evidence that brain cholesterol metabolism modulates the vulnerability for Alzheimer's disease (AD). Previous data showed that brain β-amyloid load in elderly subjects with the *CYP46* (cholesterol 24*S*-hydroxylase) TT-positive genotype was higher than in *CYP46* TT-negative elderly subjects. We investigated effects of the *CYP46* T/C polymorphism on parahippocampal and hippocampal grey matter (GM) morphology in 81 young subjects using structural magnetic resonance imaging based morphometry. We found that young TT-homozygotes exhibited smallest and CC-homozygotes largest parahippocampal and hippocampal GM volumes with the volumes of the CT-heterozygotes ranging in between. Parahippocampal and hippocampal volumes were positively correlated with delayed memory performance in C-carriers and negatively with immediate memory performance in TT-homozygotes. It has been shown that the brain cholesterol metabolism in general modulates dendrite outgrowth, synaptogenesis, and neuron survival, and it was suggested that *CYP46* indirectly influences β-amyloid metabolism. *CYP46* C-carriers are privileged both in terms of β-amyloid metabolism and in terms of brain reserve due to their larger parahippocampal and hippocampal structures. The exact cellular mechanisms that translate the *CYP46* allelic variation into volumetric brain differences in the parahippocampal gyrus and hippocampus are still unknown and need to be further investigated.

Keywords:

Cholesterol metabolism; Single nucleotide polymorphism; *CYP46* (cholesterol 24*S*-hydroxylase); Parahippocampal and hippocampal morphology; Alzheimer's disease; Voxel-based morphometry; Healthy young subjects; Brain reserve capacity; Amyloid-beta

1. Introduction

The cytochrome 450 pigment 46 enzyme (*CYP46*, cholesterol 24*S*-hydroxylase) is a subfamily of cytochrome P450 proteins. This protein is anchored in the endoplasmatic reticulum. The most important function of cholesterol is to provide eukaryotic plasma membranes both stability and flexibility. *CYP46* degrades cholesterol mainly to 24*S*-hydroxycholesterol (24-OHC). The conversion of cholesterol to 24-OHC is a mechanism for the elimination of excess cholesterol from and maintenance of cholesterol homeostasis in the brain (Björkhem et al., 1997). This mechanism is modulated by age (Lütjohann et al., 1996). There is no cholesterol import into the brain; hence, brain cholesterol availability depends entirely on local production. Being a constituent of myelin and neural

cell membranes, cholesterol is important for brain function. Studies also suggest that cholesterol plays an important role in regulating β-amyloid (Aβ) metabolism (Papassotiropoulos et al., 2003; Puglielli et al., 2003; Simons et al., 1998; Wolozin, 2003). Therefore, a loss of *CYP46* activity might produce a corresponding increase in Aβ accumulation that may lead to neurodegeneration.

Although preliminary findings point toward an influence of this cholesterol turnover mechanism on the vulnerability for Alzheimer's disease (AD), it is still disputed whether this SNP (rs754203 on intron 2) in the *CYP46* gene (on chromosome 14q32.1) is a risk factor for AD. *CYP46* TT-positive patients with AD were found to have increased cholesterol levels in cerebrospinal fluid (CSF) compared with *CYP46* TT-negative patients with AD (Papassotiropoulos et al., 2003), albeit only on a trend level toward significance ($p = 0.07$). These increased cholesterol levels presumably coincide with a loss of *CYP46* activity (Papassotiropoulos et al., 2003). The majority of studies found the TT-genotype to be the risk variant for AD, while this was the case for the CC-genotype only in a few studies (Helisalmi et al., 2006). Most of the studies on this *CYP46* SNP and its association with AD were meta-analysed by Helisalmi et al. (2006). An interaction of the *CYP46* T/C SNP with the ε4 allele of the apolipoprotein E (*ApoE*) gene synergistically increases the risk for AD (Papassotiropoulos et al., 2003). Recently, Reiman and colleagues used ^{18}fluoro-2-deoxyglucose (FDG) positron emission tomography (PET) to measure regional cerebral blood flow (rCBF) and showed that cholesterol-related genes modulate brain metabolism. These authors revealed hypometabolism in AD-affected brain regions in healthy elderly subjects who are carriers of the negative allelic variant of several cholesterol-related genes including the *CYP46* TT-genotype, even when controlling for the effects of *ApoE* ε4 gene dose (Reiman et al., 2008).

Also, there is accumulating and converging evidence that the brain cholesterol metabolism plays an important role in dendrite outgrowth, synaptogenesis, and neuronal survival. First, it has been shown that cholesterol complexed to *ApoE*-containing lipoproteins controls synaptogenesis in the central nervous system (Mauch et al., 2001). Second, it has been reported that cholesterol deficiency causes a selective inhibition of dendrite outgrowth due to the decreased stability of microtubules as a result of inhibition of microtubule-associated protein 2 (MAP2) phosphorylation (Fan et al., 2002). Third, inhibition of cholesterol production in the brain tissue cultures induced neuronal cell death (Michikawa and Yanagisawa, 1999). Fourth, it has been suggested that the deleterious effects of ethanol on the developing brain might be due, at least in part, to an effect on cholesterol homeostasis (Guzzetti and Costa, 2007). Last, there are inborn defects in cholesterol metabolism such as the Smith-Lemli-Opitz syndrome (Tint et al., 1994), a failure in cholesterol production accompanied by microcephaly, and the Niemann-Pick type C disease, a failure in cholesterol degradation accompanied by neurodegeneration (Sévin et al., 2007). Taken together, there is good evidence that brain

cholesterol and its metabolism are important for the formation and maintenance of neural tissue as well as for neural functions. Because neuropathologic changes in Alzheimer's disease precede the occurrence of the first cognitive symptoms by decades (Mondadori et al., 2006), we anticipated that there might be structural brain differences in the medial temporal lobe already in young healthy subjects with the *CYP46* TT-genotype.

Hence, we hypothesized that the *CYP46* T/C SNP affects neural tissue, preferentially in brain structures with a high metabolic turnover such as the hippocampus and in fact the whole medial temporal lobe (MTL), which is first affected by Alzheimer's pathology. Here, we report first findings of the influence of the *CYP46* T/C SNP (rs754203) on parahippocampal and hippocampal morphology in healthy young Swiss subjects of Caucasian origin, while simultaneously controlling for the allelic variation in other genes with known influences on brain morphology and memory functions such as the gene that encodes for the brain-derived neurotrophic factor and the apolipoprotein gene that is associated with AD.

2. Methods

2.1. Subjects

The 81 participants were drawn from a larger sample of 354 healthy, young Swiss subjects of Caucasian origin (de Quervain et al., 2003). The 354 volunteers were university students and employees/trainees recruited at the university of Zurich and via advertisements in local newspapers. The 81 subjects already participated in two functional magnetic resonance imaging studies that investigated brain activity elicited by memory tasks between different apolipoprotein E genotypes (Mondadori et al., 2007) and between different prion protein genotypes (Buchmann et al., 2008). Our sample is homogenous with respect to age, education, and memory performance. The subjects reported no past or current psychiatric or neurological problems and denied taking illegal drugs or medication. All subjects gave written informed consent to participate in the study after the nature and possible consequences of the study had been explained. The local ethics committee approved the experiment. The subjects were paid for participating in the study.

2.2. Genotyping

Information on polymorphic sites was derived from the database of single nucleotide polymorphisms (dbSNP) (http://www.ncbi.nlm.nih.gov/SNP/index.html). Genotyping is described in detail elsewhere: for the cholesterol 24*S*-hydroxylase (*CYP46*; rs754203) gene (Papassotiropoulos et al., 2003), for the brain-derived neurotrophic factor (*BDNF*; rs6265) gene (Egan et al., 2003), for the apolipoprotein E (*ApoE*) gene (Nauck et al., 2000), for the serotonin 2a receptor (*5-HT2a*; rs6314) gene (de Quervain et

al., 2003), and for the prion protein (*PrnP*; rs1799990) gene (Papassotiropoulos et al., 2005a). We also controlled for nonrandom genetic heterogeneity (hidden population structures) by genotyping each subject for 27 unlinked SNPs located in non-genic regions distributed over all autosomes (Papassotiropoulos et al., 2005b).

2.3. Neuropsychology

Memory performance (immediately after stimulus presentation as well as at delays of 5 min. and 24 h.) was assessed during two consecutive days using the Rey-15-figures free recall test (Rey, 1958), the recurring figures recognition test (Kimura, 1963), and an in-house developed verbal free recall test of 30 common German words, a test already applied and described in other publications (Papassotiropoulos et al., 2005a; de Quervain et al., 2003). The difficult in-house verbal free recall test had been developed to avoid ceiling effects that commonly occur when investigating cognitively high functioning subjects such as university students with other verbal memory tests. On the first day, subjects viewed six sets of semantically unrelated nouns (five nouns per set) presented at a rate of 1 word per second with the instruction to learn the words for immediate free recall after each series. In addition, subjects underwent an unexpected delayed free recall test of the learned words after 5 minutes and again after 24 hours. Both delayed free recall tests reflect episodic memory (Squire and Alvarez, 1995).

In addition to the verbal memory test, subjects performed a modified version of the Rey-15-figures free recall test (Rey, 1958), which included the presentation of 15 figures in sequence – each figure for 2 seconds – with the instruction to learn them for immediate recall. In addition, subjects underwent an unexpected delayed free recall test of the learned figures after 5 minutes and again after 24 hours.

In addition to the two free recall memory tests, we also applied a non-verbal recognition memory test using 13 complex figures of the recurring figures recognition test (Kimura, 1963). This test requires the presentation of geometric or irregular nonsense figures – each figure for 2 seconds – that have to be learned for later recognition at delays of 5 minutes and 24 hours.

All reported memory scores are hits minus false alarms. Maximal scores are: 15 for the Rey-Figures Test; 13 for the Recurring Figures Test; and 30 for the list of common words.

Additionally, we applied three different subscales of the revised Wechsler adult intelligence scale (WAIS-R) (Wechsler, 1981; German version: Tewes, 1991) to assess working memory capacity (Digit span, forward and backward), visuospatial cognition (Block design), and verbal reasoning (Similarities). A summary of the neuropsychological test results between the three different *CYP46* genotypes can be found in Table 1.

2.4. Magnetic resonance imaging data acquisition

Magnetic resonance imaging (MRI) scans were acquired on a 3T Philips Intera whole body scanner

(Philips, Best, the Netherlands) equipped with a commercial eight-element head coil array. A T1-weighted gradient echo (fast field echo) sequence was applied with a measured spatial resolution of 1.0x1.0x1.0 mm (acquisition matrix 224x224 pixels) and a reconstructed resolution of 0.9x0.9x0.8 mm, echo-time TE=2.3 ms, repetition-time TR=20 ms, flip angle FA θ=20°.

2.5. Preprocessing of magnetic resonance imaging data

Image preprocessing was done with Statistical Parametric Mapping (SPM5) software (http://www.fil.ion.ucl.ac.uk/spm) using voxel-based morphometry (VBM) (Ashburner and Friston, 2000) implemented in the VBM5 toolbox (http://dbm.neuro.uni-jena.de/vbm/). A Hidden Markov Random Field (HMRF) model was applied to enhance the accuracy of the tissue class segmentation process (http://dbm.neuro.uni-jena.de/vbm/markov-random-fields/). Customized a priori maps from the normalized, segmented, HMRF weighted, unsmoothed GM, white matter (WM), and CSF images of the subjects were constructed. Native images were again segmented with the customized a priori maps resulting in normalized, segmented, Jacobian modulated, and HMRF weighted GM images which were smoothed with a 9 mm Gaussian kernel. Images were subjected into a voxel-wise analysis on one hand and the unsmoothed versions were used for the volumes-of-interest (VOIs) approach on the other hand. VOIs for the parahippocampal gyri and for the hippocampi were derived from the Pickatlas (http://www.fmri.wfubmc.edu/cms/software#PickAtlas). These VOIs were originally drawn by others (Tzourio-Mazoyer et al., 2002) on the MNI single-subject brain (Holmes et al., 1998). We also normalized and segmented the MNI single-subject brain to obtain the warping parameters to adjust this brain onto the customized a priori maps. We then applied these transformations to the VOIs to adjust them onto the customized a priori maps, multiplied the VOIs by the GM images, and computed the volumes within these VOIs. Note that both the voxel-based and the VOI-based approach are fully automated procedures and therefore they are operator-independent.

2.6. Statistical analyses

We used SPM5 and SPSS 14 (http://www.spss.com/) to analyze voxel- and VOI-based data, respectively. Partial correlations between *CYP46* allelic frequency and parahippocampal or hippocampal volumes controlling for total GM volume (TGMV) and *BDNF* genotype as well as analysis of covariance (ANCOVA) models were applied. In the ANCOVAs, the allelic variant was the independent variable and parahippocampal and hippocampal volumes the dependent variables while TGMV and *BDNF* genotype were used as covariates. Gender and TGMV are collinear variables (Spearman correlation: $r = -0.657$, $p = 2.82*10^{-11}$, male coded as 1, female coded as 2), i.e., TGMV explains most of the gender-related variance in brain morphology; hence, gender was not included in our statistical models to preserve statistical power. Education, handedness, and age showed no significant influence on morphology (tested in multiple regression analyses together with TGMV and

BDNF genotype) and were therefore not modeled in both analyses. We controlled for SNPs with published influences on brain morphology such as found in the *BDNF* gene (Egan et al., 2003; Hariri et al., 2003; Pezawas et al., 2004; Szeszko et al., 2005; Bueller et al., 2006) and *5-HT2a* gene (Filippini et al., 2006), and for SNPs with potential influences on morphology such as found in the *ApoE* gene (Mondadori et al., 2007) and *PrnP* gene (Papassotiropoulos et al., 2005a), as well as for nonrandom genetic heterogeneity, i.e., hidden, genetic population structure (Papassotiropoulos et al., 2005b). Allelic frequencies of the SNPs with potential influences and the *5-HT2a* SNP were not significantly different between the *CYP46* genotypes and were not considered further. Although the allelic frequency of the *BDNF* SNP was not statistically different between the three *CYP46* genotypes it was included in our statistical models as a covariate because of its relevance on medial temporal lobe morphometry as well as memory functions (Egan et al., 2003; Hariri et al., 2003; Pezawas et al., 2004; Szeszko et al., 2005; Bueller et al., 2006). VBM results were thresholded with an error probability of $p < 0.001$ (uncorrected for multiple comparisons) combined with a cluster extent threshold of $k = 50$ voxels (uncorrected). In order to account for the multiple comparisons problem we applied a small volume correction (SVC) that restricts the statistical analysis to the medial temporal lobe. This SVC was combined with a false discovery rate (FDR) of $p = 0.05$. For the VOI-based data, we used a common threshold of $p < 0.05$ (uncorrected). We correlated the parahippocampal and hippocampal volumes with memory performance and with the *CYP46* T-allele frequency and the latter also with memory performance. We applied two different types of correlations, a partial product-moment correlation according to Pearson that controls for TGMV and *BDNF* genotype, and a rank correlation according to Spearman. The rank correlations were based on residual values after the effects of TGMV and *BDNF* genotype on hippocampal and parahippocampal volumes were regressed out.

3. Results

Demographic characteristics, memory performance, indices of intelligence, and global brain tissue volumes are shown in Table 1. There were neither significant differences nor trends toward significance ($0.05 < p < 0.1$) between the *CYP46* genotypes for the variables age, years of education, TGMV, total WM volume, total CSF volume, intracranial volume, indices of intelligence, and for any of the free recall and recognition memory measure as revealed by AN(C)OVAs. Nor were there significant differences in the distribution of *BDNF*, *5-HT2a*, *ApoE*, *PrnP*, *GenHet* allele frequencies, gender, and handedness between *CYP46* genotypes as assessed with χ^2-tests. As expected, *CYP46* genotype distribution was under Hardy-Weinberg equilibrium conditions.

	TT - homozygotes (n = 33)				CT - heterozygotes (n = 38)				CC - homozygotes (n = 10)				
Measures	**Mean**	**S.D.**	**Min.**	**Max.**	**Mean**	**S.D.**	**Min.**	**Max.**	**Mean**	**S.D.**	**Min.**	**Max.**	**Probability***
Age (years)	22.9	3.5	18.7	39.0	23.2	2.3	19.7	31.0	24.0	3.4	20.0	32.1	0.613
Education (years)	14.5	1.7	10.5	18.0	15.4	1.8	12.0	19.0	15.5	1.1	13.5	17.0	0.104
TGMV (ccm)	781.6	70.4	648.5	947.2	778.8	74.5	657.1	920.6	778.7	79.1	665.2	946.2	0.613
TWMV (ccm)	420.4	46.5	320.9	499.1	428.4	49.6	348.8	584.2	417.2	67.1	353.9	592.2	0.616
TCSFV (ccm)	405.5	63.3	296.1	595.1	412.4	50.6	296.8	516.7	410.3	43.8	350.0	506.5	0.912
ICV (ccm)	1,607.5	143.2	1,313.7	1,909.7	1,619.7	132.8	1,386.4	1,936.3	1,606.1	163.5	1,387.7	1,958.6	0.924
Kimura figures short delay	6.6	3.0	0	12	7.1	3.0	0	13	6.0	2.9	1	9	0.544
Kimura figures long delay	5.3	3.0	-1	11	4.9	2.7	-3	11	5.2	2.7	1	8	0.860
Rey figures short delay	5.6	3.0	1	12	5.2	2.8	-1	12	6.0	4.1	1	12	0.674
Rey figures long delay	3.9	3.4	-7	9	2.4	3.2	-6	-8	3.8	4.6	-2	12	0.178
30 words immediate	22.4	4.0	14	29	22.7	2.9	15	29	22.0	3.7	17	27	0.818
30 words short delay	5.8	3.9	-3	14	6.0	3.5	0	14	5.7	2.4	2	9	0.979
30 words long delay	5.0	3.9	-8	11	3.6	4.2	-6	11	2.3	2.5	-3	5	0.122
Digit span** (WAIS-R)	15.6	3.8	9	25	15.3	3.6	8	21	16.5	3.9	10	23	0.651
Block design (WAIS-R)	42.8	6.9	27	51	43.8	5.4	33	51	43.8	4.5	36	50	0.776
Similarities (WAIS-R)	28.3	2.7	20	32	28.4	2.6	23	32	27.4	4.0	19	32	0.602
	Frequency				**Frequency**				**Frequency**				
Gender (f/m)	21 / 12				18 / 20				7 / 3				0.755
Handedness (r/l/a)	28 / 3 / 2				32 / 4 / 2				9 / 1 / 0				0.624
	Frequency of amino acids / alleles				**Frequency of amino acids / alleles**				**Frequency of amino acids / alleles**				
BDNF val66met	22 val/val	10 val/met	1 met/met		21 val/val	16 val/met	1 met/met		7 val/val	3 val/met	0 met/met		0.526
5-HT2a his452tyr	24 his/his	9 his/tyr	0 tyr/tyr		29 his/his	9 his/tyr	0 tyr/tyr		5 his/his	5 his/tyr	0 tyr/tyr		0.255
PrnP met129val	13 met/met	12 val/met	7 val/val		16 met/met	13 val/met	9 val/val		5 met/met	3 val/met	2 val/val		0.986
ApoE ε4 vs not ε4	10 epsilon 4	19 not epsilon 4			6 epsilon 4	32 not epsilon 4			3 epsilon 4	7 not epsilon 4			0.195
GenHet 2 clusters	15 cluster 1	18 cluster 2			20 cluster 1	18 cluster 2			6 cluster 1	4 cluster 2			0.682

Table 1. Demographic characteristics, memory performance, and brain tissue volumes of *CYP46* genotypes. Memory measures are hits minus false alarms. * Confirmed by analysis of variance and covariance (two-tailed) and by χ^2 (two-tailed). ** Forward and backward. *Abbreviations:* TGMV, total gray matter (GM) volume; TWMV, total white matter (WM) volume; TCSFV, total cerebrospinal fluid (CSF) volume; ICV, intracranial volume; WAIS-R, Wechsler adult intelligence scale - revised; f, females; m, males; r, right; l, left, a, ambidexter; *BDNF*, brain-derived neurotrophic factor; *5-HT2a*, 5-Hydroxy-tryptamine 2a; *ApoE*, apolipoprotein E; *PrnP*, prion protein; GenHet, genetic heterogeneity; val, valine; met, methionine; his, histidine; tyr, tyrosine; S.D., standard deviation.

We found volumetric GM differences in the medial temporal lobe (MTL) structures between the *CYP46* genotypes (Figs. 1 and 3) as a result of both the correlations (Fig. 1 left) and ANCOVAs (Fig. 1 right). Voxel-wise (Figs. 1 and 2) and VOI-based (Fig. 3; Table 2) analyses revealed that both parahippocampal gyri and both hippocampi were smaller in TT-homozygotes than in CT-heterozygotes and in turn than in CC-homozygotes. In the voxel-wise analyses (Fig. 1), the left parahippocampal cluster size is 7984 voxels ($p < 0.001$ uncorrected; $p = 0.003$ FDR corrected) as revealed by correlation and 2322 voxels ($p < 0.001$ uncorrected; $p = 0.024$ FDR corrected) as revealed by ANCOVA. The right parahippocampal cluster size is 785 voxels ($p < 0.001$ uncorrected; $p = 0.004$ FDR corrected) as yielded by the correlation analysis. In the VOI-based analyses (Fig. 3), the differences of the parahippocampal and hippocampal volumes between TT- and CC-homozygotes were all significant, whereas the volumetric differences between the homozygotes and the CT-heterozygotes showed only a trend toward significance (see Fig. 3). As stated above in the Methods, we did not model gender in our analyses because gender is collinear to TGMV. Nevertheless, we also analyzed our data with TGMV and gender as simultaneous covariates. Theses analyses revealed qualitatively and quantitatively similar results.

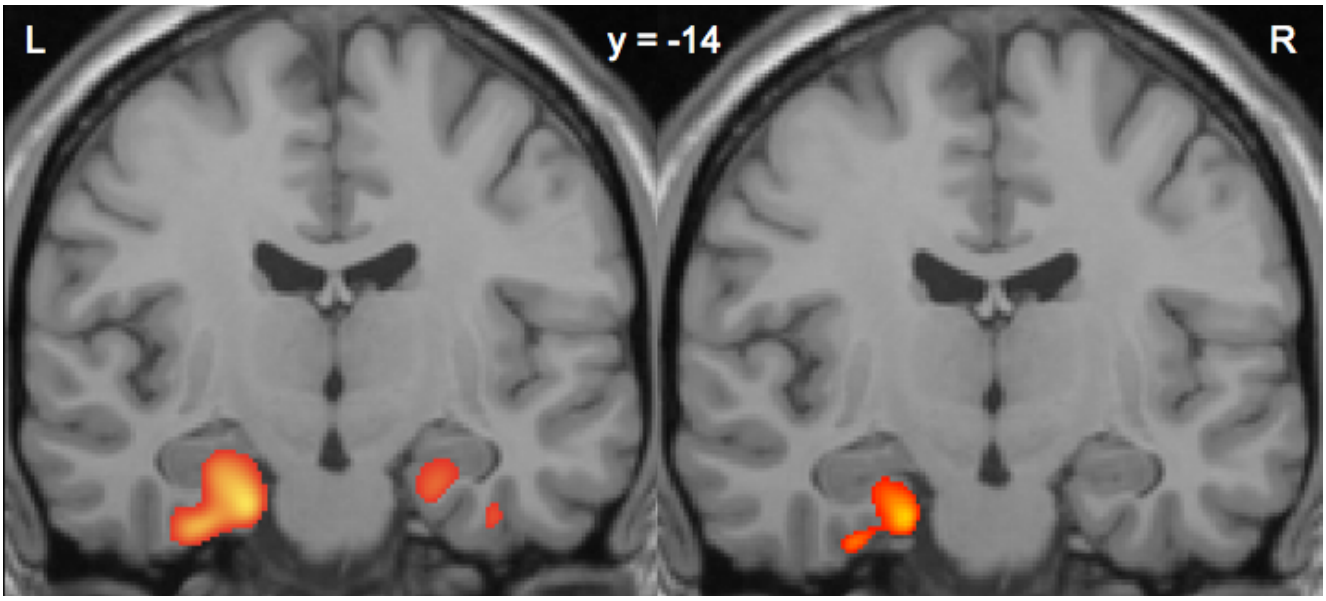

Figure 1. Main effect of *CYP46* T-alleles on parahippocampal and hippocampal volumes revealed by voxel-wise analyses using partial correlation (left) and analysis of covariance (right). Total grey matter volume and *BDNF* allele frequency were used as covariates. Less T-alleles mean larger volumes. Clusters of volumetric differences are overlaid on the Montreal Neurological Institute (MNI) single subject brain. *Abbreviations:* L, left; R, right; y, y-coordinate in MNI space.

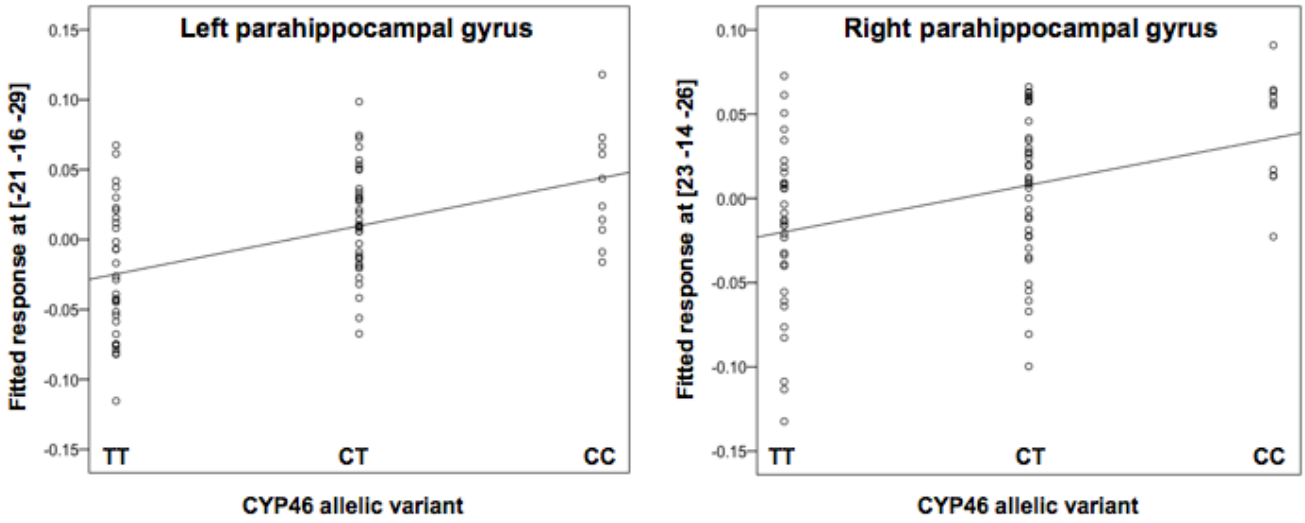

Figure 2. Correlations between *CYP46* genotypes and parahippocampal volumes. Influences of total grey matter volume and *BDNF* allele frequency were regressed out. Less T-alleles go with larger volumes. Plots are shown for two local maxima located in the left and right entorhinal cortex. Coordinates are in Montreal Neurological Institute (MNI) space. The y-axis represents the beta-values of the general linear model.

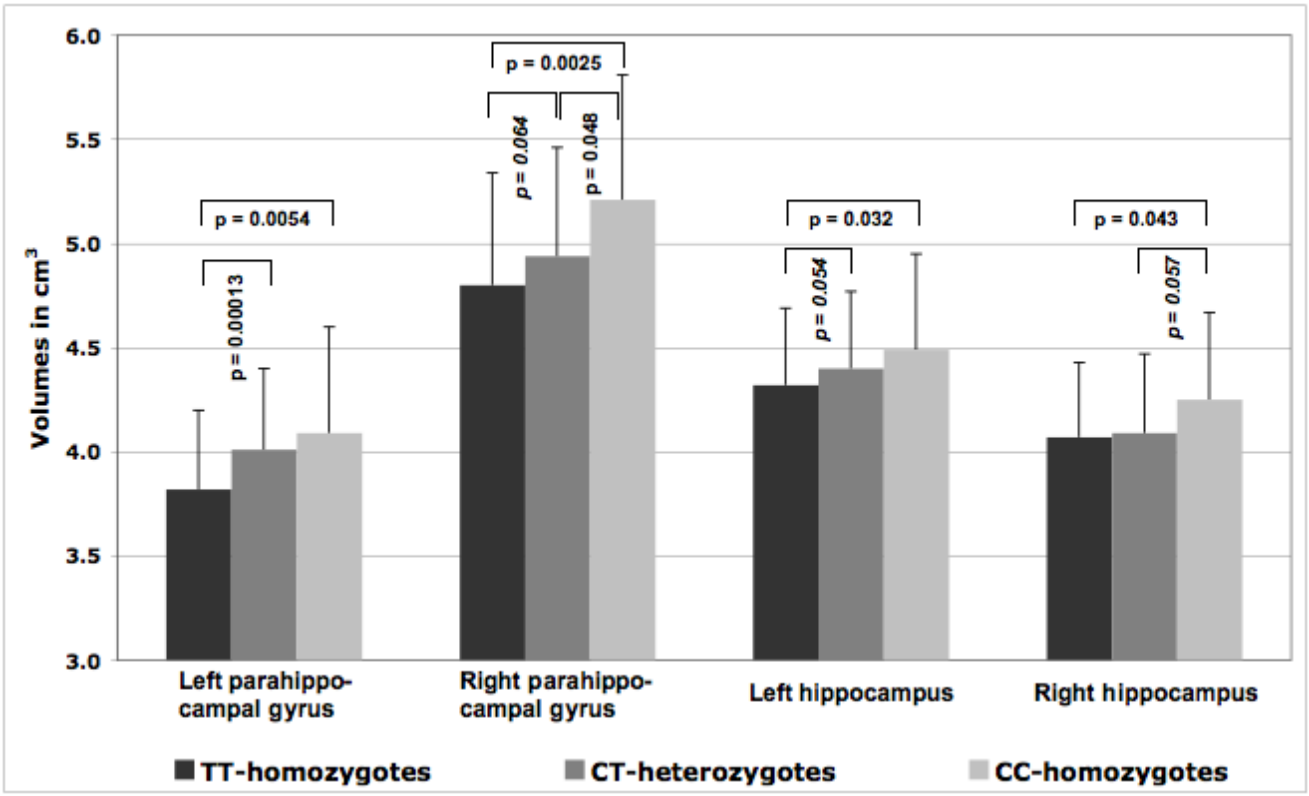

Figure 3. Parahippocampal and hippocampal volumes of the different *CYP46* genotype groups. Error probabilities are corrected for total grey matter volume and *BDNF* genotype. Shown are mean volumes and the error bar represents the standard deviation. Statistical trends ($0.05 < p < 0.1$) are printed in italic.

Structures - *CYP46* genotype correlation (n = 81)	Partial correlation*			Spearman correlation*		
	r	p	d	r	p	d
Left parahippocampal gyrus	**0.43**	**0.00004**	**0.95**	**0.39**	**0.0003**	**0.85**
Right parahippocampal gyrus	**0.36**	**0.001**	**0.78**	**0.33**	**0.002**	**0.71**
Left hippocampus	**0.26**	**0.010**	**0.52**	**0.24**	**0.032**	**0.49**
Right hippocampus	**0.23**	**0.021**	**0.46**	*0.20*	*0.068*	*0.42*

Table 2. Correlations between T-allele frequency and parahippocampal or hippocampal volumes. Less T-alleles (more C-alleles) mean larger volumes. * Partial correlations corrected for total grey matter volume and brain-derived neurotrophic factor (*BDNF*) allele frequency. Probabilities $p < 0.05$ are in bold, statistical trends towards significance ($0.05 < p < 0.1$) are in italic. *Abbreviations: CYP46*, cholesterol 24S-hydroxylase; d, Cohen's effect size; p, error probability; r, correlation coefficient.

Furthermore, we obtained negative findings with respect to an influence of the *BDNF* and the *5-HT2a* SNP on hippocampal volumes. This is in contrast with the literature where the *BDNF* val66met-allele (Egan et al., 2003; Hariri et al., 2003; Pezawas et al., 2004; Szeszko et al., 2005; Bueller et al., 2006) and the *5-HT2a* his452tyr-allele (Filippini et al., 2006) were associated with smaller hippocampal volumes. Nevertheless, there was a statistical trend in our sample pointing towards an association

between *BDNF* val66met-allele and smaller hippocampal and parahippocampal volumes. When *CYP46* genotypes were added as a second factor to a *BDNF*-MANCOVA with both hippocampi and parahippocampal gyri as dependent variables, *CYP46* genotypes explained most of the variance in these volumes (*BDNF*: F = 1.17, p = 0.327; *CYP46*: F = 1.75, p = 0.045). When the hippocampal and parahippocampal volumes were analyzed separately, all medial temporal lobe volumes were comparable between the different *BDNF* and *5-HT2a* genotypes: left hippocampus (*BDNF,* p = 0.216; *5-HT2a,* p = 0.459), right hippocampus (*BDNF,* p = 0.133; *5-HT2a,* p = 0.639), left parahippocampal gyrus (*BDNF,* p = 0.114; *5-HT2a,* p = 0.279), and right parahippocampal gyrus (*BDNF,* p = 0.063; *5-HT2a,* p = 0.765).

Memory performance in the *CYP46* genotypes is listed in Table 1. We correlated memory performance with the parahippocampal and hippocampal GM volumes derived from the VOIs (Table 3). When considering only the significant correlations, a dissociation was found in the direction of these correlations: while TT-carriers showed only negative correlations between immediate memory performance and parahippocampal and hippocampal volumes, CT- and CC-carriers showed only positive correlations between short- and long-delay memory performance and parahippocampal and hippocampal volumes. However, when looking also at the insignificant correlations there is no further support for such a kind of dissociation.

Structures - memory tests*	**Partial correlation****			**Spearman correlation****		
	r	**p**	**d**	**r**	**p**	**d**
TT-homozygotes (n = 33)						
Left hippocampus - 30 words immediate recall	**-0.58**	**0.001**	**1.44**	**-0.51**	**0.003**	**1.17**
Right hippocampus - 30 words immediate recall	**-0.45**	**0.011**	**1.01**	**-0.40**	**0.020**	**0.88**
Left parahippocampal g. - 30 words immediate recall	*-0.34*	*0.061*	*0.72*	-0.24	0.185	0.49
Right parahippocampal g. - 30 words immediate recall	**-0.45**	**0.011**	**1.01**	**-0.45**	**0.009**	**1.00**
CT-heterozygotes (n = 38)						
Right hippocampus - 30 words short delay (5 min.)	*0.30*	*0.080*	*0.62*	**0.32**	**0.048**	**0.68**
Right parahippocampal g. - 30 words short delay (5 min.)	**0.34**	**0.045**	**0.71**	*0.28*	*0.092*	*0.58*
Right hippocampus - 30 words long delay (5 min.)	0.28	0.104	**0.57**	0.27	0.106	0.55
Right parahippocampal g. - 30 words long delay (24 h.)	**0.47**	**0.004**	**1.08**	**0.45**	**0.005**	**1.00**
CC-homozygotes (n = 10)						
Left hippocampus - Rey figures long delay (24 h.)	0.52	0.187	1.22	0.47	0.171	1.06
Right hippocampus - Kimura figures short delay (5 min.)	0.30	0.474	0.62	0.23	0.527	0.47
Left parahippocampal g. - Rey figures long delay (24 h.)	0.28	0.509	0.57	0.18	0.625	0.36
Right parahippocampal g. - 30 words long delay (24 h.)	0.53	0.177	1.25	0.53	0.116	1.25

Table 3. Correlations between memory performance and parahippocampal or hippocampal volumes in the *CYP46* genotype groups. * All memory measures are hits minus false alarms. ** Correlations are corrected for total grey matter volume and brain-derived neurotrophic factor (*BDNF*) allelic variant. Probabilities $p < 0.05$ are in bold, statistical trends towards significance ($0.05 < p < 0.1$) are in italic. The whole pattern of correlations can be found in the Supplementary Table S1 online. *Abbreviations:* d, Cohen's effect size; g., gyrus; min., minutes; h., hours; p, error probability; r, correlation coefficient.

The whole pattern of correlations between the different memory measures and parahippocampal and hippocampal volumes across the different *CYP46* genotypes can be found in the Supplementary Table S1 online. There were no significant correlations between the measures of memory performance and the frequency of *CYP46* T-alleles.

Structure - memory test	TT - homozygotes (n = 33)				CT - heterozygotes (n = 38)				CC - homozygotes (n = 10)			
	Partial correlation		Spearman correlation		Partial correlation		Spearman correlation		Partial correlation		Spearman correlation	
	r	p	r	p	r	p	r	p	r	p	r	p
Left hippocampus -												
30 words immediate	**-0.58**	**0.001**	**-0.51**	**0.003**	*0.296*	*0.08*	0.132	0.43	0.006	0.989	-0.253	0.48
30 words short delay (5 min.)	-0.01	0.967	-0.05	0.774	0.08	0.642	0.107	0.523	0.069	0.871	-0.061	0.867
30 words long delay (24 h.)	0.24	0.187	0.09	0.638	0.017	0.922	-0.021	0.903	0.47	0.24	0.271	0.449
Kimura figures short delay (5 min.)	0.08	0.671	0.19	0.303	0.017	0.923	-0.061	0.717	0.034	0.937	0.191	0.598
Kimura figures long delay (24 h.)	-0.18	0.343	0.05	0.776	0.221	0.194	0.148	0.375	-0.108	0.8	-0.124	0.733
Rey figures short delay (5 min.)	0.09	0.616	0.07	0.705	0.076	0.659	-0.102	0.543	0.521	0.186	0.395	0.258
Rey figures long delay (24 h.)	-0.20	0.284	-0.03	0.856	-0.166	0.334	-0.252	0.128	0.52	0.187	0.47	0.171
Right hippocampus -												
30 words immediate	**-0.45**	**0.011**	**-0.40**	**0.020**	-0.03	0.875	-0.075	0.656	-0.309	0.456	-0.056	0.879
30 words short delay (5 min.)	0.05	0.796	0.01	0.948	*0.30*	*0.080*	**0.323**	**0.048**	0.1	0.814	0.165	0.648
30 words long delay (24 h.)	0.16	0.396	0.01	0.959	0.28	0.104	0.266	0.106	0.145	0.731	0.394	0.26
Kimura figures short delay (5 min.)	0.05	0.786	0.11	0.556	0.14	0.427	0.045	0.786	0.297	0.474	0.228	0.527
Kimura figures long delay (24 h.)	-0.12	0.516	0.03	0.855	-0.02	0.927	-0.034	0.838	-0.079	0.853	-0.062	0.865
Rey figures short delay (5 min.)	-0.02	0.908	-0.08	0.648	0.07	0.678	0.041	0.806	0.273	0.513	0.194	0.59
Rey figures long delay (24 h.)	-0.15	0.429	-0.05	0.782	-0.20	0.246	-0.158	0.342	0.302	0.467	0.134	0.712
Left parahippocampal gyrus -												
30 words immediate	*-0.34*	*0.061*	-0.24	0.185	-0.12	0.504	-0.064	0.702	0.088	0.836	-0.228	0.526
30 words short delay (5 min.)	0.15	0.416	0.20	0.264	0.03	0.866	0.043	0.797	-0.173	0.682	-0.037	0.92
30 words long delay (24 h.)	*0.32*	*0.084*	*0.30*	*0.088*	0.20	0.249	0.152	0.361	0.385	0.346	0.24	0.504
Kimura figures short delay (5 min.)	0.06	0.748	0.14	0.448	-0.02	0.918	-0.113	0.501	-0.553	0.155	-0.363	0.302
Kimura figures long delay (24 h.)	-0.14	0.453	-0.02	0.934	-0.27	0.109	-0.186	0.264	-0.102	0.81	-0.149	0.682
Rey figures short delay (5 min.)	0.23	0.216	0.27	0.134	0.23	0.178	*0.092*	*0.09*	0.514	0.193	0.358	0.31
Rey figures long delay (24 h.)	-0.02	0.923	0.17	0.347	-0.13	0.437	-0.15	0.369	0.275	0.509	0.177	0.625
Right parahippocampal gyrus -												
30 words immediate	**-0.45**	**0.011**	**-0.45**	**0.009**	-0.24	0.155	-0.154	0.355	-0.123	0.771	-0.136	0.708
30 words short delay (5 min.)	-0.11	0.560	-0.12	0.521	**0.34**	**0.045**	*0.277*	*0.092*	0.333	0.42	0.343	0.333
30 words long delay (24 h.)	0.12	0.522	-0.06	0.730	**0.47**	**0.004**	**0.447**	**0.005**	0.529	0.177	0.529	0.116
Kimura figures short delay (5 min.)	-0.05	0.776	-0.02	0.935	-0.03	0.887	0.002	0.993	0.084	0.842	0.086	0.813
Kimura figures long delay (24 h.)	-0.03	0.855	-0.01	0.950	-0.26	0.126	-0.155	0.353	0.03	0.944	-0.074	0.838
Rey figures short delay (5 min.)	0.05	0.794	-0.02	0.911	0.15	0.384	0.195	0.24	0.449	0.264	0.245	0.496
Rey figures long delay (24 h.)	-0.10	0.582	-0.04	0.807	-0.13	0.437	-0.125	0.454	0.382	0.35	0.159	0.662

Supplementary Table S1. Whole pattern of correlations between parahippocampal or hippocampal volumes and memory test performance in the different *CYP46* genotype groups. *Abbreviations:* h., hour; min., minutes; r, correlation coefficient; p, probability.

4. Discussion

We found that the *CYP46* T/C SNP (rs754203), a possible risk factor for AD, modulates parahippocampal and hippocampal volumes in young, healthy Swiss subjects of Caucasian origin. These structures were smaller in TT-homozygotes than in CT-heterozygotes and in turn than in CC-homozygotes. The MRI T1-weighted intensity profiles, on which morphometric MRI studies are based, have been shown to be best explained by a weighted sum of cytoarchitectonic and myeloarchitectonic profiles (Eickhoff et al., 2005), suggesting that the volumetric differences originate in differences in neuronal and synaptic compartments, which are very important for brain functions, rather than differences in the stroma / interstitium (including interstitial fluid) or edema.

The significant correlations of parahippocampal and hippocampal GM volumes with various measure of memory showed a dissociation between TT-carriers and CT-/CC-carriers. Correlations between parahippocampal or hippocampal volumes and immediate recall of 30 words were *negative* for TT-homozygotes. Although traditional views do not account for a role of MTL structures in short-term memory, there is mounting evidence that the MTL supports short-term memory as well, particularly with high mnemonic load and with associative learning tasks (Ranganath and Blumenfeld, 2005). It might be possible that, although MTL volume is reduced in the *CYP46* TT-genotype, there is still enough parahippocampal and hippocampal substrate in young healthy TT-carriers to perform mnemonic functions properly. However, in older age and with progressing non-pathologic neuronal loss, the amount of properly functioning MTL tissue might fall below a critical threshold and as a consequence disturbed memory functions might result in subjects with the TT-genotype. CT-heterozygotes and CC-homozygotes exhibited *positive* correlations between parahippocampal or hippocampal volumes and performance in tests of delayed recognition. Associations of larger volumes with better memory performance indicates that neurons in the measured volumes were functionally relevant and therefore carry the potential to keep memory functions up at an advanced age when pathological deposits start to disturb neural function locally. This relationship in the carriers of the favorable C-allele are interpretable in the light of the theory of brain reserve capacity (Katzman et al., 1988; Mori et al., 1997) as a protective factor against memory decline due to neurodegeneration at an advanced age. This “volume advantage” affords the individual greater physical resistance against neural degeneration. Thus, *CYP46* T-alleles might mediate a risk for AD (Helisalmi et al., 2006; Papassotiropoulos et al., 2003). The suggestion of a protective role of the *CYP46* C-alleles (SNP rs754203) is supported by recent findings in a Chinese population. Fu and colleagues showed that elderly subjects with the T allele are more likely to deteriorate in cognitive functioning over a two years period compared with those without the T allele (Fu et al., 2009).

Although several morphometric imaging studies found support for an association of the *BDNF*

val66met SNP (rs6265) with volumetric differences in MTL structures and memory performance (Egan et al., 2003; Hariri et al., 2003; Pezawas et al., 2004; Szeszko et al., 2005; Bueller et al., 2006), we were unable to replicate the finding of smaller hippocampal volumes in *BDNF* val66met carriers compared with val66val carriers within our dataset. Possible explanations include the diversity of methodological approaches applied to measure the volume of interest, the restricted age range of our subjects, the high level of education of our academic sample, the fact that we controlled for genetic variation in additional SNPs as well as background genetic heterogeneity, and/or the different numbers of *BDNF* met66met carriers between our and the other studies.

Evidence is accumulating showing that brain cholesterol metabolism plays an important role in dendrite outgrowth (Fan et al., 2002), synaptogenesis (Mauch et al., 2001), and neuronal survival (Michikawa and Yanagisawa, 1999). Inborn defects in cholesterol metabolism such as the Smith-Lemli-Opitz syndrome (Tint et al., 1994) and the Niemann-Pick type C disease (Sévin et al., 2007) disturb brain development profoundly. The exact molecular and cellular mechanisms that translate the *CYP46* allelic variation into volumetric brain differences in the parahippocampal gyrus and hippocampus are still unknown. However, intronic SNPs have been shown to modulate genetic risk for AD (Dermaut et al., 2002; Wang et al., 2002) possibly through alternative splicing, altered RNA stability, differences in the distribution of the enzyme inside the neural cell, or through a linkage disequilibrium with other so far unknown loci in the *CYP46* gene. Recently, it has been shown that three other SNPs in the *CYP46* gene (rs7157609, rs4900442, and rs3742376) influence the risk for AD (Kölsch et al., 2009; Fu et al., 2009).

If the found structural differences should turn out to persist in older persons, one might speculate that structures may be larger because *CYP46* C-alleles favor the non-amyloidogenic amyloid precursor protein cleavage pathway by inhibiting the beta-site APP-cleaving enzyme (BACE) as suggested by Wolozin (2003), meaning that less Aβ might be produced and deposited during lifetime. Less Aβ production and deposition result in less cell destruction and preserved neural functionality. Therefore, reduced atrophy and hence better memory functions in older age can be expected in *CYP46* C-carriers compared with T-carriers. Taken together the *CYP46* T/C SNP might modulate the vulnerability for AD twofold: through its direct effects on the formation of parahippocampal and hippocampal tissue, neuronal survival, and synaptogenesis in early life and through its indirect role in regulating β-amyloid metabolism at an advanced age.

Disclosure statement

The authors reported no conflicts of interest.

Acknowledgments

We thank the support by the EU contract LSHM-CT-2003-503330 (APOPIS) to C.H. This study was funded in part by the National Centre of Competence in Research on Neural Plasticity and Repair (NCCR) and by grants of the Neuroscience Centre Zurich, the Foundation for Clinical Neuropsychiatric Research, and the Swiss National Science Foundation (3100-067114) to K.H.

References

Ashburner, J., Friston, K.J., 2000. Voxel-based morphometry – The methods. Neuroimage 11, 805-821.

Björkhem, I., Lütjohann, D., Breuer, O., Sakinis, A., Wennmalm, A, 1997. Importance of a novel mechanism for elimination of brain cholesterol. J. Biol. Chem. 272(48), 30178-30184.

Buchmann, A., Mondadori, C.R., Hänggi, J., Aerni, A., Vrticka, P., Luechinger, R., Boesiger, P., Hock, C., Nitsch, R.M., de Quervain, D.J., Papassotiropoulos, A., Henke, K., 2008. Prion protein M129V polymorphism affects retrieval-related brain activity. Neuropsychologia 46(9), 2389-2402.

Bueller, J.A., Aftab, M., Sen, S., Gomez-Hassan, D., Burmeister, M., Zubieta, J.-K., 2006. BDNF Val^{66}Met Allele is Associated with Reduced Hippocampal Volume in Healthy Subjects. Biol. Psychiatry 59(9), 812-815.

de Quervain, D.J.F., Henke, K., Aerni, A., Coluccia, D., Wollmer, M.A., Hock, C., Nitsch, R.M., Papassotiropoulos, A., 2003. A functional genetic variation of the 5-HT2a receptor affects human memory. Nat. Neurosci. 6(11), 1141-1142.

Dermaut, B., Theuns, J., Sleegers, K., Hasegawa, H., van den Broeck, M., Vennekens, K., Corsmit, E., St. George-Hyslop, P., Cruts, M., van Duijn, C.M., van Broeckhoven, C., 2002. The gene encoding nicastrin, a major γ-secretase component, modifies risk for familial early-onset Alzheimer disease in a Dutch population-based sample. Am. J. Hum. Genet. 70, 1568-1574.

Egan, M.F., Kojima, M., Callicott, J.H., Goldberg, T.E., Kolachana, B.S., Bertolino, A., Zaitsev, E., Gold, B., Dean, M., Lu, B., Weinberger, D.R., 2003. The BDNF val66met polymorphism affects activity-dependent secretion of BDNF and human memory and hippocampal function. Cell 112(2), 257-269.

Eickhoff, S., Walters, N.B., Schleicher, A., Kril, J., Egan, G.F., Zilles, K., Watson, J.D., Amunts, K., 2005. High-Resolution MRI Reflects Myeloarchitecture and Cytoarchitecture of Human Cerebral Cortex. Hum. Brain Mapp. 24, 206-215.

Fan, Q.-W., Yu, W., Gong, J.-S., Zou, K., Sawamura, N., Senda, T., Yanagisawa, K., Michikawa, M.,

2002. Cholesterol-dependent modulation of dendrite outgrowth and microtubule stability in cultured neurons. J. Neurochem. 80, 178-190.

Filippini, N., Scassellati, C., Boccardi, M., Pievani, M., Testa, C., BocchioChiavetto, L., Frisoni, G.B., Gennarelli., M., 2006. Influence of serotonin receptor 2A His452Tyr polymorphism on brain temporal structures: a volumetric MR study. Eur. J. Hum. Genet. 14, 443-449.

Fu, B.Y., Ma, S.L.,Tang, N.L., Tam, C.W., Lui, V.W., Chiu, H.F., Lam, L.C., 2009. Cholesterol 24-hydroxylase (CYP46A1) polymorphisms are associated with faster cognitive deterioration in Chinese older persons: a two-year follow-up study. Int. J. Geriatr. Psychiatry doi:10.1002/ gps.2196.

Guzzetti, M., Costa, L.G., 2007. Cholesterol homoestasis in the developing brain: a possible new target for ethanol. Hum. Exp. Toxicol. 26(4), 355-360.

Hariri, A.R., Goldberg, T.E., Mattay, V.S., Kolachana, B.S., Callicott, J.H., Egan, M.F., Weinberger, D.R., 2003. Brain-Derived Neurotrophic Factor val^{66}met Polymorphism Affects Human Memory-Related Hippocampal Activity and Predicts Memory Performance. J. Neurosci. 23(17), 6690-6694.

Helisalmi, S., Vepsäläinen, S., Koivisto, A.M., Mannermaa, A., Iivonen, S., Hiltunen, M., Kiviniemi, V., Soininen, H., 2006. Association of CYP46 intron 2 polymorphism in Finnish Alzheimer's disease samples and a global scale summary. J. Neurol. Neurosurg. Psychiatry 77, 421-422.

Holmes, C.J., Hoge, R., Collins, L., Woods, R., Toga, A.W., Evans, A.C., 1998. Enhancement of MR Images Using Registration for Signal Averaging. J. Comput. Assist. Tomogr. 22(2), 324-333.

Katzman, R., Terry, R., DeTeresa, R., Brown, T., Davies, P., Fuld, P., Renbing, X., Peck, A., 1988. Clinical, pathological, and neurochemical changes in dementia: a subgroup with preserved mental status and numerous neocortical plaques. Ann. Neurol. 23(2), 138-144.

Kimura, D., 1963. Right temporal-lobe damage. Arch. Neurol. 8, 264-271.

Kölsch, H., Lütjohann, D., Jessen, F., Popp, J., Hentschel, F., Kelemen, P., Schmitz, S., Maier, W., Heun, R., 2009. *CYP46A1* variants influence Alzheimer's disease risk and brain cholesterol metabolism. European Psychiatry doi:10.1016/j.eurpsy.2008.12.005.

Lütjohann, D., Breuer, O., Ahlborg, G., Nennesmo, I., Sidén, A., Diczfalusy, U., Björkhem, I., 1996. Cholesterol homeostasis in human brain: Evidence for an age-dependent flux of 24S-hydroxycholesterol from the brain into the circulation. Proc. Nat. Acad. Sci. USA 93, 9799-9804.

Mauch, D.H., Nägler, K., Schumacher, S., Göritz, C., Müller, E.C., Otto, A., Pfrieger, F.W., 2001. CNS Synaptogenesis Promoted by Glia-Derived Cholesterol. Science 294, 1354-1357.

Michikawa, M., Yanagisawa, K., 1999. Inhibition of Cholesterol Production but Not of Nonsterol

Isoprenoid Products Induces Neuronal Cell Death. J. Neurochem. 72, 2278-2285.

Mondadori, C.R., Buchmann, A., Mustovic, H., Schmidt, C.F., Boesiger, P., Nitsch, R.M., Hock., C., Streffer, J., Henke, K., 2006. Enhanced brain activity may precede the diagnosis of Alzheimer's disease by 30 years. Brain 129(11), 2908-2922.

Mondadori, C.R., de Quervain, D.J., Buchmann, A., Mustovic, H., Wollmer, M.A., Schmidt, C.F., Boesiger, P., Hock., C., Nitsch, R.M., Papassotiropoulos, A., Henke, K., 2007. Better memory and neural efficiency in young apolipoprotein epsilon4 carriers. Cereb. Cortex 17(8), 1934-1947.

Mori, E., Girono, N., Yamashita, H., Imamura, T., Ikejiri, Y., Ikeda, M., Kitagaki, H., Shimomura, T., Yoneda, Y., 1997. Premorbid brain size as a determinant of reserve capacity against intellectual decline in Alzheimer's disease. Am. J. Psychiatry 154, 18-24.

Nauck, M., Hoffmann, M.M., Wieland, H., Marz, W., 2000. Evaluation of the apo E genotyping kit on the LightCycler. Clin. Chem. 46, 722-724.

Papassotiropoulos, A., Wollmer, M.A., Aguzzi, A., Hock, C., Nitsch, R.M., de Quervain, D.J., 2005a. The prion gene is associated with human long-term memory. Hum. Mol. Genet. 14, 2241-2246.

Papassotiropoulos, A., Wollmer, M.A., Tsolaki, M., 2005b. A cluster of cholesterol related genes confers susceptibility for Alzheimer`s disease. J. Clin. Psychiatry 66, 940-947.

Papassotiropoulos, A., Streffer, J.R., Tsolaki, M., Schmid, S., Thal, D., Nicosia, F., Iakovidou, V., Maddalena, A., Lütjohann, D., Ghebremedhin, E., Hegi, T., Pasch, T., Traxler, M., Brühl, A., Benussi, L., Binetti, G., Braak, H., Nitsch, R.M., Hock, M.D., 2003. Increased brain β-amyloid load, phosphorylated tau, and risk of Alzheimer`s disease associated with an intronic CYP46 polymorphism. Arch. Neurol. 60, 29-35.

Pezawas, L., Verchinski, B.A., Mattay, V.S., Callicott, J.H., Kolachana, B.S., Dtraub, R.E., Egan, M.F., Meyer-Lindenberg, A., Weinberger, D.R., 2004. The brain-derived neurotrophic factor val66met polymorphism and variation in human cortical morphology. J. Neurosci. 24(45), 10099-10102.

Puglielli, L., Tanzi, R.E., Kovacs, D.M., 2003. Alzheimer's disease: the cholesterol connection. Nat. Neurosci. 6(4), 345-351.

Ranganath, C., Blumenfeld, R.S., 2005. Doubts about double dissociations between short- and long-term memory. Trends Cogn. Sci. 9(8), 374-380.

Reiman, E.M., Chen, K., Caselli, R.J., Alexander, G.E., Bandy, D., Adamson, J.L., Lee, W., Cannon, A., Stephan, E.A., Stephan, D.A., Papassotiropoulos, A., 2008. Cholesterol-related genetic risk scores are associated with hypometabolism in Alzheimer's-affected brain regions. Neuroimage 40, 1214-1221.

Rey A., 1958. L'examen clinique en psychologie. Presses Universitaires de France, Paris, France.

Sévin, M., Lesca, G., Baumann, N., Millat, G., Lyon-Caen, O., Vanier, M.T., Sedel, F., 2007. The adult form of Niemann-Pick disease type C. Brain 130, 120-133.

Simons, M., Keller, P., De Strooper, B., Beyreuther, K., Dotti, C.G., Simons, K., 1998. Cholesterol depletion inhibits the generation of beta-amyloid in hippocampal neurons. Proc. Natl. Acad. Sci. USA 95, 6460-6464.

Squire, L., Alvarez, P., 1995. Retrograde amnesia and memory consolidation: a neurobiological perspective. Curr. Opin. Neurobiol. 5(2), 169-177.

Szeszko, P.R., Lipsky, R., Mentschel, C., Robinson, D., Gunduz-Bruce, H., Sevy, S., Ashtari, M., Napolitano, B., Bilder, R.M., Kane, J.M., Goldman, D., Malhotra, A.K., 2005. Brain-derived neurotrophic factor val66met polymorphism and volume of the hippocampal formation. Mol. Psychiatry 10, 631-636.

Tewes, U., 1991. HAWIE-R. Hamburg-Wechsler Intelligenztest für Erwachsene Revision 1991. Verlag Hans Huber, Bern, Switzerland.

Tint, G.S., Irons, M., Elias, E.R., Batta, A.K., Frieden, R., Chen, T.S., Salen, G., 1994. Defective Cholesterol Biosynthesis Associated with the Smith-Lemli-Opitz Syndrome. New Engl. J. Med. 330, 107-113.

Tzourio-Mazoyer, N., Landeau, B., Papathanassiou, D., Crivello, F., Etard, O., Delcroix, N., Mazoyer, B., Joliot, M., 2002. Automated Anatomical Labeling of Activations in SPM Using a Macroscopic Anatomical Parcellation of the MNI MRI Single-Subject Brain. Neuroimage 15, 273-289.

Wang, X., DeKosky, S.T., Ikonomovic, M.D., Kamboh, M.I., 2002. Distribution of plasma α1-antichymotrypsin levels in Alzheimer disease patients and controls and their genetic controls. Neurobiol. Aging 23, 377-382.

Wechsler, D., 1981. Wechsler Adult Intelligence Scale – Revised. Psychological Corporation, San Antonio, Texas.

Wolozin, B., 2003. Cyp46 (24S-cholesterol hydroxylase): a genetic risk factor for Alzheimer disease. Arch. Neurol. 60, 16-18.

3.3 Study 3: Neuromorphometric profiling in mild cognitive impairment and Alzheimer's disease: Sensitivity and specificity

Neuromorphometric profiling in mild cognitive impairment and Alzheimer's disease: Sensitivity and specificity

Jürgen Hänggi[1,2*], Johannes Streffer[1], Andri Signorell[1], Lutz Jäncke[2], and Christoph Hock[1]

[1] Division of Psychiatry Research, Psychiatric University Hospital, University of Zurich, Switzerland
[2] Division of Neuropsychology, Institute of Psychology, University of Zurich, Switzerland

[*] Corresponding author: J. Hänggi (j.haenggi@psychologie.uzh.ch)

Authors' information
Jürgen Hänggi, Ph.D.
Division of Neuropsychology
Institute of Psychology
University of Zurich
Binzmuehlestrasse 14 / PO Box 25
8050 Zurich
Phone: 0041 44 635 73 97
Fax: 0041 44 635 74 09
Email: j.haenggi@psychologie.uzh.ch

Division of Psychiatry Research
Psychiatric University Hospital
University of Zurich
Lenggstrasse 31 / PO Box 1931
8032 Zurich, Switzerland

Key words
Dementia diagnostics; Structural magnetic resonance imaging; Neuromorphometric profiling; Alzheimer's disease; Amnestic mild cognitive impairment; Sensitivity and specificity

Running head
Neuromorphometric profiling in dementia diagnostics

Abstract

Background: Diagnosing Alzheimer's disease (AD) and distinguishing it from other dementia as well as from amnestic mild cognitive impairment (MCI) depends mainly on clinical evaluation, and, ultimately, on investigator's judgement. Clinical evaluation is based primarily on neuropsychological assessments and secondary on biomarkers found in cerebrospinal fluid. The present study explores the potential of volumetric magnetic resonance imaging (MRI) to diagnose AD in vivo and to separate it from patients with amnestic MCI and healthy control subjects (HCS).

Methods: We acquired 3D volumetric T1-weighted MRI scans of 12 age-matched HCS, 18 patients with amnestic MCI, and 59 patients with probable late onset Alzheimer's disease (PRADL). These MR images were spatially normalised into a stereo-tactic space, segmented into tissue compartments, Jacobian and hidden Markov random field modulated, and the resulted grey matter segments were full automatically parcellated into 45 regions of interest (ROIs) per hemisphere and the volumes of the ROIs were computed.

Results: Promising diagnostic values for distinguishing PRADL patients from HCS were found for the total grey matter (sensitivity/specificity: 88.1%/91.7%), the hippocampi (both 93.2%/91.7%), and the right and left superior parietal gyrus (96.6%/83.3% and 93.2%/83.3%, respectively), for distinguishing MCI from PRADL patients for the left inferior temporal gyrus (86.4%/72.2%) and the right hippocampus (84.7%/66.7%), and for distinguishing MCI patients from HCS for the left Heschl's gyrus (88.9%/83.3%) and the left superior temporal gyrus (83.3/83.3%).

Conclusion: We showed potential diagnostic values of MRI-based neuromorphometric profiling in dementia diagnostics. Therefore, we propose to establish a standardised database of regional brain volumes based on large series of patients and controls. A new patient can then be compared to these norms and statistical measures for a single subject can be derived to support and corroborate the general and differential diagnosis of dementia.

Background

Diagnosing Alzheimer's disease (AD) and distinguishing it from other dementia as well as from amnestic mild cognitive impairment (MCI) depends mainly on clinical evaluation, and, ultimately, on investigator's judgement. Clinical evaluation is based primarily on neuropsychological assessments and secondary on biomarkers found in cerebrospinal fluid. Structural magnetic resonance imaging (MRI) is used almost only for exclusionary diagnostic purposes. AD is characterised by progressive cerebral atrophy that can be measured using structural MRI as well as by perfusion and metabolic deficits that can be measured using positron emission tomography and single photon emission

computed tomography. AD is accompanied by impairments in several cognitive domains (e.g., memory, executive functions, and orientation) that can be measured using neuropsychological assessments. Cerebral atrophy along with progressive cognitive decline is used to diagnose AD clinically, although definitive AD diagnosis is based on histologic post mortem analyses. From a therapeutic perspective, identifying individuals at risk for developing AD as early as possible and distinguishing AD patients from patients with other dementia as well as from patients with amnestic MCI is imperative for maximising treatment efficacy.

Episodic memory impairments are generally the earliest sign seen in AD [1]. Executive functions (which include the abilities responsible for concurrent manipulation of information, concept formation, inhibition of alternative reactions, and goal-directed behaviour) also show significant declines early in the course of AD [1]. Other cognitive domains that are impaired in the course of the AD pathology are orientation, attention, semantic and working memory, language, visuospatial functions, and perception. These cognitive deficits were confirmed also in preclinical AD patients as revealed by a meta-analysis of 47 studies published between 1985 and 2003 [2]. The neural substrates of episodic memory (the medial temporal lobe, MTL) and executive functions (the prefrontal cortex, PFC) are well known from functional imaging studies [3]. A meta-analysis of structural and functional brain imaging studies in AD [4] revealed that almost the whole brain, except occipital and sensorimotor areas, is affected by atrophy. Clearly, the extent and magnitude of atrophy depends on the stage of the disease.

There are numerous cross-sectional [5-13] and longitudinal [14-19] studies that have investigated the neural patterns of atrophy among healthy control subjects (HCS) and patients with amnestic MCI and AD using fully automated, computational, neuromorphometric procedures, e.g., voxel-based morphometry (VBM). In summary, these studies have revealed that besides MTL structures there were also atrophic regions in temporal, parietal, and frontal lobes. Other affected structures that were not found consistently across studies were the cingulate gyri, insulae, caudate nuclei, and thalami. These studies revealed qualitative and quantitative distinct patterns of atrophy among HCS and patients with amnestic MCI and AD. If the qualitative and quantitative neuroanatomical differences are measured in single subjects during the clinical evaluation using structural MRI, this information can be used to support and corroborate the general as well as the differential diagnosis of dementia in clinical daily routine. To our knowledge, with the exception of manually traced hippocampal and entorhinal volumes, there neither are reports that investigated the diagnostic values of the volumes of local neocortical structures nor reports that established the normal values of local brain structures for different pathological populations like patients with amnestic MCI and AD, although some databases exist that are able to provide data needed.

Here we report about qualitative and quantitative volumetric brain differences as neuromorphometric markers of neurodegenerative processes among HCS, patients with amnestic MCI, and patients with probable late onset AD (PRADL). We aimed at computing the diagnostic values (sensitivity, specificity, positive and negative predictive value, area under the curve) of these structural brain differences. Based on the literature [5-19] we expected qualitative as well as quantitative localised volume differences among the brains of the three groups not only in the medial temporal lobe (e.g., hippocampus) but also in neocortical brain structures (e.g., parietal lobes and lateral temporal lobes).

Methods

Participants: The 12 healthy elderly control subjects (HCS), 18 patients with amnestic mild cognitive impairment (MCI), and 59 late-onset Alzheimer's disease (PRADL) patients were drawn from our clinical database. All participants gave written informed consent to use their data for research. The data acquisition for the clinical purpose was approved by the local ethics committee of the Canton of Zurich, Switzerland, and took place from October 2001 through June 2006. Most patients included in our study were outpatients from Switzerland.

Neuropsychology: The clinical diagnosis of probable Alzheimer's disease followed National Institute of Neurological and Communicative Disorders and Stroke (NINCDS) / Alzheimer's Disease and Related Disorders Association (ADRDA) guidelines [20]. The clinical diagnosis of amnestic MCI was based on criteria published by Petersen and colleagues [21]. The cognitive status of the patients and HCS were assessed with the German version of the CERAD (Consortium to Establish a Registry for Alzheimer's Disease) test battery [22]. We used the mini mental state examination (MMSE) scores [23] as a global measure of disease severity. Memory functions were assessed with subtests from the Wechsler Memory Scale – Revised (WMS-R) in German [24]; spatial thinking with the Luria Mental Rotation Test [25]; executive functions with a verbal (S-Words) fluency task [26] and a nonverbal (5-Points) fluency task [27]; the Kramer Card Sorting Test [28] and the Stroop test [29]. For some patients, instead of the CERAD test battery the Alzheimer's Disease Assessment Scale (ADAS) cognitive part (ADAS-Cog) [30] was used. Orientation, attention, language, and praxis were assessed only excursively. Thus, the diagnoses, which were made by an interdisciplinary team comprised by neurologists, psychiatrists, and neuropsychologists, are based on the reference standard (NINCDS-ADRDA guidelines) [20]. Data collection was done retrospectively.

MRI data acquisition: MRI scans were acquired on three different scanners: on a 1.5 T GE Signa (General Electric Medical Systems, Milwaukee, WI), on a 1.5 T Siemens Sonata (Siemens, Erlangen, Germany), and on a 3.0 T Philips Intera (Philips, Best, the Netherlands) scanner. Volumetric 3D T1-

weighted gradient echo sequences (for GE Signa: Magnetisation Prepared Inversion Recovery, MPIR; for Siemens Sonata: Turbo Inversion Recovery, TIR; for Philips Intera: Turbo Field Echo, TFE) scans in the sagittal or coronal plane were obtained with three different spatial resolutions (0.94x0.94x1.5 mm; 0.94x0.94x1.8 mm; 0.49x0.49x1.0 mm) and two different acquisition matrices (256x256 pixels for the two lower resolutions and 512x512 pixels for the higher resolution). The numbers of slices were 100, 120, or 176, respectively. Scanning parameters for the different pulse sequences were as follow: repetition time / echo time / inversion time / flip angle (TR/TE/TI/FA) for MPIR (GE Signa) 12.1ms/5.16ms/450.0ms/15°; for TIR (Siemens Sonata) 1900.0ms/3.93ms/1100.0ms/15°; for TFE (Philips Intera) 9.85ms/4.59ms/0.0ms/8°.

Preprocessing of MRI data: Image preprocessing was done with the Statistical Parametric Mapping (SPM5) software (http://www.fil.ion.ucl.ac.uk/spm). Based on the 3D T1-weighted structural MRI scan that covered the whole brain, we applied the preprocessing of voxel-based morphometry (VBM) [31] implemented in the VBM5 toolbox (http://dbm.neuro.uni-jena.de/vbm/) to obtain grey matter (GM) segments. Because SPM5 enables image registration, tissue classification, and bias correction within the same generative model [32], the procedure called optimised VBM [33,34] is no longer needed when working with SPM5 [32]. Additionally, a Hidden Markov Random Field (HMRF) model was used to enhance the segmentation process [35] (http://dbm.neuro.uni-jena.de/vbm/markov-random-fields/). Instead of using the canonical a priori maps (ICBM452, international consortium for brain mapping 452 templates), we decided to construct customised a priori maps because the populations under investigation differ from the ICBM452 a priori maps with respect to age and neurodegeneration in the pathological groups.

Parcellation procedure: The cortical and subcortical GM was parcellated into 45 volumes of interest (VOIs) per hemisphere and their volumes were computed. A similar approach was used in another study [36] and is implemented in the IBASPM (Individual Brain Atlases using Statistical Parametric Mapping) software (http://www.thomaskoenig.ch/Lester/ibaspm.htm). The masks for the parcellation were derived from the software MARINA (MAsks for Region of INterest Analysis [37] (http://www.bion.de/index.php?title=Downloads&lang=deu). These masks were originally drawn by other researchers [38] on the MNI single-subject brain [39]. The preprocessing of the MR images and the parcellation procedure are in brief summarised below.

(I) After have run a first VBM in SPM5 that normalised and segmented the raw T1-weighted images, we created customised a priori maps from the normalised, segmented, HMRF (with 0.3) modulated, and unsmoothed GM, white matter (WM), and cerebrospinal fluid (CSF) images of the whole study population. (II) We then segmented the native T1-weighted images again with the customised a priori maps created in the first step. (III) We also segmented the MNI single-subject brain [39], on which the

masks were originally drawn [38], with the customised a priori maps created in step I. In this way, we got the warping parameters that have to be used to adjust the MNI single-subject brain onto the customised a priori maps. (IV) All masks implemented in the MARINA software were saved individually and some of them were combined to avoid too small VOIs. (V) We then applied the warps that were computed in step III to the masks to bring them in congruence with the structures within the customised a priori maps. (VI) Next we multiplied each mask with the unsmoothed GM image of the subjects obtained in step II. (VII) The new binary images now contain only the GM that is localised within an individual mask. (VIII) In the last step, we used an in-house MATLAB script to compute the volumes within these VOIs.

Statistical analyses: Statistical Package for the Social Sciences (SPSS 14, http://www.spss.com/) software was used for statistical analyses. We used two-factorial (diagnosis and gender) univariate analysis of covariance models (ANCOVAs) and receiver operating characteristic (ROC) curves to analyse our data. In some ANCOVAs, the error variances were heteroscedastic ($0.1 < p < 0.25$) instead of $p > 0.25$ which is the appropriate threshold to show statistical equality. Heteroscedasticity is mainly caused by the unequal sizes of the groups. For the ROC curves we used cut-off values that optimised both sensitivity and specificity. Because the MRI scans of the patients and healthy control subjects were acquired on three different scanners (in a balanced way across groups), a separate ANCOVA was performed with the different scanners as a covariate of no interest to rule out possible cross scanner effects.

Results

Demographic and behavioural characteristics of the populations are shown in Table 1. There were no significant differences among the groups with respect to gender, age, education, and total head volume. As expected, the groups significantly differed with respect to their mini mental state examination (MMSE) scores.

	HCS (n = 12) Mean	S.D.	Min.	Max.	MCI (n = 18) Mean	S.D.	Min.	Max.	PRADL (n = 59) Mean	S.D.	Min.	Max.
Age (y)	71.4	6.01	62.0	83.0	70.5	5.53	65.0	88.0	75.3	6.58	61.0	90.0
Education (y)	12.0	2.92	7.0	17.0	13.5	3.62	8.0	20.0	11.9	3.22	6.0	20.0
THV (cm^3)	1716.7	176.58	1472.5	1974.4	1846.5	142.51	1608.3	2064.8	1772.8	169.73	1407.3	2156.6
MMSE (points)*	29.0	1.04	27.0	30.0	25.9	2.80	21.0	30.0	20.7	3.45	14.0	27.0
	Frequency				**Frequency**				**Frequency**			
Gender (f/m)	6 / 6				6 / 12				33 / 26			

Table 1: Demographic characteristics of the healthy control subjects and the patients with amnestic mild cognitive impairment and Alzheimer's disease. There were no significant differences between the groups with respect to age ($p = 0.154$), education ($p = 0.206$), and THV ($p = 0.099$) (ANOVA, two-tailed) and with respect to gender ($p = 0.244$) (Chi2, two-tailed). * MMSE scores were significant ($p<0.001$) different among the three groups (independent t-Tests, two-tailed). Abbreviations: HCS, healthy control subjects; MCI, amnestic mild cognitive impairment; PRADL, probable late onset Alzheimer's disease; S.D., standard deviation; Min., minimum; Max., maximum; y, years; THV, total head volume; MMSE, mini mental state examination.

The volumes of the brain structures that provide diagnostic information (are significantly differed among the groups) are shown in Table 2. The diagnostic values (sensitivity, specificity, positive and negative predictive value, test efficiency, and the area under the curve) of these volume differences are presented in Tables 3-5. The diagnostic values of the volumes for distinguishing patients with amnestic mild cognitive impairment (MCI) from healthy control subjects (HCS) are shown in Table 3, for distinguishing patients with MCI from patients with probable late onset Alzheimer's disease (PRADL) see Table 4, and for distinguishing HCS from patients with PRADL see Table 5.

Across all 19 brain structures that showed significant volume differences among the three groups in the ANCOVA analyses (Table 2), highest mean sensitivity and specificity were found between HCS and PRADL patients (87.2% and 81.5%, respectively), lowest mean sensitivity and specificity were found between MCI and PRADL patients (79.9% and 67.5%, respectively). The magnitudes of the diagnostic values for HCS versus MCI were between the two other contrasts (84.0% and 76.0%, respectively).

Brain structures (cm^3)	HCS (n = 12) Mean	S.D.	Min.	Max.	MCI (n = 18) Mean	S.D.	Min.	Max.	PRADL (n = 59) Mean	S.D.	Min.	Max.
Total grey matter volume	668.11	51.00	593.20	731.32	601.76	59.37	508.52	695.21	526.54	80.81	379.35	724.40
Total white matter volume	456.61	42.33	407.32	543.15	460.39	59.45	360.89	545.94	400.67	58.09	281.93	517.23
Total cerebrospinal fluid plus volume*	592.03	147.75	401.28	826.53	784.31	136.14	412.33	973.64	845.60	154.29	548.26	1267.38
Left hippocampus	3.31	0.27	2.99	3.77	2.72	0.52	1.74	3.52	2.13	0.52	0.99	3.58
Right hippocampus	3.19	0.30	2.76	3.75	2.46	0.61	1.52	3.48	1.77	0.61	0.66	3.40
Left inferior temporal gyrus	11.76	0.95	10.31	12.96	10.93	1.14	9.07	13.47	9.18	1.28	6.25	12.24
Left middle temporal gyrus	17.59	1.79	14.85	19.65	16.15	1.84	13.51	19.50	13.60	2.09	10.09	18.45
Left superior temporal gyrus	7.26	0.78	5.82	8.63	6.10	0.75	4.77	7.92	5.28	1.01	3.32	7.91
Left middle temporal pole	2.22	0.22	1.88	2.57	1.95	0.32	1.43	2.34	1.60	0.33	0.89	2.63
Left superior temporal pole	2.66	0.51	1.98	3.38	2.00	0.41	1.21	2.85	1.60	0.41	0.67	2.65
Right superior temporal pole	3.63	0.43	2.83	4.27	2.98	0.47	2.14	3.69	2.48	0.58	1.34	3.79
Left Heschl's gyrus	0.84	0.19	0.48	1.08	0.52	0.16	0.23	0.81	0.40	0.18	0.10	1.00
Left superior parietal gyrus	3.28	0.52	2.57	4.54	2.62	0.53	1.93	4.07	2.09	0.57	0.73	3.34
Right superior parietal gyrus	2.75	0.49	1.96	3.49	2.14	0.50	1.29	3.40	1.63	0.49	0.47	2.64
Right precuneus	8.83	1.06	7.26	10.21	7.15	1.02	5.50	9.38	6.64	1.21	4.28	10.30
Left lingual gyrus	8.32	0.86	6.48	9.69	8.11	0.80	6.75	9.35	7.55	1.25	4.90	10.51
Right lingual gyrus	8.44	0.93	6.89	9.76	7.76	0.89	6.47	9.69	7.08	1.31	4.44	10.33
Left orbital inferior frontal gyrus	5.35	0.43	4.46	6.23	5.16	0.68	3.98	6.88	4.47	0.82	2.78	6.51
Left insula	6.93	0.78	5.36	8.23	5.96	0.96	4.61	7.82	4.82	1.05	2.76	7.55

Table 2: Absolute volumes of neuroanatomical structures that distinguish among the groups. * Total cerebrospinal fluid plus volume includes also parts of scalp, skull, and meninges. Abbreviations: HCS, healthy control subjects; MCI, amnestic mild cognitive impairment; PRADL, probable Alzheimer's disease late onset; S.D., standard deviation; Min., minimum; Max., maximum; y, years.

For distinguishing MCI patients from HCS, the left Heschl's gyrus (88.9%/83.3%), the left superior temporal gyrus (83.3%/83.3%), and the right precuneus (88.9%/75.0%) revealed most promising diagnostic values (Table 3).

Brain structures	HCS (n=12) vs MCI (n=18) % Vol. Diff.	p(Diff.)	Cut-off (cm^3)	Sensitivity %	Specificity %	PPV %	NPV %	Efficiency %	AUC	p(AUC)
Total grey matter volume	-9.9	0.001	649.0	77.8	66.7	77.8	75.0	73.3	0.792	0.008
Total cerebrospinal fluid plus volume*	32.5	0.025	701.0	83.3	75.0	83.3	75.0	80.0	0.856	0.001
Left hippocampus	-17.8	n.s	3.11	83.3	75.0	83.3	75.0	80.0	0.829	0.003
Right hippocampus	-22.9	*0.058*	2.91	83.3	75.0	83.3	75.0	80.0	0.852	0.001
Left superior temporal gyrus	-16.0	0.015	6.65	83.3	83.3	88.2	76.9	83.3	0.87	0.001
Right superior temporal pole	-17.9	0.015	3.51	83.3	75.0	83.3	75.0	80.0	0.866	0.001
Left Heschl's gyrus	-37.8	0.001	0.688	88.9	83.3	88.9	83.3	86.7	0.889	0.0004
Right precuneus	-19.0	0.038	8.06	88.9	75.0	84.2	81.8	83.3	0.875	0.001

Table 3: Diagnostic values and relative volume differences between healthy control subjects and patients with amnestic mild cognitive impairment. * Total cerebrospinal fluid plus volume includes also parts of scalp, skull, and meninges. Abbreviations: n.s., not significant ($p > 0.1$); Cursively printed probabilities are trends ($0.05 < p < 0.1$); PPV, positive predictive value; NPV, negative predictive value; AUC, area under the curve; HCS, healthy control subjects; MCI, mild cognitive impairment; % Vol. Diff.; mean volume difference relative to HCS; p, probability.

For distinguishing MCI from PRADL patients, the left inferior temporal gyrus (86.4%/72.2%) and the right hippocampus (84.7%/66.7%) revealed most promising diagnostic values, although for the hippocampi there were only trends toward significance (Table 4).

Brain structures	MCI (n=18) vs PRADL (n=59) % Vol. Diff.	p(Diff.)	Cut-off (cm^3)	Sensitivity %	Specificity %	PPV %	NPV %	Efficiency %	AUC	p(AUC)
Total grey matter volume	-12.5	0.002	576.0	78.0	61.1	86.8	45.8	74.0	0.767	0.001
Total white matter volume	-13.0	0.003	449.0	79.7	61.1	87.0	47.8	75.3	0.760	0.001
Left hippocampus	-21.7	*0.063*	2.56	79.7	72.2	90.4	52.0	77.9	0.793	0.0002
Right hippocampus	-18.0	*0.057*	2.29	84.7	66.7	89.3	57.1	80.5	0.798	0.0001
Left inferior temporal gyrus	-16.0	0.001	10.47	86.4	72.2	91.1	61.9	83.1	0.847	0.000009
Left middle temporal gyrus	-15.8	0.017	14.91	76.3	72.2	90.0	48.1	75.3	0.819	0.00004
Left insula	-19.1	0.033	5.38	74.6	66.7	88.0	44.4	72.7	0.796	0.0002

Table 4: Diagnostic values and relative volume differences between patients with amnestic mild cognitive impairment and patients with Alzheimer's disease. * Total cerebrospinal fluid plus volume includes also parts of scalp, skull, and meninges. Abbreviations: n.s., not significant ($p > 0.1$); cursively printed probabilities are trends ($0.05 < p < 0.1$); PPV, positive predictive value; NPV, negative predictive value; AUC, area under the curve; PRADL, probable Alzheimer's disease late onset; MCI, mild cognitive impairment; % Vol. Diff.; mean volume difference relative to MCI; p, probability.

For distinguishing PRADL patients from HCS, the total GM (sensitivity/specificity: 88.1%/91.7%), the total CSF plus (83.1%/83.3%), the right hippocampus (93.2%/91.7%), the left hippocampus (93.2%/91.7%), the left inferior temporal gyrus (88.1%/83.3%), and the left and right superior parietal gyrus (93.2%/83.3% and 96.6%/83.3%, respectively) revealed most promising diagnostic values (Table 5).

Brain structures	HCS (n=12) vs PRADL (n=59) % Vol. Diff.	p(Diff.)	Cut-off (cm^3)	Sensitivity %	Specificity %	PPV %	NPV %	Efficiency %	AUC	p(AUC)
Total grey matter volume	-21.2	0.00000004	605.0	88.1	91.7	98.1	61.1	88.7	0.935	0.000002
Total white matter volume	-12.3	0.0004	435.0	71.2	66.7	91.3	32.0	70.4	0.766	0.004
Total cerebrospinal fluid plus volume*	42.8	0.000000009	701.0	83.1	83.3	96.1	50.0	83.1	0.887	0.00003
Left hippocampus	-35.6	0.001	2.997	93.2	91.7	98.2	73.3	93.0	0.973	0.0000003
Right hippocampus	-44.5	0.0003	2.832	93.2	91.7	98.2	73.3	93.0	0.966	0.0000004
Left inferior temporal gyrus	-21.9	0.001	10.66	88.1	83.3	96.3	58.8	87.3	0.945	0.000001
Left middle temporal gyrus	-22.7	0.060	15.56	83.1	83.3	96.1	50.0	83.1	0.928	0.000003
Left superior temporal gyrus	-27.3	0.036	6.73	93.2	83.3	96.5	71.4	91.5	0.931	0.000003
Left middle temporal pole	-28.1	0.007	1.94	84.7	83.3	96.2	52.6	84.5	0.936	0.000002
Left superior temporal pole	-39.8	0.00006	2.10	88.1	83.3	96.3	58.8	87.3	0.956	0.000001
Right superior temporal pole	-31.7	0.016	3.16	89.8	83.3	96.4	62.5	88.7	0.939	0.000002
Left Heschl's gyrus	-51.7	0.0002	0.675	91.5	75.0	94.7	64.3	88.7	0.941	0.000002
Left lingual gyrus	-9.3	0.002	8.22	76.3	75.0	93.8	39.1	76.1	0.701	0.029
Right lingual gyrus	-16.1	0.020	8.05	81.4	66.7	92.3	42.1	78.9	0.811	0.001
Left superior parietal gyrus	-36.3	0.010	2.88	93.2	83.3	96.5	71.4	91.5	0.959	0.000001
Right superior parietal gyrus	-40.7	0.001	2.46	96.6	83.3	96.6	83.3	94.4	0.948	0.000001
Left orbital inferior frontal gyrus	-16.4	0.026	5.22	84.7	75.0	94.3	50.0	83.1	0.839	0.0002
Left insula	-30.5	0.005	6.14	89.8	83.3	96.4	62.5	88.7	0.935	0.000002

Table 5: Diagnostic values and relative volume differences between healthy control subjects and patients with Alzheimer's disease. * Total cerebrospinal fluid plus volume includes also parts of scalp, skull, and meninges. Abbreviations: n.s., not significant ($p > 0.1$); cursively printed probabilities are trends ($0.05 < p < 0.1$); PPV, positive predictive value; NPV, negative predictive value; AUC, area under the curve; HCS, healthy control subjects; PRADL, probable Alzheimer's disease late onset; % Vol. Diff.; mean volume difference relative to HCS; p, probability.

The medians, quartiles, and outliers of the best distinguishing volumes are presented in Figure 1 and 2. Volumetric brain differences were only reported when both the ANCOVA as well as the ROC curves were significantly different among the groups except for the key structure in AD – the hippocampus.

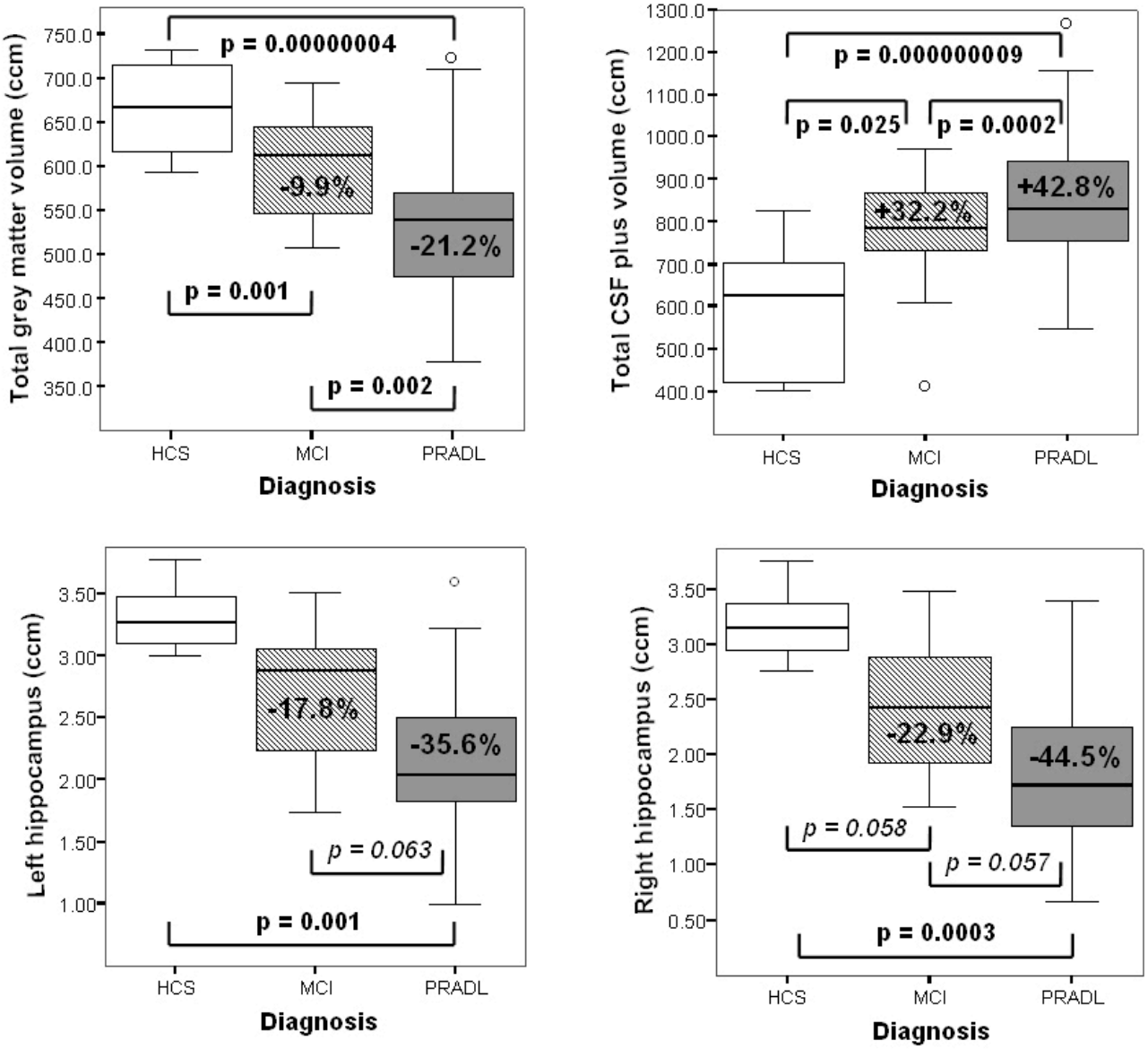

Figure 1: Medians, quartiles, and outliers (circles) of the local brain structure volumes with the most promising diagnostic values among the three different groups. Left top panel: Total grey matter volumes. Right top panel: Total cerebrospinal fluid plus (including also parts of scalp, skull, and meninges) volumes. Left bottom panel: Left hippocampal volumes. Right bottom panel: Right hippocampal volumes. Percent volume differences are relative to healthy control subjects. Number of subjects were as follow: Healthy control subjects (HCS), n = 12; patients with amnestic mild cognitive impairment (MCI), n = 18; patients with probable late onset Alzheimer's disease (PRADL), n = 59. Probabilities (p) printed cursively are trends ($0.05 < p < 0.10$).

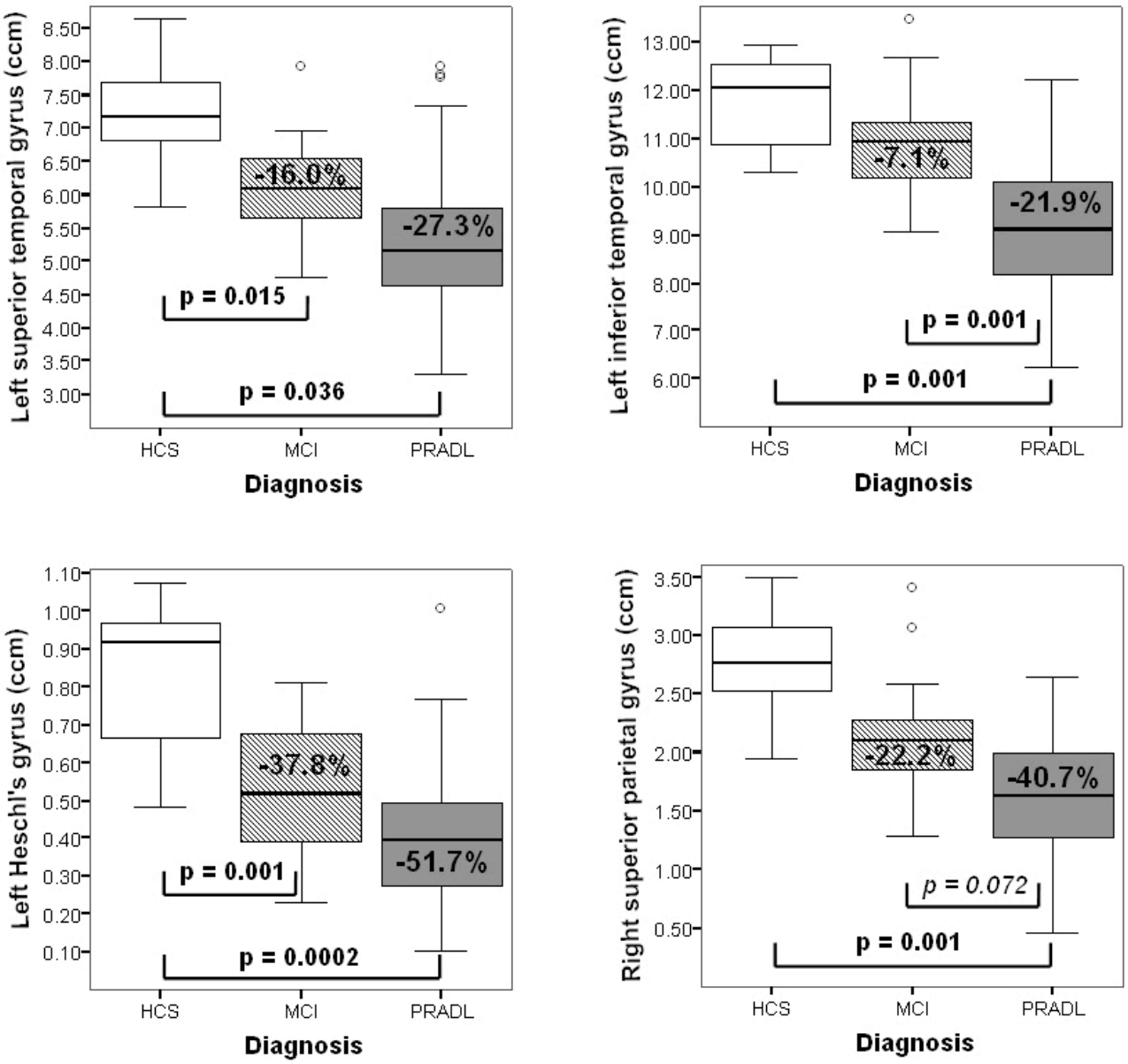

Figure 2: Medians, quartiles, and outliers (circles) of the local brain structure volumes with the most promising diagnostic values among the three different groups. Left top panel: Left superior temporal gyrus volumes. Right top panel: Left inferior temporal gyrus volumes. Left bottom panel: Left Heschl's gyrus volumes. Right bottom panel: Right superior parietal gyrus volumes. Percent volume differences are relative to healthy control subjects. Number of subjects were as follow: Healthy control subjects (HCS), n = 12; patients with amnestic mild cognitive impairment (MCI), n = 18; patients with probable late onset Alzheimer's disease (PRADL), n = 59. Probabilities (p) printed cursively are trends ($0.05 < p < 0.10$).

The additional analysis with the different scanners as a covariate of no interest revealed equal results compared to the results obtained without modelling the different scanners in the statistical models. Therefore, all results reported in this study based on statistical models that do not include the different scanners as a covariate of no interest.

Discussion

Here we report about the sensitivity and specificity of local neuroanatomical volume differences in distinguishing among healthy elderly control subjects (HCS), patients with amnestic mild cognitive impairment (MCI), and patients with probable late onset Alzheimer's disease (PRADL). Most promising diagnostic values were found for the volumes of the following structures: the left and right hippocampus (sensitivity/specificity: 93.2%/91.7% and 93.2%/91.7%, respectively) and the right superior parietal gyrus (96.6%/83.3%) for distinguishing PRADL patients from HCS; the left inferior temporal gyrus (86.4%/72.2%) and the right hippocampus (84.7%/66.7%) for distinguishing MCI from PRADL patients; the left Heschl's gyrus (88.9%/83.3%) and the left superior temporal gyrus (83.3/83.3%) for distinguishing MCI patients from HCS.

The diagnostic accuracy (an integration of sensitivity and specificity) of the local neuroanatomical volume differences was superior compared to the accuracy of common neuropsychological assessments. Comprehensive neuropsychological tests rarely surpass 70% sensitivity and specificity [40]. For the criteria of the National Institute of Neurological and Communicative Disorders and Stroke and the Alzheimer's Disease and Related Disorders Association (NINCDS-ADRDA) [20], which are commonly used for the clinical diagnosis of Alzheimer's disease, the diagnostic accuracy is relatively low, with sensitivity of around 80% and specificity of around 70% [41]. For the German version of the CERAD (Consortium to Establish a Registry for Alzheimer's Disease) test battery [22], Barth and colleagues [42] showed that only patients with moderate AD (mean ± S.D.: MMSE 15.0 ± 2.9) can sufficiently distinguished from HCS using the CERAD. For distinguishing patients with MCI, patients with mild AD, and patients with a major depression from HCS, the diagnostic values of the CERAD were insufficient.

However, the diagnostic values of biomarkers found in CSF are comparable to the diagnostic values achieved with the volumes of dedicated neuroanatomical structures as the hippocampi, the left Heschl's gyrus, and the right and left superior parietal gyrus. The focus in CSF biomarkers is on the β-amyloid (Aβ) peptide (Aβ 1-40 and Aβ 1-42) and on the tau (τ) protein (total and phosphorylated tau). In a longitudinal study on MCI patients de Leon and colleagues [43] found a classification accuracy of 87% at baseline and 81% at follow-up for phosphorylated tau (P-tau 231), and a classification accuracy of 75% at follow-up for Aβ1-40. For isoprostane – a by-product of membrane oxidative damage and hence a direct marker of neurodegeneration – the classification accuracy was 88% at both baseline and follow-up [43]. Longitudinal effects over an interval of 1.8 years were only found for isoprostane and not for Aβ and tau [43]. That study also investigated the diagnostic values of a delayed paragraph recall and of hippocampal volumes. The diagnostic accuracy was 73% at follow-up for the delayed paragraph recall and 94% at baseline and 88% at follow-up for the hippocampal volumes [43].

Other CSF biomarker studies reported higher diagnostic values when using combinations of these CSF markers. E.g., Hansson and colleagues [44] reported a sensitivity of 95% and a specificity of 83% for the detection of incipient AD in patients with MCI when using a combination of total tau and Aβ1-42. But other CSF biomarker studies reported much smaller diagnostic values. E.g., Blasko and colleagues [45] investigated Aβ1-42 and reported sensitivities of 60% for HCS-to-MCI converters and 54% for HCS-to-AD converters and specificities of 63% for both converter groups.

Our study showed promising results with respect to the diagnostic accuracy of the volumes of dedicated local brain structures. Prospective studies with larger samples are needed to evaluate our promising findings. Because it is recommended to use structural MRI in dementia diagnostics to exclude other causes like tumours or vascular lesions that could also explain cognitive deficits, no additional brain images have to be acquired to use MRI-based neuromorphometric profiling. The only thing that has to be changed is the manner of MR image acquisition. Instead of acquiring a so called "clinical" T1-weighted MR image comprising of only about 20-40 slices and hence does not cover the whole brain, a volumetric 3D T1-weighted MR image of the whole brain without gaps have to be acquired in order to be used in computational MRI-based neuromorphometric profiling.

Conclusion

Therefore, we propose to standardise local brain structure volumes in a large series of patients and controls in order to establish the neuromorphometric normal values in these populations. A new patient can then be compared to these norms and statistical measures (e.g., z-scores and confidence intervals) for a single subject can be derived to support and corroborate the general and differential diagnosis of dementia. Obviously, this standardisation has to be done in a multi-centre study due to the large number of patients and controls needed. Because our neuroanatomical parcellation procedure can be fully automated, it could easily be used in clinical daily routine assessment of dementia once the normative values will be established. Our findings also point to the importance of focusing on neocortical structures in AD and not only on the medial temporal lobe. A multi-centre study with a similar aim like the study we proposed here has already being started in the United States of America (ADNI – Alzheimer's Disease Neuroimaging Initiative; http://www.loni.ucla.edu/ADNI/). At the time we are collecting additional MCI patients and HCS and extending our approach on frontotemporal lobar degeneration and on vascular dementia. Further we were starting to measure also local white matter volumes as well as other neuromorphometric measures like cortical thickness that also revealed diagnostic values among healthy control subjects and patients with AD and amnestic MCI in another study [46].

Abbreviations

AD, Alzheimer's disease; ADAS-Cog, Alzheimer's Disease Assessment Scale – cognitive part; ANCOVA, analysis of covariance; AUC, area under the curve; CERAD, Consortium to Establish a Registry for Alzheimer's Disease; CSF, cerebrospinal fluid; Diff., difference; FA, flip angle; GM, grey matter; HCS, healthy control subjects; HMRF, hidden Markov random field; IBASPM, individual brain atlases using SPM; ICBM, international consortium for brain mapping; MARINA, masks for region of interest analysis; MCI, amnestic mild cognitive impairment; MMSE, mini mental state examination; MNI, Montreal neurological institute; MPIR, magnetisation prepared inversion recovery; (s)MRI, (structural) magnetic resonance imaging; MTL, medial temporal lobe; NINCDS-ADRDA, National Institute of Neurological and Communicative Disorders and Stroke and the Alzheimer's Disease and Related Disorders Association; NPV, negative predictive value; P, error probability; PFC, prefrontal cortex; PPV, positive predictive value; PRADL, probable late onset Alzheimer's disease; ROC, receiver operating characteristic; SPM, statistical parametric mapping; SPSS, statistical package for the social sciences; TE, echo time; TFE, turbo field echo; TI, inversion time; TIR, turbo inversion recovery; TR, repetition time; VBM, voxel-based morphometry; VOIs, volumes of interest; WM, white matter; WMS-R, Wechsler memory scale – revised.

Competing interests

The authors declare that they have no competing financial or any other conflict of interests.

Authors' contributions

J.H. and C.H. proposed the project and designed the study. A.S. programmed and managed the database. L.J. contributed to the critical discussion of the methods and results. J.S. recruited, clinically investigated, and diagnosed the patients. C.H. made the motion to the ethics committee, critically evaluated the results, edited the manuscript, and contributed to the interpretation. J.H. preprocessed and analysed the MRI data and wrote the preliminary version of the manuscript.

Acknowledgments

We thank all the physicians, neuropsychologists, nurses, and IT people for their help in care and diagnosis of the patients and data acquisition and databasing. We acknowledge also the participation of the patients in our study and the support by the EU contract LSHM-CT-2003-503330 (APOPIS). This study was funded in parts by the National Centre of Competence in Research on Neural Plasticity and Repair (NCCR Neuro; grant to C.H.). Jürgen Hänggi thanks for the support by the Handschin

Foundation and by the Jubilee Foundation of the Bank of Basle-Country and for the grants received from the University of Zurich and from the Canton Basle-Country.

References

1. Albert MS: **Cognitive and neurobiologic markers of early Alzheimer disease**. *Proc Natl Acad Sci USA* 1996, **93**:13547-13551.
2. Bäckman L, Jones S, Berger AK, Laukka EJ, Small BJ: **Cognitive impairment in preclinical Alzheimer's disease: A meta-analysis**. *Neuropsychology* 2005, **19(4)**:520-531.
3. Cabeza R, Nyberg L: **Imaging cognition II: An empirical review of 275 PET and fMRI studies**. *J Cog Neurosci* 2000, **12(1)**:1-47.
4. Zakzanis KK, Graham SJ, Campbell Z: **A meta-analysis of structural and functional brain imaging in dementia of the Alzheimer's type: A neuroimaging profile**. *Neuropsychol Rev* 2003, **13(1)**:1-18.
5. Karas GB, Scheltens P, Rombouts SARB, Visser PJ, van Schijndel RA, Fox NC, Barkhof F: **Global and local gray matter loss in mild cognitive impairment and Alzheimer`s disease**. *Neuroimage* 2004, **23**:708-716.
6. Karas, GB, Burton EJ, Rombouts SARB, van Schijndel RA, O'Brien JT, Scheltens P, McKeith IG, Williams D, Ballard C, Barkhof F: **A comprehensive study of gray matter loss in patients with Alzheimer's disease using optimized voxel-based morphometry**. *Neuroimage* 2003, **18**:895-907.
7. Frisoni GB, Testa C, Sabattoli F, Beltramello A, Soininen H, Laakso MP: **Structural correlates of early and late onset Alzheimer's disease: voxel-based morphometric study**. *J Neurol Neurosurg Psychiatry* 2005, **76**:112-114.
8. Frisoni GB, Testa C, Zorzan A, Sabattoli F, Beltramello A, Soininen H, Laakso MP: **Detection of grey matter loss in mild Alzheimer's disease with voxel-based morphometry**. *J Neurol Neurosurg Psychiatry* 2002, **73**:657-664.
9. Chételat G, Desgranges B, de la Sayette V, Viader F, Eustache F, Baron JC: **Mapping gray matter loss with voxel-based morphometry in mild cognitive impairment**. *Neuroreport* 2002, **13(15)**:1939-1943.
10. Baron J-C, Chételat G, Desgranges B, Perchey G, Landeau B, de la Sayette V, Eustache F: **In vivo mapping of gray matter loss with voxel-based morphometry in mild Alzheimer's disease**. *Neuroimage* 2001, **14**:298-309.
11. Rombouts SARB, Barkhof F, Witter MP, Scheltens P: **Unbiased whole-brain analysis of gray**

matter loss in Alzheimer's disease. *Neurosci Lett* 2000, **285**:231-233.

12. Thompson PM, Mega MS, Woods RP, Zoumalan CI, Lindshield CJ, Blanton RE, Moussai J, Holmes CJ, Cummings JL, Toga AW: **Cortical change in Alzheimer's disease detected with a disease-specific population-based brain atlas**. *Cereb Cortex* 2001, **11**:1-16.
13. Thompson PM, Moussai J, Zohoori S, Goldkorn A, Khan AA, Mega MS, Small GW, Cummings JL, Toga AW: **Cortical variability and asymmetry in normal aging and Alzheimer's disease**. *Cereb Cortex* 1998, **8**:492-509.
14. Chételat G, Landeau B, Eustache F, Mézenge F, Viader F, de la Sayette V, Desgranges B, Baron JC: **Using voxel-based morphometry to map the structural changes associated with rapid conversion in MCI: A longitudinal MRI study**. *Neuroimage* 2005, **27**:934-946.
15. Scahill RI, Schott JM, Stevens JM, Rossor MN, Fox NC: **Mapping the evolution of regional atrophy in Alzheimer's disease: Unbiased analysis of fluid-registered serial MRI**. *Proc Nat Acad Sci USA* 2002, **99(7)**:4703-4707.
16. Mungas D, Harvey D, Reed BR, Jagust WJ, DeCarli C, Beckett L, Mack WJ, Kramer JH, Weiner MW, Schuff N, Chui HC: **Longitudinal volumetric MRI change and rate of cognitive decline**. *Neurology* 2005, **65**:565-571.
17. Thompson PM, Hayashi KM, de Zubicaray GI, Janke AL, Rose SE, Semple J, Herman D, Hong MS, Dittmer SS, Doddrell DM, Toga AW: **Dynamics of gray matter loss in Alzheimer's disease**. *J Neurosci* 2003, **23(3)**:994-1005.
18. Rusinek H, de Santi S, Frid D, Tsui WH, Tarshish CY, Convit A, de Leon MJ: **Regional brain atrophy rate predicts future cognitive decline: 6-year longitudinal MR imaging study of normal aging**. *Radiology* 2003, **229**:691-696.
19. Fox NC, Scahill RI, Crum WR, Rossor MN: **Correlation between rates of brain atrophy and cognitive decline in AD**. *Neurology* 1999, **52**:1687-1689.
20. McKhann G, Drachman D, Folstein M, Katzman R, Price D, Stadlan EM: **Clinical diagnosis of Alzheimer's disease: report of the NINCDS/ADRDA Work Group under the auspices of Department of Health and Human Services Task Force on Alzheimer`s Disease**. *Neurology* 1984, **34**:939-944.
21. Petersen RC, Doody R, Kurz A, Mohs RC, Morris JC, Rabins PV, Ritchie K, Rossor M, Thal L, Winblad B: **Current concepts in mild cognitive impairment**. *Arch Neurol* 2001, **58**:1985-1992.
22. Morris JC, Heyman A, Mohs RC, Hughes JP, van Belle G, Fillenbaum G, Mellits ED, Clark C: **The Consortium to Establish a Registry for Alzheimer's Disease (CERAD). Part I. Clinical and neuropsychological assessment of Alzheimer's disease**. *Neurology* 1989, **39**:1159-1165.
23. Folstein MF, Folstein SE, McHugh PR: **The Mini-Mental State. A practical method for grading**

the cognitive state of patients for the clinician. *J Psychiatr Res* 1975, **12**:189-198.

24. Härting C, Markowitsch HJ, Neufeld H, Calabrese P, Deisinger K, Kessler J: *Deutsche Adaptation der revidierten Fassung der Wechsler Memory Scale*. Bern, Switzerland: Verlag Hans Huber; 1999.
25. Luria AR: *Higher cortical functions in man*. London: Tavistock; 1966.
26. Lezak M: *Neuropsychological assessment (2nd edition)*. New York: Oxford University Press; 1983.
27. Regard M, Strauss E, Knapp P: **Children's production on verbal and non-verbal fluency tasks**. *Percep Mot Skills* 1982, **55**:839-844.
28. Kramer J: *Intelligenztest*. Solothurn, Antonius; 1965.
29. Stroop J: **Studies of interference in serial verbal reactions**. *J Exp Psychol* 1935, **18**:643-661.
30. Rosen WG, Mohs RC, Davis KL: **A new rating scale for Alzheimer's disease**. *Am J Psychiatry* 1984, **141**:1356-1364.
31. Ashburner J, Friston KJ: **Voxel-based morphometry – The methods**. *Neuroimage* 2000, **11**:805-821.
32. Ashburner J, Friston KJ: **Unified segmentation**. *Neuroimage* 2005, **26**:839-851.
33. Good CD, Johnsrude IS, Ashburner, J, Henson RN, Friston KJ, Frackowiak RS: **A voxel-based morphometric study of ageing in 465 normal adult human brains**. *Neuroimage* 2001, **14**:21-36.
34. Senjem ML, Gunter JL, Shiung MM, Petersen RC, Jack CR Jr.: **Comparison of different methodological implementations of voxel-based morphometry in neurodegenerative disease**. *Neuroimage* 2005, **26**:600-608.
35. Cuadra MB, Cammoun L, Butz T, Cuisenaire O, Thiran JP: **Comparison and Validation of Tissue Modelization and Statistical Classification Methods in T1-Weighted MR Brain Images**. *IEEE Trans Med Imaging* 2005, 24(12):1548-1565.
36. Wilke M, Sohn J-H, Byars AW, Holland SK: **Bright spots: correlations of gray matter volume with IQ in a normal pediatric population**. *Neuroimage* 2003, **20**:202-215.
37. Walter B, Blecker C, Kirsch P, Sammer G, Schienle A, Stark R, Vaitl D: MARINA: **An easy to use tool for the creation of MAsks for Region of INterest Analyses** [abstract]. Presented at the 9th International Conference on Functional Mapping of the Human Brain, June 19-22, 2003, New York, NY.
38. Tzourio-Mazoyer N, Landeau B, Papathanassiou D, Crivello F, Etard O, Delcroix N, Mazoyer B, Joliot M: **Automated Anatomical Labeling of Activations in SPM Using a Macroscopic Anatomical Parcellation of the MNI MRI Single-Subject Brain**. *Neuroimage* 2002, **15**:273-289.

39. Holmes CJ, Hoge R, Collins L, Woods R, Toga AW, Evans AC: **Enhancement of MR Images Using Registration for Signal Averaging**. *J Comput Assist Tomogr* 1998, **22(2)**:324-333.
40. Modrego PJ: **Predictors of Conversion to Dementia of Probable Alzheimer Type in Patients with Mild Cognitive Impairment**. *Curr Alzheimer Res* 2006, 3(2):161-170.
41. Knopman DS, DeKosky ST, Cummings JL, Chui H, Corey-Bloom J, Relkin N, Small GW, Miller B, Stevens JC: **Practice parameter: Diagnosis of dementia (an evidence-based review): Report of the Quality Standards Subcommittee of the American Academy of Neurology**. *Neurology* 2001, 56:1143-1153.
42. Barth S, Schönknecht P, Pantel J, Schröder J: **Neuropsychologische Profile in der Demenz-diagnostik: Eine Untersuchung mit der CERAD-NP-Testbatterie**. *Fortschr Neurol Psychiat* 2005, 73:568-576.
43. de Leon MJ, DeSanti S, Zinkowski R, Mehta PD, Pratico D, Segal S, Rusinek H, Li J, Tsui W, Saint Louis LA, Clark CM, Tarshish C, Li Y, Lair L, Javier E, Rich K, Lesbre P, Mosconi L, Reisberg B, Sadowski M, DeBernadis JF, Kerkman DJ, Hampel H, Wahlund LO, Davies P: **Longitudinal CSF and MRI biomarkers improve the diagnosis of mild cognitive impairment**. *Neurobiol Aging* 2006, **27**:394-401.
44. Hansson O, Zetterberg H, Buchhave P, Londos E, Blennow K, Minthon L: **Association between CSF biomarkers and incipient Alzheimer's disease in patients with mild cognitive impairment: a follow-up study**. *Lancet Neurol* 2006, **5**:228-234.
45. Blasko I, Jellinger K, Kemmler G, Krampla W, Jungwirth S, Wichart I, Tragl KH, Fischer P: **Conversion from cognitive health to mild cognitive impairment and Alzheimer's disease: Prediction by plasma amyloid beta 42, medial temporal lobe atrophy and homocysteine**. *Neurobiol Aging* 2006, **29(1)**:1-11.
46. Singh, V, Chertkow, H, Lerch, JP, Evans AC, Dorr AE, Kabani NJ: **Spatial patterns of cortical thinning in mild cognitive impairment and Alzheimer's disease**. *Brain* 2006, **129**:2885-2893.

4 General discussion

Due to the centrality of the neuromorphometric methodology in this Ph.D. thesis on the one hand and due to the large diversity of the contents of my studies on the other hand (the studies do not suit well to do a synthesis of their results), I decided to not additionally discuss the results of the three papers in more detail here. Furthermore, these studies were done three years ago and meanwhile, I succeeded in morphometric methodologies and complemented and substituted the VBM methodology by other morphometric approaches and tools. Therefore, I will discuss shortcomings and drawbacks of the methods applied in the three publications that constitute the experimental part of my Ph.D. thesis. Additionally and more important are other approaches, new developments, and progresses in the field of neuromorphometry and the solutions or workarounds provided for the shortcomings and drawbacks.

4.1 Shortcomings of the classical voxel-based morphometry methodology

There are several shortcomings that are associated with the classical voxel-based morphometry methodology. These drawbacks are not dependent on the specific software package used in this Ph.D. thesis, i.e., they are not dependent on the SPM software. Due to the similar and even identical implementations of the classical VBM method across software packages, almost all of the commercial and freely available VBM tools are affected by these shortcomings.

4.1.1 Volume-based versus surface-based coordinate systems of the brain

The cerebral cortex is the largest part of the human brain. Although it is highly folded in many mammalian species, the intrinsic “unfolded” structure of the cortex is that of a 2D sheet, several millimetres thick. With respect to the geometric feature of high folding, the cerebral cortex is similar to the surface of the earth (Fig. 30).

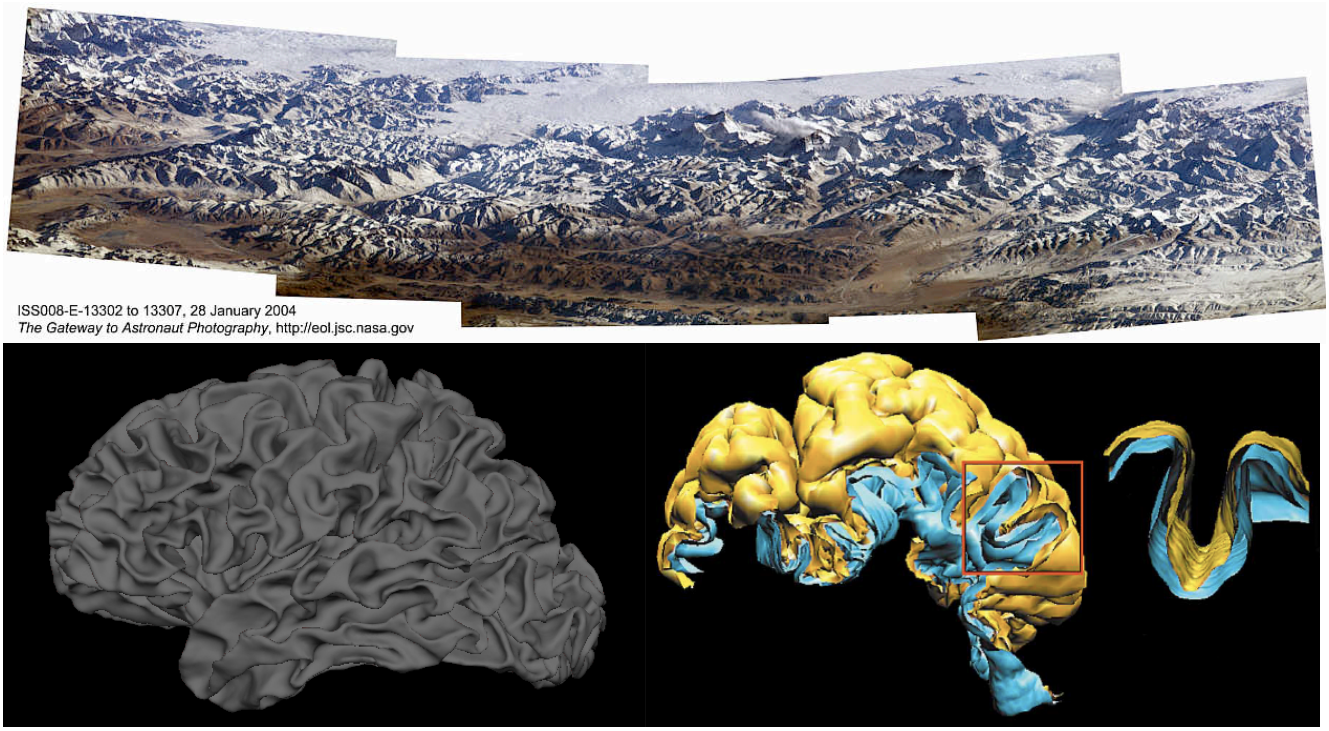

Figure 30: Comparison of the earth's surface with the surface of the human cerebral cortex.
Upper panel: The Himalayas photographed from the international space station (ISS). ***Lower panel left:*** White matter surface model of my left hemisphere created with FreeSurfer software. ***Lower panel right:*** Surface models (grey matter in yellow; white matter in blue) of a part of the human brain and a model of an isolated sulci (see inset). Figure adopted from Chung et al., 2003.

In order to relate and compare anatomical features or functional activations across subjects, it is necessary to establish a mapping that specifies a unique correspondence between each location in one brain and the corresponding location in another – that is, to bring the two brains into spatial register. Most comparisons of data across subjects in the human brain have relied on the 3-D normalisation approach described by Talairach and Tournoux (1988) and Talairach et al. (1967). Although this type of approach has certain advantages (ease of use, widespread acceptance, applicability to subcortical structures), it also has significant drawbacks (Fischl et al., 1999b).

These drawbacks derive directly from the fact that the intrinsic topology of the cerebral cortex is that of a 2-D sheet that is highly convoluted, as described above. For instance, estimates of the amount of 'buried' cortex range from 60–70% (van Essen et al., 1998; Zilles et al., 1988). Thus distances measured in 3-D space between two points on the cortical surface will substantially underestimate the true distance along the cortical sheet, particularly in cases where the points lie on different banks of a sulcus. For example, the lateral tip of the central sulcus frequently lies within a centimetre of the superior temporal gyrus when the distance is measured in the Cartesian embedding space. The distance between the same two points as measured along the actual cortical surface is 10 cm due to the depth of the Sylvian fissure. This problem is compounded by the poor anatomical accuracy afforded by the

Talairach normalisation approach. As numerous studies have demonstrated, the between-subject variability in the location of cortical anatomical landmarks after Talairach alignment is on the order of several centimetres (Steinmetz et al., 1984; Hunton et al., 1996; Thompson & Toga, 1996; van Essen & Drury, 1997). Since many human functional areas (e.g., visual areas V2, V3, VP, V4v, MT+) are 2 cm wide, the Talairach coordinate system does not have sufficient accuracy to differentiate neighbouring cortical areas. This type of error makes it impossible to distinguish topographical and fine structural features of the cortical architecture based solely on Talairach coordinates (Fischl et al., 1999b). In summary, it is widely accepted by the experts in the field of neuromorphometry that a geodesic (vertex) coordinate system is better suited than a Cartesian (voxel) coordinate system in order to represent the complex architectonics of human and non-human cerebral cortices appropriately. This is immediately recognised when deliberating about the geodesic mapping of the surface of our planet. Any point on the surface of the planet in described by a longitude, a latitude, and a height, defining a unique point (vertex) on the earth's surface. In contrast to classical voxel based morphometry procedures, which are operationalised in a Cartesian coordinate system, surface-based approaches based on geodesic coordinate systems are destined for separating out the effects of structural translocation and surface area change from the effects of changes in cortical thickness and curvature (Lyttelton et al., 2009). In this way, the confound of these morphometric features inherent in VBM studies can be easily resolved. How such a geodesic coordinate system of the cortical sheet is implemented can be seen in Figure 31.

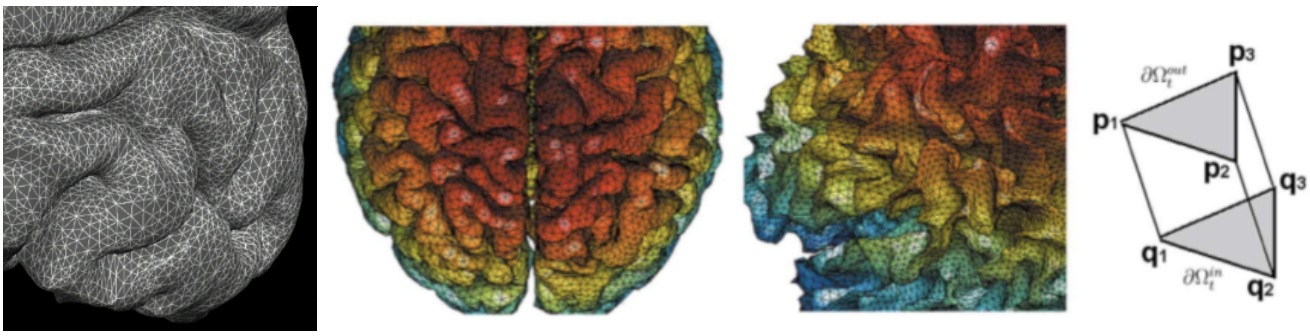

Figure 31: Surface tesselation of the human cerebral cortex.
Left panel: A surface tesselation comprised by vertices that are interconnected by triangles as implemented in the FreeSurfer software. Left panel adopted from the FSL-FreeSurfer course 2006 in Siena (D.N. Greve). ***Middle panel:*** Surface tesselation with evenly spaced vertices and constant triangle area size. ***Right panel:*** p_1 to p_3 are three vertices on the grey matter surface and q_1 to q_3 are the corresponding vertices on the white matter surface. The distance between p_1 and q_1 represents the cortical thickness at that location. Middle and right panel adopted from Chung et al., 2003.

The above mentioned problem of a Cartesian coordinate system are only related to the cerebral cortex, i.e., the highly convoluted sheet. When investigating neural features (mostly volume) of subcortical structures such as the thalamus, the basal ganglia, or the corpus callosum, the Cartesian coordinate

system is appropriate for the representation of the shapes of these structures. The thalamus, an egg-shaped subcortical complex comprised by different nuclei, can be described in a Cartesian (voxel) based coordinate system without the the problems that one encounter when describing the highly convoluted cortical sheet within a voxel frame. Standard functional MRI analyses nowadays use a spatial resolution of 2 mm^3; hence, the cerebral cortex, which is on average about 2.8 mm (1-4 mm) thick, is represented in their statistical models only by one or two voxels, of which a majority are affected by partial volume effects, i.e., comprising mixtures of neural tissue such as GM and WM or GM and CSF within one voxel. The additional problem of averaging different structural or functional areas that arise from the spatial blurring (smoothing) procedures in a Cartesian space will be discussed in detail below.

4.1.2 What do we actually measure with voxel-based morphometry?

When we do a classical VBM analysis as implemented in most available software packages such as SPM (http://www.fil.ion.ucl.ac.uk/spm/), FSL (http://www.fmrib.ox.ac.uk/fsl/index.html), AFNI and SUMA (http://afni.nimh.nih.gov/afni/), ANIMAL and INSECT (http://www.bic.mni.mcgill.ca/~louis/papers/hbm98c/), BrainVoyager (http://www.brainvoyager.com/), and others, there is actually only one measure derived from the preprocessing of the structural MRI data, that is the "probability with which a particular voxel belongs to a particular neural tissue class". More precisely, the "probable mm^3 of grey or white matter per mm^3 spatially normalised image" is measured. Of course, this probability is related to morphometric features; hence, also to volumetric properties of the brain. But, it is not really a explicit measure that one would encounter when working with postmortem brains. When sectioning a brain, features such as cortical thickness can immediately be recognised and measured with high precision. When applying the classical probability approach with one of the above mentioned software packages and finding a structural brain difference, one is unable to determine which of the two cortical features cortical thickness or cortical surface area, which constitute cortical volume, drove the cortical volume difference. With surface-based morphometric procedures such as implemented in the FreeSurfer software suite (http://surfer.nmr.mgh.harvard.edu/fswiki) or in the CARET (computerised anatomical reconstruction and editing toolkit) software package (http://brainvis.wustl.edu/wiki/index.php/Caret:About) more intuitive measures of the brain such as cortical thickness, cortical surface area, and cortical volume can be measured. This kind of neuromorphometric tools also provide information about additional brain features such as curvature indices (bending of gyri and sulci) and gyrification indices (surface area on the cortex in relation to the surface area buried under this area on the cortex). The surface-based procedure for measuring cortical thickness, as implemented in the FreeSurfer software suite, have been validated against histologic thickness data (Rosas et al., 2002) as

well as against manual thickness measurements (Kuperberg et al., 2003; Salat et al., 2004).

4.1.3 Low versus high parametric spatial normalisation

There are several issues that have to be considered when brain images are spatially normalised (registered). One issue is related to the number of parameters used for modelling the spatial transformations between an individual brain and a reference brain (template). Most of the available software packages for functional and structural brain image analyses use only several Hundreds or about one thousand parameters for modelling the transformations. Crivello and colleagues investigated four different kinds of spatial normalisation procedures and quantified their impact on functional maps (Crivello et al., 2002). The four procedures investigated were a simple affine transformation (AFF; 12 parameters), a fifth order polynomial warp (WARP; 168 parameters), discrete cosine basis functions (SPM; 1,536 parameters), and a movement model (based on Navier-Lamé continuum mechanics theory) called full multi grid (FMG; 10,861,086 parameters). Thanks to the large number of degrees of freedom of the technique, FMG was found to provide enhanced alignment accuracy as compared to the other three methods, both for grey and white matter tissue; WRP and SPM exhibited very similar performances whereas AFF had the lowest registration accuracy. Furthermore, this study also suggested that the functional variability is much larger than the anatomical one and that precise alignment of anatomical features has low influence on the resulting intersubject functional maps. The accuracy of the tissue classification procedure (segmentation) that followed the spatial normalisation is greatly enhanced when using the FMG approach, i.e., there were less misclassified voxels; hence, the resulting tissue probability maps are of increased quality (Crivello et al., 2002). Another problem arises from the fact that a spatial normalisation procedure is more suited for registering one brain structure (e.g. the cerebral cortex), whereas the normalisation of another structure (e.g. the hippocampus) is hampered by the same registration procedure. An example that revealed a more accurate registration in the medial temporal lobe with less parameters compared with the same registration procedure with more parameters can be found by Salmond and colleagues (Salmond et al., 2002). In the context of medical image registration, three concepts are important: correspondence, homology, and quality. More details about these three concepts can be found by Crum (Crum et al., 2003). How spatial normalisation algorithms can be tuned is described by Robbins (Robbins et al., 2004). Generally spoken, an increased number of parameters is advantageous in most applications, but one has to be careful not to run into the over-fitting problem. An over-fit of a statistical model can occur when the degrees of freedom in parameter selection exceed the information content of the data, this leads to arbitrariness in the final (fitted) model parameters which reduces or destroys the ability of the model to generalize beyond the fitting data.

4.1.4 Intensity-based versus intensity- and conditional-based segmentation

How the brain can be segmented into its different tissue types such as GM, WM, CSF, and skull was described in section 2.2.4. I also discussed the additional application of hidden Markov random fields to increase the accuracy of the segmentations (2.2.4.1). This segmentation is mainly based on intensity information encoded by the MRI scan, although some kind of a priori information about the spatial distribution of these intensities is also used (tissue a priori maps, templates). The segregation of different subcortical structures form each other, e.g., amygdala and hippocampus or caudate nucleus and putamen, is quite more demanding. Whereas the overlap of the MRI intensity profiles of grey and white matter is rather small (see Fig. 16), the MRI intensity profiles of the amygdala and the hippocampus are almost identical (see Fig. 32, left panel).

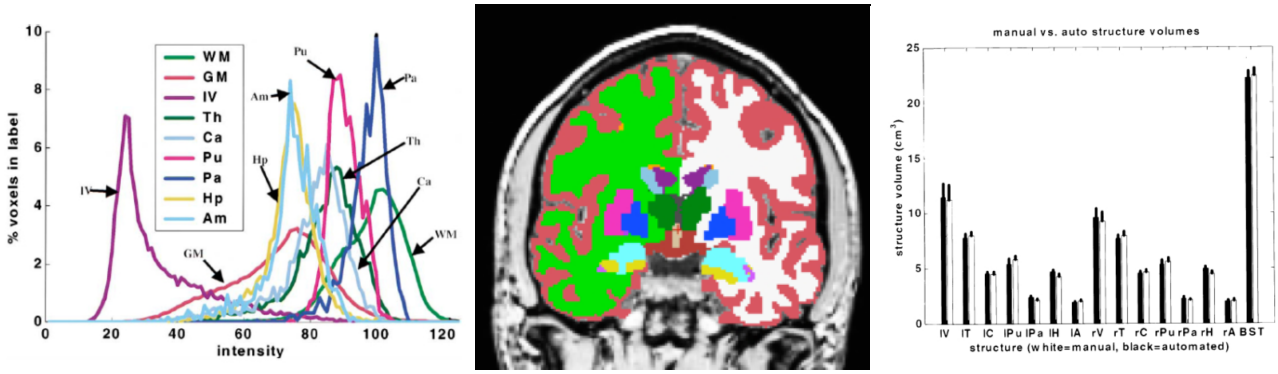

Figure 32: Gaussian classifier array and the evaluation of the subcortical segmentation algorithm.
Left panel: Gaussian classifier array. Shown are the MRI intensity distributions of the various subcortical components and of cortical grey matter (GM), white matter (WM), and cerebrospinal fluid (CSF). *Abbreviations:* lV, CSF of lateral ventricle; Th, thalamus; Ca, caudate nucleus; Pu, putamen; Pa, pallidum; Hp, hippocampus; Am, amygdala. Figure adopted from Fischl et al., 2002. ***Middle panel:*** Labelled volumetric subcortical and cortical segmentations are overlaid on a structural MR image. The colours correspond to the colours shown in the left panel. ***Right panel:*** Evaluation of the subcortical segmentation algorithm (ICM, iterated conditional modes algorithm) that is implemented in the FreeSurfer software suite. Figure adopted from Fischl et al., 2002.

Hence, additional information is needed to distinguish the two structures. There are three sources of information that help in this disambiguation process: I) the number of possible anatomical classes at a given global position is small. II) Neuroanatomical structures occur in a characteristic spatial pattern relative to each other (e.g., the amygdala is located anterior and superior to the hippocampus). III) Tissue classes have spatially heterogenous MRI properties that vary in a spatially predictable fashion (e.g., T1 relaxation time is 20% longer in the frontal than in motor and somatosensory cortex) (Fischl et al., 2002).

4.1.5 Cartesian spatial blurring versus surface-based diffusion smoothing

The advantage of using a geodesic compared with a Cartesian coordinate system in order to model morphometric brain features becomes obvious when considering the preprocessing step called spatial

blurring or spatial smoothing (discussed under 2.2.5). When the cortical sheet is parameterised with vertices in a geodesic space, then neighbouring vertices of the digital brain model represent neighbouring points on the cortical surface. This is not the case when the cortex is parameterised with voxels in a Cartesian space; here, neighbouring voxels of the digital brain model represent points on the cortical surface that are actually not in direct neighbourhood. When we blur the voxels in a Cartesian coordinate system, the new computed (weighted) intensity values of these voxels are derived from functionally segregated brain areas. According to the matched filter theorem, one should apply a smoothing kernel similar in size as the extent of the expected structural difference in order to sensitise the data. The applied smoothing kernels (FWHM) in common structural voxel-based analyses vary between 6-15 mm, so the expected effects should be within this range. On a geodesically (spherically) parameterised 2D surface model of the cortex, diffusion smoothing kernels with a size up to 30 mm (FWHM) are possible. An illustration of the difference between the geometry preserving diffusion smoothing blurring over a 2-D surface manifold and the more commonly employed 3-D volumetric blurring kernels can be found in Figure 33 below.

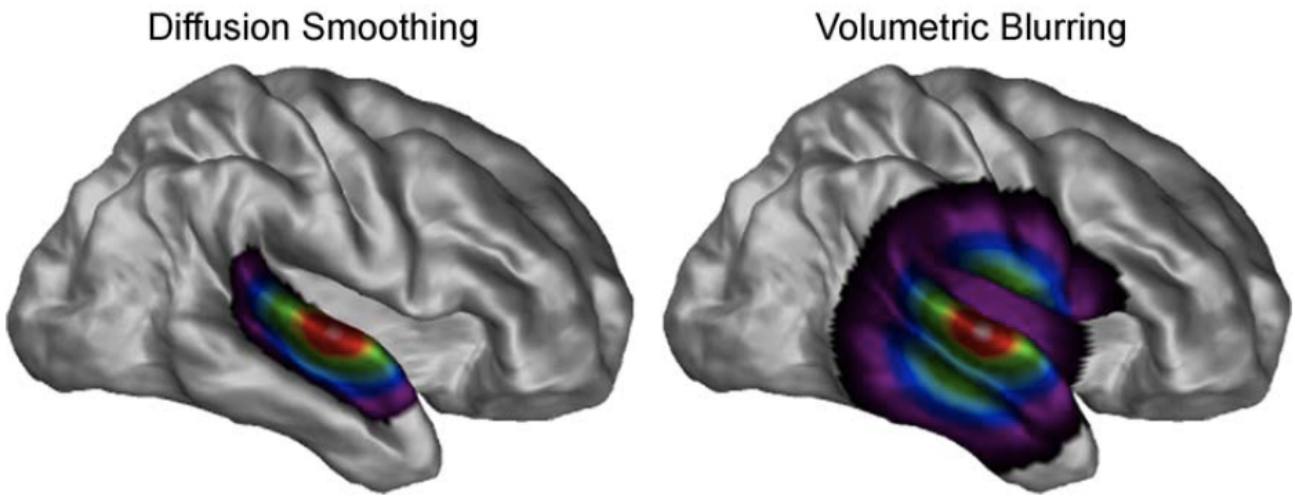

Figure 33: Surface-based diffusion smoothing versus volumetric spatial blurring.
An illustration of the difference between the geometry preserving diffusion smoothing blurring over a 2D surface manifold and the more commonly employed 3D volumetric blurring kernels. The FWHM was set at 30 mm in both cases. One can see how anatomically disparate areas such as the inferior motor and sensorimotor areas are influenced by the volumetric kernel but not by diffusion smoothing. Figure adopted from Lerch and Evans, 2005.

More details about the advantages of the geometry preserving diffusion smoothing over a 2D surface manifold can be found by Chung and colleagues (Chung et al., 2001, 2003) and by Lerch & Evans, 2005.

4.1.6 Averaging brains in a voxel- versus a vertex-based space and the influence on statistical power

One of the main potential applications of volume- and surface-based coordinate systems is for averaging functional (and structural) data across subjects. Minimising spatial blurring of the functional data introduced by this averaging process has several benefits: I) it preserves more information about the detailed relationship between structure and function, II) it improves the statistical power of statistical parametric maps by more accurately aligning corresponding functional activations across subjects, and III) it provides a mechanism for reporting of more accurate coordinates, which facilitates cross-study comparisons (Fischl et al., 1999b). One important benefit of the improved alignment of functional areas in the spherical coordinate system is increased statistical power for cross-subject averaging of functional (and structural) data (Fischl et al., 1999b). This is illustrated in Fig. 34, which shows statistical parametric maps of fMRI repetition effects in a visual size-judgment task (Dale et al., 1997; 2000) in individual subjects together with the corresponding average maps computed in Talairach and spherical coordinates. Reducing the statistical threshold reveals an extensive pattern of activation in each subject (second row), although valid statistical inference cannot be drawn at such a low significance level. Typically, Talairach-based cross-subject averaging is used in order to obtain statistically reliable activation patterns (lower left). The improved statistical power afforded by averaging in spherical coordinates results in a more extensive pattern of activation, as illustrated by the map at the lower right (Fischl et al., 1999b).

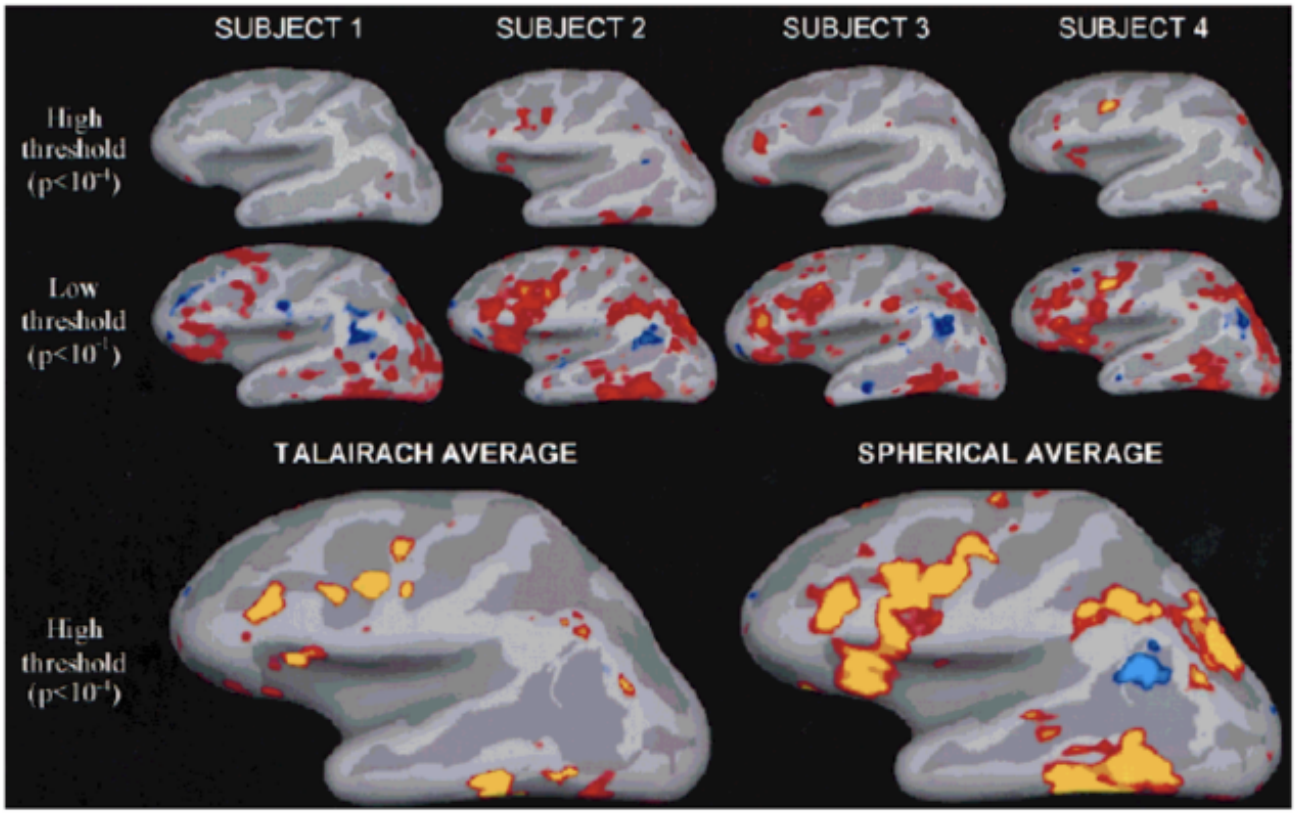

Figure 34: Averaging brains in a voxel- versus a vertex-based space and the influence on statistical power. Increased statistical power due to averaging in spherical coordinates (bottom right) as opposed to Talairach coordinates (bottom left). See text for more details. Figure adopted from Fischl et al., 1999b.

4.2 FreeSurfer software suite

The FreeSurfer software suite was created by Bruce Fischl, Anders Dale, and coworkers at the Athinoula A. Martinos center for biomedical imaging, Massachusetts general hospital, Boston and is freely available under http://surfer.nmr.mgh.harvard.edu/fswiki. This software overcomes some of the shortcomings reported above. The whole procedure consists of three parts. First, a voxel-based (Cartesian space), volumetric processing stream that resulted in subcortical as well as global cortical segmentations, of which the volumes are computed. Second, in a vertex-wise (spherical space), surface-based processing stream that resulted in statistical parametric maps of different brain parameters such as cortical thickness, cortical volume, cortical surface-area, and curvature indices as well as in cortical parcellations (regions of interest), for which the mean cortical thickness, volume, surface area, and curvature are computed. Third, the statistical analysis of global (GM, WM, CSF, other), semi-local (segmentations and parcellations), and local (vertex-wise) maps of the different tissue parameters as well as further options such as cortical flattening of the maps and computing of local gyrification indices. The volumetric pipeline consists of about 15 single processing steps and the

surface-based processing stream is comprised by about 17 individual steps. These steps are applied serially and the volumetric processing stream precedes the surface-based stream. An overview listing the functions of both FreeSurfer's processing streams is shown in Figure 35.

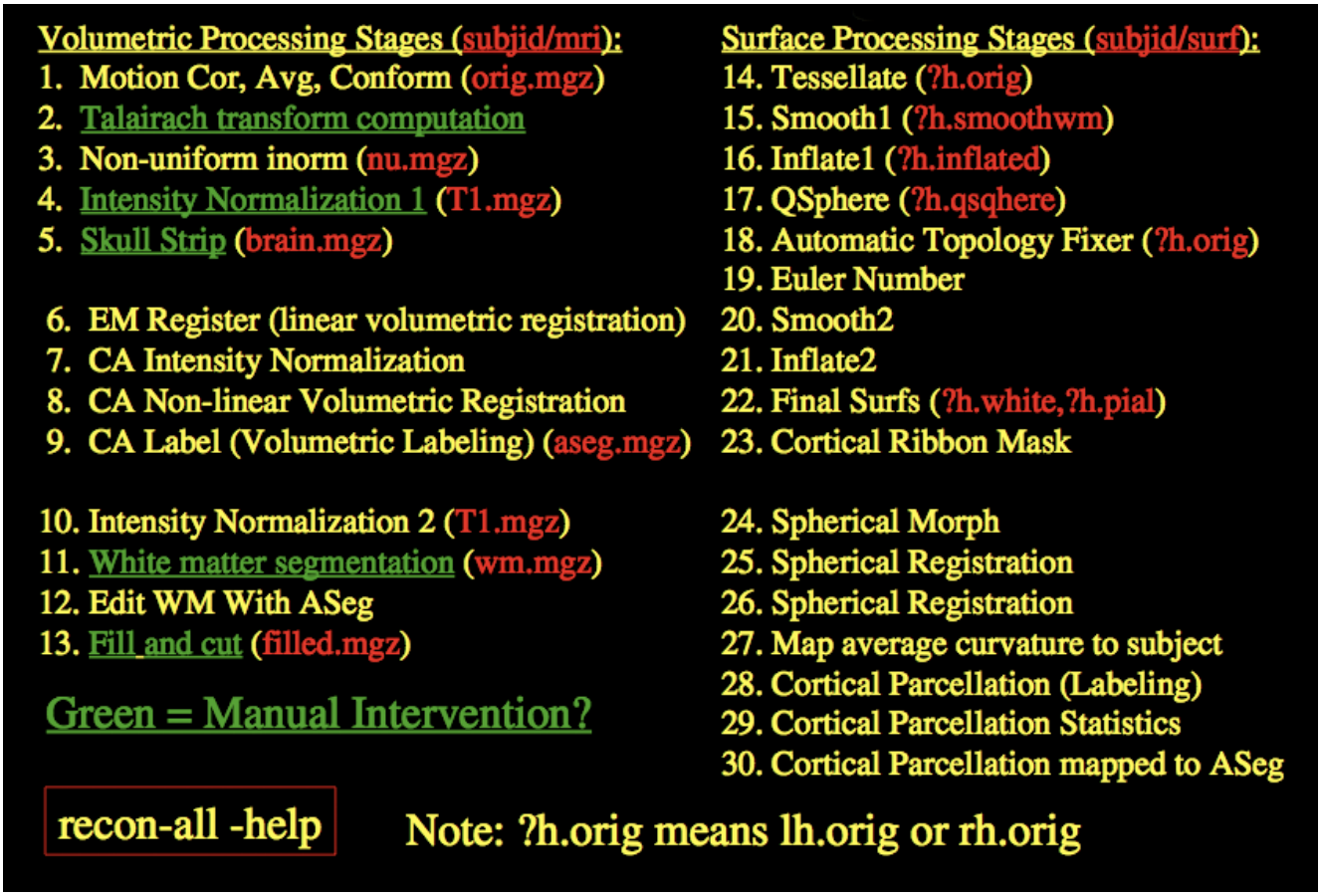

Figure 35: Overview of the FreeSurfer's volumetric and surface-based processing stream.
Figure adopted from the FSL-FreeSurfer course 2006 in Siena (presentation by D.N. Greve).

To recapitulate in detail all the volumetric and surface-based processing steps (functions) implemented in FreeSurfer is not the aim of this general discussion. A lot of functions used in the two pipelines of FreeSurfer were already described in the method section of this Ph.D. thesis. In the following paragraphs I will focus on important processing steps that help to understand the benefits of the FreeSurfer methodology compared with other common neuromorphometric analysis methods that mainly based on a Cartesian voxel space such as the classical VBM. The technical details of these procedures are described in prior publications elsewhere (Dale et al., 1999; Dale & Sereno, 1993; Fischl & Dale, 2000; Fischl et al., 1999a, 1999b, 2001, 2002, 2004a, 2004b; Han et al., 2006; Jovicich et al., 2006; Ségonne et al., 2004, 2007; Desikan et al., 2006).

4.2.1 Volumetric processing pipeline for subcortical segmentation

The flow chart of FreeSurfer's volumetric processing stream is depicted in Figure 36. When more than one structural MRI scan were acquired, FreeSurfer's volumetric processing stream starts with a motion correction [MC, see flow chart] of the multiple volumetric T1-weighted images (when more than one is available), averages the motion corrected images, and transforms [Conform] the motion corrected, averaged image into the FreeSurfer's volumetric file format [.mgh and .mgz; 256^3 matrix; 1 mm^3 resolution; 8-bit encoded]. Nonparametric, nonuniform intensity inhomogeneities, also called bias fields, are estimated [NU] using the N3 algorithm (Sled et al., 1998) and the Talairach transformation [Talairach] between the individual MR image and the reference template (MNI 305) is computed (no resampling). Here, one has the opportunity to manually edit the transformation if registration problems occur [tkregister2], the results of which can be fed into other processing functions as control points [CP]. The formerly estimated bias field is applied [INorm1], the skull is stripped away [SkullStrip] using a hybrid watershed/surface deformation procedure (Ségonne et al., 2004), and the resulting brain mask including only neural tissue can be edited if any problem occur [BM-tkmedit].

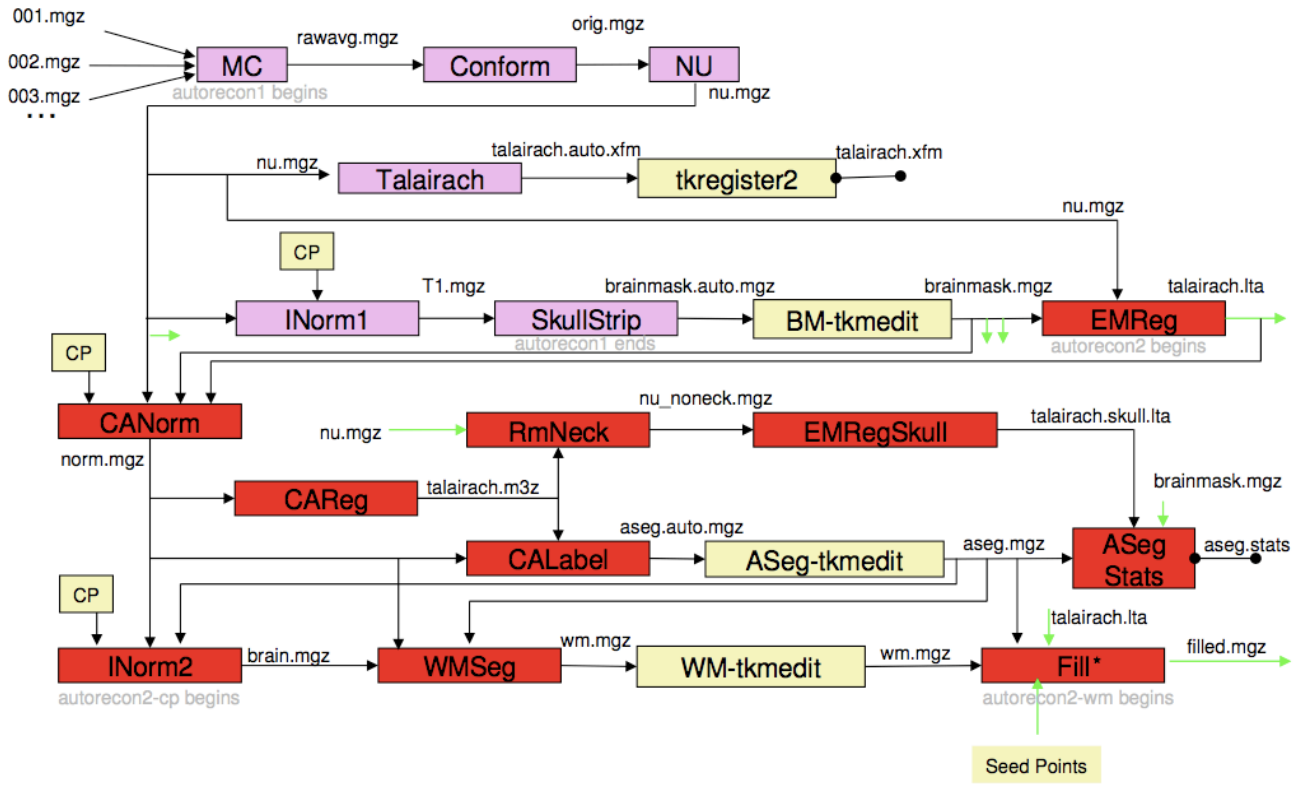

Figure 36: Flow chart of FreeSurfer's volumetric processing stream.
Pink, red, and yellow boxes represent individual preprocessing steps (functions) that are applied to the MR images by FreeSurfer. In the yellow boxes, manual intervention is possible, the results of which can be fed into other functions [CP, control points]. Resulting brain images, transformation matrices, and statistical tables are printed in black. Figure adopted from the FSL-FreeSurfer course 2006 in Siena (presentation by D.N. Greve).

The next four steps are the core functions of the subcortical segmentation procedure that also includes the labelling (computation of volumes) of global brain tissue such as cerebral GM, cerebral WM, cerebellar GM, cerebellar WM, sulcal and ventricular CSF, and estimated total intracranial volume (eTIV). A linear volumetric registration [EMReg] precedes an intensity normalisation onto the Gaussian classifier array (GCA) [CANorm] followed by a nonlinear volumetric registration onto that GCA [CAReg] (Fischl et al., 2002, 2004a). The volumetric registrations are then labelled to indicate to which brain structure each voxel belongs to [CALabel]. These labelled anatomical segmentations (including hippocampus, amygdala, thalamus, caudate, putamen, pallidum, ventricles, others) can be edited if any problem occur [ASeg-tkmedit]. The neck was removed from the formerly bias field corrected brain image nu.mgz by the function [RmNeck], the skull was linearly registered, and this information is combined with the already labelled volumetric registrations to compute the volumes of the final segmentations [ASegStats]. Here the actual volumetric subcortical segmentation stream is finished and the last three steps are devoted to prepare the brain image for the surface model reconstructions, i.e., for the surface processing stream. The initial linearly normalised image norm.mgz is intensity normalised, aiming at separating the white matter from everything else [INorm2]. The brain is then segmented into white matter [WMSeg], segmentations that can be edited if necessary [WM-tkmedit]. Holes in this WM segment such as the ventricles will be filled [Fill]. Control points [Seed points] can be used to edit this filling. This filled WM segment [filled.mgz] is then fed into FreeSurfer's surface-based processing stream as a starting volume for the reconstructions of the surface models.

4.2.2 Surface processing pipeline for cortical surface models and its parcellation

The flow chart of FreeSurfer's surface processing stream is depicted in Figure 37. This stream starts with the tesselation [Tess1] of the filled WM volume into a triangular mesh (see Fig. 31), the nodes of which are comprised by vertices. Then this initial surface model will be smoothed [Smooth1], inflated [Inflate1], and transformed into a quasi-sphere [qsphere1]. Any topological failure or inaccuracy in the surface reconstructions are detected and automatically fixed [TopoFix]. A (surface) brain mask is constructed [BFSMask] from the two images brainmask.mgz and brain.mgz (see Fig. 36) that is fed into the reconstruction of the final surface models [FinalSurfs]. The final surface models are smoothed [Smooth2] and inflated [Inflate2]. The cortical ribbon is then extracted [Ribbon] on which an initial cortical parcellation procedure is applied that takes into account the already volume-based cortical segmentations [AParc+ASeg]. The remaining green boxes are dealing with the spherical registration of the surface-based brain models.

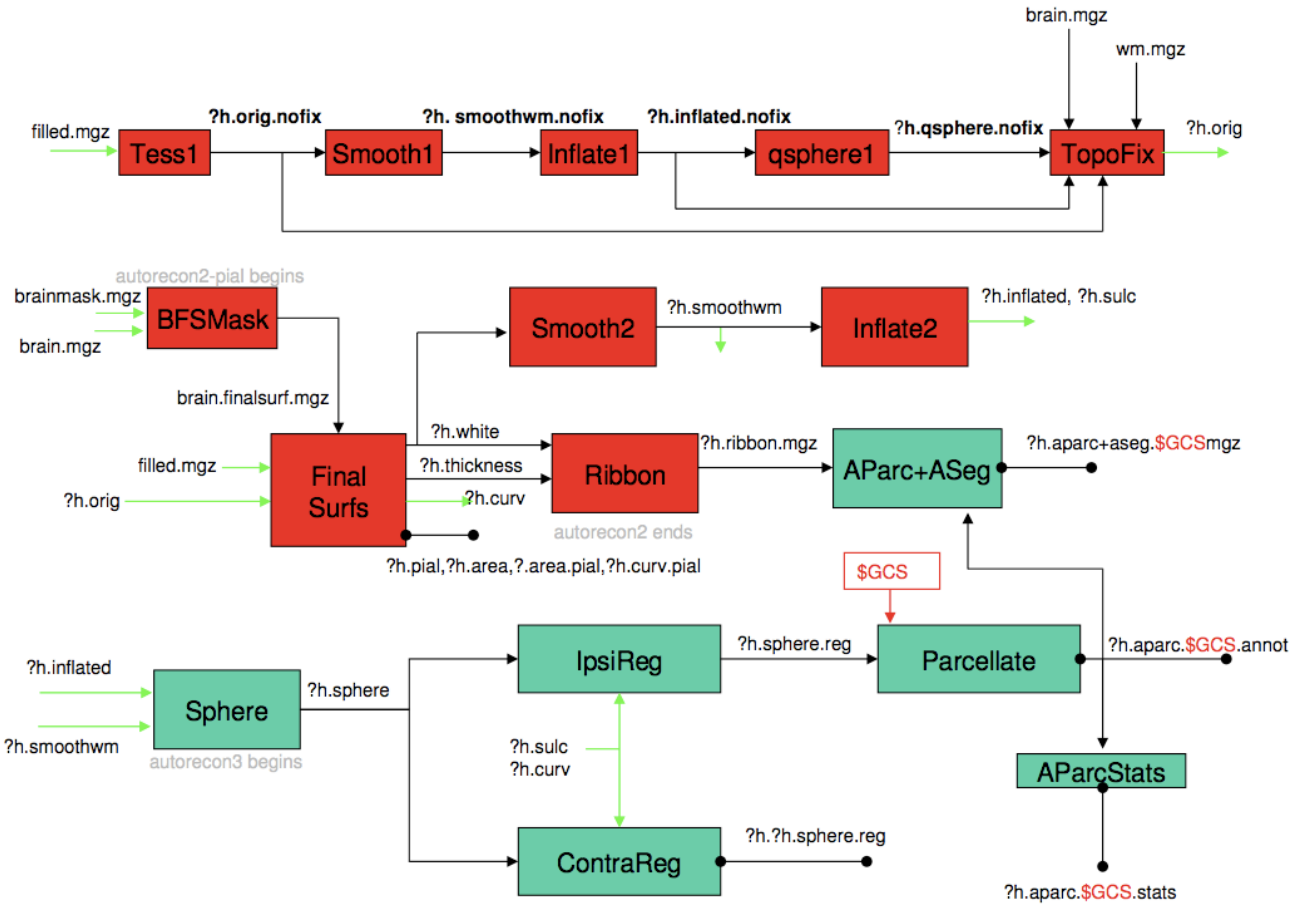

Figure 37: Flow chart of FreeSurfer's surface processing stream.
Red and green boxes represent individual preprocessing steps (functions) that are applied to the MR images by FreeSurfer. Resulting brain images, transformation matrices, and statistical tables are printed in black. Figure adopted from the FSL-FreeSurfer course 2006 in Siena (presentation by D.N. Greve).

The surface models that resulted from the functions [Smooth2] and [Inflate2] are used to initialise the spherical registration process [Sphere]. After the construction of the spherical models they are registered onto the ipsilateral hemisphere [IpsiReg] as well as onto the contralateral hemisphere [ContraReg] of the spherical reference brain. The ipsilateral registered spheres are then used to compute the final cortical parcellations [Parcellate]. These cortical parcellations are then used to compute their final (statistical) parameters [AParcStats] taking into account the initial parcellations / segmentations.

4.2.3 Subcortical and cortical indices

A bunch of morphometric brain parameters results from the Freesurfer's processing streams. Global as well as local volumetric measures are derived from the volumetric/subcortical processing stream. Volumetric measures, separated for the left and right hemisphere, are obtained from the following

brain structures: cerebral GM (cortex), cerebellar GM, cerebral WM, cerebellar WM, WM hypointensities, lateral ventricle, thalamus, hippocampus, amygdala, caudate nucleus, putamen, pallidum, ventral diencephalon, and the nucleus accumbens. Other volumes are derived from the brain stem, the third and fourth ventricle, the intracranium, the corpus callosum (divided into 5 parts), and blood vessels.

Note that in contrast to a classical VBM analysis, where voxel-wise volumetric or density measures are obtained, there is no such voxel-wise volumetric measure of the subcortical structures in FreeSurfer. In common VBM software tools the signal intensities of the MR image are computed with a priori information about the distributions of GM, WM, and CSF in the population, resulting in the a posteriori probability that a particular voxel belongs to a particular tissue class (e.g., GM). This a posteriori probability is related to the volumetric measure one is interested in. In the FreeSurfer analysis suite, there is no computation of such probabilities. Instead, the signal intensities found in the MR image are compared with the intensities that are mapped in the Gaussian classifier array (see Fig. 32). When we look at the number of voxels used in the two approaches, a striking difference can be seen. Assumed that the spatial resolution of the preprocessed MR image is 1 mm^3 and we are interested in the volume of the thalamus, then within the framework of the FreeSurfer software suite the thalamus is comprised by about 8000 voxels that directly reflect the volume of the thalamus (about 8000 mm^3). When using the probabilistic approach implemented in other VBM tools such as SPM and FSL, the thalamus is comprised by much more voxels each of them representing a probability that vary between 0.5 to 0.9. If the probabilities of all these voxels are integrated one obtains a volumetric measure called concentration (without modulation with the Jacobian determinant) or volume (with modulation with the Jacobian determinant). Remember that this volume is relative. It reflects "probable mm^3 of grey or white matter per mm^3 spatially normalised image" as described in section 4.1.2, a measure that we do not encounter when sectioning a postmortem brain. There were also efforts by the FreeSurfer creators to implement a VBM-like procedure that solely based on the MR intensities (without a probabilistic framework). These efforts apparently did not result in a satisfied solution (Bruce Fischl, personal communication).

In order to characterise the cortical architecture in more detail, FreeSurfer uses its surface-based brain reconstructions to compute the following measures: cortical thickness, cortical surface area, cortical volume, and indices of the curvature and gyrification / fissurisation. These measures can be investigated vertex-wise (preserving precise localisation) or aggregated across the vertices of a structural (e.g., precentral gyrus) or across a functional unit / parcellation (e.g., supplementary motor area). At the time, there are two parcellation schemes implemented in FreeSurfer: A coarser parcellation scheme (comprised by 34 parcellations per hemisphere) that do not distinguish between

gyrus and sulcus, and a finer parcellation scheme (comprised by 78 parcellations per hemisphere) that labels gyri and sulci separately. The separation of the sulci from the gyri can be achieved with information derived directly from the surface reconstructions: the transition between a sulcus and a gyrus is the point where the surface topology changes from concavity to convexity.

5 Conclusions

In the first third of my Ph.D. thesis, I introduced the individual steps of the classical voxel-based morphometry processing stream. The second third constituted the experimental part comprised by three experimental studies. The last part of the thesis deals with shortcomings and drawbacks of the classical VBM analysis and it introduced the approach of surface-based morphometry. Furthermore, a fully automated subcortical segmentation procedure was also described.

In this Ph.D. thesis, it has been shown that the neuromorphometric methodology based on structural magnetic resonance imaging (MRI) can be used to investigate the relations between brain structure and brain function. Different computational, neuromorphometric methods were applied to investigate basic neuroscientfic hypotheses about the morphology of brain structures and its associated functions as well as to answer clinical neuroscience questions about pathological conditions of brain structures in disease. These kinds of methods are heavily dependent on 3D high resolution, high quality, and high contrast MRI scans and need a lot of computational hardware was well as software resources. With the advent of high field MR scanners working at 7 Tesla, new opportunities such as the investigation of the different cortical layers arise for the field of structural neuromorphometry.

In the first experimental study of my thesis, we were able to isolate structural correlates associated with visuospatial cognition independent of general intelligence. These correlates were sexually dimorphic, i.e., were found in parietal white matter in males and in parietal grey matter in females. In a second study, I investigated the influence of a single nucleotide polymorphism (SNP) on brain structures in young healthy subjects. This SNP is proposed to be a risk factor for Alzheimer's disease and it is located in the gene that encodes for an important brain cholesterol degrading enzyme. We found that this SNP influences parahippocampal and hippocampal volumes in a dose-dependent manner, i.e., the more T-alleles the smaller the volumes of the hippocampus and parahippocampal gyrus. In the third experiment, we showed how computational neuromorphometry can be use to support/evaluate/corroborate clinical diagnoses of mild cognitive impairment and Alzheimer's disease. This neuromorphometric approach revealed sensitivities and specificities that were superior compared to the sensitivities and specificities obtained with neuropsychological (cognitive) assessments and comparable with the sensitivities and specificities obtained with CSF-biomarker investigations.

In the last part of this Ph.D. thesis, I will describe future perspectives that might be fruitful for the field of neuroscience in general and for computational neuromorphometry specifically.

6 Future perspectives

The number of published studies about the brain and its functions increased exponentially within the last two decades resulting in a huge number of new neuroscientific results. These results were acquired with a bunch of experimental methods. Attempts to integrate this huge amount of new insights into a unified theory of the brain and its functions are rarely. When posing questions about brain structure (architecture) and function (physiology) on a system level, structural and functional MR imaging methods are central.

In my opinion, it would be fruitful for the whole field of neuroscience to change its maxim. Instead of augmenting the flood of neuroscientific data further, it might be worth thinking about how this flood of scientific information can be integrated, evaluated, and subsequently reduced to the essence about brain architecture and its physiology. Although classical reviews might help to overlook a particular neuroscientific topic, meta-analytic approaches are needed in order to quantify and evaluate effects that were reported across studies. Another problem arise from the tasks used to evoke brain activity in functional imaging studies. Most of these experimental designs do not any longer targeting elementary cognitive or affective brain functions (tasks); hence, the results of such functional studies are strongly dependent on the tasks applied and it is difficult to compare the results obtained with different tasks. Furthermore, whether basic methodological assumptions such as e.g. the concept of pure insertion are also true when investigating more complex cognitive or affective brain functions such as theory of mind and prospective memory or love and morality, respectively, was in my opinion not persuasively shown yet.

In the field of computational neuromorphometry, the maxim is to obtain multimodal structural as well as functional atlases of the human brain. A comprehensive review about cartographic approaches towards computational, multimodal atlases (databases) can be found by Toga and colleagues (Toga et al., 2006). Such atlases can now combine data describing multiple aspects of brain architecture and physiology at different scales from different subjects, yielding a truly integrative and comprehensive description of this organ. Due to the interindividual variability in neuroarchitecture as well as neurophysiology, these atlases are probabilistic in nature, i.e. they also include these two kinds of interindividual variability; hence, these atlases and databases can be regarded as representative brain models for a particular population (Toga et al., 2006).

6.1 Integration of cyto-, myelo-, and chemoarchitectonic atlases with physiological, genetic, and behavioural data

Cytoarchitectonic maps of the cerebral cortex are based on cellular features such as the size and shape of neural cells, the cell packing densities in different cortical layers, and/or the width of the cortical layers, and are identified in cell body-stained specimens and by using structural T1-weighted MRI (Toga et al., 2006). Myeloarchitectonic maps of the cerebral cortex are based on features such as myelinisation, fibre bundle coherence, and other measures of white matter connectivity, and are identified in myelin-stained histologic specimens and/or by using diffusion-weighted MRI methods such as diffusion tensor imaging (DTI) and diffusion spectrum imaging (DSI), the latter is also called q-ball or q-space imaging (Tuch, 2004). In contrast to DTI, DSI is capable to resolve more than one fibre direction within a single voxel, although multi-tensor models exist for DTI. Chemoarchitectonic maps represent differences in the molecular composition of cortical and subcortical brain regions assessed using enzyme- or immunohistochemistry, in situ hybridisation, and/or receptor autoradiography (Toga et al., 2006). The expression of different neurotransmitter receptors throughout the brain can be visualised with such chemoarchitectonic maps. If these multimodal brain atlases will be exist in the near future, physiological, genetic, and behavioural data acquired with e.g., functional MRI or electroencephalography, genotyping of single nucleotide polymorphisms or genome-wide arrays, and cognitive or affective assessments, respectively, can be related to the cytoarchitecture, myeloarchitecture, and chemoarchitecture of the brain and integrated into these multimodal atlases (databases). As brain imaging data from different studies can now be compared in a common coordinate system, large databases of functional and structural imaging data - and associated meta-data on experimental paradigms and findings - are now beginning to be assembled, along with tools to interact with these data (van Horn, 2005). Notable examples of these neuroinformatics efforts include the International Consortium for Brain Mapping (ICBM; http://www.loni.ucla.edu/ICBM/) and the Alzheimer's Disease Neuroimaging Initiative (ADNI; http://www.adni-info.org/) consortium project to build a data repository of MRI, PET, and other clinical and biomarker data on ageing and Alzheimer's disease.

7 References

Abell, F., Krams, M., Ashburner, J., Passingham, R., Friston, K., Frackowiak, R., Happé, F., Frith, C. & Frith, U. (1999). **The neuroanatomy of autism: a voxel-based whole brain analysis of structural scans.** *Neuroreport;* 10: 1647-1651.

Aguirre, G.K., Zarahn, E. & D'Esposito, M. (1998). **The Inferential Impact of Global Signal Covariates in Functional Neuroimaging Analyses.** *Neuroimage;* 8: 302-306.

Andrade, A., Paradis, A.-L., Rouquette, S. & Poline, J.-B. (1999). **Ambiguous Results in Functional Neuroimaging Data Analysis Due to Covariate Correlation.** *Neuroimage;* 10: 483-486.

Ashburner, J. & Friston, K.J. (2005). **Unified segmentation.** *Neuroimage;* 26: 839-851.

Ashburner, J. & Friston, K.J. (2003). **Morphometry.** In Frackowiak, R.S.J., Friston, K.J., Frith, C., Dolan, R., Price, C.J., Zeki, S., Ashburner, J. & Penny, W.D. Editors, ***Human Brain Function.*** Academic Press, USA, 2nd edition, 2003.

Ashburner, J. & Friston, K.J. (2001). **Why Voxel-Based Morphometry Should Be Used.** *Neuroimage;* 14: 1238-1243.

Ashburner, J. & Friston, K.J. (2000). **Voxel-Based morphometry – The methods.** *Neuroimage;* 11: 805-821.

Ashburner, J. (2000). **Computational Neuroanatomy.** PhD thesis, University College London, 2000.

Ashburner, J. & Friston, K.J. (1999a). **Nonlinear Spatial Normalization Using Basis Functions.** *Hum. Brain Mapp.;* 7: 254-266.

Ashburner, J. & Friston, K.J. (1999b). **Spatial Normalization**. In Toga, A.W. Editor, ***Brain Warping,*** Academic Press, USA, 1999.

Ashburner, J., Hutton, C., Frackowiak, R., Johnsrude, I., Price, C. & Friston, K. (1998). **Identifying Global Anatomical Differences: Deformation-Based Morphometry.** *Hum. Brain Mapp.;* 6: 348-357.

Ashburner, J. & Friston, K.J. (1997a). **Spatial transformation of images**. In Frackowiak, R.S.J., Friston, K.J., Frith, C., Dolan, R. & Mazziotta, J.C. Editors, ***Human Brain Function.*** Academic Press, USA, 1997.

Ashburner, J. & Friston, K.J. (1997b). **Multimodal Image Coregistration and Partitioning – A Unified Framework.** *Neuroimage;* 6: 209-217.

Bailey, P. & von Bonin, G. (1951). ***The Isocortex of Man.*** Univ. Illinois Press, Urbana, 1951.

Baron, J.-C., Chételat, G., Desgranges, B., Perchey, G., Landeau, B., de la Sayette, V. & Eustache, F. (2001). **In vivo mapping of gray matter loss with voxel-based morphometry in mild Alzheimer`s disease.** *Neuroimage;* 14: 298-309.

Bell-McGinty, S., Butters, M.A., Meltzer, C.C., Greer, P.J., Reynolds III, C.F. & Becker, J.T. (2002). **Brain Morphometric Abnormalties in Geriatric Depression: Long-Term Neurobiological effects of Illness Duration.** *Am. J. Psychiatry;* 159: 1424-1427.

Bjaalie, J.G. (2001). **Advances in computational neuroanatomy.** *Anat. Embryol.;* 204: 253-254.

Bookstein, F.L. (2001). **„Voxel-Based Morphometry" Should Not Be Used with Imperfectly Registred Images.** *Neuroimage;* 14: 1454-1462.

Boyke, J., Driemeyer, J., Gaser, C., Büchel, C. & May, A. (2008). **Training-induced brain structure changes in the elderly.** *J. Neurosci.;* 28(28): 7031-7035.

Brenneis, C., Wenning, G.K., Egger, K.E., Schocke, M., Trieb, T., Seppi, K., Marksteiner, J., Ransmayr, G., Benke, T. & Poewe, W. (2004). **Basal forebrain atrophy is a distinctive pattern in dementia with Lewy bodies.** *Neuroreport;* 5 (11): 1711-1714.

Brodmann, K. (1908). **Beiträge zur histologischen Lokalisation der Grosshirnrinde. VI. Die Cortexgliederung des Menschen.** *J. Psychol. Neurol.;* 10: 231-246, 287-334 [in German].

Brodmann, K. (1909). ***Vergleichende Lokalisationslehre der Großhirnrinde in ihren Prinzipien dargestellt auf Grund ihres Zellenbaues.*** Barth, Leipzig, 1909 [in German].

Brodmann, K. (1914). **Physiologie des Gehirns.** *Neue Dtsch. Chir.*; 11: 85-426 [in German].

Bruno, S.D. (2005). **Neuroimaging of Bipolar Disorder: Emphasis on Novel MRI Techniques.** *Epilepsia;* 46 (Suppl. 4): 14-18.

Busatto, G.F., Garrido, G.E.J., Almeida, O.P., Castro, C.C., Camargo, C.H.P., Cid, C.G., Buchpiguel, C.A., Furuie, S. & Bottino, C.M. (2003). **A voxel-based morphometry study of temporal lobe gray matter reductions in Alzheimer's disease.** *Neurobiol. Aging;* 24: 221-231.

Chételat, G., Landeau, B., Eustache, F., Mézenge, F., Viader, F., de la Sayette, V., Desgranges, B. & Baron, J.-C. (2005). **Using voxel-based morphometry to map the structural changes associated with rapid conversion in MCI: A longitudinal MRI study.** *Neuroimage;* 27, 934-946.

Chételat, G., Desgranges, B., de la Sayette, V., Viader, F., Eustache, F. & Baron, J.-C. (2002). **Mapping gray matter loss with voxel-based morphometry in mild cognitive impairment.** *Neuroreport;* 13 (15): 1939-1943.

Christensen, G.E., Rabbitt, R.D. & Miller, M.I. (1996). **Deformable templates using large deformation kinemathics.** *IEEE Trans. Image Process.;* 5: 1435-1447.

Christensen, G.E., Rabbitt, R.D. & Miller, M.I. (1994). **3D brain mapping using a deformable neuroanatomy.** *Phys. Med. Biol.;* 39: 609-618.

Chumbley, J.R. & Friston, K.J. (2009). **False discovery rate revisited: FDR and topological inference using Gaussian random fields.** *Neuroimage;* 44: 62-70.

Chung, M.K., Worsley, K.J., Robbins, S., Paus, T., Taylor, J., Giedd, J.N., Rapoport, J.L. & Evans, A.C. (2003). **Deformation-based surface morphometry applied to gray matter deformation.** *Neuroimage;* 18(2): 198-213.

Chung, M.K., Worsley, K.J., Paus, T., Cherif, C., Collins, D.L., Giedd, J.N., Rapoport, J.L. & Evans, A.C. (2001). **A Unified Statistical Approach to Deformation-Based Morphometry.** *Neuroimage;* 14: 595-606.

Collins**,** D.L., Zijdenbos, A.P., Barré, W.F.C. & Evans, A.C. (1999). **ANIMAL+INSECT: Improved cortical structure segmentation,** in ***Proc. of the Annual Symposium on Information Processing in Medical Imaging*** (A. Kuba, M. Samal, and A. Todd-Pokropek, eds.), vol. 1613 of LNCS, pp. 210-223, Springer, 1999.

Collins, D.L., Holmes, C.J., Peters, T.M. & Evans, A.C. (1995). **Automatic 3D Model-Based Neuroanatomical Segmentation.** *Hum. Brain Mapp.;* 3: 190-208.

Collins, D.L., Neelin, P., Peters, T.M. & Evans, A.C. (1994). **Automatic 3D intersubject registration of MR volumetric data in standardized Talairach space.** *J. Comput. Assist. Tomogr.;* 18: 192-205.

Colom, R., Jung, R.E. & Haier, R.J. (2006a). **Distributed brain sites for the g-factor of intelligence.** *Neuroimage;* 31: 1359-1365.

Colom, R., Jung, R.E. & Haier, R.J. (2006b). **Finding the g-factor in brain structure using the method of correlated vectors.** *Intelligence;* 34 (6): 561-570.

Cormack, F., Gadian, D.G., Vargha-Khadem, F., Cross, J.H., Connelly, A. & Baldeweg, T. (2005). **Extra-hippocampal grey matter density abnormalties in paediatric mesial temporal sclerosis.** *Neuroimage;* 27: 635-643.

Crivello, F., Schormann, T., Tzourio-Mazoyer, N., Roland, P.E., Zilles, K. & Mazoyer, B.M. (2002). **Comparison of Spatial Normalization Procedures and Their Impact on Functional Maps.** *Hum. Brain Mapp.;* 16: 228-250.

Crum, W.R., Griffin, L.D., Hill, D.L.G. & Hawkes, D.J. (2003). **Zen and the art of medical image registration: correspondence, homology, and quality.** *Neuroimage;* 20: 1425-1437.

Csernansky, J.G., Joshi, S., Wang, L., Haller, J.W., Gado, M., Miller, J.P., Grenander, U. & Miller, M.I, (1998). **Hippocampal morphometry in schizophrenia by high dimensional brain mapping.** *Proc. Natl. Acad. Sci. U.S.A.;* 95(19): 11406-11411.

Cuadra, M.B., Cammoun, L., Butz, T. Cuisenaire, O. & Thiran, J.-P. (2005). **Comparison and Validation of Tissue Modelization and Statistical Classification Methods in T1-Weighted MR Brain Images.** *IEEE Trans. Med. Imaging;* 24(12): 1548-1565.

Dale, A.M., Liu, A.K., Fischl, B.R., Buckner, R., Belliveau, J.W., Lewine, J., Halgren, E. (2000). **Dynamic statistical parametric mapping: combining fMRI and MEG for high-resolution imaging of cortical activity.** *Neuron;* 26(1): 55-67.

Dale, A.M., Fischl, B. & Sereno, M.I. (1999). **Cortical Surface-Based Analysis: I. Segmentation and Surface Reconstruction.** *Neuroimage;* 9: 179-194.

Dale, A.M., Halgren, E., Lewine, J., Buckner, R., Paulson, K., Marinkovic, K. & Rosen, B. (1997). **Spatiotemporal localization of cortical word repetition effects in a size-judgment task using combined fMRI/MEG [abstract].** Presented at the 3th International Conference on Human Brain Mapping, May 19-23, 1997, Copenhagen, DK.

Dale, A.M. & Sereno, M.I. (1993). **Improved localisation of cortical activity by combining EEG and MEG with MRI cortical surface reconstruction: a linear approach.** *J. Cogn. Neurosci.;* 5: 162-176.

Davatzikos, C. (2004). **Why voxel-based morphometric analysis should be used with great caution when characterizing group differences.** *Neuroimage;* 23: 17-20.

Davatzikos, C., Genc, A., Xu, D. & Resnick, S.M. (2001). **Voxel-based morphometry using the RAVENS maps: methods and validation using simulated longitudinal atrophy.** *Neuroimage;* 14(6): 1361-1369.

Davatzikos, C., Vaillant, M., Resnick, S.M., Prince, J.L., Letovsky, S. & Bryan, R.N. (1996). **A Computerized Approach for Morphological Analysis of the Corpus Callosum.** *J. Comp. Assist. Tomogr.;* 20(1): 88-97.

Deichmann, R., Good, C.D., Josephs, O., Ashburner, J. & Turner, R. (2000). **Optimization of 3-D MP-RAGE Sequences for Structural Brain Imaging.** *Neuroimage;* 12: 112-127.

Desikan, R.S., Ségonne, F., Fischl, B., Quinn, B.T., Dickerson, B.C., Blacker, D., Buckner, R.L., Dale, A.M., Maguire, R.P., Hyman, B.T., Albert, M.S. & Killiany, R.J. (2006). **An automated labeling system for subdividing the human cerebral cortex on MRI scans into gyral based regions of interest.** *Neuroimage;* 31(3): 968-980.

Draganski, B., Gaser, C., Kempermann, G., Kuhn, H.G., Winkler, J., Büchel, C. & May, A. (2006a). **Temporal and Spatial Dynamics of Brain Structure Changes during Extensive Learning.** *J. Neurosci;* 26 (23): 6314-6317.

Draganski, B., Moser, T., Lummel, N., Gänssbauer, S., Bogdahn, U., Haas, F. & May, A. (2006b). **Decrease of thalamic gray matter following limb amputation.** *Neuroimage;* 31: 951-957.

Draganski, B., Gaser, C., Busch, V., Schuierer, G., Bogdahn, U. & May, A. (2004). **Changes in grey matter induced by training.** *Nature;* 427: 311-312.

Draganski, B., Geisler, P., Hajak, G, Schuierer, G., Bogdahn, U., Winkler, J. & May, A. (2002). **Hypothalamic grey matter changes in narcoleptic patients.** *Nat. Med.;* 427: 311-312.

Driemeyer, J., Boyke, J., Gaser, C., Büchel, C. & May, A. (2008). **Changes in gray matter induced by learning - revisited.** *PLoS ONE;* 3(7): e2669.

Duning, T., Kloska, S., Steinsträter, O., Kugel, H., Heindel, W. & Knecht, S. (2005). **Dehydration confounds the assessment of brain atrophy.** *Neurology;* 64: 548-550.

Duvernoy, H. M. (1991). ***The Human Brain.*** Springer, New York, 1991.

von Economo, C. & Koskinas, G.N. (1925). ***Die Cytoarchitektonik der Hirnrinde des Erwachsenen Menschen.*** Springer, Berlin, 1925 [in German].

von Economo C. (1929). ***The cytoarchitectonics of the human cerebral cortex***. Oxford Medical Publications, London, 1929.

Eickhoff, S., Schleicher, A., Scheperjans, F., Palomero-Gallagher, N. & Zilles, K. (2007). **Analysis of neurotransmitter receptor distribution patterns in the cerebral cortex.** *Neuroimage;* 34(3): 1317-1330.

Eickhoff, S.B., Heim, S., Zilles, K. & Amunts, K. (2006). **Testing anatomically specified hypotheses in functional imaging using cytoarchitectonic maps.** *Neuroimage;* 32 (2): 570-582.

Eickhoff, S.B., Stephan, K.E., Mohlberg, H., Grefkes, C., Fink, G.R., Amunts, K. & Zilles, K. (2005a). **A new SPM toolbox for combining probabilistic cytoarchitectonic maps and functional imaging data.** *Neuroimage;* 25: 1325–1335.

Eickhoff, S.B., Walters, N.B., Schleicher, A., Kril, J., Egan, G.F., Zilles, K., Watson, J.D. & Amunts, K. (2005b). **High-resolution MRI reflects myeloarchitecture and cytoarchitecture of human cerebral cortex.** *Hum. Brain Mapp.;* 24(3): 206-215.

van Essen, D.C., Drury, H.A., Joshi, S. & Miller, M.I. (1998). **Functional and structural mapping of human cerebral cortex: solutions are in the surfaces.** *Proc. Natl. Acad. Sci. USA;* 95: 788-795.

Etgen, T., Draganski, B., Ilg, C., Schröder, M., Geisler, P., Hajak, G., Eisensehr, I., Sander, D. & May, A. (2005). **Bilateral thalamic gray matter changes in patients with restless legs syndrome.** *Neuroimage;* 24: 1242-1247.

Evans, A.C., Kamber, M., Collins, D.L. & MacDonald, D. (1994). **An MRI based probabilistic atlas of neuroanatomy.** In: Shorvon, S., Fish, D., Andermann, F., Bydder, G.M., Stefan, H. (Eds.), ***Magnetic Resonance Scanning and Epilepsy,*** NATO ASI Ser., Ser. A: Life Sci., vol. 264. Plenum Press, pp. 263–274.

Evans, A.C., Collins, D.L. & Milner, B. (1992). **An MRI-based stereotactic brain atlas from 300 young normal subjects.** *Soc. Neurosci. Abstr.;* 408.

Fischl, B., Salat, D.H., van der Kouwe, A.J.W., Makris, N., Ségonne, F., Quinn, P.T. & Dale, A.M. (2004a). **Sequence-independent segmentation of magnetic resonance images.** *Neuroimage;* 23: S69-S84.

Fischl, B., van der Kouwe, A., Déstrieux, C., Halgren, E., Ségonne, F., Salat, D.H., Busa, E., Seidman, L.J., Goldstein, J., Kennedy, D., Caviness, V., Makris, N., Rosen, B. & Dale, A.M. (2004b). **Automatically parcellating the human cerebral cortex.** *Cereb. Cortex;* 14: 11-22.

Fischl, B., Salat, D.H., Busa, E., Albert, M., Dieterich, M., Haselgrove, C., van der Kouwe, A., Killiany, R., Kennedy, D., Klaveness, S., Montillo, A., Makris, N., Rosen, B. & Dale, A.M. (2002). **Whole Brain Segmentation: Automated Labeling of Neuroanatomical Structures in the Human Brain.** *Neuron;* 33: 341-355.

Fischl, B., Liu, A. & Dale, A.M. (2001). **Automated manifold surgery: constructing geometrically accurate and topologically correct models of the human cerebral cortex.** *IEEE Trans. Med. Imaging;* 20: 70-80.

Fischl, B. & Dale, A.M. (2000). **Measuring the thickness of the human cerebral cortex from magnetic resonance images.** *Proc. Natl. Acad. Sci. USA;* 97: 11050-11055.

Fischl, B., Sereno, M.I. & Dale, A.M. (1999a). **Cortical Surface-Based Analysis: II. Inflation, Flattening, and a Surface-Based Coordinate System.** *Neuroimage;* 9: 195-207.

Fischl, B., Sereno, M.I., Tootell, R.B.H. & Dale, A.M. (1999b). **High-Resolution Intersubject Averaging and a Coordinate System for the Cortical Surface.** *Hum. Brain Mapp.;* 8: 272-284.

Flechsig, P. (1920). ***Anatomie des menschlichen Gehirns und Rückenmarks auf myelogenetischer Grundlage.*** Thieme, Leipzig, 1920 [in German].

Frangou, S., Chitins, X., & Williams, S.C.R. (2004). **Mapping IQ and gray matter density in healthy young people.** *Neuroimage;* 23: 800-805.

Free, S.L., Mitchell, T.N., Williamson, K.A., Churchill, A.J., Shorvon, S.D., Moore, A.T., van Heyningen, V. & Sisodiya, S.M. (2003). **Quantitative MR image analysis in subjects with defects in the *PAX6* gene.** *Neuroimage;* 20: 2281-2290.

Freeborough, P.A. & Fox, N.C. (1998). **Modeling brain deformations in Alzheimer disease by fluid registration of serial 3D MR images.** *J. Comp. Assist. Tomogr.;* 22(5): 838-843.

Frisoni, G.B., Testa, C., Sabattoli, F., Beltramello, A., Soininen, H. & Laakso, M.P. (2005). **Structural correlates of early and late onset Alzheimer`s disease: voxel-based morphometric study.** *J. Neurol. Neurosurg. Psychiatry;* 76: 112-114.

Frisoni, G.B., Testa, C., Zorzan, A., Sabattoli, F., Beltramello, A., Soininen, H. & Laakso, M.P. (2002). **Detection of grey matter loss in mild Alzheimer`s disease with voxel-based morphometry.** *J. Neurol. Neurosurg. Psychiatry;* 73: 657-664.

Friston, K.J., Ashburner, J.T., Kiebel, S.J., Nichols, T.E. & Penny, W.D. (2007). ***Statistical Parametric Mapping: The Analysis of Functional Brain Images.*** Elsevier, London, 2007.

Friston, K. (1997). **Testing for Anatomically Specified Regional Effects.** *Hum. Brain Mapp.;* 5: 133-136.

Friston, K.J., Holmes, A.P., Poline, J.-B., Price, C.J. & Frith, C.D. (1996). **Detecting activations in PET and fMRI: Levels of inference and power.** *Neuroimage;* 4: 223–235.

Friston, K.J., Ashburner, J., Frith, C., Poline, J.B., Heather, J.D. & Frackowiak, R.S.J. (1995a). **Spatial Registration and Normalization of Images.** *Hum. Brain Mapp.;* 2: 165-189.

Friston, K.J., Holmes, A.P., Worsley, K.J., Poline, J.-B., Frith, C.D. & Frackowiak, R.S.J. (1995b). **Statistical parametric maps in functional imaging: A general linear approach.** *Hum. Brain Mapp.;* 2: 189–210.

Gaser, C. & Schlaug, G. (2003). **Brain Structures Differ Between Musicians and Non-Musicians.** *J. Neurosci.;* 23 (27): 9240-9245.

Gaser, C., Nenadic, I., Buchsbaum, B.R., Hazlett, E.A. & Buchsbaum, M.S. (2001). **Deformation-Based Morphometry and Ist Relation to Conventional Volumetry of Brain Lateral Ventricles in MRI.** *Neuroimage;* 13: 1140-1145.

Gaser, C. (2001). **Deformations-basierte Morphometrie - eine Methode zur Analyse hirnstruktureller Veränderungen.** PhD thesis, Otto-von-Guericke University Magdeburg, 2001.

Gaser, C., Volz, H.P., Kiebel, S., Riehemann, S. & Sauer, H. (1999). **Detecting structural changes in whole brain based on nonlinear deformations - application to schizophrenia research.** *Neuroimage;* 10(2): 107-113.

Gale, S.D., Baxter, L., Roundy, N. & Johnson, S.C. (2005). **Traumatic brain injury and grey matter concentration: a preliminary voxel based morphometry study.** *J. Neurol. Neurosurg. Psychiatry;* 76: 984-988.

Genovese, C.R., Lazar, N.A. & Nichols, T. (2002). **Thresholding of Statistical Maps in Functional Neuroimaging Using the False Discovery Rate.** *Neuroimage;* 15: 870-878.

Gerig, G., Styner, M., Shenton, M.E. & Lieberman, J.A. (2001). **Shape versus Size: Improved Understanding of the Morphology of Brain Structures.** *Proc. MICCAI (Springer LNCS);* 2208; 24-32.

Golestani, N., Molko, N., Dehaene, S., LeBihan, D. & Pallier, C. (2007a). **Brain Structures Predicts the Learning of Foreign Speech Sounds.** *Cereb. Cortex;* 17: 575-582.

Golestani, N. & Pallier, C. (2007b). **Anatomical Correlates of Foreign Speech Sound Production.** *Cereb. Cortex;* 17: 929-934.

Golestani, N., Paus, T. & Zatorre, R.J. (2002). **Anatomical correlates of learning novel speech sounds.** *Neuron;* 35: 997-1010.

Gong, Q.-Y., Sluming, V., Mayes, A., Keller, S., Barrick, T., Cezayirli, E. & Roberts, N. (2005). **Voxel-based morphometry and stereology provide convergent evidence of the importance of medial prefrontal cortex for fluid intelligence in healthy adults.** *Neuroimage;* 25: 1175-1186.

Good, C.D., Johnsrude, I.S., Ashburner, J., Henson, R.N.A., Friston, K.J. & Frackowiak, R.S.J. (2001a). **A Voxel-Based Morphometric Study of Ageing in 465 Normal Adult Human Brains.** *Neuroimage;* 14: 21-36.

Good, C.D., Johnsrude, I.S., Ashburner, J., Henson, R.N.A., Friston, K.J. & Frackowiak, R.S.J. (2001b). **Cerebral Asymmetry and the Effects of Sex and Handedness on Brain Structure: A Voxel-Based Morphometric Analysis of 465 Normal Adult Human Brains.** *Neuroimage;* 14: 685-700.

Good, C.D., Ashburner, J. & Frackowiak, R.S.J. (2001c). **Computational neuroanatomy: new perspectives for neuroradiology.** *Rev. Neurol. (Paris);* 157(8-9 Pt 1): 797-806.

Hänggi, J., Beeli, G., Oechslin, M.S. & Jäncke, L. (2008). **The multiple synaesthete E.S.: neuroanatomical basis of interval-taste and tone-colour synaesthesia.** *Neuroimage;* 43(2): 192-203.

Hänggi, J., Mondadori, C.R.A., Buchmann, A., Henke, K. & Hock, C. (2009). **A *CYP46* T/C SNP modulates parahippocampal and hippocampal morphology in young subjects.** *Neurobiol. Aging;* doi:10.1016/j.neurobiolaging.2009.07.001.

Hänggi, J., Buchmann, A., Mondadori, C.R.A., Henke, K., Jäncke, L. & Hock, C. (2008). **Sexual dimorphism in the parietal substrate associated with visuospatial cognition independent of general intelligence.** *J. Cogn. Neurosci.;* doi:10.1162/jocn.2008.21175.

Hänggi, J., Streffer, J., Signorell, A., Jäncke, L. & Hock, C. **Neuromorphometric profiling in mild cognitive impairment and Alzheimer's disease: Sensitivity and specificity.** (submitted).

Haier, R.J., Jung, R.E., Yeo, R.A., Head, K. & Alkire, M.T. (2005). **The neuroanatomy of general intelligence: sex matters.** *Neuroimage;* 25: 320-327.

Haier, R.J., Jung, R.E., Yeo, R.A., Head, K. & Alkire, M.T. (2004). **Structural brain variation and general intelligence.** *Neuroimage;* 23: 425-433.

Han, X., Jovicich, J., Salat, D., van der Kouwe, A., Quinn, B., Czanner, S., Busa, E., Pacheco, J., Albert, M., Killiany, R., Maguire, P., Rosas, D., Makris, N., Dale, A.M., Dickerson, B. & Fischl, B. (2006). **Reliability of MRI-derived measurements of human cerebral cortical thickness: the effects of field strength, scanner upgrade and manufacturer.** *Neuroimage;* 32: 180-194.

Haug, H. (1986). **History of neuromorphometry.** *J. Neurosci. Methods;* 18: 1-17.

Hayasaka, S., Phan, K.L., Liberzon, I., Worsley, K.J. & Nichols, T.E. (2004). **Nonstationary cluster-size inference with random field and permutation methods.** *Neuroimage;* 22: 676-687.

Honea, R., Crow, T.J., Passingham, D. & Mackay, C.E. (2005). **Regional Deficits in Brain Volume in Schizophrenia: A Meta-Analysis of Voxel-Based Morphometry Studies.** *Am. J. Psychiatry;* 162: 2233-2245.

Holmes, C.J., Hoge, R., Collins, L., Woods, R., Toga, A.W. & Evans, A.C. (1998). **Enhancement of MR Images Using Registration for Signal Averaging.** *J. Comput. Assist. Tomogr.;* 22 (2): 324-333.

van Horn, J.D. (2005). **Neuroimaging databases as a resource of scientific discovery.** *Int. Rev. Neurobiol.;* 66: 55-87.

Howarth, C., Hutton, C. & Deichmann, R. (2005). **Improvements of the image quality of T1-weighted anatomical brain scan.** *Neuroimage;* 29: 930-937.

Jatzko, A., Rothenhöfer, S., Schmitt, A., Gaser, C., Demirakca, T., Weber-Fahr, W., Wessa, M., Magnotta, V. & Braus, D.F. (2006). **Hippocampal volume in chronic posttraumatic stress disorder (PTSD): MRI study using two different evaluation methods.** *J. Affect. Disord.;* 94: 121-126.

Jäncke, L., Koeneke, S., Hoppe, A., Rominger, C. & Hänggi, J. (2009a). **The architecture of the golfer's brain.** *PLoS ONE;* 4(3): e4785.

Jäncke, L., Beeli, G., Eulig, C. & Hänggi, J. (2009b). **The neuroanatomy of grapheme-color synesthesia.** *Eur. J. Neurosci.;* 29(6): 1287-1293.

Jäncke, L., Siegenthaler, Th., Preis, S. & Steinmetz, H. (2006). **Decreased white-matter density in a left-sided fronto-temporal network in children with developmental language disorder: Evidence for anatomical anomalies in a motor-language network.** *Brain Lang.;* 102(1): 91-98.

Jäncke, L., Hänggi, J. & Steinmetz, H (2004). **Morphological brain differences between adult stutterers and non-stutterers.** *BMC Neurology;* 4(1): 23.

Jayakumar, P.N., Venkatasubramanian, G., Gangadhar, B.N., Janakiramaiah, N. & Keshavan, M.S. (2005). **Optimized voxel-based morphometry of gray matter volume in first-episode, antipsychotic-naïve schizophrenia.** *Prog. Neuropsychopharmacol. Biol. Psychiatry;* 29: 587-591.

Jennings, C & Aamodt, S. (2000). **Computational approaches to brain function.** *Nat. Neurosci. Supp.;* 3: 1160.

Job, D.E., Whalley, H.C., McConnell, S., Glabus, M., Johnstone, E.C. & Lawrie, S.M. (2002). **Structural Gray Matter Differences between First-Episode Schizophrenics and Normal Controls Using Voxel-Based Morphometry.** *Neuroimage;* 17: 880-889.

Joshi, S., Grenander, U. & Miller, M.I. (1997). **On the geometry and shape of brain sub-manifolds.** *IEEE Trans. Pattern Anal. Mach. Intell.*; 11: 1317-1343.

Jovicich, J., Czanner, S., Greve, D., Haley, E., van der Kouwe, A., Gollub, R., Kennedy, D., Schmitt. F., Brown, G., Macfall, J., Fischl, B. & Dale, A.M. (2006). **Reliability in multi-site structural MRI studies: effects of gradient non-linearity correction on phantom and human data.** *Neuroimage;* 30: 436-443.

Jung, R.E. & Haier, R.J. (2007). **The Parieto-Frontal Intergration Theory (P-FIT) of intelligence: converging neuroimaging evidence.** *Behav. Brain Sci.;* 30(2): 135-154; discussion 154-187.

Karas, G.B., Scheltens, P., Rombouts, S.A.R.B., Visser, P.J., van Schijndel, R.A., Fox, N.C. & Barkhof, F. (2004). **Global and local gray matter loss in mild cognitive impairment and Alzheimer`s disease.** *Neuroimage;* 23: 708-716.

Karas, G.B., Burton, E.J., Rombouts, S.A.R.B., van Schijndel, R.A., O`Brien, J.T., Scheltens, P., McKeith, I.G., Williams, D., Ballard, C. & Barkhof, F. (2003). **A comprehensive study of gray matter loss in patients with Alzheimer`s disease using optimized voxel-based morphometry.** *Neuroimage;* 18: 895-907.

Kennedy, D.N., Lange, N., Makris, N., Bates, J., Meyer, J. & Caviness, V.S. Jr. (1998). **Gyri of the human neocortex: an MRI-based analysis of volume and variance.** *Cereb. Cortex;* 8(4): 372-84.

Keller, S.S., Wilke, M., Wieshmann, U.C., Sluming, V. & Roberts, N. (2004). **Comparison of standard and optimized voxel-based morphometry for analysis of brain changes associated with temporal lobe epilepsy.** *Neuroimage;* 23: 860-868.

Kuperberg, G.R., Broome, M.R., McGuire, P.K., David, A.S., Eddy, M., Ozawa, F., Goff, D., West, W.C., Williams, S.C., van der Kouwe, A.J., Salat, D.H., Dale, A.M. & Fischl, B. (2003). **Regionally localized thinning of the cerebral cortex in schizophrenia.** *Arch. Gen. Psychiatry;* 60: 878-888.

Lerch, J.P. & Evans, A.C. (2005). **Cortical thickness analysis examined through power analysis and a population simulation.** *Neuroimage;* 24: 163-173.

Luders, E., Gaser, C., Jancke, L. & Schlaug, G. (2004). **A voxel-based approach to gray matter asymmetries.** *Neuroimage;* 22: 656-664.

Lüders, E., Steinmetz, H. & Jäncke, L. (2002). **Brain size and grey matter volume in the healthy human brain.** *Neuroreport;* 13(17): 2371-2374.

Lyttelton, O.C., Karama, S., Ad-Dab'bagh, Y., Zatorre, R.J., Carbonell, F., Worsley, K. & Evans, A.C. (2009). **Positional and surface area asymmetry of the human cerebral cortex.** *Neuroimage;* 46: 895-903.

Maguire, E.A., Gadian, D.G., Johnsrude, I.S., Good, C.D., Ashburner, J., Frackowiak, R.S.J. & Frith, C.D. (2000). **Navigation-related structural change in the hippocampi of taxi drivers.** *Proc. Natl. Acad. Sci. USA;* 97 (8): 4398-4403.

Mai, J., Assheuer, J. & Paxinos, G. (1997). ***Atlas of the Human Brain***. Academic Press, San Diego, 1997.

Makris, N., Kaiser, J., Haselgrove, C., Seidman, L.J., Biederman, J., Boriel, D., Valera, E.M., Papadimitriou, G.M., Fischl., B., Caviness Jr., V.S. & Kennedy, D.N. (2006). **Human cerebral cortex: A system for the integration of volume- and surface-based representations.** *NeuroImage;* 33(1); 139-153.

May, A. & Gaser, C. (2006). **Magnetic resonance-based morphometry: a window into structural plasticity of the brain.** *Curr. Opin. Neurol.;* 19: 407-411.

Mazziota, J., Toga, A., Evans, A., Fox, P., Lancaster, J., Zilles, K., Woods, R., Paus, T., Simpson, G., Pike, B., Holmes, C., Collins, L., Thompson, P., MacDonald, D., Iacoboni, M., Schormann, T., Amunts, K., Palomero-Gallagher, N., Geyer, S., Parson, L., Narr, K., Kabani, N., Le Goualher, G., Boomsma, D., Cannon, T., Kawashima, R. & Mazoyer, B. (2001). **A probabilistic atlas and reference system for the human brain: International Consortium for Brain Mapping (ICBM).** *Phil. Trans. R. Soc. Lond. B;* 356: 1293-1322.

MacDonald, D. (1998). **A Method for Identifying Geometrically Simple Surfaces from Three Dimensional Images.** Ph.D. Thesis, McGill University, Canada.

Mechelli, A., Friston, K.J., Frackowiak, R.S. & Price, C.J. (2005a). **Structural Covariance in the Human Cortex.** *J. Neurosci.;* 25(36): 8303-8310.

Mechelli, A., Price, C.J., Friston, K.J. & Ashburner, K. (2005b). **Voxel-Based Morphometry of the Human Brain: Methods and Applications.** *Curr. Med.Imaging Rev.;* 1(2): 105-113.

Miller, M.I., Trouve, A. & Younes, L. (2002). **On the metrics and Euler-Lagrange equations of computational anatomy.** *Annu. Rev. Biomed. Eng.;* 4: 375-405.

Molko, N., Cachia, A., Riviere, D., Mangin, J.F., Bruandet, M., LeBihan, D., Cohen, L. & Dehaene, S. (2004). **Brain Anatomy in Turner Syndrome: Evidence for Impaired Social and Spatial-Numerical Networks.** *Cereb. Cortex;* 14 (8): 840-850.

Mummery, C.J., Patterson, K., Price, C.J., Ashburner, J., Frackowiak, R.S.J. & Hodges, J.R. (2000). **A Voxel-Based Morphometry Study of Semantic Dementia: Relationship between Temporal Lobe Atrophy and Semantic Memory.** *Ann. Neurol.;* 47: 36-45.

Nichols, T.E. & Holmes, A.P. (2001). **Nonparametric Permutation Tests For Functional Neuroimaging: A Primer with Examples.** *Hum. Brain Mapp.;* 15: 1-25.

Ono, M., Kubik, S. & Abernathey, C.D. (1990). ***Atlas of the Cerebral Sulci***. Thieme, Stuttgart, 1990.

Pennanen, C., Testa, C., Laakso, M.P., Hallikainen, M., Helkala, E.-L., Hänninen, T., Kivipelto, M., Könönen, M., Nissinen, A., Tervo, S., Vanhanen, M., Vanninen, R., Frisoni, G.B. & Soininen, H. (2005). **A voxel based morphometry study on mild cognitive impairment.** *J. Neurol. Neurosurg. Psychiatry;* 76: 11-14.

Pezawas, L., Verchinski, B.A., Mattay, V.S., Callicott, J.H., Kolachana, B.S., Straub, R.E., Egan, M.F., Meyer-Lindenberg, A. & Weinberger, D.R. (2004). **The brain-derived neurotrophic factor val66met polymorphism and variation in human cortical morphology.** *J. Neurosci.;* 24 (45): 10099-10102.

Poldrack, R.A., Fletcher, P.C., Henson, R.N., Worsley, K.J., Brett, M. & Nichols, T.E. (2008). **Guidelines for reporting an fMRI study.** *Neuroimage;* 40: 409-414.

Pujol, J., Soriano-Mas, C., Alonso, P., Cardoner, N., Menchon, J.M., Deus, J. & Vallejo, J. (2004). **Mapping Structural Brain Alterations in Obsessive-Compulsive Disorder.** *Arch. Gen. Psychiatry;* 61: 720-730.

Raz, A., Lieber, B., Soliman, F., Buhle, J., Posner, J., Peterson, B.S. & Posner, M.I. (2005). **Ecological nuances in functional magnetic resonance imaging (fMRI): psychological stressor, posture, and hydrostatics.** *Neuroimage;* 25: 1-7.

Ridgway, G.R., Henley, S.M.D., Rohrer, J.D., Scahill, R.I., Warren, J.D. & Fox, N.C. (2008). **Ten simple rules for reporting voxel-based morphometry studies.** *Neuroimage;* 40(4): 1429-1435.

Richardson, M.P., Friston, K.J., Sisodiya, S.M., Koepp, M.J., Ashburner, J., Free, S.L., Brooks, D.J. & Duncan, J.S. (1997). **Cortical grey matter and benzodiazepine receptors in malformations of cortical development: A voxel-based comparison of structural and functional imaging data.** *Brain;* 120: 1961-1973.

Robbins, S., Evans, A.C., Collins, D.L. & Whitesides, S. (2004). **Tuning and comparing spatial normalization methods.** *Med. Image Anal.;* 8: 311-323.

Rombouts, S.A.R.B., Barkhof, F., Witter, M.P. & Scheltens, P. (2000). **Unbiased whole-brain analysis of gray matter loss in Alzheimer`s disease.** *Neurosci. Lett.;* 285, 231-233.

Rosas, H.D., Liu, A.K., Hersch, S., Glessner, M., Ferrante, R.J., Salat, D.H., van der Kouwe, A., Jenkins, B.G., Dale, A.M. & Fischl, B. (2002). **Regional and progressive thinning of the cortical ribbon in Huntington's disease.** *Neurology;* 58: 695-701.

Rosen, H.J., Gorno-Tempini, M.L., Goldman, W.P., Perry, R.J., Schuff, N., Weiner, M., Feiwell, R., Kramer, J.H. & Miller, B.L. (2002). **Patterns of brain atrophy in frontotemporal dementia and semantic dementia.** *Neurology;* 58: 198-208.

Salat, D.H., Buckner, R.L., Snyder, A.Z., Greve, D.N., Desikan, R.S., Busa, E., Morris, J.C., Dale, A.M. & Fischl, B. (2004). **Thinning of the cerebral cortex in aging.** *Cereb. Cortex;* 14: 721-730.

Salmond, C.H., Ashburner, J., Vargha-Khadem, F., Connelly, A., Gadian, D.G. & Friston, K.J. (2002). **Distributional Assumptions in Voxel-Based Morphometry.** *Neuroimage;* 17: 1027-1030.

Salmond, C.H., Ashburner, J., Vargha-Khadem, F., Connelly, A., Gadian, D.G. & Friston, K.J. (2002). **The Precision of Anatomical Normalization in the Medial Temporal Lobe Using Spatial Basis Functions.** *Neuroimage;* 17: 507-512.

Sanides, F. (1962). ***Die Architektonik des menschlichen Stirnhirns.*** Springer, Berlin & New York, 1962) [in German].

Sarkisov, S.A., Filimonoff, I.N., Kononowa, E.P., Preobrachenskaja, I.S. & Kukuew, L.A. (1955). ***Atlas of the Cytoarchitectonics of the Human Cerebral Cortex.*** Medgiz, Moscow, 1955.

Saykin, A.J., Wishart, H.A., Rabin, L.A., Santulli, R.B., Flashman, L.A., West, J.D., McHugh, T.L. & Mamourian, A.C. (2006). **Older adults with cognitive complaints show brain atrophy similar to that of amnestic MCI.** *Neurology;* 67: 834-842.

Scahill, R.I., Schott, J.M., Stevens, J.M., Rossor, M.N. & Fox, N.C. (2002). **Mapping the evolution of regional atrophy in Alzheimer`s disease: Unbiased analysis of fluid-registered serial MRI.** *Proc. Natl. Acad. Sci. U.S.A.;* 99 (7): 4703-4707.

Schleicher, A., Amunts, K., Geyer, S., Morosan, P. & Zilles K. (1999). **Observer-independent method for microstructural parcellation of cerebral cortex: a quantitative approach to cytoarchitectonics.** *Neuroimage;* 9: 165–177.

Senjem, M.L., Gunter, J.L., Shiung, M.M., Petersen, R.C. & Jack, C.R. Jr. (2005). **Comparison of different methodological implementations of voxel-based morphometry in neurodegenerative disease.** *Neuroimage;* 26: 600-608.

Ségonne, F., Pacheco, J. & Fischl, B. (2007).**Geometrically accurate topology correction of cortical surfaces using nonseparating loops.** *IEEE Trans. Med. Imaging;* 26: 518-529.

Ségonne, F., Dale, A.M., Busa, E., Glessner, M., Salat, D., Hahn, H.K. & Fischl, B. (2004). **A hybrid approach to the skull stripping problem in MRI.** *Neuroimage;* 22: 1060-1075.

Shaffer, J.P. (1995). **Multiple Hypothesis Testing.** *Annu. Rev. Psychol.;* 46: 561-584.

Shen, D., Liu, D., Liu, H., Clasen, L., Giedd, J. & Davatzikos, C. (2004). **Automated morphometric study of brain variation in XXY males.** *Neuroimage;* 23: 648-653.

Sled, J.G., Zijdenbos, A.P. & Evans, A.C. (1998). **A nonparametric method for automatic correction of intensity nonuniformity in MRI data.** *IEEE Trans. Med. Imaging;* 17: 87-97.

Sluming, V., Barrick, T., Howard, M., Cezayirli, E., Mayes, A. & Roberts, N. (2002). **Voxel-Based Morphometry Reveals Increased Gray Matter Density in Broca's Area in Male Symphony Orchestral Musicians.** *Neuroimage;* 17: 1613-1622.

Sowell, E.R., Thompson, P.M., Leonard, C.M., Welcome, S.E., Kan, E. & Toga, A.W. (2004). **Longitudinal Mapping of Cortical Thickness and Brain Growth in Normal Children.** *J. Neurosci.;* 24 (38): 8223-8231.

Staff, R.T., Murray, A.D., Deary, I.J. & Whalley, L.J. (2006). **Generality and specificity in cognitive aging: A volumetric brain analysis.** *Neuroimage;* 30: 1433-1440.

Studholme, C., Cardenas, V., Song, E., Ezekiel, F., Maudsley, A. & Weiner, M. (2004). **Accurate template-based correction of brain MRI intensity distortion with application to dementia and aging.** *IEEE Trans. Med. Imaging;* 23(1): 99-110.

Talairach, J. & Tournoux, P. (1988). ***Co-planar Stereotaxic Atlas of the Human Brain.*** Thieme, New York, 1988.

Talairach, J. & Szikla, G. (1967). ***Atlas d'Anatomie Stereotaxique du Telencephale: Etudes Anatomo-Radiologiques.*** Masson & Cie, Paris, 1967 [in French].

Testa, C., Laakso, M.P., Sabattoli, F., Rossi, R., Beltramello, A., Soininen, H. & Frisoni, G.B. (2004). **A Comparison Between the Accuracy of Voxel-Based Morphometry and Hippocampal Volumetry in Alzheimer's Disease.** *J. Magn. Reson. Imaging;* 19: 274-282.

Thompson, P.M., Hayashi, K.M., Sowell, E.R., Gogtay, N., Giedd, J.N., Rapoport, J.L., de Zubicaray, G.I., Janke, A.L., Rose, S.E., Semple, J., Doddrell, D.M., Wang, Y., van Erp, T.G.M., Cannon, T.D. & Toga, A.W. (2004). **Mapping cortical change in Alzheimer`s disease, brain development, and schizophrenia.** *Neuroimage;* 23: S2-S18.

Thompson, P.M., Rapoport, J.L., Cannon, T.D. & Toga, A.W. (2003). **Automated Analysis of Structural MRI Data.** In Lawrie, S., Johnstone, E.C. & Weinberger, D. Editors, ***Brain Imaging in Schizophrenia.*** Oxford University Press, UK, 2003.

Thompson, P.M. & Toga, A.W. (2002). **A framework for computational anatomy.** *Comput. Vis. Sci.;* 5: 13-34.

Thompson, P.M., Mega, M.S., Woods, R.P., Zoumalan, C.I., Lindshield, C.J., Blanton, R.E., Moussai, J., Holmes, C.J., Cummings, J.L. & Toga, A.W. (2001). **Cortical Change in Alzheimer's Disease Detected with a Disease-specific Population-based Brain Atlas.** *Cereb. Cortex;* 11: 1-16.

Thompson, P.M., Giedd, J.N., Woods, R.P., MacDonald, D., Evans, A.C. & Toga, A.W. (2000). **Growth Patterns in the Developing Brain Detected By Using Continuum-Mechanical Tensor Maps.** *Nature;* 404: 190-193.

Tisserand, D.J., van Boxtel, M.P.J., Pruessener, J.C., Hofman, P., Evans, A.C. & Jolles, J. (2004). **A Voxel-based Morphometric Study to Determine Individual Differences in Gray matter Associated with Age and Cognitive Change Over Time.** *Cereb. Cortex;* 14 (9): 966-973.

Thompson, P.M., Schwartz, C. & Toga, A.W. (1996). **High-Resolution Random Mesh Algorithms for Creating a Probabilistic 3D Surface Atlas of the Human Brain.** *Neuroimage;* 3: 19-34.

Tisserand, D.J., Pruessener, J.C., Sanz Arigita, E.J., van Boxtel, M.P.J., Evans, A.C., Jolles, J. & Uylings, H.B.M. (2002). **Regional Frontal Cortical Volumes Decreased Differentially in Aging: An MRI Study to Compare Volumetric Approaches and Voxel-Based Morphometry.** *Neuroimage;* 17: 657-669.

Toga, A.W., Thompson, P.M., Mori, S., Amunts, K. & Zilles, K. (2006). **Towards multimodal atlases of the human brain.** *Nat. Rev. Neurosci.;* 7 (12): 952-966.

Toga, A.W. & Mazziotta, J.C. (2002) in ***Brain Mapping: The Methods 2nd edition.*** Eds. Toga, A.W. & Mazziotta, J.C., p. 3-25; Academic Press, San Diego, 2002.

Tuch, D.S. (2004). **Q-Ball Imaging.** *Magn. Reson. Med.;* 52: 1358-1372.

Tzourio-Mazoyer, N., Landeau, B., Papathanassiou, D., Crivello, F., Etard, O., Delcroix, N., Mazoyer, B. & Joliot, M. (2002). **Automated Anatomical Labeling of Activations in SPM Using a Macroscopic Anatomical Parcellation of the MNI MRI Single-Subject Brain.** *Neuroimage;* 15: 273-289.

Vargha-Khadem, F., Watkins, K.E., Price, C.J., Ashburner, J., Alcock, K.J., Connelly, A., Frackowiak, R.S.J., Friston, K.J., Pembrey, M.E., Mishkin, M., Gadian, D.G. & Passingham, R.E. (1998). **Neural Basis of an Inherited Speech and Language Disorder.** *Proc. Natl. Acad. Sci. USA;* 95(21): 12695-12700.

Vogt, C. & Vogt, O. (1919). **Allgemeinere Ergebnisse unserer Hirnforschung.** *J. Psychol. Neurol.;* 25, 292-398 [in German].

Wells III, W.M., Grimson, W.E.L., Kikinis, R. & Jolesz, F.A. (1996). **Adaptive segmentation of MRI data**. *IEEE Trans. Med. Imaging;* 15(4): 429-442.

Walter, B., Blecker, C., Kirsch, P., Sammer, G., Schienle, A., Stark, R. & Vaitl, D. (2003). **MARINA: An easy to use tool for the creation of MAsks for Region of INterest Analyses [abstract].** Presented at the 9th International Conference on Functional Mapping of the Human Brain, June 19-22, 2003, New York, NY.

Wechsler, D. (1981). **Wechsler Adult Intelligence Scale – Revised.** Psychological Corporation, San Antonio, Texas, USA, 1981.

Wilke, M., Kowatch, R.A., DelBello, M.P., Mills, N.P. & Holland, S.K. (2004). **Voxel-based morphometry in adolescent with bipolar disorder: first results.** *Psychiatry Res. (Neuroimaging);* 131: 57-69.

Wilke, M., Sohn, J.-H., Byars, A.W. & Holland, S.K. (2003). **Bright spots: correlations of gray matter volume with IQ in a normal pediatric population.** *Neuroimage;* 20: 202-215.

Woermann, F.G., Free, S.L., Koepp, M.J., Sisodiya, S.M., & Duncan, J.S. (1999). **Abnormal cerebral structure in juvenile myoclonic epilepsy demonstrated with voxel-based analysis of MRI.** *Brain;* 122: 2101-2107.

Woermann, F.G., Sisodiya, S.M., Free, S.L. & Duncan, J.S. (1998). **Quantitative MRI in patients with idiopathic generalized epilepsy.** *Brain;* 121: 1661-1667.

Worsley, K.J., Andermann, M., Koulis, T., MacDonald, D. & Evans, A.C. (1999). **Detecting Changes in Nonisotropic Images.** *Hum. Brain Mapp.;* 8: 98-101.

Worsley, K.J., Marrett, S., Neelin, P., Vandal, A.C., Friston, K.J., & Evans, A.C. (1996). **A unified statistical approach for determining significant voxels in images of cerebral activation.** *Hum. Brain Mapp.;* 4: 58–73.

Wright, I.C., Ellison, Z.R., Sharma, T., Friston, K.J., Murray, R.M. & McGuire, P.K. (1999). M**apping of grey matter changes in schizophrenia.** *Schizophr. Res.;* 35: 1-14.

Wright, I.C., McGuire, P.K., Poline, J.B., Travere, J.M., Murray, R.M., Frith, C., Frackowiak, R.S.J. & Friston, K.J. (1995). **A voxel-based method for the statistical analysis of gray and white matter density applied to schizophrenia.** *Neuroimage;* 2: 244-252.

Zilles, K., Armstrong, E., Schleicher, A. & Kretschmann, H.-J. (1988). **The human pattern of gyrification in the cerebral cortex.** *Anat. Embryology;* 179: 173–179.

8.2 Education

- Junior school (Primarschule) from 1978 to 1983 in Bubendorf, Basle-Country, Switzerland.
- Secondary school (Realschule) from 1983 to 1986 in Bubendorf.
- Professional choice class (Berufswahlklasse) from 1986 to 1987 in Ziefen, Basle-Country, Switzerland.
- Apprenticeship as chemical laboratory assistant (Chemielaborant) in biochemistry from 1987 to 1990 in the firm Bachem Holding AG in Bubendorf, Basle-Country, Switzerland.
- Grammar school for adults - second education (Gymnasium für Erwachsene - Zweitausbildung) from 1994 to 1998 to achieve a federal G.C.E. A level (General Certificate of Education Advanced level = eidgenössische Matura Typus B) at Minerva Schools in Basel, Basel, Switzerland.
- Commencement of studies in psychology as main subject and neuropsychology and neurophysiology as the two beside subjects in 1998 at the Institute of Psychology, University Zurich, Zurich, Switzerland.
- First examination (1. Zwischenprüfung) passed in autumn 1999 in psychology at the Institute of Psychology, University Zurich.
- Second examination (2. Zwischenprüfung) passed in autumn 2000 in psychology at the Institute of Psychology, University Zurich.
- Master and Ph.D. congress (Lizentianden- und Doktorandenkongress, LiDoKo,) at the Institute of Psychology, University Zurich, June 26, 2003, Place: University Zurich. Title of poster: Neuroanatomical anomalies in adults with persistent developmental stuttering (PDS).
- Master exam (Lizentiatsprüfung) in main subject psychology and in beside subjects neuropsychology and neurophysiology at the philosophical faculty of the University Zurich. Date of the received Master of Science (Lizentiat) May 28, 2004. Title of master thesis: Neuroanatomical anomalies in adults with persistent developmental stuttering (PDS).
- From December 01, 2004 to February 28, 2007 I was a Ph.D. student in neuroscience at the Division of Psychiatry Research, Psychiatric University Hospital, University of Zurich, and I participated in the international Ph.D. program in neuroscience at the Neuroscience Center Zurich (ZNZ). The Swiss Federal Institute of Technology Zurich and the University of Zurich founded the ZNZ.
- Written exam (in English), March 21, 2005, an obliged part of the international Ph.D. program in neuroscience at the Neuroscience Center Zurich (ZNZ): Introductory course in neuroscience I (winter term 2004/2005): Passed with the mark 5.5 (maximum 6.0).

- Symposium: Dementia – Vessel disease or Alzheimer`s disease? At the Clinic of Neurology, University Hospital Zurich, June 09, 2005.
- Statistical Parametric Mapping (SPM) course about functional and structural neuroimaging, September 26-29, 2005 at the University Clinic Hamburg-Eppendorf, Hamburg, Germany.
- Written exam (in English), October 17, 2005, an obliged part of the international Ph.D. program in neuroscience at the Neuroscience Center Zurich (ZNZ): Introductory course in neuroscience II (summer term 2005): Passed with the mark 4.5 (maximum 6.0).
- GCP (Good Clinical Practice) course for investigators and study coordinators at the Psychiatry University Hospital Zurich: April 12, 2006.
- Brain section course at the Institute of Anatomy, University Zurich, June 07-09, 2006. Part of the international Ph.D. program in neuroscience at the Neuroscience Center Zurich.
- Doctor of Philosophy (Dr. phil., Ph.D.) in neuroscience at the Faculty of Philosophy, University of Zurich, Switzerland and at the Neuroscience Center Zurich (ZNZ) (international Ph.D. program). Zurich, April 25, 2007. Doctorfather: Prof. Dr. rer. nat. Lutz Jäncke (Ph.D.), Division of Neuropsychology, Institute of Psychology, University of Zurich, Switzerland.

8.3 Universitary activities

- Tutor in lecture statistical methods: An introduction for psychologists I and II at the Division of Psychological Methods at the Institute of Psychology, University Zurich, from winter term 2000/2001, total six terms.
- Student representative in the vocation commission for the new professorship of general psychology (motivational psychology) at the Institute of Psychology, University Zurich, in winter term 2001/2002.
- Tutor in lecture statistical methods: An introduction in SPSS for psychologists at the Division of Psychological Methods at the Institute of Psychology, University Zurich, from winter term 2002/2003, total two terms.
- Tutor in lecture statistical methods: Methodological basis of test-psychology at the Division of Psychological Methods at the Institute of Psychology, University Zurich, from winter term 2002/2003, total two terms.
- Tutor in lecture brain and behaviour (biopsychology I) at the Division of Neuropsychology at the Institute of Psychology, University Zurich, from summer term 2003, total two terms.

8.4 Work experience

- I worked on a regular salary and temporary in different firms in different branches from 1990 to 1994. E.g., chemical and pharmaceutical firms (Bachem AG, Bubendorf ; Stia AG, Pratteln ; Knoll AG, Liestal), care man of refugees for government of Basle-Country (Kanton BL), roofing and building firm (Kellenberger Bedachungs AG, Liestal), building enterprise (Beat Wenger AG, Liestal), co-worker at the swimming pool (Town of Liestal) and several others.
- Care man of the SPSS (PC statistic program package) information centre for students of the Divisions of Clinical Psychology I and II at the Institute of Psychology, University Zurich in summer term 2000.
- Practical work at the Division of General Psychology at the Institute of Psychology, University Zurich, experimental psychological research (face perception), July to September 2001.
- Terminable assistance position (50%) at the Division of General Psychology at the Institute of Psychology, University Zurich, experimental psychological research (face perception / face recognition), from August 2001 to March 2002.
- Practical work at the Addiction Research Institute in Zurich, analysis und reanalysis of data from the study of heroin substitution therapy with opioid-addictive people in Switzerland, February and March 2002.
- Practical work at the Division of Neuropsychology at the Institute of Psychology, University Zurich, morphometric analysis of the brains of women with Turner-Syndrom, installation, incorporation, and preparation of a driving simulator, November 2002 to July 2003.
- Terminable term assistance (in winter term 2003/2004) at the Division of Neuropsychology at the Institute of Psychology, University Zurich.

8.5 Interests and activities

- Science, Animals, Plants, LP`s
- Reading, Politics, Farming
- Impartial local parliamentarian (parteiloser Einwohnerrat) of the town of Liestal from 2003 to 2004. Re-election for legislature 2004-2008, waiver of mandate.

8.6 Languages

- German, vocally and written (mother tongue)
- English, vocally and written
- French, vocally and written

- Latin, only written

8.7 Publications

Peer reviewed papers

2009

- Valko, P.**, Hänggi, J.,** Meyer, M. & Jung, H. (2009). **Evolution of striatal generation in McLeod syndrome.** *Europ. J. of Neurol.* (in press).

- **Hänggi, J.**, Koeneke, S., Bezzola, L. & Jäncke, L. (2009). **Structural neuroplasticity in the sensorimotor network in professional female ballet dancers.** *Hum. Brain Mapp.* (in press).

- Jäncke, L., Koeneke, S., Hoppe, A., Rominger, C. & **Hänggi, J.** (2009). **The architecture of the golfer's brain.** *PLoS ONE;* 4(3): e4785.

- Jäncke, L., Beeli, G., Eulig, C. & **Hänggi, J.** (2009). **The neuroanatomy of grapheme-color synesthesia.** *Eur. J. Neurosci.;* 29(6): 1287-1293.

- **Hänggi, J.,** Mondadori, C.R.A., Buchmann, A., Henke, K. & Hock, C. (2009). **A *CYP46* T/C polymorphism modulates parahippocampal and hippocampal morphology in healthy subjects.** *Neurobiol. Aging,* doi:10.1016/j.neurobiolaging.2009.07.001.

2008

- **Hänggi, J.,** Buchmann, A., Mondadori, C.R.A., Henke, K., Jäncke, L. & Hock, C. (2008). **Sexual Dimorphism in the Parietal Substrate Associated with Visuospatial Cognition Independent of General Intelligence.** *J. Cogn. Neurosci.,* doi:10.1162/jocn.2008.21175.

- **Hänggi, J.,** Beeli, G., Oechslin, M.S. & Jäncke, L. (2008). **The multiple synaesthete E.S.: neuroanatomical basis of interval-taste and tone-colour synaesthesia.** *Neuroimage,* 43(2), 192-203.

- Buchmann, A., Mondadori, C.R.A., **Hänggi, J.**, Aerni, A., Vrticka, P., Luechinger, R., Boesiger, P., Hock, C., Nitsch, R.M., de Quervain, D.J., Papassotiropoulos, A. & Henke, K. (2008). **Prion Protein M129V polymorphism affects retrieval-related brain activity.** *Neuropsychologia,* 46(9), 2389-2402.

2007

- Huentelman, M.J., Papassotiropoulos, A., Craig, D.W., Hoerndli, F.J., Pearson, J.V., Huynh, K.-D., Corneveaux, J., **Hänggi, J.,** Mondadori, C.R.A., Buchmann, A., Reiman, E.M., Henke, K., de Quervain, D.J. & Stephan, D.A. (2007). **Calmodulin-binding transcription activator 1 (CAMTA1) alleles predispose human episodic memory performance.** *Hum. Mol. Genet.,* 16(12), 1469-1477.

2006

- Papassotiropoulos, A., Stephan, D.A., Huentelman, M.J., Hoerndli, F.J., Craig, D.W., Pearson, J.V., Huynh, K.-D., Brunner, F., Corneveaux, J., Osborne, D., Wollmer, M.A., Aerni, A., Coluccia, D., **Hänggi, J.,** Mondadori, C.R.A., Buchmann, A., Reiman, E.M., Caselli, R.J., Henke, K. & de Quervain, D.J. (2006). **Common KIBRA Alleles Are Associated with Human Memory Performance.** *Science*, 314, 475-478.

2004

- Jäncke, L., **Hänggi, J.** & Steinmetz, H. (2004). **Morphological brain differences between adult stutterers and non-stutterers**. *BMC Neurology,* 4:23. http://www.biomedcentral.com/1471-2377/4/23

Talks & Abstracts

2007

- 3nd Winter Brain Symposium 2007 of the Psychogeriatric University Hospital and the Division of Psychiatry Research, Sils-Maria, Switzerland, February 3-7, 2007. Title of talk: **Neuromorphometric profiles of patients with amnestic mild cognitive impairment and Alzheimer's disease: Sensitivity and Specificity.**

2006

- ZNZ Symposium 2006: Symposium of the Neuroscience Center Zurich (ZNZ), October 20, 2006 at the University of Zurich, Zurich-Irchel. Title of talk: **Gender-specific neuromorphological substrates of human visuospatial intelligence: A computational neuroanatomical study.**

- INS (International Neuropsychological Society) congress 2006 in Zurich, Switzerland, July 26-30, 2006: Topic: From plasticity to rehabilitation. Title of talk: **Computational neuroanatomy supports the diagnosis of dementias in clinical daily routine.**

- 2nd Winter Brain Symposium 2006 of the Psychogeriatric University Hospital and the Division of Psychiatry Research, Sils-Maria, Switzerland, January 29 – February 2, 2006. Title of talk: **Longitudinal effects of β-amyloid immunization (AN1792) on whole brain atrophy rates and hippocampal volumes in patients with Alzheimer`s disease.**

Posters

2009

- NCCR (National Center of Competence in Research) Symposium on neural plasticity and repair 2009, January 30-31, 2009, Berlingen, Switzerland.
  Title of poster: **The architecture of the reverse piano player's brain.**

2008

- ZNZ Symposium 2008: Symposium of the Neuroscience Center Zurich (ZNZ), September 12, 2008 at the Swiss Federal Institute of Technology Zurich, Hönggerberg Zurich, Switzerland.
  Title of poster: **Structural neuroplasticity in the sensorimotor system of professional female ballet dancers.**
  Title of poster: **The neuroanatomical basis of grapheme-colour synaesthesia – a surface-based morphometry study.**
  Title of poster: **Structural brain anomalies in Turner syndrome – revisited.**

- NCCR (National Center of Competence in Research) Symposium on neural plasticity and repair 2008, March 7-8, 2008, Berlingen, Switzerland.
  Title of poster: **Structural neuroplasticity in the sensorimotor system of professional**

female ballet dancers.

Title of poster: **Training-induced structural plasticity in professional handball players: voxel-based morphometry & DTI.**

2007

- ZNZ Symposium 2007: Symposium of the Neuroscience Center Zurich (ZNZ), September 14, 2007 at the University of Zurich, Zurich-Irchel, Switzerland.
  Title of poster: **Neuromorphometric profiles of patients with amnestic mild cognitive impairment and Alzheimer's disease: Sensitivity and Specificity.**
  Title of poster: **Training-induced structural plasticity in professional handball players: voxel-based morphometry & DTI.**

2006

- ZNZ Symposium 2006: Symposium of the Neuroscience Center Zurich (ZNZ), October 20, 2006 at the University of Zurich, Zurich-Irchel, Switzerland. Title of poster: **Gender-specific neuromorphological substrates of human visuospatial intelligence: A computational neuroanatomical study.**

2005

- ZNZ Symposium 2005: Symposium of the Neuroscience Center Zurich (ZNZ), October 21, 2005 at the Swiss Federal Institute of Technology Zurich, Switzerland.
  Title of poster: **Longitudinal effects of β-amyloid immunization on hippocampal volumes in patients with Alzheimer`s disease.**

2003

- Master and Ph.D. congress (Lizentianden- und Doktorandenkongress, LiDoKo,), June 26, 2003, at the Institute of Psychology, University Zurich, Switzerland. Title of poster: **Neuroanatomical anomalies in adults with persistent developmental stuttering (PDS).**